REHABILITATION OF MAJOR STEEL BRIDGES IN MYANMAR UNDER SEISMIC RISKS

Khin Maung Zaw

2017

REHABILITATION OF MAJOR STEEL BRIDGES IN MYANMAR UNDER SEISMIC RISKS

A Thesis submitted to the Faculty of Engineering of Kyoto University
in partial fulfillment of the requirements for
the Degree of Doctor of Engineering

Khin Maung Zaw

2017

ABSTRACT

Many long span steel bridges were built all over the country with limited resources in limited construction time by the former Myanmar government around 1990's, in order to develop the transportation network of the county. Accordingly, there had been some background problems for the design, construction and maintenance of these long span bridges due to the rapid rate of construction. Many of the bridges were built in coastal and delta area, and some were built near the active faults. Bridges in the coastal and delta area suffered severe corrosion and damage due to the chloride attack, the movement of substructures on soft ground, unqualified bridge painting works, fracture of high tension bolts and, cracks in floor beams and pavements. Moreover, these long span bridges were usually designed with the assumed earthquake load of 0.1 g without considering local seismic demands but the new Seismic Zone Map of Myanmar (2012) stated higher ground acceleration values especially along the Sagaing fault and in the northern regions. Hence, the seismic performance of these long span steel bridges should be reviewed urgently.

Maubin Bridge was selected as a case study bridge, and preliminary analysis with FE bridge model showed higher overstresses in some diagonal members under design loads as well as increased seismic loads of 0.2 g and 0.4 g. Resistance of piles against the earthquake also cannot be assured anymore when the earthquake intensity is greater than 0.1g, and the earthquake resistance of the bridge in the longitudinal direction is relatively weaker than that in the transverse direction due to the arrangement of bearings and piles. Hence, static and dynamic loading tests were done on the bridge with two (60 ton) trucks in September 2016 to investigate the dynamic characteristics and current performance of the bridge, and measured results were used to compare and update the FE bridge model. After updating, the bridge model was analyzed under the time history dynamic analysis using modified Thabeikkyin Earthquake (2012) data for before and after retrofitting conditions using elastomeric rubber bearings. Bridge model with existing bearings showed 4 over-yield-stress diagonal members together with 160 over-allowable-stress members. However, the retrofitted bridge model showed only 140 over-allowable-stress members while eliminating over-yield-stress members. Moreover, magnitudes of horizontal reactions for after-retrofitting condition were reduced significantly about 6 times comparing with before-retrofitting condition due to the load sharing effect, improving the weakness in earthquake resistance of the bridge in the longitudinal direction. Based on Thabeikkyin earthquake data, the design spectrums for level I and level II earthquakes in the delta region were also proposed as an initiative for the emergence of the design standard for the construction of long span bridges in Myanmar.

ACKNOWLEDGEMENT

The author wants to express his utmost and heartiest gratitude to his academic supervisor, Professor Kunitomo Sugiura, Structural Mechanics Laboratory, Department of Civil and Earth Resources Engineering, Kyoto University, for his encouragement, precious guidance and continuous support through the study. Sincere appreciations are also extended to Professor Hiromichi Shirato of Bridge Engineering Laboratory, and Professor Junji Kiyono of Earthquake and Lifeline Engineering Laboratory for co-supervising the research and their kindness to review this Doctoral thesis.

The author acknowledges Associate Professor Masahide Matsumura and Assistant Professor Yasuo Suzuki of Structural Mechanics Laboratory for sharing their knowledge and kind assistance during his study in Japan. Special thanks go to Ms. Namie Kawano and other members of Structural Mechanics Laboratory for helping his life easier in Japan.

Appreciation is also extended to Dr. Hisato Kato of CTI Engineering for his kind sharing of experiences during the field test in Myanmar as well as in Japan. Special thanks to Mr. Gen Hayashi and Mr. Tomohiro Tsujita of Structural Mechanics Lab, and Mr. Taku Hirai of Yokogawa Bridge for their kind assistance during the field test on Maubin Bridge.

The author wants to express his thanks to Sumitomo Riko Co. Ltd. for providing elastomeric rubber bearing specimens in order to perform the experiments, and also to JFE Engineering for accepting him in 2016 summer internship.

Sincere thanks are to the officials from Bridge Section of the Ministry of Construction of Myanmar for allowing him to conduct experiments on Maubin Bridge, and for sharing their experiences and knowledge to him during the visits to Myanmar.

The author is greatly indebted to JICA and, the people and government of Japan for providing him the scholarship, and also to YTU for allowing him to study in Japan so that he can have a chance to fulfill his dream to study in the prestigious Kyoto University.

Finally, the author heartily thanks his beloved family for supporting him and making his life easier during his study in Japan.

TABLE OF CONTENTS

CHAPTER 1
Introduction

1.1 General

Myanmar, also known as Burma, is the second largest country in South East Asia with a population of 51.4 million people living within the wide land area of 676,578 km^2, and also possess 1,930 km long coast line along its perimeter from the west to the south [1]. In addition to numerous rivers flowing all over the country, there are four major rivers flowing from the north to the south, the Ayeyarwaddy, the Chindwin, the Sittaung, and the Thanlwin, which are vital for the surface transportation network of the country, but there were only five long span bridges to cross these rivers before 1988.

According to the Ministry of Construction of Myanmar [2], there were 528 long span bridges (over 180 ft or 55m) built over 148,690 km long road network (as of 18.7.2013) and, of these bridges, 330 bridges were built only after 1988 and only 26.16% of road network are paved roads. Hence, the number of long span bridges has drastically increased within two decades, especially between 1990 and 2010, but there were some drawbacks in the design, construction and maintenance of these bridges due to such a rapid rate of construction without any technical assistance from foreign countries except from China at that time.

1.2 Background of Research

After 1988, in addition to some bridges in delta and coastal areas, the number of long span steel bridges over four major rivers and around Yangon also increases rapidly from 5 to 28 within two decades, and many of the newly constructed bridges, especially in coastal and delta regions, become deteriorated due to unfavorable environmental conditions such as the sea salt contamination and foundation problems due to soft soil conditions, as well as due to unqualified bridge painting works, and fracture of high tension bolts, in addition to the poor maintenance budget.

Moreover, some of the long span bridges, such as Yadanarpon Bridge and Yadanar Theinga Bridge, were constructed near fault lines with assumed design earthquake load of 0.1 g, which may not be sufficient according to the new Seismic Zone Map of Myanmar 2012 due to the lack of bridge design standards specifically issued for Myanmar. Myanmar Seismic Zone Map was first issued in 2005 by Myanmar Earthquake Committee and now it was updated into a newer version in 2012 based on more research data [3, 4]. Hence, in 2009,

Myanmar government inspected the reliability of major long span bridges in the delta and coastal regions with the support of some local institutions, such as Public Works and Yangon Technological University, forming five inspection teams for different regions. Later, Ministry of Construction (MOC) of Myanmar requested the Japanese government to send the experts through JICA for the construction and maintenance of bridges and, now there is an office arranged for JICA Experts in the Head Office of Ministry of Construction at Nay Pyi Taw.

On top of this, Japanese professors and researchers from Kyoto University, Osaka City University and Public Work Research Institute (PWRI) as well as from the University of Tokyo are also contributing their knowledge through various researches in the bridge sector under JICA programs in collaboration with some local universities, such as Yangon Technological University (YTU) and Mandalay Technological University (MTU), and Ministry of Construction.

1.3 Literature Review on the Seismic Retrofitting and Field Load Testing of Bridges

Bridges are one of the most essential infrastructures to pass through obstacles, and play an important role for the emergence and development of various civilizations in the history of mankind. Bridges made of wood and stone may be the very first kind of bridge types before reinforced concrete bridges and steel bridges become popular. With the invention of concrete and steel, the construction of long span bridges, such as truss bridges, cable-stayed bridges, and suspension bridges became possible by using different steel sections and steel cables together with reinforced concrete piers and cable anchorages. Since long span bridges are regarded as one of the lifelines for the human community by connecting different parts of the region, they are critical not to occur functional failure after natural disasters such as earthquakes. Hence, seismic retrofitting of long span bridges become popular in developed countries, such as US and Japan, after the introduction of seismic codes around late 1960's [5, 6, 7, 8, 9], and Japan revised the seismic codes again after the 1995 Kobe Earthquake based on past experiences. Many technical papers have been published on the seismic retrofitting of bridges and field load testing for dynamic characterization and damage detection by various researchers since then, and some of them were reviewed so as to support the present study.

1.3.1 Review on Seismic Retrofit of Long Span Bridges

Imbsen, R.A. [10] demonstrated the increasing acceptance of seismic isolation for bridges by referring four bridges in the United States of America, the North Viaduct of Golden Gate Bridge in San Francisco, Benicia-Martinez Bridge in California, I-40 Bridge

across Mississippi River in Memphis, JFK Air Train Light-Rail Structure in New York, which were retrofitted by lead core rubber bearings and friction pendulum bearings.

Saaf, M. and Bruneau, M. [11] studied the seismic resistance of steel deck-truss bridges and proposed ductile seismic retrofit method, in which the deck slabs were converted into composite slabs, and the end cross frames and lower lateral braced frames adjacent to supports were replaced by special ductile diaphragms so as to create ductile fuses to protect other parts.

Farhey, D. N., et al. [12] made deterioration assessment to the existing steel truss bridge together with diagnostic truck-load tests and proposed a two-step rehabilitation procedure instead of demolishing and constructing a new bridge.

Seim, C., Yen, P., and O'Connor, J. S. [13] introduced the seismic retrofitting manual with some examples of retrofit strategies for the superstructure of steel truss highway bridges, including complex trusses which were not covered in AASHTO standard specifications.

Spyrakos, C. C. et al. [14] analyzed the condition of the existing steel truss railway bridge by static and dynamic field measurements as well laboratory tests, and then validated FE bridge model was used to evaluate the load carrying capacity of existing bridge before strengthening and replacement measures were proposed with an estimation of remaining fatigue life.

Aramaki, E. [15] introduced the damage control design concept to improve the earthquake resistance of Minato Bridge in Japan, the third longest steel truss bridge in the world. After 1995 Kobe Earthquake, Minato Bridge was retrofitted to meet the new seismic requirements by installing floor base isolation system with sliding isolation bearings together with buckling restrained braces in lower diagonal bracings and sway brace towers over the supports.

Lima, K., et al. [16] made the condition assessment of a 100-year-old historic steel truss bridge in Canada and retrofitted the bridge by replacing 40% of main truss members without changing the historical significance of the bridge.

Brencich, A., and Gambarotta, L. [17] assessed the 90-year-old Campasso steel truss bridge in Italy to reclassify it to carry a higher loading due to increased traffic. From the results of material characterization, load testing on the bridge, 3D FE analysis of bridge model, the bridge condition was upgraded from C3 (20 tons/axle) to D4 (22.5 tons/axle) after retrofitting processes which included replacing corroded truss members and connecting plates.

Costa, B. J. A., et al. [18, 19] performed the rehabilitation assessment of a centenary steel bridge based on modal analysis. Ambient vibration tests were done by using tri-axial

strong motion recorders before and after the rehabilitation, and compared the measured frequencies of the bridge with the FE model frequencies in order to confirm the effectiveness of rehabilitation.

DesRoches, R., et al. [20, 21, 22] studied the seismic response of multi-span simply supported and continuous steel girder bridges in the central and southern United States under 475 year and 2475 year return period earthquakes, and verified that the response under 475 year return period showed linear behaviour, but showed significant demands on non-ductile columns, fixed and expansion bearings, and abutments. However, the analysis results showed lower demands for the bridges retrofitted with lead-rubber bearings, elastomeric bearings and restrainer cables. Full-scale tests were also done for simply supported steel girder bridges attached with cable restrainers.

Pantelides, C. P., et al. [23] discussed the seismic retrofit of the State Street Bridge, a composite welded steel plate girder bridge with reinforced concrete bents by using CFRP jacketing wrapped on piers and bent caps as well as joints between them based on the analysis results of FE bridge model.

Murphy, T. P., and Collins, K.R. [24] proposed a strategy for retrofitting suspension bridges located in central and eastern United States due to the long period content of earthquakes in the region, by using distributed dampers installed in the stiffening truss under the deck.

Wright, T., DesRoches, R., and Padgett, J.E. [25] reviewed seismic retrofitting practices in the central and southern United States, such as seismic isolation by using elastomeric bearings and slider bearings, longitudinal and transverse retrofits by shear keys, seat extenders, bumper blocks, dampers and restrainers, and column bent retrofits by steel, RC and FRP jacketing.

Hoshikuma, J., Zhang, G, and Sakai, J. [26] examined the seismic behaviour of retrofitted bridges during the 2011 Great East Japan Earthquake, most of which were retrofitted in the step-by-step seismic retrofit projects after 1995 Kobe Earthquake by using RC jacketing, cable restrainers and shear keys, and compare the damage between retrofitted and un retrofitted bridges.

Lin, W.W., Yoda, T., and Taniguchi, N. [27] introduced a strengthening method for old steel railway bridges by using rubber-latex motor, GFRP plates, light weight rapid hardening concrete and reinforcing bars after doing static loading tests in the laboratory as well as field tests.

Moustafa, M. A. and Mosalam, K. M. [28] performed a combined experimental and computational research to investigate the seismic response of bent caps in as-built and retrofitted RC box girder bridges by fabricating two large scale as-built and retrofitted column-bent cap-box girder specimens and testing under bi-directional quasi-static cyclic loading together with detailed FE models.

Gingery, J. R., et al. [29] and Johnson, N. S., et al. [30] performed the seismic retrofit of a 15-span PC girder bridge by the combination of geotechnical retrofit measures, such as ground improvement and new foundation system, and structural retrofit measures, such as partial isolation and strengthening of some bridge bents and replacing new girders, after seismic hazard and site response analysis as well as FE structural analysis.

Usami, T., Lu, Z, and Ge, B. [31] numerically studied the use of buckling restrained braces (BRB) as energy dissipation dampers, which were installed in the place of diagonal truss members, for seismic performance upgrading of steel arch bridges against strong earthquakes by nonlinear time history analyses.

Wang, Y., et al. [32] performed nonlinear time history analysis to assess the seismic performance of a three span RC box girder bridge and buckling restrained braces (BRB) in order to implement the seismic retrofit by installing BRB members between bent columns.

1.3.2 Review on Field Load Testing and FE Model Analysis of Bridges

Wang, M. L., Heo, G. and Satpathi, D. [33] performed the dynamic characterization of a long span bridge by creating a base line FE bridge model and updated the model later by comparing the frequencies obtained from model and obtained from field tests.

Farrar, C. R. and James, G. H. [34] proposed a method of analyzing the ambient vibration data by using standard time domain curve fitting procedures, which were typically applied to impulse functions, now applied to cross correlation functions in order to estimate the resonant frequencies and modal damping of the structure.

Shama, A. A., et al. [35] conducted ambient vibration experiments on a cantilever truss bridge and validated the FE bridge model against the experimental results. Results from time history analyses were used to assess the damage threshold of the bridge, and nonlinear static procedure was used to evaluate the expected seismic performance.

Brownjohn, J. M. W., et al. [36] presented the dynamic testing and the modal analysis to identify the vibration properties and the quantification of the effectiveness of upgrading through subsequence model updating by monitoring strain and acceleration on the bridge for

one month, by carrying out the full scale dynamic testing without closing the bridge, and by FE model updating.

Ren, W. X., Zhao, T., and Harik, I. E. [37] carried out the ambient vibration test on a steel arch bridge, used the peak picking method and stochastic subspace identification method for output only modal identification and validated FE bridge models to match field frequencies and mode shapes.

Cunha, A., and Caetano, E. [38] described the evolution of experimental modal analysis in the field of civil engineering, such as input-output modal identification, output-only modal identification using forced vibration, ambient vibration, free vibration, and finite element correlation and model updating.

Rodrigues, C., et al. [39] performed the rehabilitation of a double deck centenary wrought iron truss bridge by carrying out FPG (fiber optic sensors) based strain monitoring before and after the retrofitting and during the load tests in order to confirm the structural behavior in step-by-step during the rehabilitation process.

Bacinskas, D., et al. [40] presented the field load testing of an old narrow-gauge railway steel truss bridge, in which both the static and dynamic loading tests were done by two test locomotives, and then discussed the measured displacement and frequency results. The authors [41] also presented the static and dynamic load testing of a newly constructed single span steel concrete railway bridge by using the same locomotives, and used the field results in model updating the FE bridge model.

Moen, C. D., Shapiro, E. E., and Hart, J. [42] examined an old wrought iron bowstring truss bridge by static loading tests in order to evaluate the interaction between the arch and the truss elements, and then comparing the field results with the FE bridge model.

Costa, B. J. A., et al. [43] reported the modal analysis of a unique centenary steel arch bridge by performing dynamic loading tests under ambient vibration before and after rehabilitation conditions. Then the field results were analyzed and compare with FE bridge models in order to confirm the efficiency of retrofitting processes.

1.3.3 Comments on Literature Review

According to the review on literature, there are three major methods for seismic retrofitting of bridges – strengthening, base isolation and damping. Strengthening is the simplest way to retrofit a deteriorated structure and it can be achieved by adding some additional members or overlays to the existing structure by increasing the cross sectional dimensions or stiffness, such as RC and FRP jacketing to bridge piers. Base isolation is

another popular method for seismic retrofitting of bridges by decoupling the superstructure from its substructure to control the vibration during an earthquake, and elastomeric bearings and slider bearings are usually used for base isolation together with bumper blocks and cable restrainers to control displacements. Damping is another method of seismic isolation in which the increased kinetic energy due to the vibration or an earthquake is released from frictional losses or changing into other forms of energy by attenuating the oscillations to decay gradually, and friction dampers and buckling restraining braces (BRB dampers) are generally used for seismic retrofitting of bridges.

Although Myanmar is vulnerable to strong earthquakes historically, long span bridges in Myanmar are mostly steel truss bridges constructed with lower design earthquake loads due to the absence of bridge design specifications and lack of data at that time. Hence, the earthquake performance of these bridges should be reviewed urgently and seismic retrofitting should be done, if required, by using the methods discussed above. However, due to the lack of modern technology and equipment, the application of strengthening method or the use of elastomeric rubber bearings and BRB dampers, would be preferable to accomplish the task because of easier and simpler installation procedures.

1.4 Objectives and Scope of the Study

There are three main objectives for commencing the present study for the retrofit of long span steel bridges in Myanmar. The first one is to highlight the urgent requirement for the seismic retrofitting of long span steel truss bridges in Myanmar, which were constructed after 1988 with superstructure steel trusses fabricated by Chinese manufactures with the lower design earthquake loads, due to the possibility in increase of seismic hazards described in new Seismic Zone Map of Myanmar 2012. The second objective is to propose a feasible seismic retrofitting procedure for similar types of long span steel truss bridges, which were constructed all over the country possibly with the same design earthquake loads even when the bridge was close to an active fault. The third objective of the study is to propose suggestions for seismic retrofitting methods for the long span steel bridges in Myanmar so as to include in the future Myanmar design standard and specifications for long span bridges. Currently, there is still no design code for long span bridges specifically issued for Myanmar, except for Myanmar National Building Code issued for low and high rise residential buildings.

The scope of the study was limited to the static and dynamic analysis, field loading tests and the seismic retrofit of a four span continuous warren steel truss bridge. As the recommendation from the Ministry of Construction of Myanmar at the time of the initial

study, Maubin Bridge in Ayeyarwady delta region was chosen as a case study bridge, which is a 480 m long, four span continuous warren steel truss bridge. Most of the long span bridges in Myanmar after 1988, fabricated by Chinese manufactures, were constructed in the same configurations like Maubin Bridge possibly with the same design loading conditions. This is the reason why the bridge was selected for the case study.

1.5 Organization of Thesis

The thesis is organized into eight chapters including Chapter 1, which is the introductory chapter about the background conditions and literature review of the current research, the objectives and scope of the present study and, the organization of thesis.

Chapter 2 states the current situation of construction and maintenance of bridges in Myanmar, in which the causes of deterioration and deteriorating conditions of bridges in Myanmar, especially bridges in lower Myanmar and along Yangon-Mandalay rail track, were discussed mainly based on the inspection reports prepared by consultants from JICA, which had supported Myanmar bridge sector since 1979.

Chapter 3 discusses about the seismic activities in Myanmar, the development of linear and nonlinear response spectrums, the ductility and response of nonlinear systems, and the frequency characteristics and response spectrum of Thabeikkyin Earthquake, which is the last largest earthquake recorded on Sagaing Fault occurred in 2012. Based on Thabeikkyin Earthquake response spectrums, design spectrum for the Ayeyarwady delta region (or regions with peak ground accelerations of 0.2g and 0.4g) due to the earthquakes along the Sagaing Fault was also proposed.

Chapter 4 describes the preliminary finite element analysis of Maubin Bridge, the case study bridge located in the Ayeyarwady delta region. The superstructure steel truss of the bridge, designed according to AASHO specifications, was analyzed under 1973 AASHO [44] static load combinations as well as under static push over analysis using explicit method under increased earthquake loading according to Seismic Zone Map of Myanmar 2012. The earthquake resistance of pile foundation under the pier P5 with fixed (hinge) bearings was also analyzed using the SPT values obtained from soil reports.

Chapter 5 reviews the results of field load testing on Maubin Bridge done in September 2016, which included both static and dynamic loading tests as well as measurements for member thickness, paint thickness and surface salinity of some members. Measured results of member strain, deflection, and bridge frequencies due to (60 ton) trucks were compared with

simulated results from FE analysis, and model updating was also done for the first four bridge frequencies in bending mode.

Chapter 6 consists of the discussion on experimental results of elastomeric rubber bearings with high damping rubber. Tests were done in the Structural Engineering Laboratory of Kyoto University to determine the shear modulus (horizontal stiffness), vertical stiffness, dissipated energy, and equivalent damping ratio of specimens in various loading conditions according to AASHTO [45].

Chapter 7 makes the dynamic assessment of the FE model of Maubin Bridge retrofitted with elastomeric bearings, which were designed according to the method B of AASHTO-LRFD [46] specifications, to replace the existing steel bearings. Then the results were compared between the bridge model with existing bearings and the one retrofitted with elastomeric rubber bearings.

Chapter 8 summarizes each chapter of the thesis, including the results from field loading tests and laboratory experiments as well as the analytical results from computer simulation of FE bridge models before and after retrofitting conditions. Then, the recommendations were given for future studies.

FORTRAN programs for the computation of linear and nonlinear response spectrums were attached in Appendix A and B, calculation of earthquake resistance of piles under the pier P5 of Maubin Bridge was described in Appendix C, and the preliminary design of elastomeric bearings for the bridge according to AASHTO was included in Appendix D.

References

[1] Department of Population, The 2014 Myanmar Population and Housing Census – The Union Report (Volume 2), Ministry of Immigration and Population, Union of Myanmar, May 2015.

[2] Han Zaw, Panel Discussion of Bridge, *30th Japan Road Conference*, Toshi Center Hotel, Tokyo, Japan, 30-31 October 2013.

[3] Myanmar Earthquake Committee, The Seismic Zone Map of Myanmar (2005), Union of Myanmar, 2005.

[4] Myanmar Earthquake Committee, The Seismic Zone Map of Myanmar (2012), Union of Myanmar, 2012.

[5] Priestley, M.J.N., Seible, F., and Calvi, G.M., Seismic Design and Retrofit of Bridges, 1st edition, John Wiley & Sons, Inc., 1996.

[6] Tonias, D.E., and Zhao, J.J., Bridge Engineering: Design, Rehabilitation, and Maintenance of Modern Highway Bridges, 2nd edition, McGraw-Hill, 2007.

[7] Baker, R.M., and Puckett, J.A., Design of Highway Bridges: An LRFD Approach, 3rd edition, John Wiley & Sons, Inc., 2013.

[8] Fu, G., Bridge Design and Evaluation: LRFD and LRFR, 1st edition, John Wiley & Sons, Inc., 2013.

[9] Taly, N., Highway Bridge Superstructure Engineering: LRFD Approaches to Design and Analysis, 1st edition, CRC Press, Taylor and Francis Group, 2015.

[10] Imbsen, R.A., Use of Isolation for Seismic Retrofitting Bridges, *Journal of Bridge Engineering*, Vol. 6 (6), pp. 425-438, 2001.

[11] Saaf, M. and Bruneau, M., Ductile Seismic Retrofit of Steel Deck-Truss Bridges I: Strategy and Modeling, *Journal of Structural Engineering*, Vol. 124 (11), pp. 1253-1262, 1998.

[12] Farhey, D. N., et al., Deterioration Assessment and Rehabilitation Design of Existing Steel Bridge, *Journal of Bridge Engineering*, Vol. 5 (1), pp. 39–48, 2000.

[13] Seim, C., Yen, P., and O'Connor, J. S., Seismic Retrofitting of Highway Truss Bridges, *Advanced Steel Construction*, Vol. 2 (4), pp. 374-388, 2006.

[14] Spyrakos, C. C. et al., Condition assessment and retrofit of a historic steel-truss railway bridge, *Journal of Constructional Steel Research*, Vol. 60, pp. 1213–1225, 2004.

[15] Aramaki, E., Seismic Retrofit of the Minato Bridge, the Third Longest Truss Bridge in the World, *Japanese Infrastructure Newsletter*, Infrastructure Development Institute – Japan, No.37, October 2006.

[16] Lima, K., et al., Rehabilitation of a 100-year-old steel truss bridge, *CSCE 2008 Annual Conference*, Quebec, Canada, 10-13 June 2008.

[17] Brencich, A., and Gambarotta, L., Assessment procedure and rehabilitation of riveted railway girders: The Campasso Bridge, *Engineering Structures*, Vol. 31, pp. 224-239, 2009.

[18] Costa, B. J. A., et al., Rehabilitation assessment of a centenary steel bridge based on modal analysis, *Engineering Structures*, Vol. 56, pp. 260-272, 2013.

[19] Costa, B. J. A., and Figueiras, J.A., Rehabilitation and condition assessment of a centenary steel bridge, *Journal of Constructional Steel Research*, Vol. 89. Pp. 185–197, 2013.

[20] DesRoches, R., et al., Full Scale Tests of Seismic Cable Restrainer Retrofits for Simply Supported Bridges, *Journal of Bridge Engineering*, Vol. 8 (4), pp. 191-198, 2003.

[21] DesRoches, R., et al., Seismic Response of Multiple Span Steel Bridges in Central and Southeastern United States. I: As Built, *Journal of Bridge Engineering*, Vol. 9 (5), pp. 464-472, 2004.

[22] DesRoches, R., et al., Seismic Response of Multiple Span Steel Bridges in Central and Southeastern United States. II: Retrofitted, *Journal of Bridge Engineering*, Vol. 9 (5), pp. 473-479, 2004.

[23] Pantelides, C. P., et al., Seismic Retrofit of State Street Bridge on Interstate 80, *Journal of Bridge Engineering*, Vol. 9 (4), pp. 333-342, 2004.

[24] Murphy, T. P., and Collins, K.R., Retrofitting Suspension Bridges Using Distributed Dampers, *Journal of Structural Engineering*, Vol. 130 (10), pp. 1466-1474, 2004.

[25] Wright, T., DesRoches, R., and Padgett, J.E., Bridge Seismic Retrofitting Practices in the Central and Southeastern United States, *Journal of Bridge Engineering*, Vol. 16 (1), pp. 82–92, 2011.

[26] Hoshikuma, J., Zhang, G, and Sakai, J., Seismic Behavior of Retrofitted Bridges During the 2011 Great East Japan Earthquake, *Proceedings of the International Symposium on Engineering Lessons Learned from the 2011 Great East Japan Earthquake*, Tokyo, Japan, 1-4 March 2012.

[27] Lin, W.W., Yoda, T., and Taniguchi, N., Rehabilitation and Restoration of Old Steel Railway Bridges: Laboratory Experiment and Field Test, *Journal of Bridge Engineering*, Vol. 19 (5), [04014004], 2014.

[28] Moustafa, M. A. and Mosalam, K. M., Seismic Response of Bent Caps in As-built and Retrofitted Reinforced Concrete Box-girder Bridges, *Engineering Structures*, Vol. 98, pp. 59-73, 2015.

[29] Gingery, J. R., et al., North Torrey Pines Bridge Seismic Retrofit: Part I, Seismic Hazard and Geotechnical Design, *Earthquake Spectra*, Vol. 31 (4), pp. 2195–2210, 2015.

[30] Johnson, N. S., Creveling, M. L., and Gazaway, K. J., North Torrey Pines Bridge Seismic Retrofit: Part II, Structural Analysis and Design, *Earthquake Spectra*, Vol. 31 (4), pp. 2211–2233, 2015.

[31] Usami, T., Lu, Z, and Ge, B., A Seismic Upgrading Method for Steel Arch Bridges Using Buckling Restrained Braces, *Earthquake Engineering and Structural Dynamics*, Vol. 34, pp. 471-496, 2005.

[32] Wang, Y., Ibarra, L, and Pantelides, C., Seismic Retrofit of a Three-Span RC Bridge with Buckling Restrained Braces, *Journal of Bridge Engineering*, Vol. 21 (11), [04016073], 2016.

[33] Wang, M. L., Heo, G. and Satpathi, D., Dynamic Characterization of a Long Span Bridge: A Finite Element Based Approach, *Soil Dynamics and Earthquake Engineering*, Vol.16, pp. 503-512, 1997.

[34] Farrar, C. R. and James, G. H., System Identification from Ambient Vibration Measurements on a Bridge, *Journal of Sound and Vibration*, Vol. 205 (1), pp. 1-18, 1997.

[35] Shama, A. A., et al., Ambient Vibration and Seismic Evaluation of a Cantilever Truss Bridge, *Engineering Structures*, Vol. 23, pp. 1281-1292, 2001.

[36] Brownjohn, J. M. W., et al., Assessment of Highway Bridge Upgrading by Dynamic Testing and Finite-Element Model Updating, *Journal of Bridge Engineering*, Vol. 8 (3), pp. 162-172, 2003.

[37] Ren, W. X., Zhao, T., and Harik, I. E., Experimental and Analytical Modal Analysis of Steel Arch Bridge, *Journal of Structural Engineering*, Vol. 130 (7), pp. 1022–1031, 2004.

[38] Cunha, A., and Caetano, E., Experimental Modal Analysis of Civil Engineering Structures, *Sound and Vibration*, pp. 12-20, June 2006.

[39] Rodrigues, C., et al., FBG based strain monitoring in the rehabilitation of a centenary metallic bridge, *Engineering Structures*, Vol. 44, pp. 281-290, 2012.

[40] Bacinskas, D., et al., Load Testing and Model Updating of a Single Span Composite Steel-Concrete Railway Bridge, *Procedia Engineering*, Vol. 57, pp. 127-135, 2013.

[41] Bacinskas, D., et al., Field Testing of Old Narrow-Gauge Railway Steel Truss Bridge, *Procedia Engineering*, Vol. 57, pp. 136-143, 2013.

[42] Moen, C. D., Shapiro, E. E., and Hart, J., Structural Analysis and Load Test of a Nineteenth-Century Iron Bowstring Arch-Truss Bridge, *Journal of Bridge Engineering*, Vol. 18 (3), pp. 261-271, 2013.

[43] Costa, B. J. A., et al., Modal Analysis for the Rehabilitation Assessment of the Luiz I Bridge, *Journal of Bridge Engineering*, Vol. 19 (2), [05014006], 2014.

[44] AASHO, Standard Specifications for Highway Bridges, 11th edition, American Association of State Highway Officials, 1973.

[45] NCHRP, Elastomeric Bridge Bearings: Recommended Test Methods, National Cooperative Highway Research Program, National Academic Press, 2001.

[46] AASHTO, LRFD Bridge Design Specifications. SI Units, 3rd edition, American Association of State Highway and Transportation Officials, 2004.

CHAPTER 2

Current Situation of Construction and Maintenance of Bridges in Myanmar

2.1 Introduction

There are four major rivers flowing from the north to the south of Myanmar, namely the Ayeyarwaddy, the Chindwin, the Sittaung, the Thanlwin, and especially the first three rivers are essential for the transport of people and goods among the towns and villages situated along them. However, until 1988, there were only five long span bridges in Myanmar due to the lack of technology: (i) Inwa Bridge (1934) over the Ayeyarwaddy River; (ii) Sittaung Bridge (Thein Zayat, 1963) and (iii) Sittaung Bridge (Taunggu-Mawchi-Loikaw, 1985) over the Sittaung River; (iv) Kunlon Bridge (1966) and (v) Tarkaw Bridge (1974) over the Thanlwin River. After 1988, the new government constructed several long span bridges with the help of Chinese bridge manufacturers all over the country for better transportation to promote the economy but newly constructed bridges were quickly deteriorated due to several factors. These deteriorating conditions were confirmed by various reports submitted by JICA consultants as well as from local institutions, such as Yangon Technological University (YTU) and Public works, and most of the reviews on the current situation of bridges in this chapter was based on these reports in addition to some new findings based on the site visits during the author's trip to Myanmar in cooperation with the Ministry of Construction.

2.2 Assistance of JICA for Bridge Construction Sector in Myanmar

In Myanmar, Ministry of Construction, and Ministry of Transport and Communications are two main authorities which are responsible for the construction of long span bridges. Starting from 1979, Japan International Cooperation Agency (JICA) established the Bridge Engineering Training Center (BETC) in Yangon for the engineers from Public Works under the Ministry of Construction, and conducted in-house trainings for 57 engineers and on-job trainings for 25 engineers and 120 technicians under the guidance of Japanese experts dispatched to Myanmar until 1985 [1]. Since that time over 30 years, several engineers from Ministry of Construction have been trained in the field of bridge design and construction especially for short and medium span RC and PC girder bridges, and new generation of engineers and technicians are still being trained there until now [2].

In 2009, Myanmar government consulted relevant organizations, such as Public Works and Yangon Technological University, to investigate the reliability of major bridges in the

delta and coastal regions of Myanmar in light of recent collapses of bridges around the world. In 2010 and 2011, with the help of the Japanese government, Ministry of Land, Infrastructure and Transport of Japan commissioned Japan Infrastructure Partners (JIP) to conduct a survey on the current situation of Myanmar bridge construction based on the results of field investigation of bridges in 2009 [3]. Moreover, in 2013 September, experts from JICA also investigated 54 bridges along Yangon-Mandalay railway track, which is under the control of Myanma Railway (MR) of the Ministry of Transport and Communications, for the rehabilitation and modernization of the railway track between Yangon and Mandalay [4]. These studies showed that most of the bridges (mostly steel truss and steel plate girder bridges) along Yangon-Mandalay railway track and some of the long span bridges (mostly steel truss bridges) in delta and coastal regions were suffering from serious corrosion [3, 4].

2.3 Background Problems

There are some major issues concerning with the construction and maintenance of bridges in Myanmar, especially for the bridges constructed after the change of government in 1988. Bridges during these periods were constructed in limited construction time, materials and technology without almost any technical and financial assistance from foreign countries except from China. Although JICA experts gave trainings to Myanmar engineers for the design and construction of RC and PC girder bridges, they have no experiences in the design and construction of long span steel bridges due to the lack of technology, in addition to the absence of steel production plants in Myanmar at that time. Moreover, nearly half of these new bridges were constructed in the delta and coastal regions due to the presence of several rivers flowing within these areas. Since the delta and coastal regions are close to the sea, corrosion of bridges due to the sea salt carried by the wind as well as the use of sea water in concrete substructures also become major maintenance problems.

Furthermore, Myanmar, as shown in Figure 2.1, is one of the disaster prone countries in South-East Asia with the population of 51.4 million and the population growth rate of 1.07 % per year [5]. The population density is about 76 people/km^2 and most of the people are living along and near the Central Belts, Delta regions and Coastal areas. One of the active faults, Sagaing Fault, runs from the north to the south passing through the central region of Myanmar. According to the historical records, many strong earthquakes had occurred along the Sagaing Fault and the Sunda-Andaman Trench which is parallel to the coastal line of Myanmar [6]. These earthquake generators had been the focal point of many great earthquakes, and Table 2.1 shows some of major earthquakes which had occurred in

Myanmar. In addition, there is still no standard and specifications for the design and construction of long span bridges issued for Myanmar, so bridge designers in Myanmar often referred AASHTO and JRA standards with the assumed design earthquake load of 0.1 g for long span bridges, which may not be sufficient according to the higher probable ground acceleration values described in the new Seismic Zone Map of Myanmar (2012) [7].

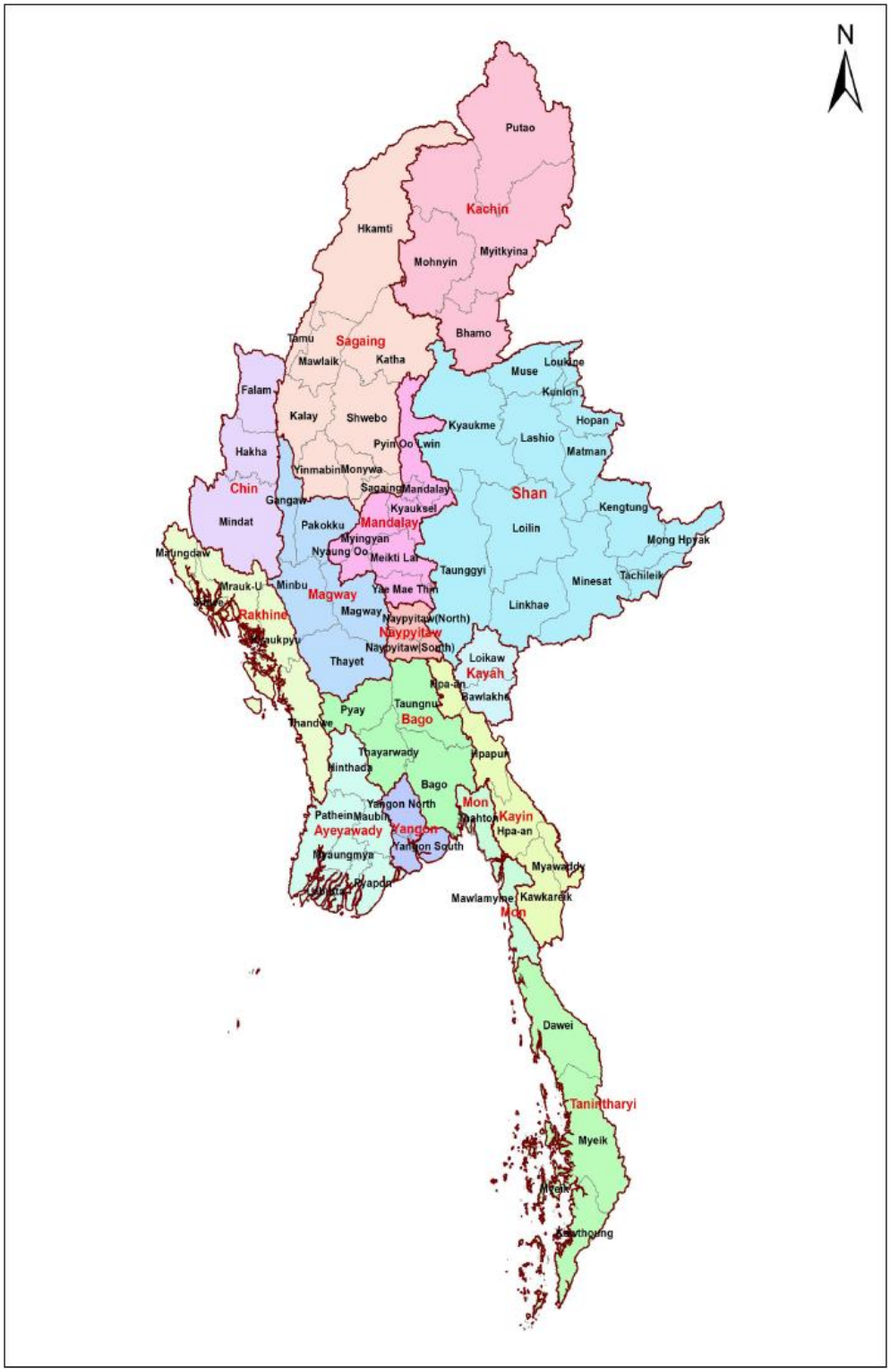

Figure 2.1: Map of Myanmar by state, region and district [5].

Table 2.1: List of major earthquakes occurred in Myanmar.

Sr.	Major earthquakes occurred in Myanmar	Intensity (M_w)
1.	Arakan Earthquake (1762)	8.8
2.	Pyu Earthquake (1930)	7.3
3.	Myitkyina Earthquake (1931)	7.6
4.	Sagaing Earthquake (1956)	7.1
5.	Myanmar Earthquake (2011)	6.9
6.	Thabeikkyin Earthquake (2012)	6.8
7.	Myanmar Earthquake (2016)	6.8

Table 2.2: Number of long span bridges (180 ft or 54 m and above) in Myanmar.

Sr.	State/Region	Bridges constructed before 1988	Bridges constructed after 1988
1.	Yangon Region	7	30
2.	Ayeyarwady Region	11	78
3.	Mandalay Region	18	22
4.	Bago Region	36	25
5.	Tanintharyi Region	8	7
6.	Magwe Region	20	38
7.	Sagaing Region	17	30
8.	Rakhine State	11	38
9.	Mon State	3	4
10.	Kayin State	8	10
11.	Shan State	24	20
12.	Kachin State	27	23
13.	Chin State	2	3
14.	Kayah State	6	2
Total		198	330
Grand Total		528	

Source: Public Works, Ministry of Construction (as of 18.7.2013)

2.4 Inventory of Long Span Bridges in Myanmar

According to the data from the Ministry of Construction (as of 18.7.2013), a total of 528 long span bridges (span longer than 180 ft or 54 m) have been constructed in various regions of Myanmar [2] and the total number of bridges in Myanmar before and after 1988 are presented in Table 2.2. According to the Table, among the total 528 long span bridges, 198

bridges were constructed before 1988, and 330 bridges were constructed after 1988. Hence, the number of bridges constructed after 1988 is about 1.6 times as many as those before 1988. This rapid rate of construction of bridges cannot be achieved without the assistance of the previous JICA bridge training program.

In Myanmar, there are 4 major rivers, which are important for the transport of people and merchandises, flowing from the north to the south across the country, the Ayeyarwaddy, the Chindwin, the Sittaung and the Thanlwin. However, before 1988, there were only 5 bridges across the Ayeyarwaddy, the Sittaung and the Thanlwin. Now, the number of long span bridges over 4 major rivers of Myanmar dramatically increase from 5 to 28 within 20 years and the list of these bridges are presented in Table 2.3. Moreover, the Bridge Section of Public Works under the Ministry of Construction was awarded the ASEAN Outstanding Award for 2011 in CAFEO-30 for the completion of 3 major bridge projects across the Ayeyarwady River within 2 years from 2009 to 2011 [8].

Although Yangon is the former capital and economic center of Myanmar surrounded by Yangon River and Bago River as well as some creeks, there were no long span bridges around the city before 1988. However, eight long span bridges connecting the central area of Yangon to the suburb regions of the city were constructed after 1988, and the list of these bridges were presented in Table 2.4. Most of the bridges were steel truss bridges except two cable stay bridges, Aungzaya Bridge and Mahar Bandoola Bridge, a suspension Bridge, Twantay Bridge, and a steel arch bridge, Bayint Naung Bridge-2.

Although there is no exact data on the ratio of two different types of bridges, i.e. steel bridges and concrete bridges, PC and RC girder bridges are usually constructed for short and medium span bridges (shorter than 180 ft) due to the lack of technology and economic reasons while steel bridges are normally used for constructing long span bridges. Although PC and RC girder bridges can be designed and constructed by locally available construction materials, there were still no steel production plants in Myanmar which can produce qualified construction steel sections at that time. Hence, almost all the superstructure of the long span steel truss bridges constructed in Myanmar were designed and fabricated from the Chinese bridge manufactures, and only some from Myanmar - Japanese joint enterprises. Particularly in 2013, J & M Solutions was founded as a joint venture company including the Ministry of Construction and JFE Engineering, and started to produce steel box girder sections and steel truss members in Thaketa, Yangon with the steel plates imported from Japan. J & M Solutions even manufactured bridge sections for the projects outside Myanmar, such as for the projects in Sri Lanka.

Table 2.3: List of long span bridges across four major rivers in Myanmar.

Name of the River	Sr.	Name of the Bridge	Length (m)	Type of Bridge
Ayeyarwady	1.	Innwa Bridge (1934)*	1207	Steel Truss
	2.	Nawaday Bridge (1997)	1275	Steel Truss
	3.	Maubin Bridge (1998)	720	Steel Truss
	4.	Bala Min Htin Bridge (1998)	819	Steel Truss
	5.	Bo Myat Htun Bridge (1998)	2604	Steel Truss
	6.	Anaw Ra Htar Bridge (2001)	1583	Steel Truss
	7.	Daedaye Bridge (2003)	1246	Steel Truss
	8.	Ayeyarwady Bridge (Magwe) (2002)	2740	Steel Truss
	9.	Ayeyarwady Bridge (Yadanarbon) (2008)	1719	Steel Arch
	10.	Ayeyarwady Bridge (Nyaung Done) (2011)	2195	Steel Truss
	11.	Ayeyarwady Bridge (Pakokku) (2011)	3484	Steel Truss
	12.	Ayeyarwady Bridge (Sinkhan) (2012)	980	Steel Truss
	13.	Ayeyarwady Bridge (Malun) (2013)	1780	Steel Truss
	14.	Yadana Theinga Bridge (2013)	756	Steel Truss
Sittaung	15.	Sittaung Bridge (Thein Zayat) (1963)*	707	Steel Truss
	16.	Sittaung Bridge (Taunggu-Mawchi-Loikaw) (1985)*	207	Steel Girder
	17.	Sittaung Bridge (Shwekyin-Madauk) (2003)	457	PC + RC
	18.	Sittaung Bridge (Moppalin) (2008)	729	Steel Truss
	19.	Sittaung Bridge (Nat Than Kwin) (2012)	219	Steel Truss
Thanlwin	20.	Kunlon Bridge (1966)*	240	Suspension
	21.	Tarkaw Bridge (1974)*	238	Suspension
	22.	Thanlwin Bridge (Pha An) (1997)	686	Steel Truss
	23.	Thanlwin Bridge (Tarsan) (1999)	274	Suspension
	24.	Thanlwin Bridge (Maw La Myine) (2005)	3528	Steel Truss
	25.	Thanlwin Bridge (Tarpar) (2005)	183	Suspension
	26.	Thanlwin Bridge (Tar Kaw At) (1997)	183	Suspension
Chindwin	27.	Sin Phyu Shin Bridge (1999)	1511	Steel Truss
	28.	Chindwin Bridge (Monywa) (2003)	1442	Steel Truss

* Old bridges constructed before 1988.

Source: Public Works, Ministry of Construction (as of 18.7.2013)

Table 2.4: List of long span bridges around Yangon City after 1988.

Sr.	Name of Bridge	Main Span (m)	Total Length (m)	Type of Bridge
1.	Thanlyin Bridge (1993)	112	1,808	Steel Truss
2.	Bayint Naung Bridge (1994)	123	501	Steel Truss
3.	Bo Mya Tun Bridge (1999)	120	1872	Steel Truss
4.	Aung Zeya Bridge (2000)	300	582	Cable-stayed
5.	Mahar Bandoola Bridge (2000)	130	240	Cable-stayed
6.	Shwe Pyithar Bridge (2001)	120	528	Steel Truss
7.	Twantay Bridge (2006)	263	425	Suspension
8.	Bayint Naung Bridge-2 (2014)	494	1262	Steel Arch

Source: Public Works, Ministry of Construction (as of 18.7.2013)

2.5 Inspection of Bridges in Lower Myanmar and along Yangon-Mandalay Rail Track

2.5.1 Inspection of Bridges in Delta and Coastal Regions by JIP

Most of the bridges constructed during the previous government (1988 ~ 2011) were mainly in the delta and coastal regions because there are numerous rivers flowing across this area, causing difficulties in local transportation. Since these regions are close to the sea, most of the bridges are deteriorated by chloride attack due to the sea salt contamination problems as well as damaged by the foundation failure due to the soft soil with large tidal range.

In 2009, various local organizations, such as Public Works, Irrigation Department and Yangon Technological University, started to investigate the condition of major bridges and dams in the delta and coastal regions (Yangon, Ayeyarwady, Rakhine, Mon and Tanintharyi regions) according to the request from the Government of Myanmar. Hence, five inspection teams were formed with the relevant professors and engineers from these organizations to review the major bridges and dams in the lower Myanmar, and then the inspection reports had been submitted to the government. Prof. Dr. Khin Than Yu, the Pro-rector of Yangon Technological University, was then the head of the department of civil engineering at YTU and one of the leaders of Inspection Teams responsible for the review of bridges in Yangon and Ayeyarwady regions. She also had a chance to share her findings with the Japanese experts from Japan Infrastructure Partners (JIP) in 2010 [3].

Based on the results of field investigation of bridges in 2009 and, according to the request from the Ministry of Construction (MOC) of Myanmar, Ministry of Land, Infrastructure and Transport (MLIT) of Japan commissioned Japan Infrastructure Partners (JIP) through JICA to conduct a survey on the current situation of the construction of bridges in Myanmar during 2010 and 2011 [3, 9]. During the survey of long span bridges around

Yangon, Rakhine and Ayeyarwady regions, a total of 19 bridges had been inspected by JIP and the list of the inspected bridges are summarized in Table 2.5.

Table 2.5: List of bridges inspected by JIP in Yangon, Ayeyarwady and Rakhine Regions.

Sr.	Name of Bridge	Total Length (m)	Type of Bridge	Region
1.	Thanlyin Bridge (1993)	1,808	Steel Truss	Yangon Region
2.	Dagon Bridge (2007)	836	PC Girder	
3.	Bo Myat Tun Bridge (1999)	1872	Steel Truss	
4.	Aung Zeya Bridge (2000)	582	Cable-stayed	
5.	Mahar Bandoola Bridge (2000)	240	Cable-stayed	
6.	Shwe Pyithar Bridge (2001)	528	Steel Truss	
7.	Bayint Naung Bridge (1994)	501	Steel Truss	
8.	Twantay Bridge (2006)	425	Suspension	
9.	Pathein Bridge (2004)	427	Suspension	Ayeyarwady Region
10.	Thakhut Bridge (1991)	149	PC Girder	
11.	Myaung Mya Bridge (1996)	262	Suspension	
12.	Maubin Bridge (1998)	2362	Steel Truss	
13.	Yar Yamaung Bridge (1999)	305	Suspension	
14.	Dalet Chaung Bridge (1999)	302	Bailey	
15.	Kyaung Kong Bridge (1989)	183	Steel Truss	
16.	Lone Daw Pauk Bridge (2004)	130	Steel Truss	Rakhine Region
17.	Min Chaung Bridge (2006)	212	Steel Truss	
18.	Min Kyaung Chaung Bridge (2006)	270	Steel Truss	
19.	Tha Yupa Padone Bridge (2010)	122	Suspension	

Source: Japan Infrastructure Partners (JIP)

2.5.2 Inspection of Bridges along Yangon-Mandalay Railway Track by Oriental Consultant

In Myanmar, rail transport is run by the state-owned agency, Myanma Railway (MR) under the Ministry of Transport and Communications, and Yangon-Mandalay rail network is one of the oldest rail network in the world constructed by the British since 1889. However, due to the poor maintenance budget and lack of modern technologies, the quality of the rail network became poor with the maximum speed for freight trains as 24 km/h, and an urgent upgrade of the rail system as well as the infrastructures along the network is urgently required.

In March 2017, JICA signed ODA loan agreements with the Myanmar government for six projects in Myanmar, one of which is Yangon - Mandalay Railway Improvement Project Phase I with the loan amount of 25 billion yen [10]. The objective of the project is to improve the railway transportation capacity by rehabilitating and modernizing the existing railway and

related facilities from Yangon to Taungoo along the Yangon-Mandalay Railway, thereby contributing to the economic development of Myanmar. Before Yangon-Mandalay Railway Improvement Project was approved in 2017, JICA sent experts from Oriental Consultant Firm to investigate the condition of bridges along Yangon-Mandalay railway track from 9th to 13th September 2013, according to the request from Ministry of Transport and Communications of Myanmar. During this investigation, the inspection team checked a total of 54 bridges, mainly steel plate girder bridges, some steel truss bridges and some PC girder bridges of short and medium span along the rail network, and then the findings were reported [4].

2.6 Causes of Deterioration and Deteriorating Conditions of Bridges

According to the survey of the inspected bridges, the main causes of deterioration of the bridges in Lower Myanmar, specifically in the delta and coastal regions, may be due to the chloride attack, the movement of substructures on soft ground, unqualified bridge painting works, fracture of high tension bolts, cracks in floor beams and pavements, settlement and scouring at the base of piers, soil erosion and corroded substructures due to high flood and poor maintenance. The brief summarize findings of the deterioration of bridges in Myanmar, based on the reports from JIP and JICA [3, 4], had been reported by Khin Maung Zaw et al. [9] at JSSC Symposium held at Tokyo in November 2015.

2.6.1 Deterioration due to Chloride Attack

Rakhine, Ayeyarwady, Yangon, Mon and Tanintharyi regions [See Figure 2.1] of Myanmar are situated along the coastal and delta areas and, during the monsoon season, the wind containing sea salt from the Bay of Bengal blows from the southwest direction. Not only due to the salt contaminated wind but also the use of seawater and sea sand in construction works because of the shortage of fresh water in some areas, bridge superstructures and substructures built of concrete suffer from chloride attack, and steel superstructures suffer from corrosion problems. According to the report from JIP [3], the corrosion of concrete piers, bents and concrete decks were the worst in the Rakhine state due to the possible use of seawater and sea sand in the concrete mix. For examples, the corrosion of bridge bent in Min Chaung Bridge and the corrosion of bottom cover underneath the side walk of Lone Daw Pauk Bridge from Rakhine State are shown in Figure 2.2.

There is no reference data about the air borne salt concentration, corrosion rate and thickness loss for these areas except for Yangon and Mandalay, where Kyoto University is conducting joint researches with Yangon Technological University and Mandalay

Technological University using carbon steel (SM) and weathering steel (SMA) specimens supplied by Japanese steel makers. According to these research data, the average chloride deposition rate is 0.022 mdd for Yangon, and 0.014 mdd for Mandalay, which are well below 0.05 mdd, the limit for corrosion of weathering steel. Corrosion rate and thickness loss for Yangon are 25.68 g/m^2/year and 0.0033 mm for SM steel and 27.58 g/m^2/year and 0.0035 mm for SMA steel. For Mandalay, corrosion rate and thickness loss are 10.50 g/m^2/year and 0.0013 mm for SM steel and 8.26 g/m^2/year and 0.0011 mm for SMA steel [11].

2.6.2 Movement of Substructures on Soft Ground

The movement of bridge substructures on soft ground has been a major issue in Myanmar because there are numerous rivers flowing in the coastal and delta regions and most of the bridge abutments are built on the soft ground, in addition to changes of water level due to the tidal flow coming from the sea. According to the inspection records from JICA [3], the bridges from No. 7 to No. 12 of Table 2.5 had been facing problems with the movement of bridge abutments, piers, cable anchorages due to the soft ground movement and changes of riverbed level. The movement of bridge abutments due to lateral earth pressure causes the dislocation and unseating of bridge superstructures and suspension bridge anchorages which may lead to the total collapse of the whole bridge. Figure 2.3 shows the deformation of abutment due to lateral earth pressure in Maubin Bridge, and the inclined tower of Myaung Mya Bridge in Ayeyarwady Region due to the movement of cable anchorages during the construction.

(a) (b)

Figure 2.2: (a) Corrosion of bridge bent in Min Chaung Bridge; (b) Corrosion of bottom cover underneath the side walk in Lone Daw Pauk Bridge.

Source: Public Works, Ministry of Construction and JICA

(a) (b)

Figure 2.3: (a) Deformation of bridge abutment in Maubin Bridge; (b) Inclined tower of Myaung Mya Bridge.

Source: Public Works, Ministry of Construction and JICA

2.6.3 Requirements in Bridge Painting Works

It is obvious that the paint on steel bridges in coastal areas is susceptible to damage from humid salty air as well as the temperature difference between day time and night time. In Myanmar, in terms of damage to steel bridges, corrosion of the overall bridge structure usually occurs within ten years after construction due to unfavorable weather conditions, and so the need for regular painting is a critical problem for the bridge maintenance due to poor maintenance budget [3].

Some of the reasons for early deterioration of paintings on the bridge may be because of the use of lower quality paints and thinner paint thickness, or the incompatibility between the types of original paint and overlaying new paint, or the lack of reliable standards for painting procedures. Moreover, there are also no other anticorrosion methods used in Myanmar other than surface painting. Durability of paints and trial paints should be also tested to accommodate the severe weather conditions of Myanmar before applying them in order to reduce the life cycle costs. Weathering steel should also be used for the bridges which are more than 2 km far from the coast line. Figure 2.4 shows the peeled paint film from Lone Daw Pauk Bridge from Rakhine State and the peeling of paint layers on a diagonal member in Maubin Bridge in Ayeyarwady Region.

(a) (b)

Figure 2.4: (a) Peeled paint film from Lone Daw Pauk Bridge; (b) Peeling of paint layers on a diagonal member in Maubin Bridge.

Source: Public Works, Ministry of Construction, JICA and Khin Maung Zaw et al. [12]

2.6.4 Failure of High Tension Bolts

According to the inspection records from JICA [1, 3], Ministry of Construction [13] and the report from the Infrastructure Group of the SATREPS Project [14], which is collaborating between the University of Tokyo and Yangon Technological University, the fracture of the high tension bolts was found on Pathein Bridge and Yadanarpon Bridge. Both of the bridges were manufactured by Chinese companies and, hence, high tension bolts from China were used for them.

The fracture of bolts may be the result of delayed fracture, which particularly occur in stronger steels such as high tension bolts due to the penetration of hydrogen ions, or fatigue fracture due to repeated loading, or ductile fracture by excessive loading. Hence, it was recommended to examine the cause of the bolt fracture from the tensile strength tests, from fractured surface of bolts by electron microscope to check the material composition and also by using an inspection hammer in the field.

Fracture of high tensile bolts were more severe in Yadanarpon Bridge than in Pathein Bridge, and 4641 bolts have been replaced with the JIS standard bolts in Yadanarpon Bridge between June 2010 and January 2014 [13]. The inspection team from Bridge Fabricators Association visited the bridge in October 2013 and gave comments and suggestions. According to their inspection, the damage of bolts and nuts may be due to the defect of bolt material, over tightening of bolts and the corrosion due to the water entering through the gap of splice plates while using longer bolts (than Japanese standards) with lower torque moment for tightening and consequently cause loosening due to large vibration. Then, they

recommend to seal off the gap with water tight sealant and to change the fractured bolts to Japanese bolts (S10T) with proper torque moment and also to check the structural design calculations of the bridge again. Aye Mya Cho et al. [15] also investigated the magnitude of axial force and the strength of bolts on Yadanarpon Bridge and reported the findings in ICSE 2016. Missing high tension bolts from Pathein Bridge and fractured high tension bolts with different levels of corrosion from Yadanarpon Bridge are shown in Figure 2.5.

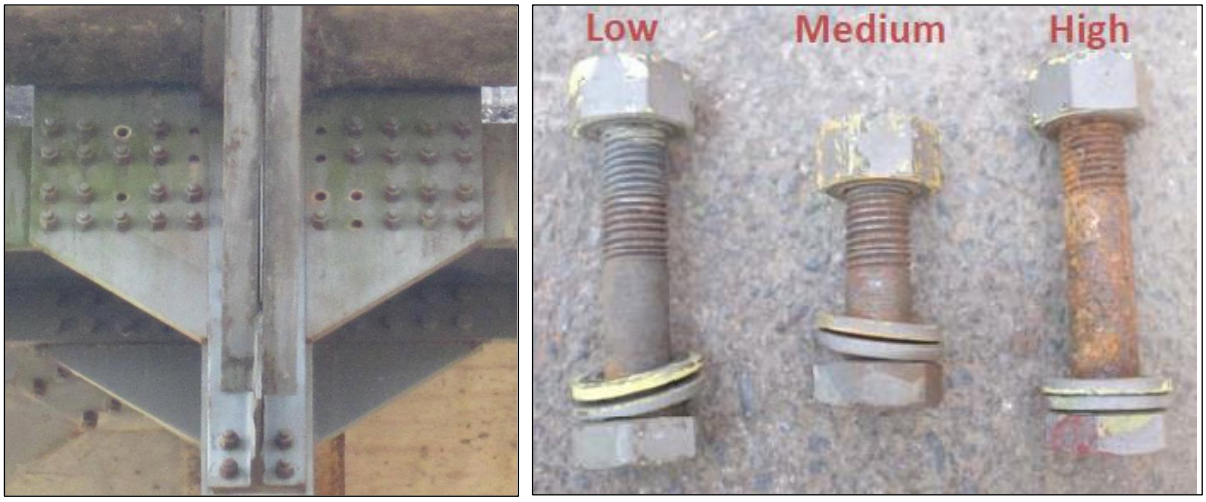

(a) (b)

Figure 2.5: (a) Missing high tension bolts on Pathein Bridge; (b) Fractured high tension bolts with different levels of corrosion from Yadanarpon Bridge.

Source: Public Works, Ministry of Construction, and JICA

2.6.5 Cracks in the Ends of Floor Beams and in the Pavements in Yadanarpon Bridge

Yadanarpon Bridge over the Ayeyarwady River connecting Mandalay and Sagaing was constructed in October 2001 and opened to public in February 2008. However, in 2012, only 4 years after the opening, cracks were found at the end of some floor beams especially at the welded connection between top flange and web of the beams near the end [16, 17] as shown in Figure 2.6. CAME company, the Chinese company which designed and fabricated the bridge, inspected the bridge and suggested to drill the stop holes (10 mm to 25 mm diameter) at the crack tip in order to stop the proceeding of cracks after identifying the cracks with Magnetic Particle Test Machine. This method stopped the cracks up to 92% but more cracks were still occurring in some other beams over some time until now. This may be due to the requirements in structural design and joint detailing or due to over loading or due to the use of precast concrete ribbed decks only without the steel stringers (along the longitudinal direction of the bridge) as shown in Figure 2.7 (a).

(a) (b)

Figure 2.6: (a) Crack in the welded joint between the top flange and the web; (b) Stop hole drilled at the tip of crack.

Source: Public Works, Ministry of Construction

Moreover, the cracks in pavements due to the deflection of precast concrete slabs underneath were found during the visit of Japanese professors and engineers on the bridge in January 2017 as shown in Figure 2.7 (b). Hence, professors and postgraduate students from Kyoto University and Osaka City University jointly formed a research group to study the dynamic characteristics of Yadanarpon Bridge, and to find out the cause of these cracks in floor beams in order to give suggestions to the Ministry of Construction for proper retrofitting of the bridge. This joint research group visited Yadanarpon Bridge from 19th to 22nd June 2017 and, made vibration tests and static loading tests with heavy trucks, and bolt tension tests successfully, with the cooperation of Ministry of Construction and Mandalay Technological University.

2.6.6 Deteriorating Bridges along Yangon-Mandalay Rail Track

For the Rehabilitation and Modernization of Yangon – Mandalay Railway Project, JICA experts from Oriental Consultants investigated 54 bridges along Yangon – Mandalay railway track in September 2013 [4]. According to the investigation report, most of the bridges are steel plate girder bridges with some steel truss bridges and some prestressed concrete girder bridges, and the abutments and piers of most bridges are aging, dislocating, showing cracks, and bearing shoes of some plate girders were missing. Some of the piers were suffering from scouring, differential settlement and some were even totally submerged under high water level during the monsoon. These conditions caused the erosion of soil around the abutments,

retaining walls, piers, and hence greatly reduced their service life. Therefore, the inspection team suggested to replace most bearings as well as to reconstruct most of the abutments and piers because they were the main reasons to reduce the speed of trains while crossing those bridges. Figure 2.8 shows the unseen bridge pier during high water level in bridge No. 111 and aging abutment and absence of shoes in bridge No. 42 along the Yangon – Mandalay rail track. Pier scouring at the base of pier in bridge No. 393 and the cracked pier in bridge No. 21 were also shown in Figure 2.9.

(a) (b)

Figure 2.7: (a) Precast concrete deck slab seen from underneath the bridge; (b) Cracks in pavement on the bridge due to the deflection of precast concrete slab.

(a) (b)

Figure 2.8: (a) Unseen bridge pier during high water level in bridge No. 111; (b) Aging abutment and absence of shoes in bridge No. 42.

Source: Oriental Consultants, JICA

(a) (b)

Figure 2.9: (a) Pier scouring in bridge No. 393; (b) Cracked pier in Bridge No. 21.

Source: Oriental Consultants, JICA

2.7 Summary

Former Myanmar government constructed several long span bridges starting around 1990's with the rapid rate of construction and, as a result, the number of long span steel bridges rapidly increased from 5 to 36 within 20 years over four major rivers and around Yangon, and also increased from 198 to 528 all over the country. Almost all of the newly constructed long span steel bridges were designed and fabricated by Chinese companies except very few from Japanese companies, such as JFE at that time. Many of the bridges were steel truss bridges of the same configurations constructed in the coastal and delta regions and some were constructed near the active faults with the assume earthquake load of 0.1 g without considering local seismic activities.

According to the investigations from various local and foreign agencies, deterioration of long span bridges were generally caused by the chloride attack, the movement of substructures on soft ground, unqualified bridge painting works, fracture of high tension bolts, cracks in floor beams and pavements, settlement and scouring at the base of piers, soil erosion and corroded substructures due to high flood and poor maintenance. Since Yadanarpon Bridge is located near the Sagaing Fault, professors and postgraduate students from Kyoto University and Osaka City University formed a joint research group to study the dynamic characteristics of the bridge, and to find out the cause of cracks in the end of floor beams in order to give suggestions to the Ministry of Construction for proper retrofitting of the bridge.

Since there are no standards or specifications of the paint coating system for different types of buildings and bridges in Myanmar, local researchers should conduct necessary

exposure tests under various local weather conditions using locally available paints in collaboration with local paint manufacturing companies such as United Paints Group (UPG). On the other hand, the use of weathering steel in steel bridges would reduce the life cycle cost because of its resistance to corrosion by forming a protective layer on its surface and no painting is required but the initial cost may be higher than using ordinary steel. Hence, the use of weathering steel in the construction of bridges (located beyond 2 km from coast line), should also be considered.

Moreover, according to the higher probable ground acceleration values indicated in the second edition of Myanmar Seismic Zone Map of Myanmar (2012) [18], the earthquake resistant performance of old bridges should be evaluated again, especially for the bridges located in higher seismic zones along the Sagaing Fault and on the northern regions.

References

[1] JICA, Research Study on Review and Application of the Bridge Engineering Training Center Project in Myanmar, Final Report, Japan International Cooperation Agency, September 2012.

[2] Public Works, Current Situation of Road Networks and Bridges, Ministry of Construction, Union of Myanmar, February 2013.

[3] JIP, Current Situation and Issues of Myanmar's Bridge Work, Situation Report, Japan Infrastructure Partners, Japan, September 2012.

[4] Oriental Consultants, JICA, Investigation Record Books for Substructures of Bridges (Reference Data), The National Transport Development Plan, Rehabilitation and Modernization of Yangon-Mandalay Railway Project, September 2013.

[5] Department of Population, The 2014 Myanmar Population and Housing Census – The Union Report (Volume 2), Ministry of Immigration and Population, Union of Myanmar, May 2015.

[6] Kyaw Kyaw Lin, Seismic and Tsunami Activities in Myanmar, JICA Training Course, Nagoya University, Japan, July 2007 – March 2008.

[7] Myanmar Earthquake Committee, The Seismic Zone Map of Myanmar (2012), Union of Myanmar, 2012.

[8] Han Zaw, Panel Discussion of Bridge, *30th Japan Road Conference*, Toshi Center Hotel, Tokyo, Japan, 30-31 October 2013.

[9] Khin Maung Zaw, Suzuki, Y. and Sugiura, K., Current Situation of Construction and Maintenance of Bridges in Myanmar, *Proceedings of Construction Steel*, Vol. 23, pp. 364-371, JSSC Symposium, Tokyo, Japan, 19 - 20 November 2015.

[10] https://www.jica.go.jp/english/news/press/2016/170301_01.html

[11] Yu Yu Kyi Win et al., Comparative Study on Atmospheric Corrosivity of Under Shelter Exposure in Yangon and Mandalay (Myanmar), *American Scientific Research Journal for Engineering, Technology, and Sciences*, Vol. 27(1) , 2017.

[12] Khin Maung Zaw, Suzuki, Y., Nishizaki, I. and Sugiura, K., Report for the Preliminary Test at Yadanarpon Bridge and Maubin Bridge, Inspection Report to Ministry of Construction, August 2016.

[13] Public Works, Ayeyarwady Bridge (Yadanarpon): Maintenance, Ministry of Construction, Union of Myanmar, Inspection Report, February 2014.

[14] SATREPS Infrastructure Group, Installation of Monitoring System and Investigation of Bridges in Yangon & Mandalay, SATREPS Report, February 2016.

[15] Aye Mya Cho, et al, Investigation into Axial Force of Bolts at Yadanapon Bridge, *Proceedings of the 7th International Conference on Science and Engineering*, Yangon Technological University, Myanmar, 10 - 11 December 2016.

[16] Public Works, Field Study Report on Ayeyarwady Bridge (Yadanarpon): Investigation of Cracks in Floor Beam Ends, Bridge Maintenance Section, Bridge Construction Group (1), Bridge Research and Quality Control Section, Ministry of Construction, Union of Myanmar, December 2015.

[17] Metropolitan Expressway, Field Investigation Result Report of Yadanapon Bridge, Inspection Report for the Ministry of Construction of Myanmar, February 2014.

[18] Myanmar Earthquake Committee, The Seismic Zone Map of Myanmar (2012), Union of Myanmar, 2012.

CHAPTER 3

Seismicity in Myanmar, Characteristics of Thabeikkyin Earthquake and Proposed Design Spectrum

3.1 Introduction

According to the World Risk Index 2012 issued by the United Nations University for Environment and Security (UNU-EHS) [1], Myanmar is ranked 42nd among 173 countries in the world with high vulnerability and susceptibility due to high exposure but ranked 6th among the top 15 countries with the lowest coping capabilities due to the lack of capacities and resources for a disaster event. Many disaster events have occurred in Myanmar almost every year, such as, earthquake, flood, land slide, and cyclone. Myanmar is also one of the disaster prone countries in South-East Asia with 51.4 million population and 1.07 % per year population growth rate [2]. The population density is about 76 people/km^2 and most of the people are living along and near the Central Belts, Delta regions and Coastal areas. One of the active faults, Sagaing Fault, runs from the north to the south passing through the central region of Myanmar. According to historical records, many strong earthquakes had occurred along the Sagaing Fault, Sunda-Andaman Trench which is parallel to Myanmar coastal line, and some other local faults [3] and, some of them are described in section 2.3 of Chapter 2.

3.2 Seismicity in Myanmar

There are two major generating sources of earthquakes in Myanmar in addition to some local faults. They are the Sagaing Fault and the Sunda-Andaman Trench (also called Java Trench or Sumatra Trench). In terms of tectonic plates, Myanmar lies in the front zone where two major plates, namely India Plate and Eurasia Plate, meet each other. India Plate is composed of the Indian continent and Indian Ocean while Eurasia Plate is composed of Europe, part of Asia including Eastern Highlands of Myanmar, and South China Sea. Myanmar can be subdivided into four main tectonic regions namely Eastern Highland, Central Myanmar Basin, Western Ranges, and Rakhine Coastal Strip [4]. The tertiary tectonic and structural features of Myanmar as a part of Southeast Asia is shown in Figure 3.1.

3.2.1 Sagaing Fault

Sagaing Fault is known as the plate boundary between the India Plate and Eurasia Plate with transform activity. Moreover, Myanmar can be divided into two different tectonic

terrains centering the Sagaing fault, namely the Sunda Plate, which comprised the Eastern Highlands of Myanmar, and the Burma (Myanmar) Plate, which is composed of the west side of the Sagaing Fault [4]. The Sagaing Fault is a major right-lateral strike-slip fault which has long and straight traces across the entire length of Myanmar for about 1000 km. The rate of motion of the Burma plate with respect to the Sunda plate has a rate of 18 ~ 25 mm/yr towards the north [5] and several severe earthquakes had occurred along the Sagaing fault zone, especially in the Segment 1 (Putao-Indawgyi), Segment 2 (Tagaung-Sagaing), and Segment 4 (Taungoo-Bago) over the last thirteen centuries according to the records. Strong earthquakes on the Sagaing fault occurred within the last century are shown in Table 3.1.

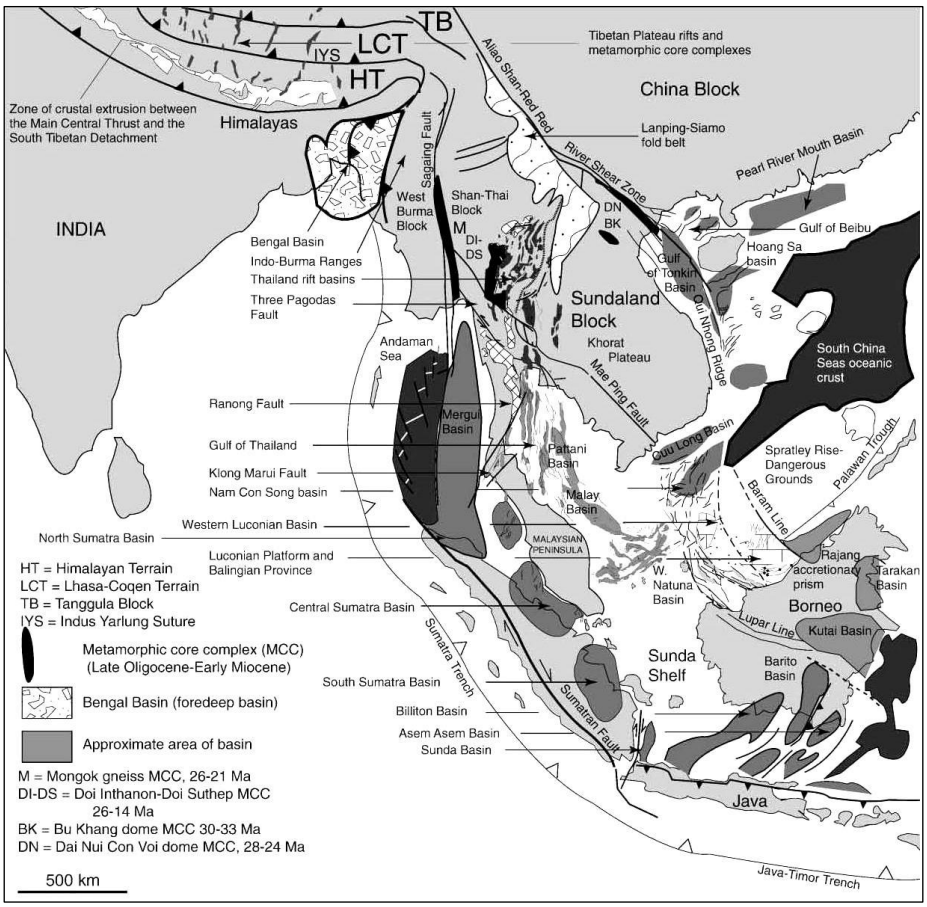

Figure 3.1: Tertiary tectonic and structural features of Myanmar in Southeast Asia [4].

3.2.2 Sunda-Andaman Trench

Another major source of earthquakes in Myanmar is the Sunda-Andaman Trench which is considered to be a part of the Pacific Ring of Fire as well as one of a ring of oceanic trenches around the northern edges of the Australian Plate [6] as shown in Figure 3.1. It is formed where the Australian Plate subducts under a part of the Eurasian Plate with a length of

3200 km and the maximum depth of 7725 m at the deepest point in the Indian Ocean. The trench stretches from the Lesser Sunda Islands past Java, around the southern coast of Sumatra on to the Andaman Islands, parallel to the Rakhine coastal line, and forms the boundary between Indo-Australian Plate and Eurasian plate. Arakan Earthquake (1762), which caused tsunami in the Rakhine coastal region, and Indian Ocean Earthquake (2004), which caused tsunami along the coastal line of Myanmar were due to the movement of this trench. Generally, Sunda-Andaman Trench caused earthquakes around the Sumatra and Java regions along Sumatra and Java segments frequently with great intensities.

Table 3.1: List of historical earthquakes along Sagaing Fault during the last century [4].

Sr.	Date	Location	Magnitude or brief description
1.	1913.03.06	Bago	Shwemawdaw Pagoda damaged
2.	1917.07.05	Bago	Shwemawdaw Pagoda fell
3.	1927.09.10	Yangon	
4.	1927.12.17	Yangon	M = 7; extended to Dedaye
5.	1929.08.08	Near Taungoo	Bent railroad tracks, bridges and culverts collapsed, and loaded trucks
6.	1930.05.05	Near Khayan	M=7.3, Imax = IX; in a zone trending north-south for 37 km south of Bago
7.	1930.12.03	Nyaunglebin	M=7.3, railroad tracks twisted (Pyu Earthquake)
8.	1931.01.27	East of Indawgyi	M=7.6, Imax = IX; numerous fissures and cracks (Myitkyina Earthquake)
9.	1931.08.10	Pyinmana	
10.	1931.03.27	Yangon	
11.	1931.05.16	Yangon	
12.	1931.05.21	Yangon	
13.	1946.09.12	Tagaung	M = 7.5
14.	1946.09.12	Tagaung	M = 7.75
15.	1956.07.16	Sagaing	Several pagodas severely damaged (Sagaing Earthquake)
16.	2012.11.11	Thabeikkyin	M = 6.8. One span of Yadanar Theinga Bridge during in construction fell into the Ayeyarwady River. 201 houses, 25 schools, 13 hospitals, 45 pagodas and 35 monasteries collapsed.

3.2.3 Other Major Faults in Myanmar

Apart from the Sagaing Fault and Sunda-Andaman Trench, there are some other major faults in Myanmar which had caused some earthquakes of high magnitude according to the previous records. They are: (i) Kaladan – Mrauk-U fault system; (ii) Kabaw fault system; (iii)

Pyay fault system; (iv) Tangyidaung-Yenangyaung-Chauk thrust; (v) Tuyin Taung-Gwegyo thrust; (vi) Momeik fault system; (vii) Phapun fault system; and (viii) Three Pagodas fault. Some of the strong earthquakes, which had occurred during the recent past due to these faults, are Bagan earthquake (1976), Taungdwingyi earthquake (2003) [4] and Myanmar earthquake (2016). The map showing various major fault systems in Myanmar is shown in Figure 3.2.

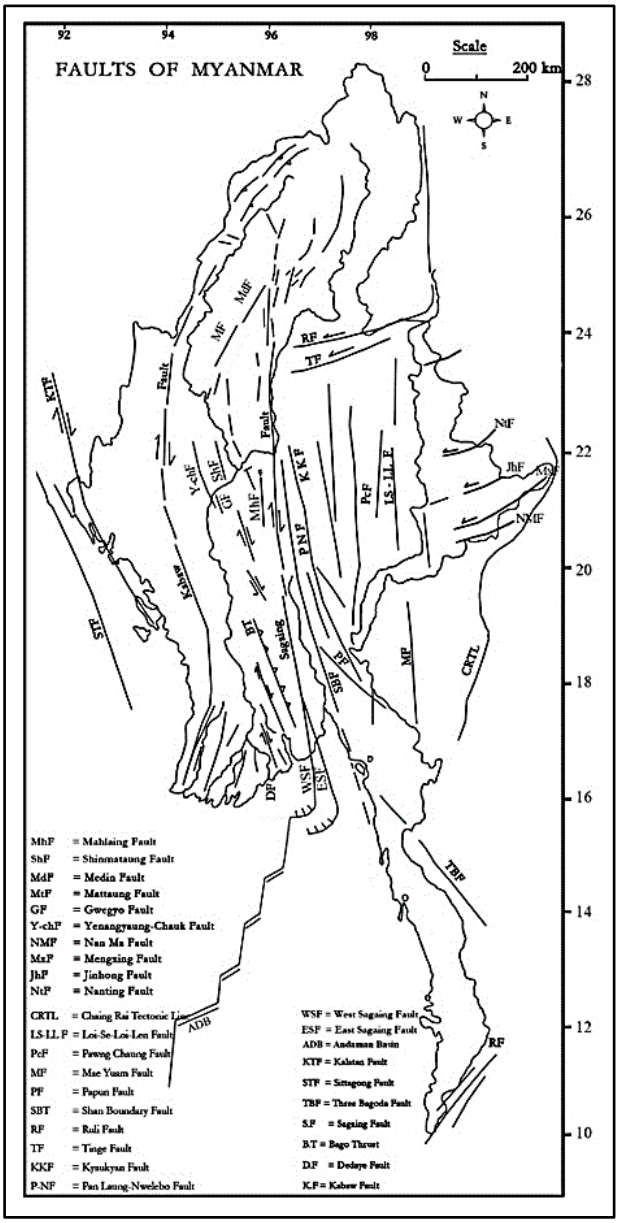

Figure 3.2: Major faults in Myanmar [5].

3.3 Development of Response Spectrums

For a civil engineer in the field of earthquake engineering, it is most important to know the maximum response of a structure, such as buildings and bridges, due to the strong ground motion in order to design it to be safe against an earthquake. In this case, the response spectrum is a useful tool for determining these responses. Response spectrum is a curve which

shows the relationship between the maximum responses (acceleration, velocity, and displacement) of a system related to its periods (or frequencies) for different values of damping ratio due to a seismic event [7]. The response spectrum can be developed by using the following dynamic equilibrium equation (3.1) of a single degree of freedom (SDF) system due to the ground motion where *m, c, k* are the mass, damping, stiffness, and $u, \dot{u}, \ddot{u},$ are the displacement, velocity and acceleration of the system, and $\ddot{u}_g$ is the ground acceleration [7].

$$m\ddot{u} + c\dot{u} + ku = -m\ddot{u}_g \tag{3.1}$$

This equation can be divided by the mass (*m*) and then changed into another form, as in equation (3.2), by using the basic relationships of structural dynamics; $k = m\omega^2$ and $c = 2m\zeta\omega$, where ω and ζ are the angular frequency and the damping ratio of the system [7].

$$\ddot{u} + 2\zeta\omega\dot{u} + \omega^2 u = -\ddot{u}_g \tag{3.2}$$

The above equation can be solved by using standard numerical methods to obtain the time histories of the required responses (acceleration, velocity, and displacement) of the system for various frequencies (or periods) and various damping ratios. The following steps can be applied to develop the response spectrum for a given ground motion $\ddot{u}_g(t)$ [8]:

1. Numerically define the ground acceleration $\ddot{u}_g(t)$; typically, the ground motion ordinates are defined every 0.01 or 0.02 sec.
2. Select the natural vibration period T_n and damping ratio ζ of an SDOF system.
3. Compute the deformation response *u(t)* of this SDOF system due to the ground motion $\ddot{u}_g(t)$ by any of the numerical methods discussed in reference books [8, 9].
4. Determine u_0, the absolute peak value of *u(t)*.
5. Then the spectral ordinates can be obtained as $D = u_0$, $V = (2\pi / T_n) D$, and $A = (2\pi / T_n)^2 D$, where *D, V, A* are the required responses (displacement, velocity, acceleration) and T_n is the natural period.
6. Repeat steps 2 to 5 for a range of T_n and ζ values covering all possible systems of engineering interest.
7. Present the results of steps 2 to 6 graphically to produce three separate spectra or a combined spectrum using log scale graphs which are called response spectrums.

In using the standard numerical methods to solve the dynamic equilibrium equation, numerical time-stepping methods were greatly efficient due to their accuracy, convergence, and stability as well as for computer implementation. These methods can be divided into explicit methods such as central difference method, where the solution u_{i+1} at time ($i + 1$) is determined from the equilibrium condition at time (i) without using the equilibrium condition at time ($i + 1$), and implicit methods such as Newmark's method, where the solution u_{i+1} is determined from the equilibrium condition at time ($i+1$) [8]. The first method can be used to solve only linear systems but the second method can be used to solve both linear and non-linear systems by changing the dynamic equilibrium equation into the time-step form as follows:

$$m\ddot{u}_{i+1} + c\dot{u}_{i+1} + (f_s)_{i+1} = p_{i+1} \tag{3.3}$$

3.3.1 Calculation of Linear Response Spectrum

In this study, pursuing the seven steps described above, response spectrums for linear elastic structures were developed by using the Newmark's method, one of the well-known time-stepping methods in combination with FORTRAN programming, based on the following equations (3.4) and (3.5) together with the dynamic equilibrium equation (3.3) in the time-step form [8]:

$$\dot{u}_{i+1} = \dot{u}_i + [(1-\gamma)\Delta t]\ddot{u}_i + (\gamma\Delta t)\ddot{u}_{i+1} \tag{3.4}$$

$$u_{i+1} = u_i + (\Delta t)\dot{u}_i + [(0.5-\beta)(\Delta t)^2]\ddot{u}_i + [\beta(\Delta t)^2]\ddot{u}_{i+1} \tag{3.5}$$

where β and γ define the variation of acceleration over a time step and also determine the stability and accuracy characteristics of the Newmark's method. The values of γ and β were usually selected as $\gamma = 1/2$, and $1/6 \leq \beta \leq 1/4$ and, satisfactory from all aspects, including the accuracy [8]. These two equations, combined with the dynamic equilibrium equation at the end of the time step, provided the basis for computing $u_{i+1}, \dot{u}_{i+1}, \ddot{u}_{i+1}$ at time ($i + 1$) from the known $u_i, \dot{u}_i, \ddot{u}_i$ at time (i). As special cases, Newmark's method can be subdivided into constant average acceleration method and linear acceleration method, as shown in Figure 3.3, based on the assumptions that the value of acceleration over a time step is constant (equal to the average acceleration), or it varies linearly. The following values for γ and β were used for the two methods: $\gamma = 1/2$ and $\beta = 1/4$ for constant average acceleration method; and $\gamma = 1/2$ and $\beta = 1/6$ for linear acceleration method [8].

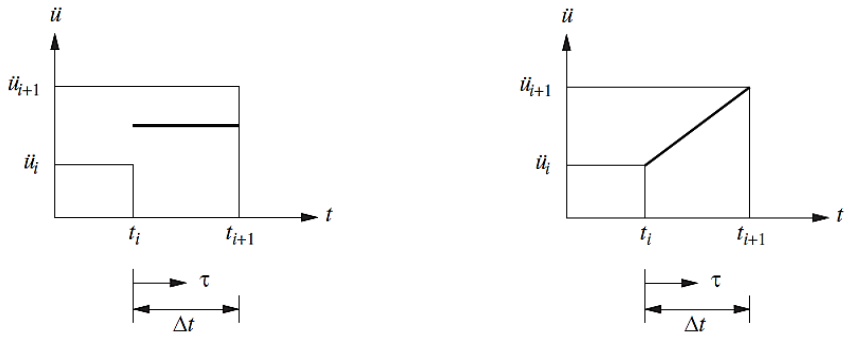

(a) (b)

Figure 3.3: (a) Constant average acceleration method; (b) Linear acceleration method [8].

For linear systems, it was possible to modify to get the solutions of equations (3.3), (3.4) and (3.5) without iteration by assuming $(f_s)_{i+1}$ equivalent to ku_{i+1} in equilibrium equation (3.3). From equations (3.3), (3.4), and (3.5), $\ddot{u}_{i+1}$ and $\dot{u}_{i+1}$ can be expressed in terms of u_{i+1} as follows:

$$\ddot{u}_{i+1} = \frac{1}{\beta(\Delta t)^2}(u_{i+1} - u_i) - \frac{1}{\beta \Delta t}(\dot{u}_i) - \left(\frac{1}{2\beta} - 1\right)\ddot{u}_i \tag{3.6}$$

and

$$\dot{u}_{i+1} = \frac{\gamma}{\beta \Delta t}(u_{i+1} - u_i) + \left(1 - \frac{\gamma}{\beta}\right)\dot{u}_i + \Delta t\left(1 - \frac{\gamma}{2\beta}\right)\ddot{u}_i \tag{3.7}$$

or these equations can be written in incremental form as:

$$\Delta\ddot{u}_i = \frac{1}{\beta(\Delta t)^2}\Delta u_i - \frac{1}{\beta \Delta t}\dot{u}_i - \frac{1}{2\beta}\ddot{u}_i \tag{3.8}$$

and

$$\Delta\dot{u}_i = \frac{\gamma}{\beta \Delta t}\Delta u_i - \frac{\gamma}{\beta}\dot{u}_i + \Delta t\left(1 - \frac{\gamma}{2\beta}\right)\ddot{u}_i \tag{3.9}$$

where $\Delta\ddot{u}_i \equiv \ddot{u}_{i+1} - \ddot{u}_i$, $\Delta\dot{u}_i \equiv \dot{u}_{i+1} - \dot{u}_i$ and $\Delta u_i \equiv u_{i+1} - u_i$.

By substituting equations (3.8) and (3.9) into the equation of motion in incremental form of equation (3.3) with $(f_s)_{i+1}$ equivalent to ku_{i+1}, the following equation is obtained:

$$\hat{k}\Delta u_i = \Delta\hat{p}_i \tag{3.10}$$

where

$$\hat{k} = k + \frac{\gamma}{\beta \Delta t} c + \frac{1}{\beta (\Delta t)^2} m \tag{3.11}$$

and

$$\Delta \hat{p}_i = \Delta p_i + \left[\frac{1}{\beta \Delta t} m + \frac{\gamma}{\beta} c \right] \dot{u}_i + \left[\frac{1}{2\beta} m + \Delta t \left(\frac{\gamma}{2\beta} - 1 \right) c \right] \ddot{u}_i \tag{3.12}$$

and the incremental displacement can be computed from equations (3.11) and (3.12) as follows:

$$\Delta u_i = \frac{\Delta \hat{p}_i}{\hat{k}} \tag{3.13}$$

Once Δu_i is known, the incremental velocity $\Delta \dot{u}_i$ and incremental acceleration $\Delta \ddot{u}_i$ can be obtained from equations (3.9) and (3.8) respectively. Then the responses for the next time step $(u_{i+1}, \dot{u}_{i+1}, \ddot{u}_{i+1})$ can be calculated from initial responses $(u_i, \dot{u}_i, \ddot{u}_i)$ and response increments $(\Delta u_i, \Delta \dot{u}_i, \Delta \ddot{u}_i)$. The acceleration $\ddot{u}_{i+1}$ can also be obtained from the equation of motion at time i+1 as follows and this is required to calculate the initial acceleration $\ddot{u}_0$ to start the time-stepping computations [8].

$$\ddot{u}_{i+1} = \frac{p_{i+1} - c\dot{u}_{i+1} - k u_{i+1}}{m} \tag{3.14}$$

The stability of Newmark's method can be checked by the following equation (3.15), which implies that the constant average acceleration method is stable for any Δt but linear acceleration method will be stable only if $\Delta t / T_n$ is less than or equal to 0.551 [8].

$$\frac{\Delta t}{T_n} \leq \frac{1}{\pi \sqrt{2}} \frac{1}{\sqrt{\gamma - 2\beta}} \tag{3.15}$$

Using Newmark's method, Table 3.2 summarized the time-stepping procedures to find the response of S.D.O.F linear systems without iteration so as to implement it on the computer with an appropriate programming language such as FORTRAN. For this study, the procedures shown in Table 3.1 was written by using a FORTRAN program [See Appendix A] after modifying the dynamic equilibrium equation with basic relationships of structural dynamics, such as $k/m = \omega^2$ and $c/m = 2\zeta\omega$ with $p_i/m = -\ddot{u}_{gi}$. Response spectrums (acceleration, velocity and displacement) of linear S.D.O.F structures for Thabeikkyin Earthquake (2012) in

Myanmar, which was shown in Figure 3.4, were derived as shown in Figures 3.5, 3.6 and 3.7 for three different damping ratios of 2%, 5% and 10%.

Table 3.2: Newmark's method for linear systems [8].

1.0	*Initial Calculations*
	1.1 $\ddot{u}_0 = \frac{p_0 - c\dot{u}_0 - ku_0}{m}$
	1.2 Select Δt.
	1.3 $\hat{k} = k + \frac{\gamma}{\beta \Delta t} c + \frac{1}{\beta (\Delta t)^2} m$
	1.4 $a = \frac{1}{\beta \Delta t} m + \frac{\gamma}{\beta} c$ and $b = \frac{1}{2\beta} m + \Delta t \left(\frac{\gamma}{2\beta} - 1 \right) c$
2.0	*Calculations for each time step, i*
	2.1 $\Delta \hat{p}_i = \Delta p_i + a\dot{u}_i + b\ddot{u}_i$
	2.2 $\Delta u_i = \frac{\Delta \hat{p}_i}{\hat{k}}$
	2.3 $\Delta \dot{u}_i = \frac{\gamma}{\beta \Delta t} \Delta u_i - \frac{\gamma}{\beta} \dot{u}_i + \Delta t \left(1 - \frac{\gamma}{2\beta} \right) \ddot{u}_i$
	2.4 $\Delta \ddot{u}_i = \frac{1}{\beta (\Delta t)^2} \Delta u_i - \frac{1}{\beta \Delta t} \dot{u}_i - \frac{1}{2\beta} \ddot{u}_i$
	2.5 $u_{i+1} = u_i + \Delta u_i$, $\dot{u}_{i+1} = \dot{u}_i + \Delta \dot{u}_i$ and $\ddot{u}_{i+1} = \ddot{u}_i + \Delta \ddot{u}_i$
3.0	*Repetitions for the next time step*
	3.1 Replace i by i+1 and implement steps 2.1 to 2.5 for the next time step.

Note: To derive the response spectrum, p_i is replaced by $-m\ddot{u}_{gi}$ in the table.

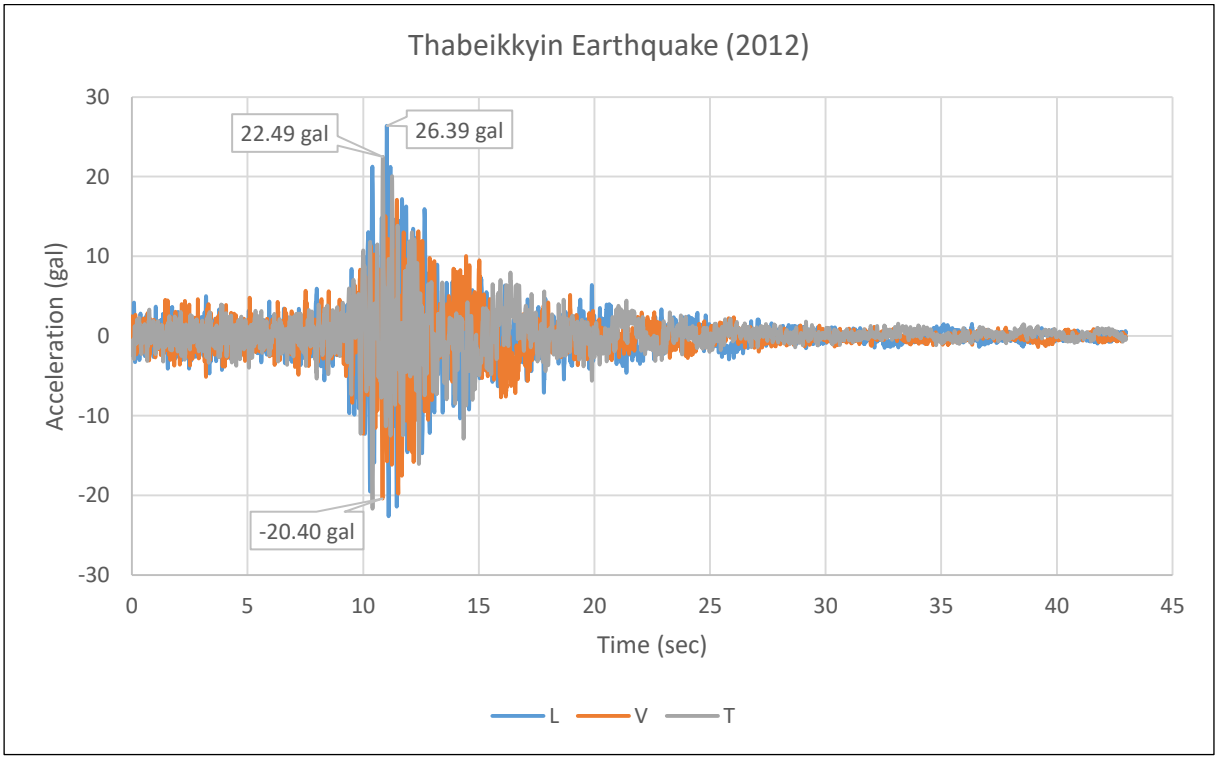

Figure 3.4: Acceleration record of Thabeikkyin Earthquake from Mandalay station.

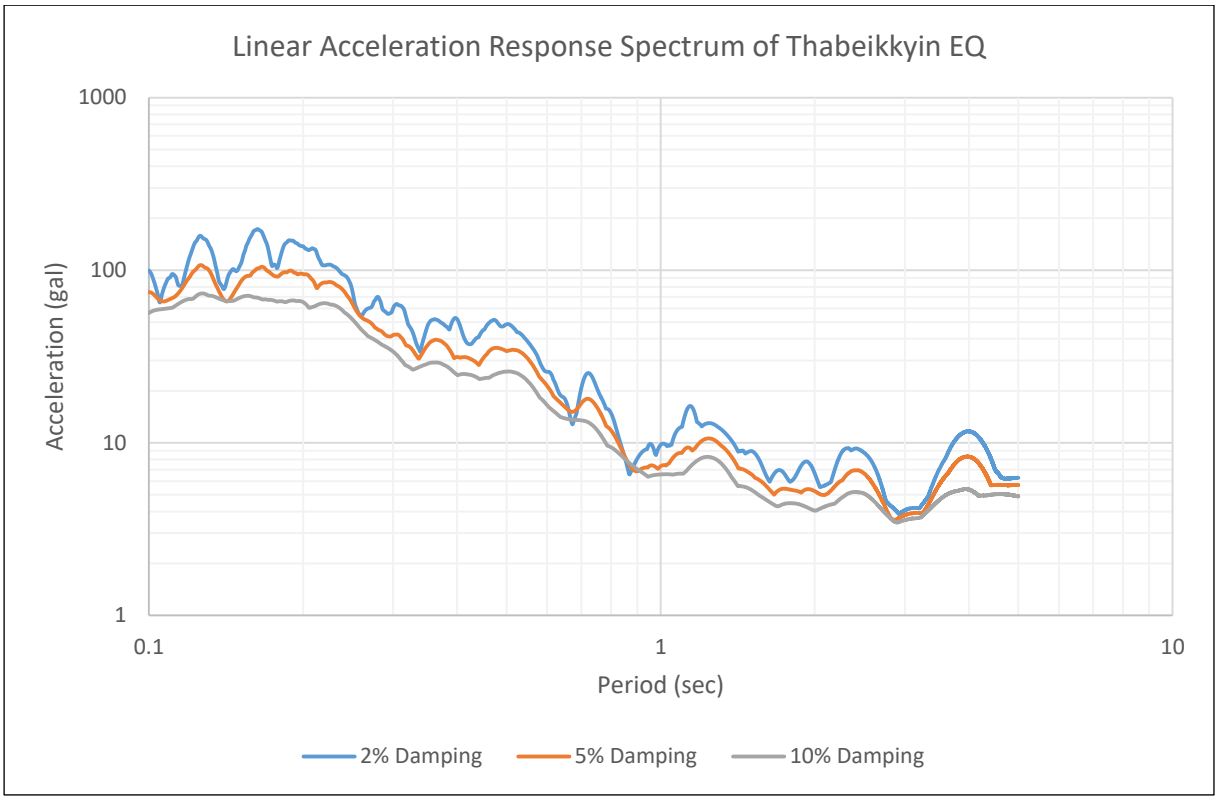

Figure 3.5: Linear acceleration response spectrum for Thabeikkyin Earthquake (2012).

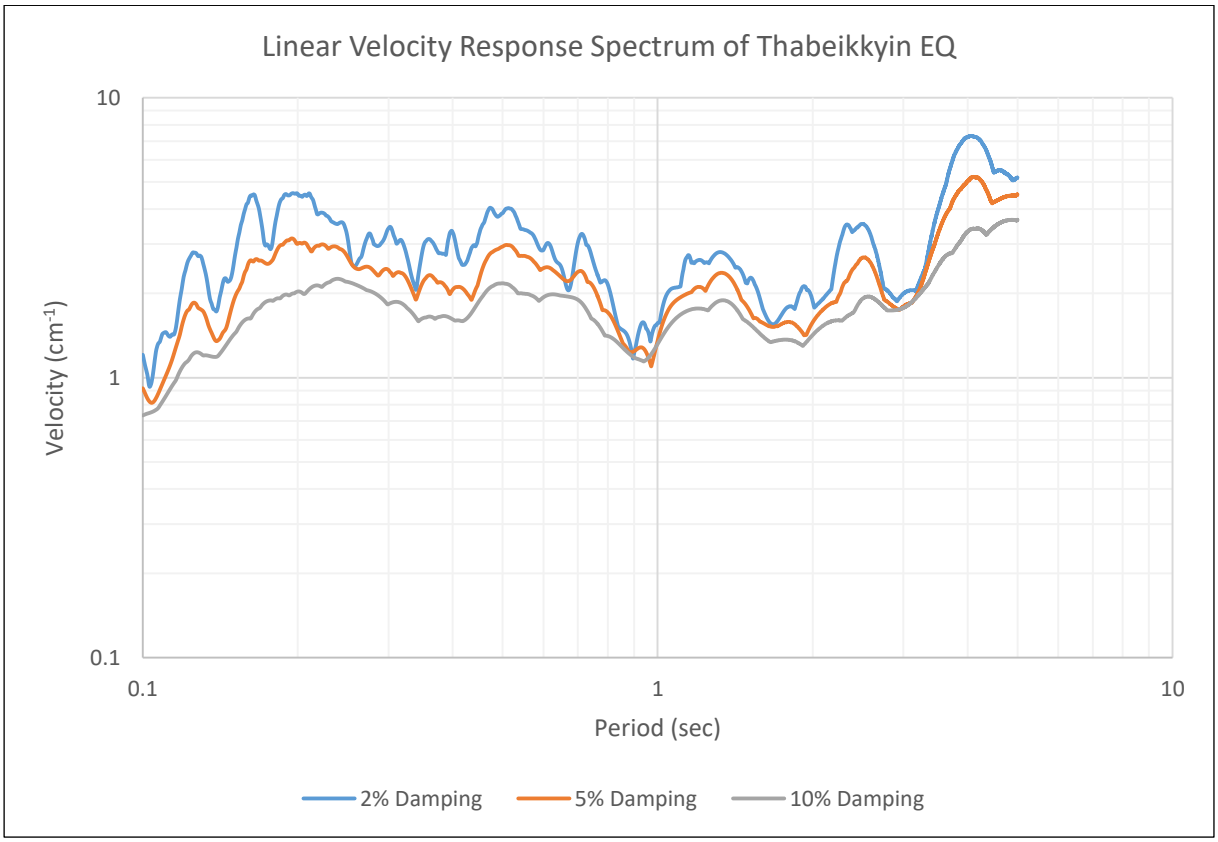

Figure 3.6: Linear velocity response spectrum for Thabeikkyin Earthquake (2012).

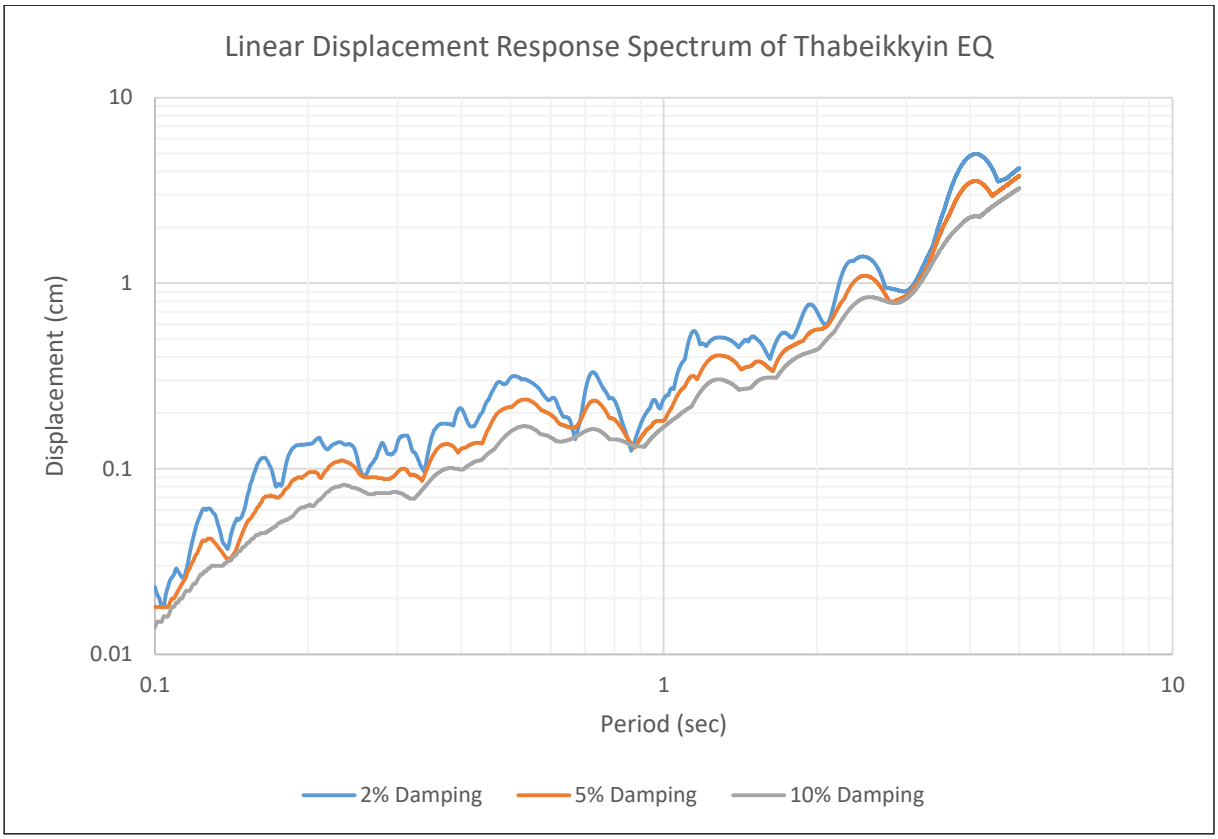

Figure 3.7: Linear displacement response spectrum for Thabeikkyin Earthquake (2012).

3.3.2 Calculation of Nonlinear Response Spectrum

Newmark's method for linear systems, which were discussed in the previous section, can be extended to produce non-linear response spectrums for elastic-perfectly plastic or bi-linear S.D.O.F systems by using the tangent stiffness (k_i) at u_i in the equation of motion in incremental form as follows [8] where $(\Delta f_s)_i = k_i \Delta u_i$:

$$m\Delta\ddot{u}_i + c\Delta\dot{u}_i + (\Delta f_s)_i = \Delta p_i \qquad (3.16)$$

For elastic-perfectly plastic systems and bilinear systems, it was necessary to consider only two different values of stiffness, stiffness for the elastic portion (k_e) and for the plastic portion (k_p) and, hence, no iteration is required to find the tangent stiffness. Almost all the steps were the same as in linear systems but, before Δu_i is calculated as shown in Table 3.2, an additional step was introduced to determine the proper value of stiffness, whether to use k_e or k_p in place of tangent stiffness (k_i). There were three main conditions in the program which are necessary to decide whether the response for next step was on the elastic part or, on the plastic part or, at the junction point between elastic and plastic parts in order to select the

proper stiffness value (k_e or k_p). In order to choose this, it was necessary to check the sign of velocity ($\dot{u}_{i+1}$), whether it was increasing (+) or, decreasing (−) or, changing from (+) to (−) or vice versa. When the velocity changed its sign, it means that the stiffness of the system also changes.

Moreover, the acceleration ($\ddot{u}_{i+1}$) was computed from two additional steps (2.7 and 2.8), instead of iteration, to ensure dynamic equilibrium at the end of each time step. Time stepping procedures to find the response of a non-linear system by Newmark's method were shown in Table 3.3, and a computer program [See Appendix B] was written in FORTRAN to generate the non-linear response spectrums. Force-displacement curves were also drawn to check the accuracy of the program as shown in Figure 3.8 and 3.9 before response spectrums were produced. Then, response spectrums of non-linear S.D.O.F structures for the Thabeikkyin Earthquake were developed as shown in Figure 3.10, 3.11 and 3.12 for elastoplastic systems, and in Figure 3.13, 3.14 and 3.15 for bilinear systems.

Table 3.3: Newmark's method for non-linear systems [8].

1.0	*Initial Calculations*
	1.1 $\ddot{u}_0 = \frac{p_0 - c\dot{u}_0 - k_0 u_0}{m}$
	1.2 $(f_s)_0 = -m\ddot{u}_{g0} - m\ddot{u}_0 - c\dot{u}_0$
	1.3 Select Δt.
	1.4 $a = \frac{1}{\beta \Delta t} m + \frac{\gamma}{\beta} c$ and $b = \frac{1}{2\beta} m + \Delta t \left(\frac{\gamma}{2\beta} - 1\right) c$
2.0	*Calculations for each time step, i*
	2.1 $\Delta \hat{p}_i = \Delta p_i + a\dot{u}_i + b\ddot{u}_i$
	2.2 Determine the proper value of tangent stiffness (k_i) whether to use k_e or k_p.
	2.3 $\hat{k} = k_i + \frac{\gamma}{\beta \Delta t} c + \frac{1}{\beta (\Delta t)^2} m$
	2.4 $\Delta u_i = \frac{\Delta \hat{p}_i}{\hat{k}}$
	2.5 $\Delta \dot{u}_i = \frac{\gamma}{\beta \Delta t} \Delta u_i - \frac{\gamma}{\beta} \dot{u}_i + \Delta t \left(1 - \frac{\gamma}{2\beta}\right) \ddot{u}_i$
	2.6 $u_{i+1} = u_i + \Delta u_i$ and $\dot{u}_{i+1} = \dot{u}_i + \Delta \dot{u}_i$
	2.7 $(f_s)_{i+1} = (f_s)_i + k_i \Delta u_i$ where $(f_s)_{i+1} - (f_s)_i = (\Delta f_s)_i$
	2.8 $\ddot{u}_{i+1} = \frac{p_{i+1} - c\dot{u}_{i+1} - (f_s)_{i+1}}{m}$
3.0	*Repetitions for the next time step*
	3.1 Replace i by i+1 and implement steps 2.1 to 2.8 for the next time step.

Note: To drive the response spectrum, p_i is replaced by $-m\ddot{u}_{gi}$ in the table.

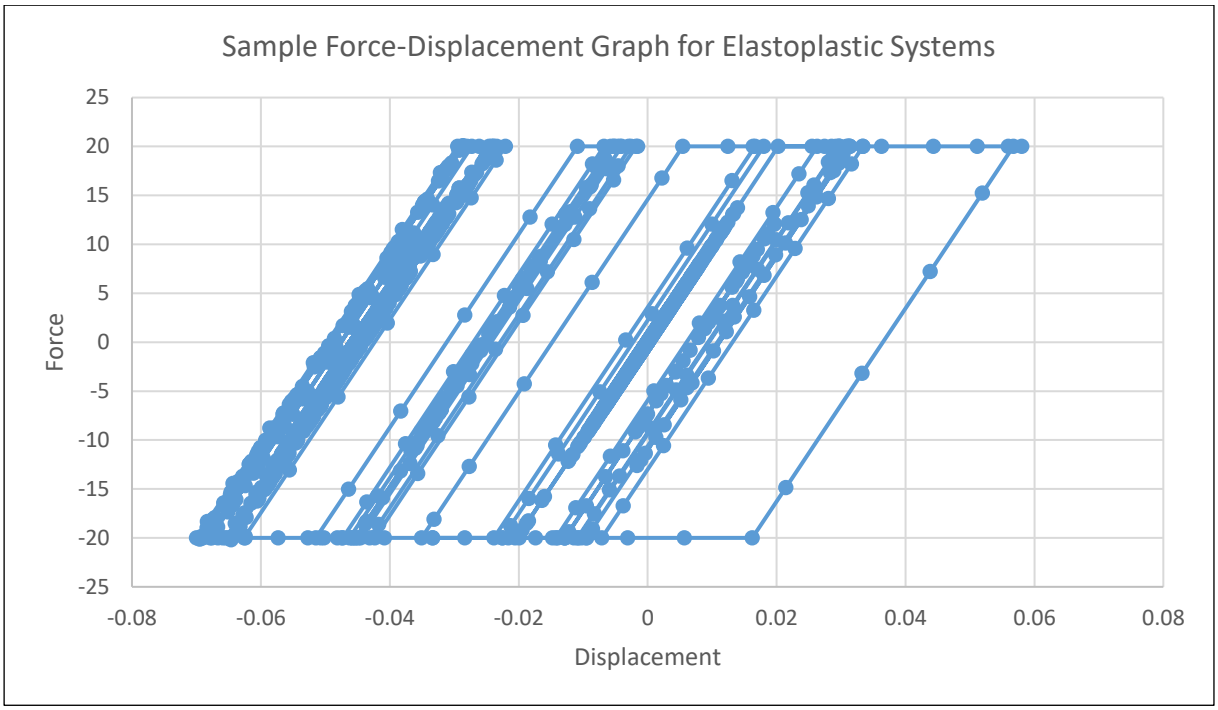

Figure 3.8: Sample of force-displacement graph for elastoplastic systems.

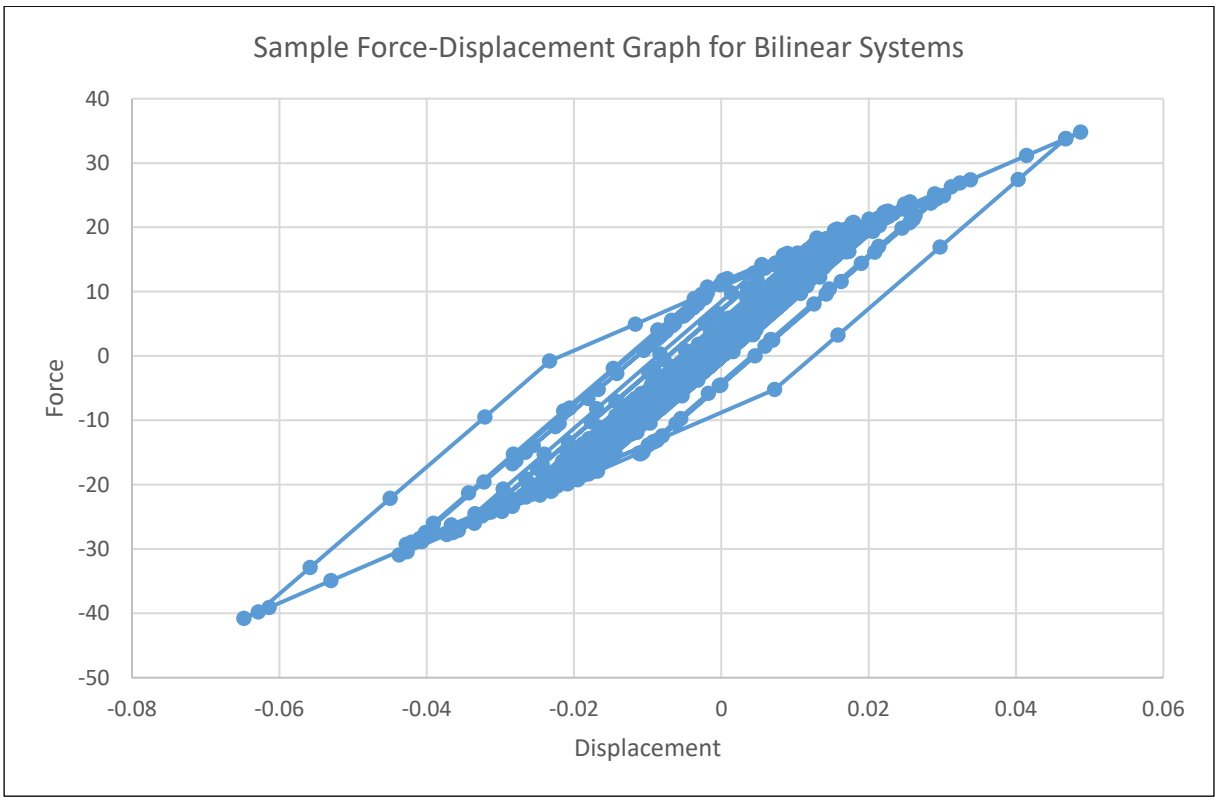

Figure 3.9: Sample of Force-displacement graph for bilinear systems.

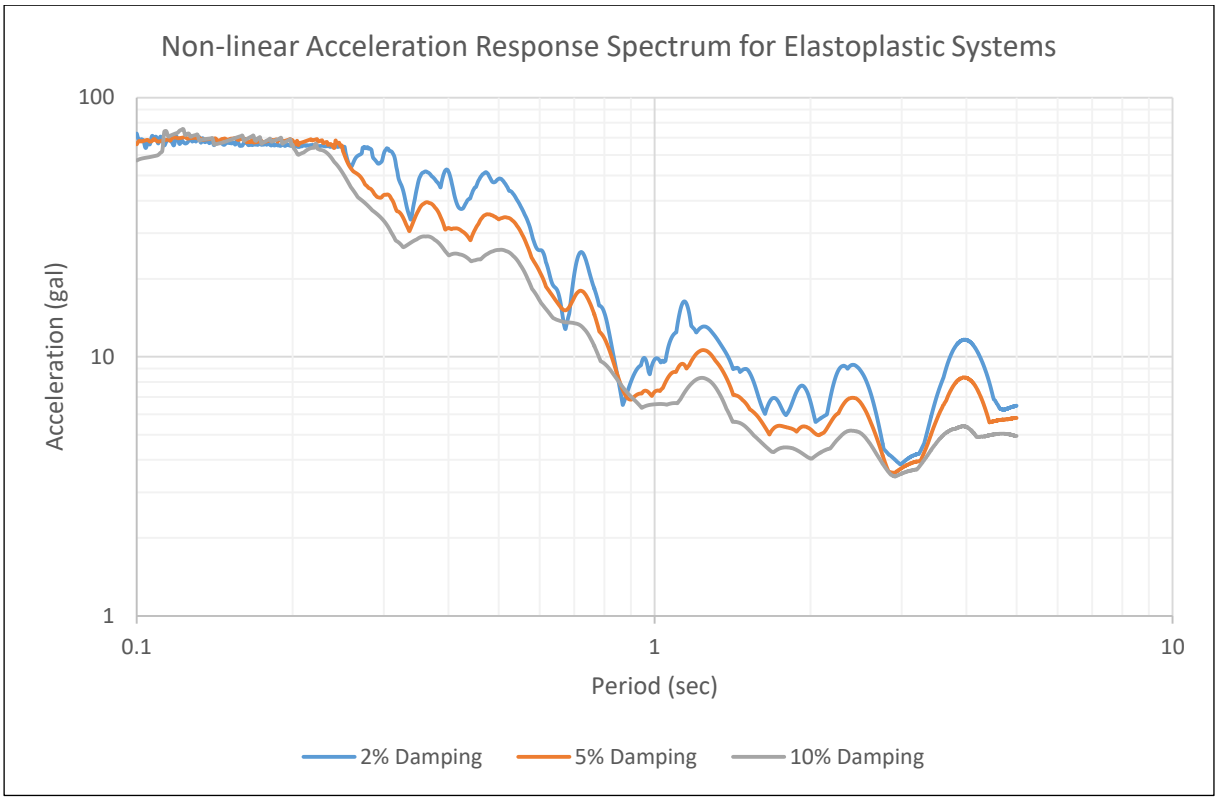

Figure 3.10: Non-linear acceleration response spectrum for elastoplastic systems due to Thabeikkyin Earthquake.

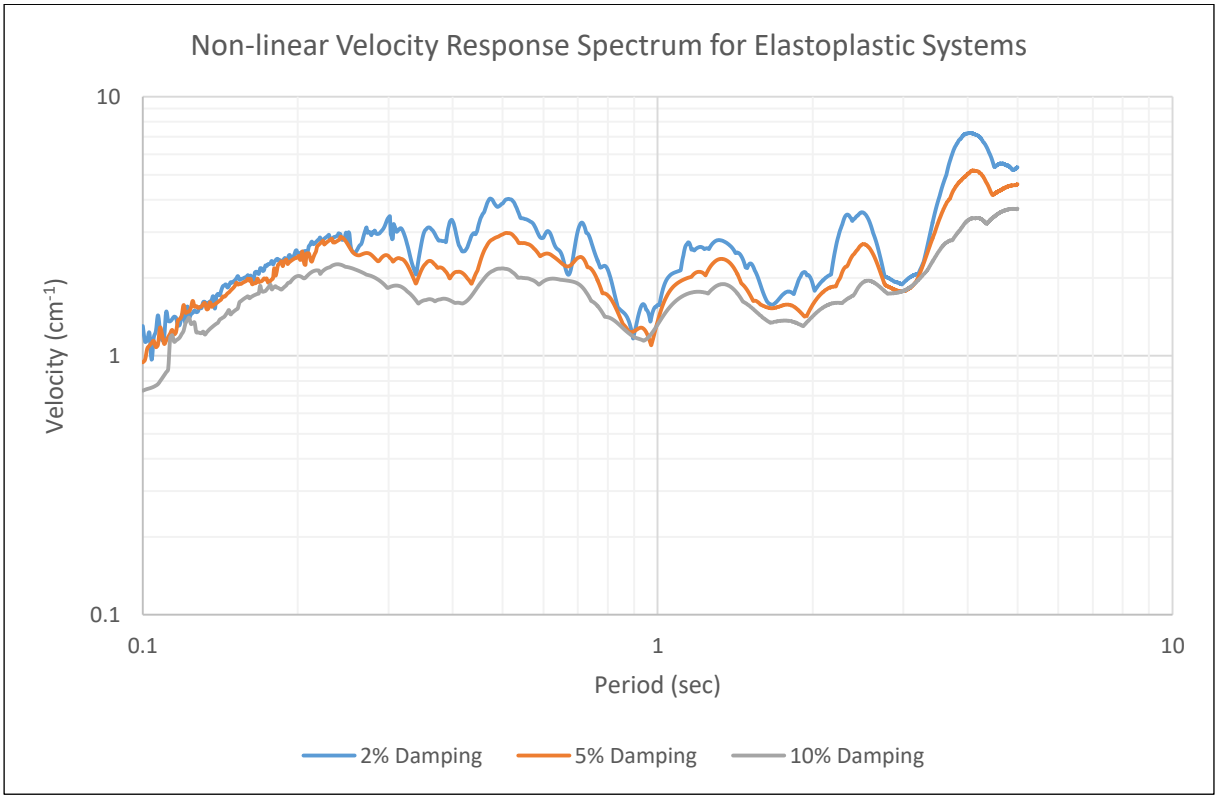

Figure 3.11: Non-linear velocity response spectrum for elastoplastic systems due to Thabeikkyin Earthquake.

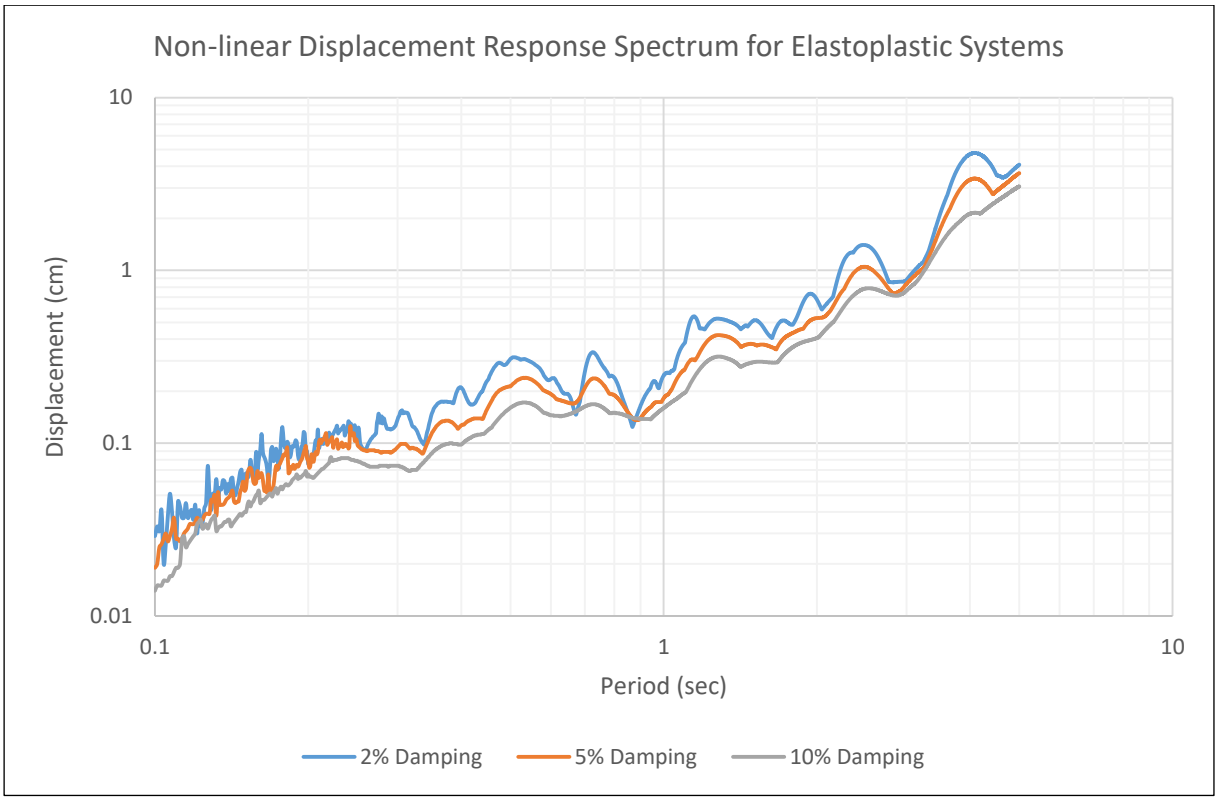

Figure 3.12: Non-linear displacement response spectrum for elastoplastic systems due to Thabeikkyin Earthquake.

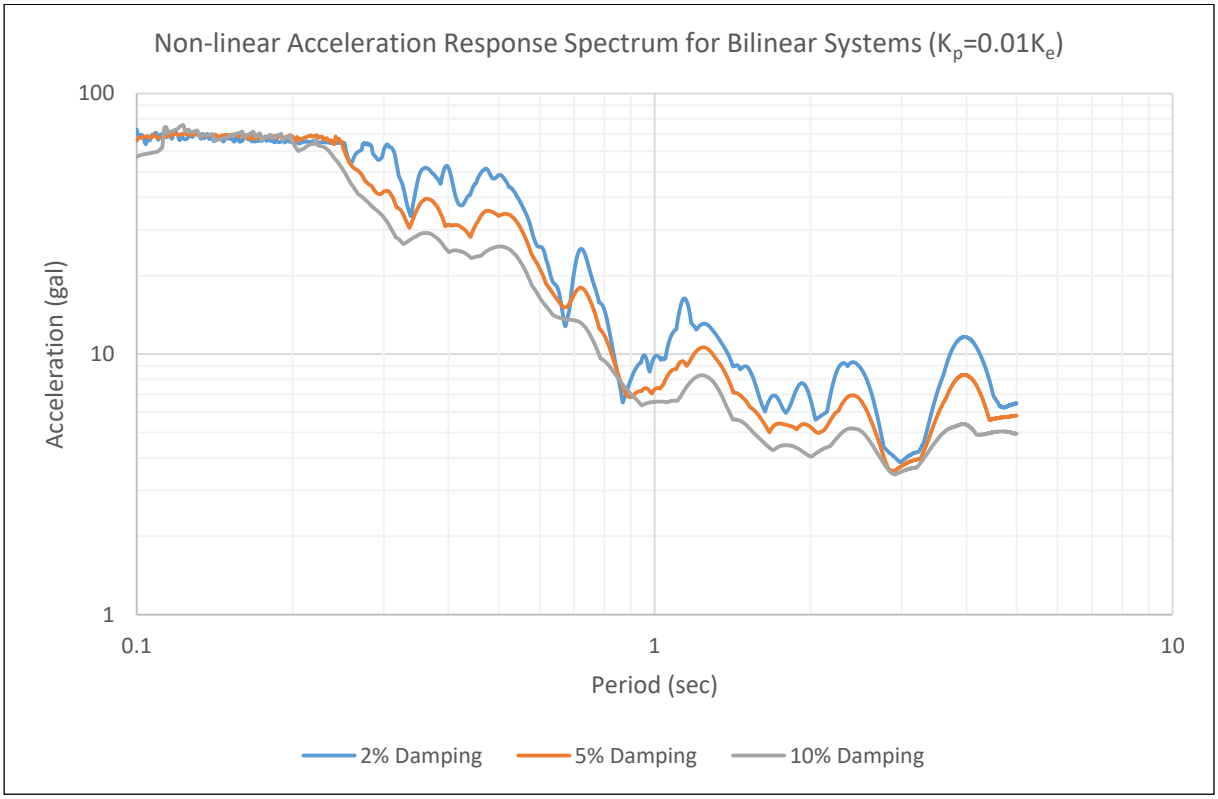

Figure 3.13: Non-linear acceleration response spectrum for bilinear systems due to Thabeikkyin Earthquake.

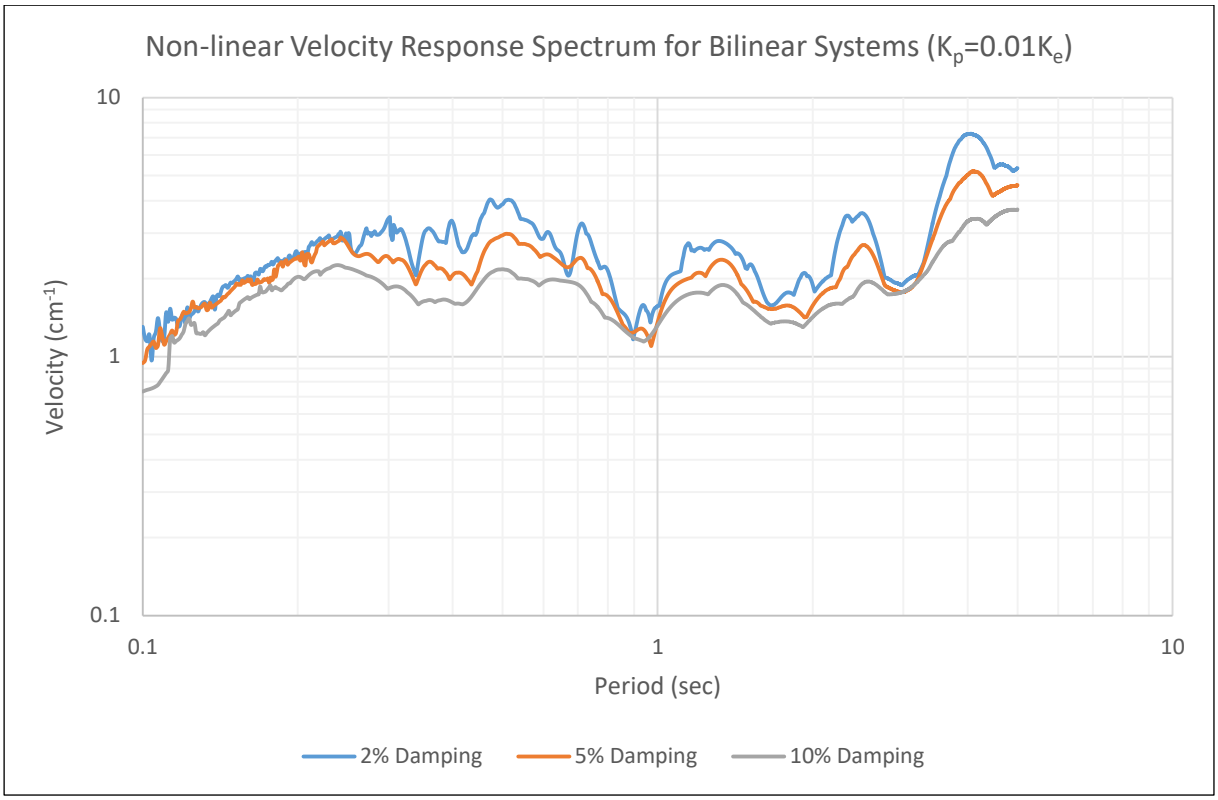

Figure 3.14: Non-linear velocity response spectrum for bilinear systems due to Thabeikkyin Earthquake.

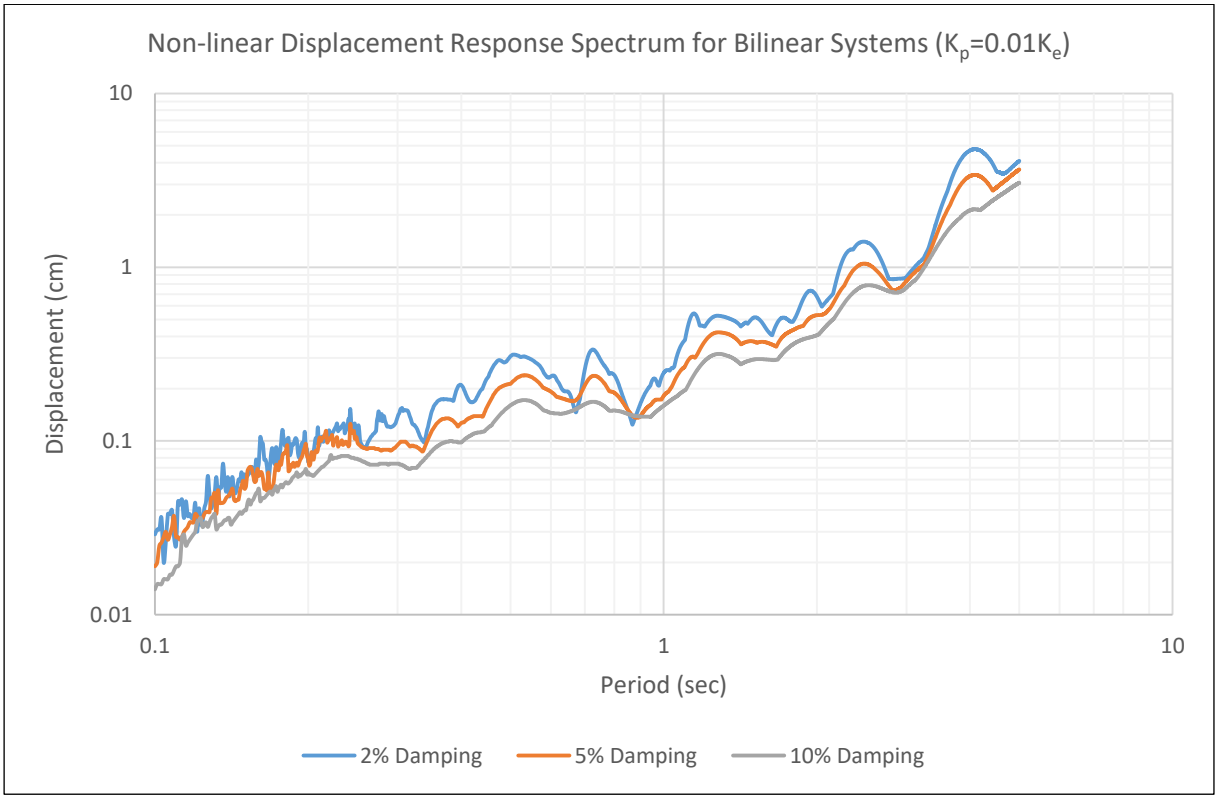

Figure 3.15: Non-linear displacement response spectrum for bilinear systems due to Thabeikkyin Earthquake.

3.4 Ductility and Response of Nonlinear Systems

3.4.1 Force-deformation Relationship

For linear systems, the relationship between the force and deformation shows a straight line (or linear) phenomenon, with a constant stiffness, as shown in Figure 3.16, which is the force-displacement graph of a linear system with m = 1 kg, T = 0.5 sec and ζ = 5% under the Thabeikkyin Earthquake (2012). For nonlinear systems, the relationship between the force and deformation is still linear as long as the response is below the yield limit, but the slope of the graph (or the stiffness) changes suddenly when the response goes beyond the elastic limit or the yield point. There are two types of idealization for the response of nonlinear systems, elastic-perfectly plastic (or elastoplastic) response or bilinear response, as shown in Figures 3.8 and 3.9, according to the type of material or system.

3.4.2 Ductility of Nonlinear Systems

For the nonlinear response of a system with steel or reinforced concrete members, the actual force-deformation relation is usually idealized by the elastoplastic nature as shown in Figure 3.17, so that the area under the two curves, which represents the dissipated energy of the system, are the same at the maximum displacement (u_m) [8]. Moreover, it is often preferred to compare the peak deformation of an elastoplastic system due to the earthquake ground motion to the peak deformation caused by the same excitation in the corresponding linear system. In that case, the initial stiffness of elastoplastic system is the same as the stiffness of linear system but the post-yield stiffness changes beyond the elastic limit.

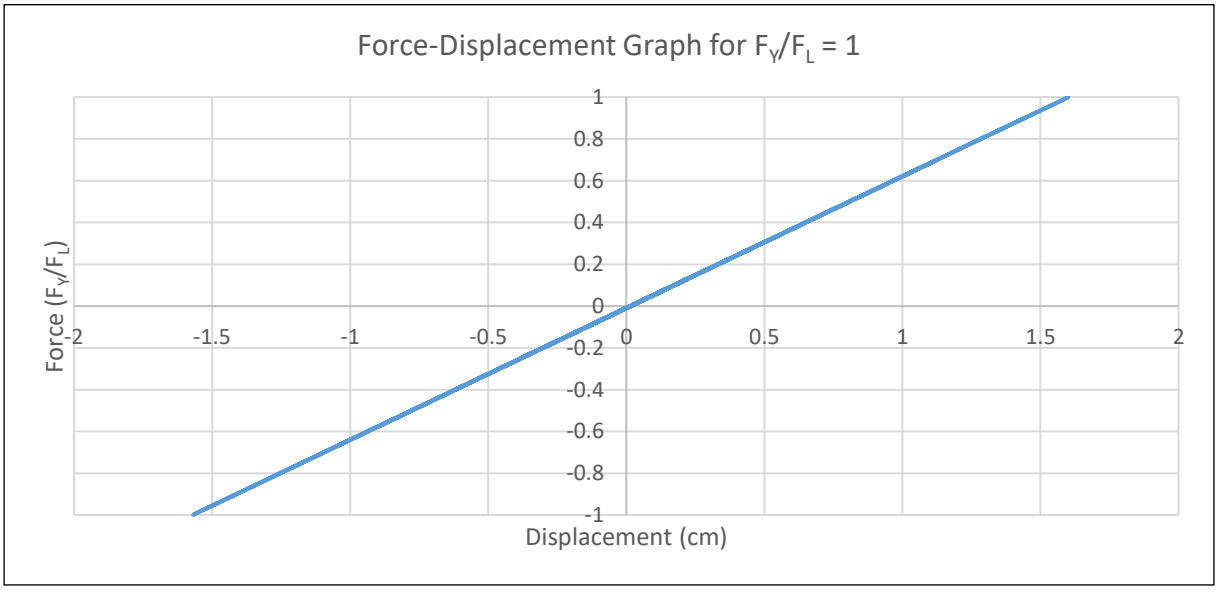

Figure 3.16: Force-displacement graph of a linear system with T = 0.5 sec and ζ = 5% under Thabeikkyin Earthquake.

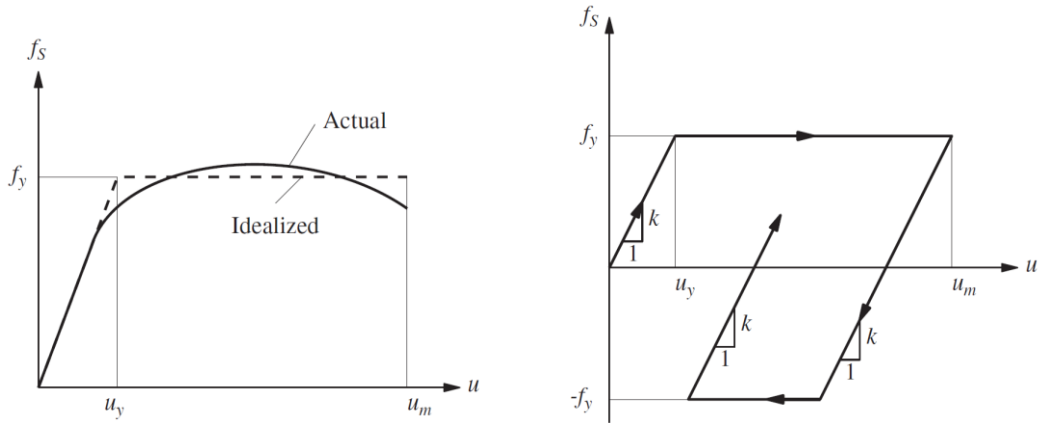

(a) (b)

Figure 3.17: (a) Force-deformation relation between actual and elastoplastic idealization; (b) Idealized elastoplastic force-deformation relation [8].

Such a comparison between linear and nonlinear elastoplastic systems can be interpreted as shown in Figure 3.18 by using a parameter, called the ductility factor (μ) of the system, which is the ratio of maximum displacement (U_M) and displacement at yield (U_Y), and the force reduction factor (R_y), which is the ratio of maximum response (F_L *or* U_L) of linear system and the response at yield (F_Y *or* U_Y) of the corresponding nonlinear system. By using the equal energy theorem, the relation between ductility factor (μ), and force reduction factor (R_y) or normalized yield strength ($\bar{F}_Y$) can be derived as follows [8,10].

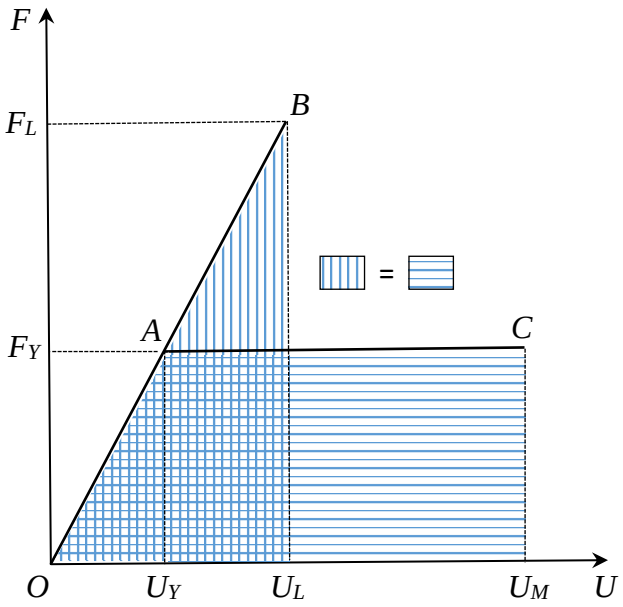

Figure 3.18: Comparison between elastoplastic system and corresponding linear system [10].

By using the equal energy theorem, it can be assumed that the area under the linear curve OAB is assumed equal to the area under the nonlinear curve OAC in Figure 3.18,

$$1/2\ (F_L - F_Y)(U_L - U_Y) = F_Y(U_M - U_L)$$

$$F_L U_L - F_L U_Y + F_Y U_Y = 2F_Y U_M - F_Y U_L$$

$$F_L \frac{U_L}{U_Y} - F_L + F_Y = 2F_Y \frac{U_M}{U_Y} - F_Y \frac{U_L}{U_Y}$$

where $\mu = \frac{U_M}{U_Y}$ and $R_y = \frac{F_L}{F_Y} = \frac{U_L}{U_Y}$ or $\bar{F}_Y = \frac{1}{R_y} = \frac{F_Y}{F_L} = \frac{U_Y}{U_L}$ can be replaced. Then the equation can be transformed into:

$$R_y = \sqrt{2\mu - 1} \text{ or } \bar{F}_Y = \frac{1}{\sqrt{2\mu - 1}} \quad (3.15)$$

or

$$\frac{U_M}{U_L} = \mu \bar{F}_Y = \frac{\mu}{R_y} \quad (3.16)$$

where R_y and $\bar{F}_Y$ are force reduction factor and normalized yield strength, respectively.

3.4.3 Effect of Yielding and Ductility Demand

In order to see the effect of yielding on a S.D.O.F system due to its nonlinear nature, the responses of a linear system and those of the corresponding nonlinear system due to an earthquake were compared by using the acceleration data from Thabeikkyin Earthquake (2012). Moreover, the ductility factor or the ductility demand of the nonlinear system for different values of normalized yield strength were evaluated from the responses of linear and corresponding nonlinear systems.

Figure 3.19, and 3.20 showed the responses of a linear S.D.O.F system with m = 1 kg, ζ = 5% and T = 0.5 sec due to the Thabeikkyin Earthquake data. It can be seen from figures that the system oscillates about the equilibrium position with the maximum displacement value of 0.213 cm and the maximum resisting force to remain the system elastic was 0.034 g.

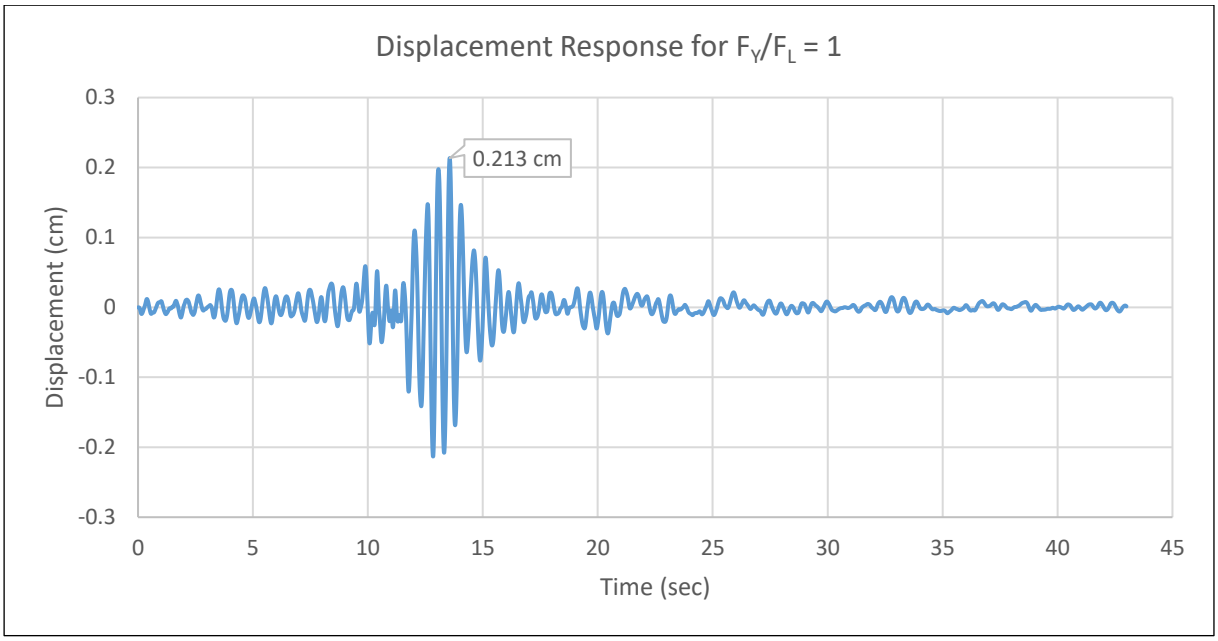

Figure 3.19: Displacement response of a linear system (m = 1 kg, ζ = 5% and T = 0.5 sec) due to Thabeikkyin Earthquake.

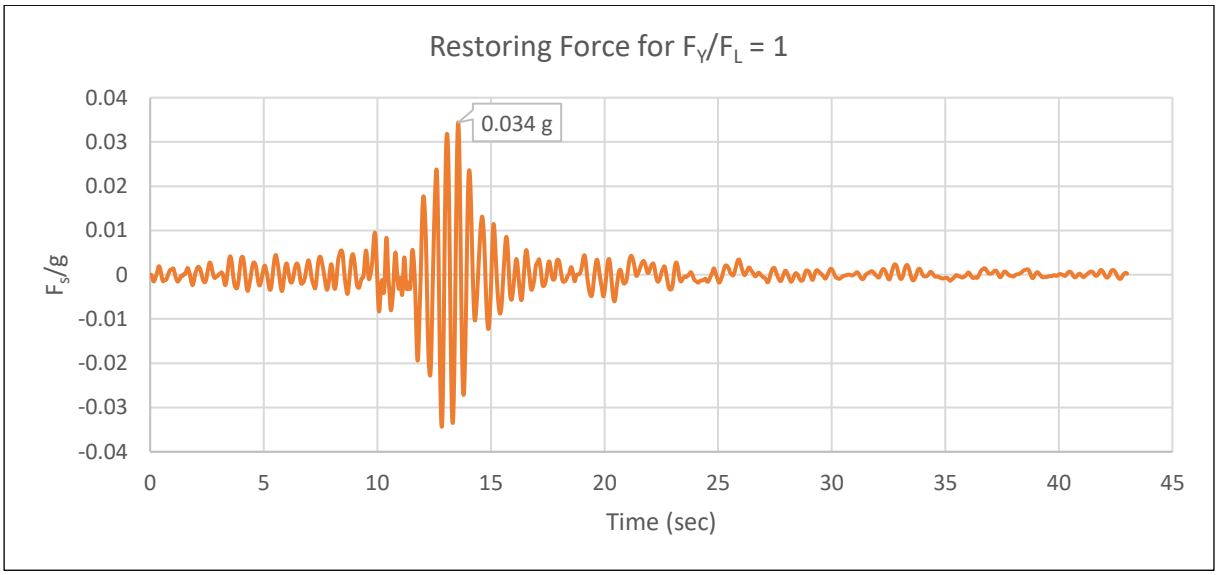

Figure 3.20: Restoring force necessary for a linear system (m = 1 kg, ζ = 5% and T = 0.5 sec) due to Thabeikkyin Earthquake.

The responses of three nonlinear (elastoplastic) S.D.O.F systems with the same m, ζ and T values were also drawn for three different values of normalized yield strength (0.5, 0.25, 0.125) as shown in Figures 3.21 to 3.23 and it can be seen that the deformation responses were no more oscillating around the equilibrium after yielding showing some permanent deformation. The ductility demand of these three different systems can be found out from equation (3.16) as, $\mu_{0.5}$ = 1.76, $\mu_{0.25}$ = 3.0, $\mu_{0.125}$ = 10.25 respectively.

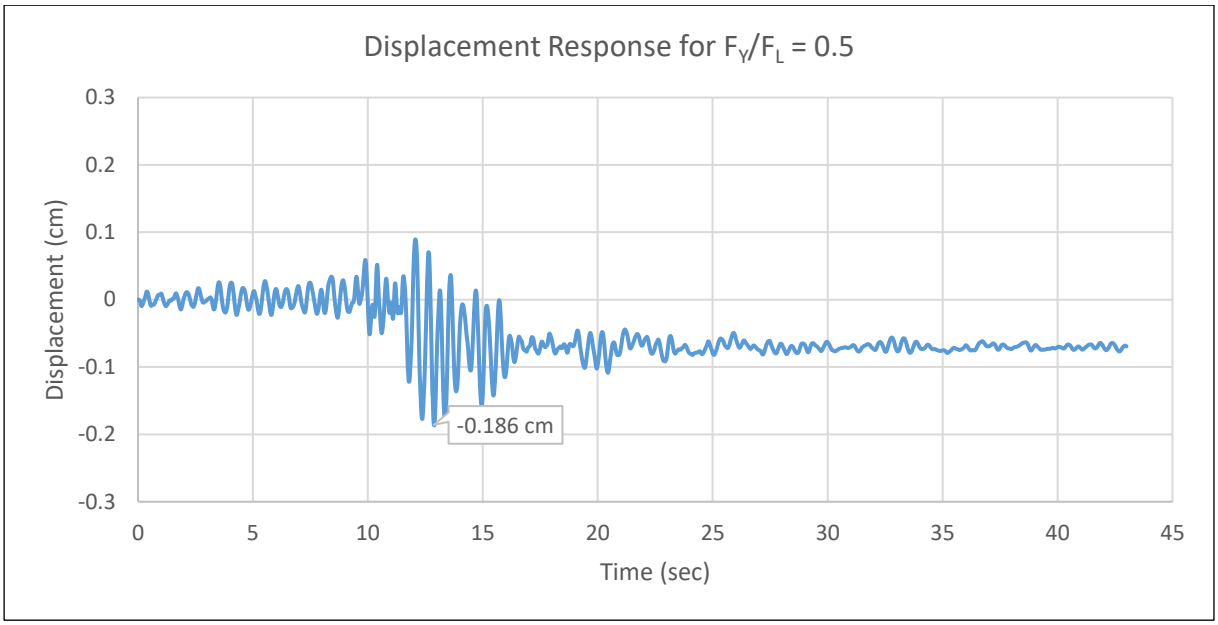

Figure 3.21: Displacement response of nonlinear system (m = 1 kg, ζ = 5% and T = 0.5 sec) with ($\bar{F}_Y$ = 0.5) due to Thabeikkyin Earthquake.

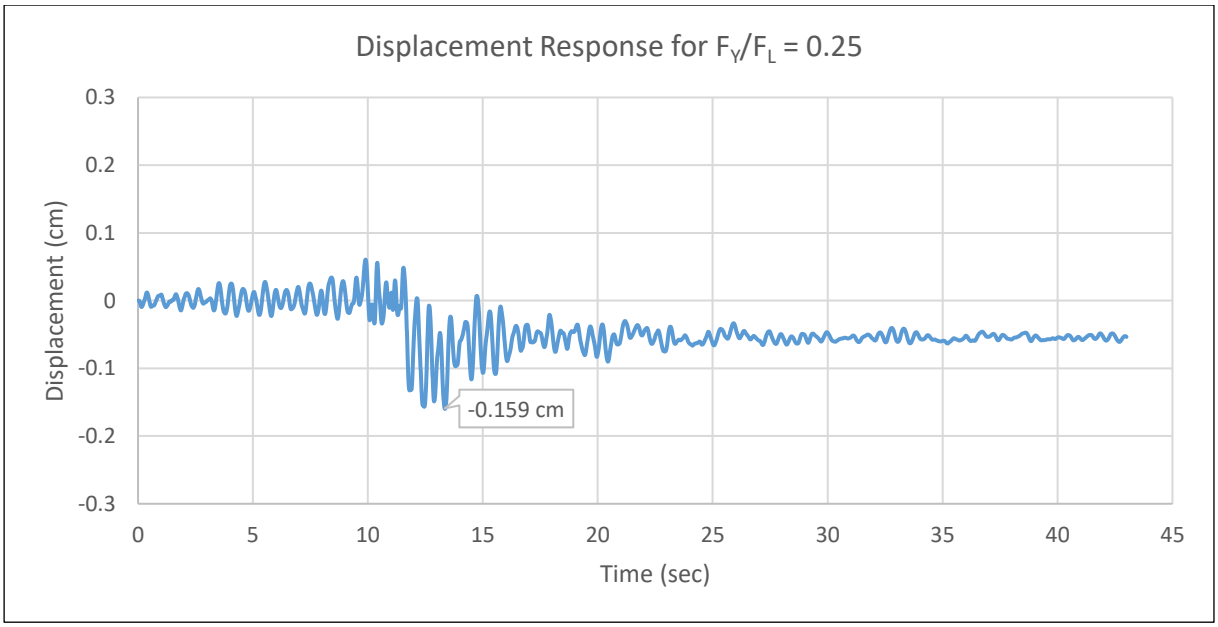

Figure 3.22: Displacement response of nonlinear system (m = 1 kg, ζ = 5% and T = 0.5 sec) with ($\bar{F}_Y$ = 0.25) due to Thabeikkyin Earthquake.

However, the maximum restoring forces (or yielding force) for three different systems necessary for stable equilibrium were decreasing with 0.017 g, 0.009 g, 0.004 g as shown in Figure 3.24 to 3.26 due to the decreasing normalized yield strength with 0.5, 0.25, and 0.125 of the corresponding linear system. It can also be seen that more yielding occurs when the yield strength of the system decreases from 0.5 to 0.25 and 0.125, increasing the chance to occur permanent deformation of the system after ground shaking.

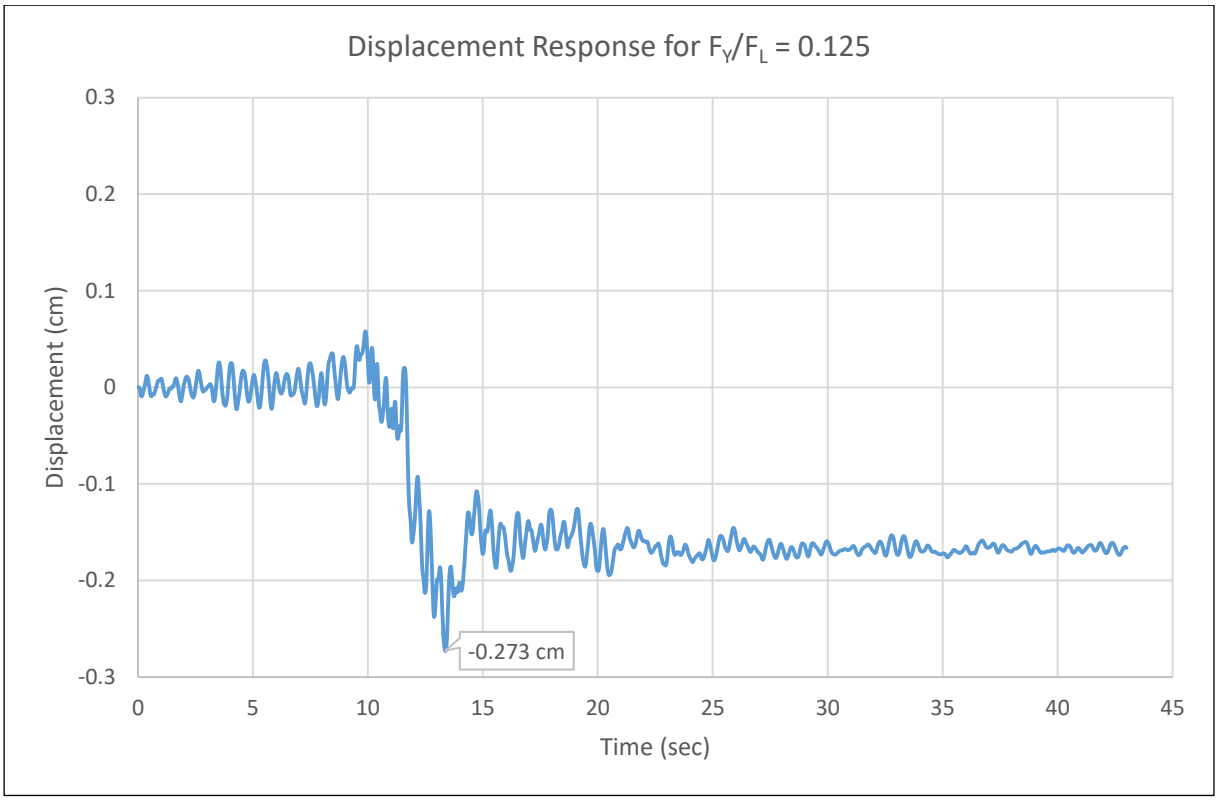

Figure 3.23: Displacement response of nonlinear system (m = 1 kg, ζ = 5% and T = 0.5 sec) with ($\bar{F}_Y$ = 0.125) due to Thabeikkyin Earthquake.

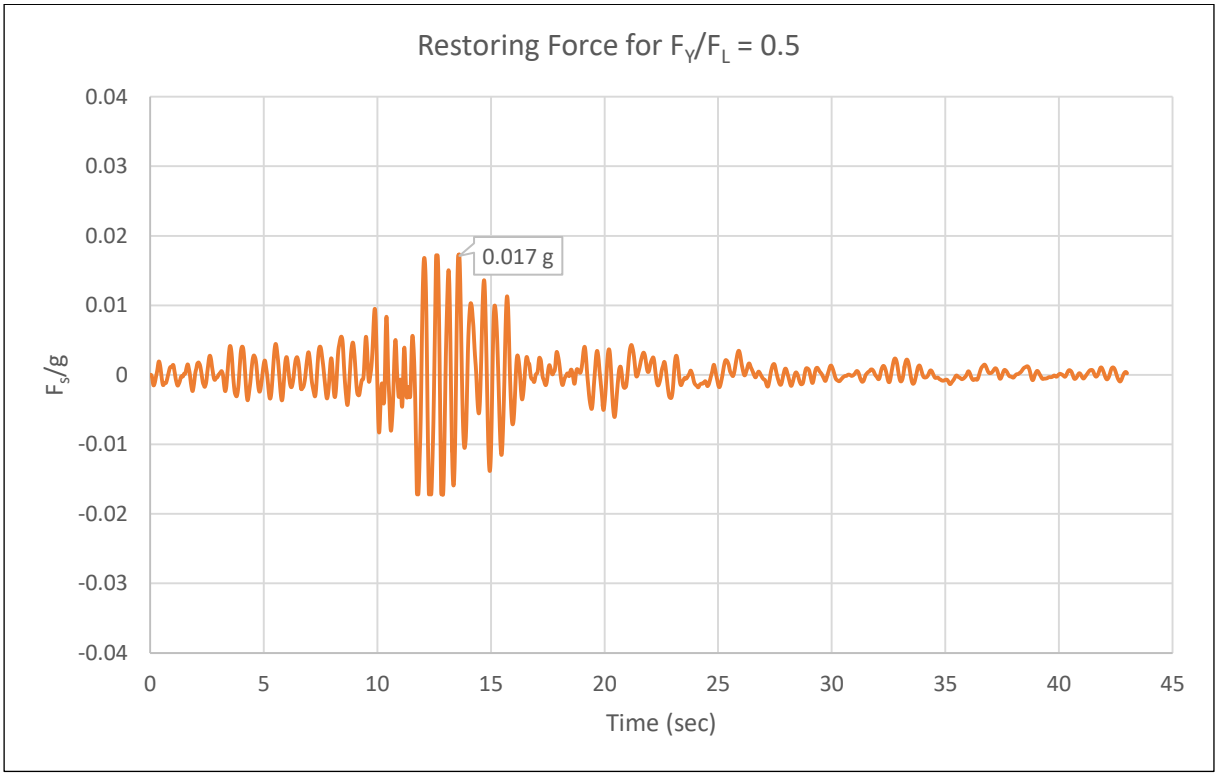

Figure 3.24: Restoring force necessary for a nonlinear system (m = 1 kg, ζ = 5% and T = 0.5 sec) with ($\bar{F}_Y$ = 0.5) due to Thabeikkyin Earthquake.

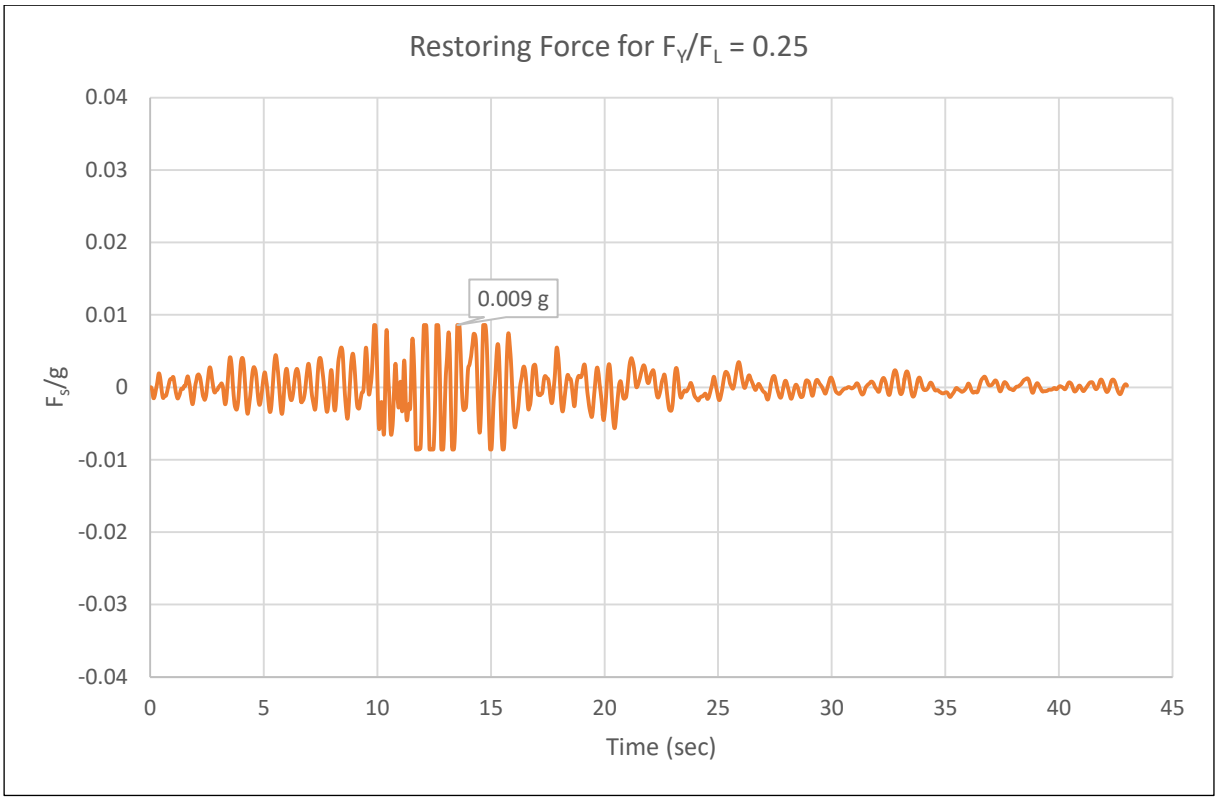

Figure 3.25: Restoring force necessary for a nonlinear system (m = 1 kg, ζ = 5% and T = 0.5 sec) with ($\bar{F}_Y$ = 0.25) due to Thabeikkyin Earthquake.

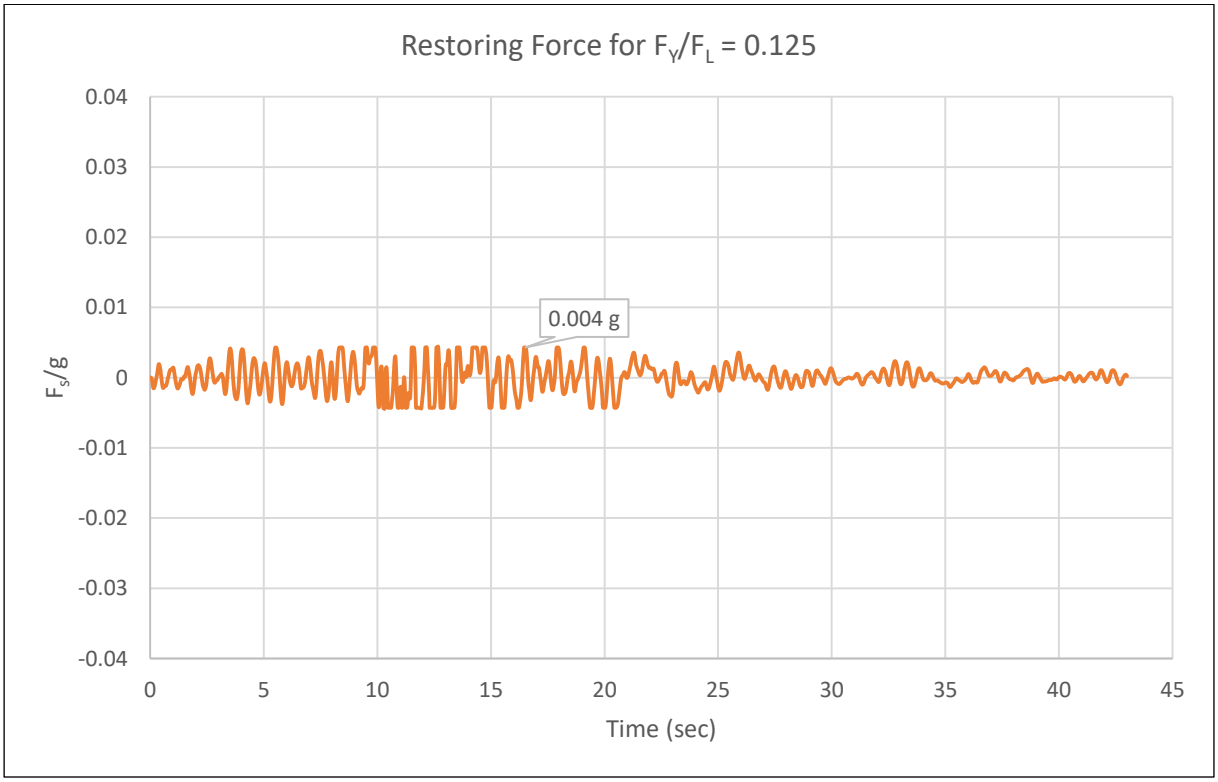

Figure 3.26: Restoring force necessary for a nonlinear system (m = 1 kg, ζ = 5% and T = 0.5 sec) with ($\bar{F}_Y$ = 0.125) due to Thabeikkyin Earthquake.

Then, the relation between the normalized yield strength ($\bar{F}_Y$) and the ductility ratio (μ) of different S.D.O.F systems with different periods was presented in Figure 3.27. From the graph, it can be seen that the required ductility ratio or (ductility demand) of a nonlinear system is inversely related to the normalized yield strength of the system, and more ductility is required if the ratio between the yield strength (F_Y) and the linear elastic strength (F_L) is reduced. Moreover, response of nonlinear systems with different periods (0.1s ~ 5s) and different ratios of F_Y/F_L (0.125, 0.25, 0.5, and 1) under Thabeikkyin Earthquake showed the same characteristics comparing with theoretical relation.

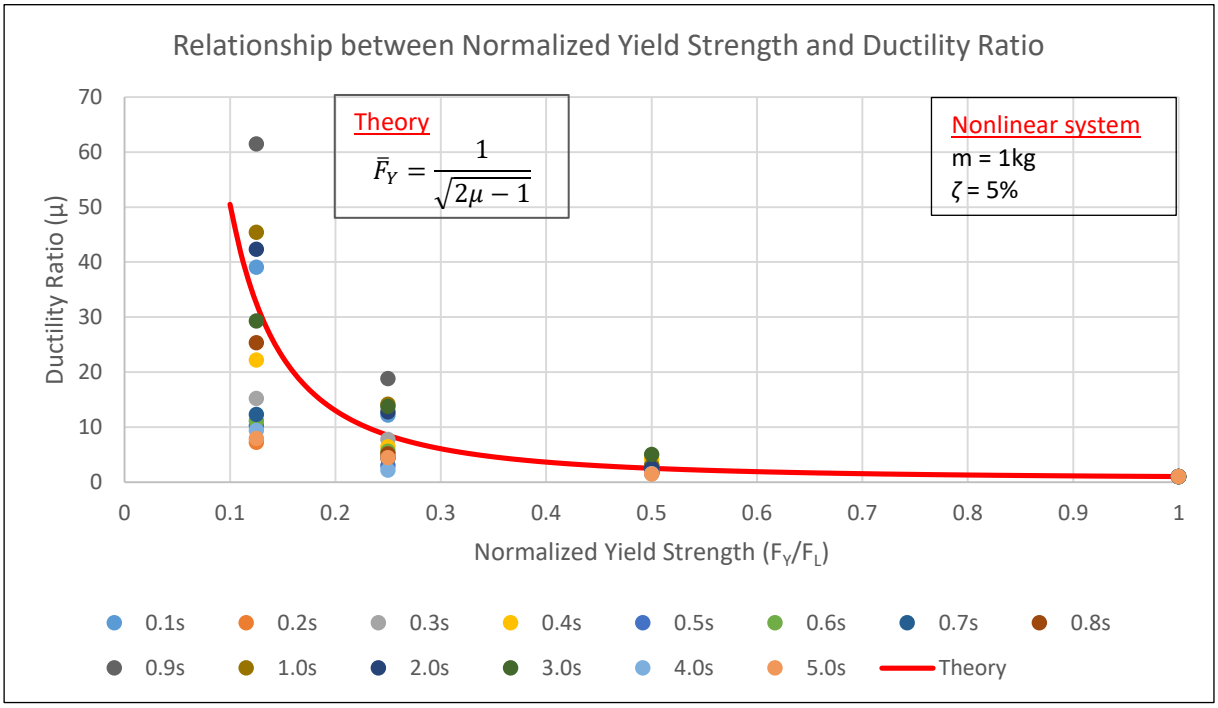

Figure 3.27: Relation between the normalized yield strength ($\bar{F}_Y$) and the ductility ratio (μ).

3.5 Characteristics of Thabeikkyin Earthquake and Proposed Design Spectrum

Thabeikkyin Earthquake was the latest large earthquake recorded on the Sagaing Fault occurred on 11th November 2012 near Thabeikkyin, 100 km north of Mandalay, at 9.9 km depth with the intensity of 6.8 [5, 11, 12]. According to the records, 201 houses, 25 schools, 13 hospitals/clinics, 35 monasteries and 45 pagodas were totally collapsed or partially damaged due to the earthquake. Moreover, one span of the bridge in construction over the Ayeyarwady River, Yadanar Theinga Bridge in Kyauk Myaung Township in Shwebo District, Sagain Region, fell into the river due to the earthquake [11]. The amplitude of Thabeikkyin Earthquake recorded from Mandalay seismic station at 0.01sec interval is shown in Figure 3.28, with the maximum acceleration values of 26.39 gal, 20.40 gal and 22.49 gal for longitudinal, vertical and transverse directions respectively.

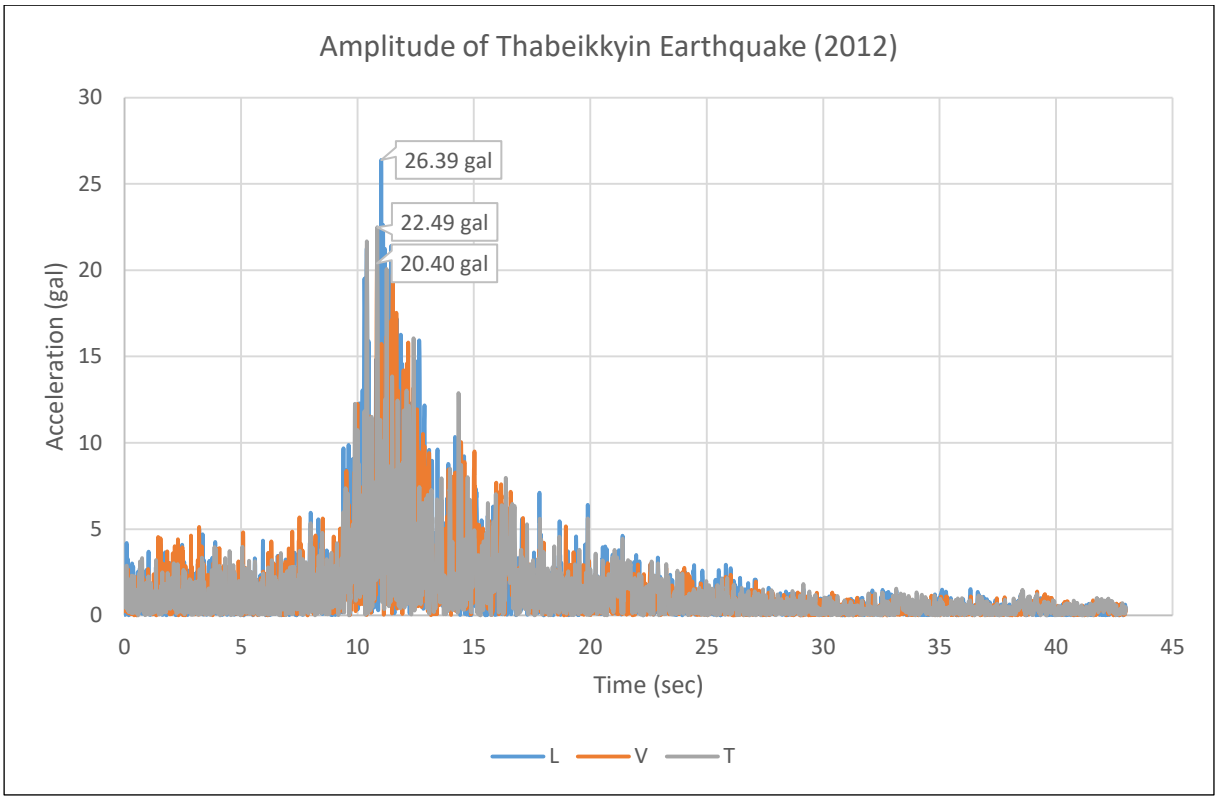

Figure 3.28: Amplitude of Thabeikkyin Earthquake (2016).

3.5.1 Fourier and Power Spectrums for Thabeikkyin Earthquake

To know the frequency characteristics of Thabeikkyin Earthquake, Fourier and Power spectrums of the earthquake in three directions (L, V, T) are produced as shown in Figure 3.29, 3.30, 3.31 and 3.32. According to the Fourier spectrums, the dominant frequencies of the earthquake occur within the range of 1 Hz to 10 Hz with the maximum frequency occurs at 0.26 Hz for longitudinal and vertical directions and at 0.19 Hz for transverse direction. Secondary peaks occur at 6.09 Hz, 3.56 Hz, and 4.65 Hz for longitudinal, vertical and transverse directions.

Power spectrum also showed the same phenomenon as Fourier spectrums that maximum amplitudes occurred around 0.26 Hz for all directions and followed by other peaks at 6.09 Hz, 3.56 Hz, and 4.65 Hz for longitudinal, vertical and transverse directions. Hence, it can be said that higher frequency range is dominant for Thabeikkyin Earthquake. According the linear acceleration response spectrums shown in Figure 3.5, maximum response occurred between 0.1 sec and 0.2 sec periods based on different damping ratios. Hence, low frequency structures such as long span bridges were assumed to be less vulnerable during the earthquake than high frequency structures such as highrise buildings.

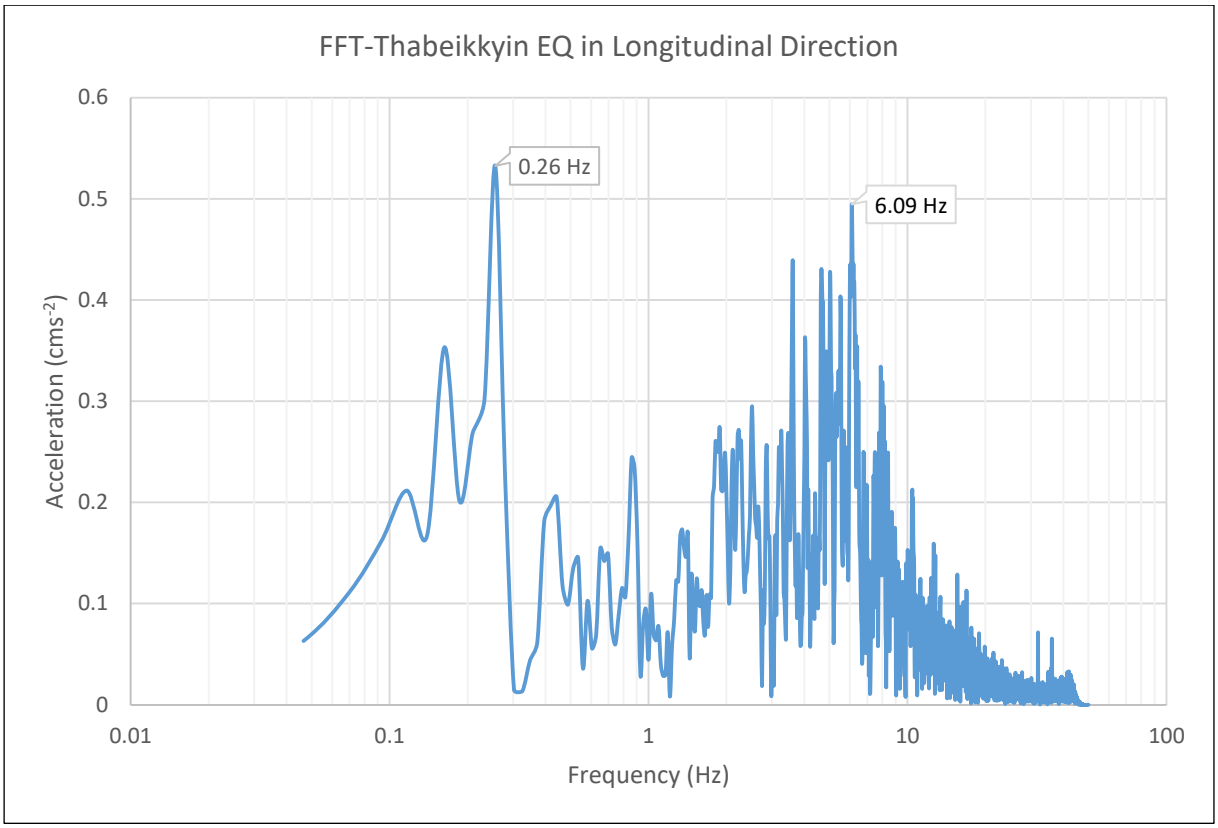

Figure 3.29: Fourier spectrum of Thabeikkyin Earthquake in longitudinal direction.

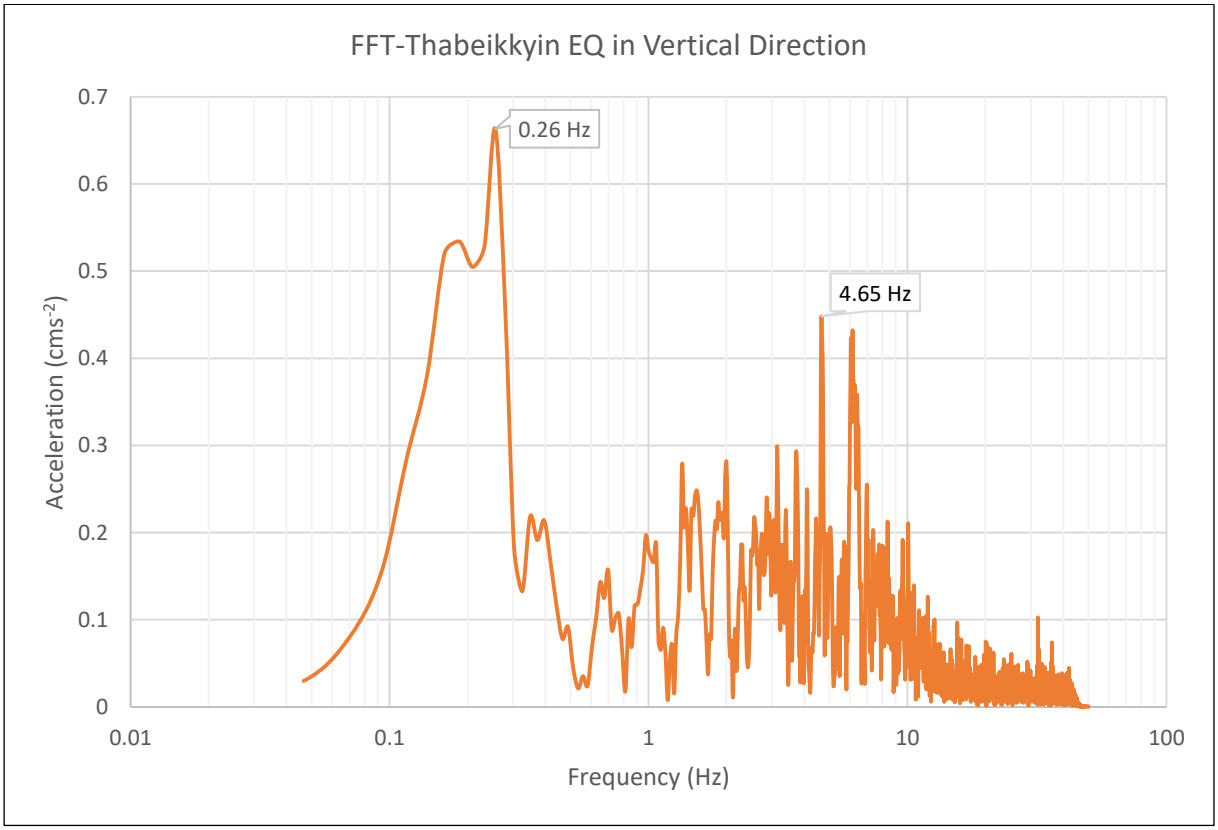

Figure 3.30: Fourier spectrum of Thabeikkyin Earthquake in vertical direction.

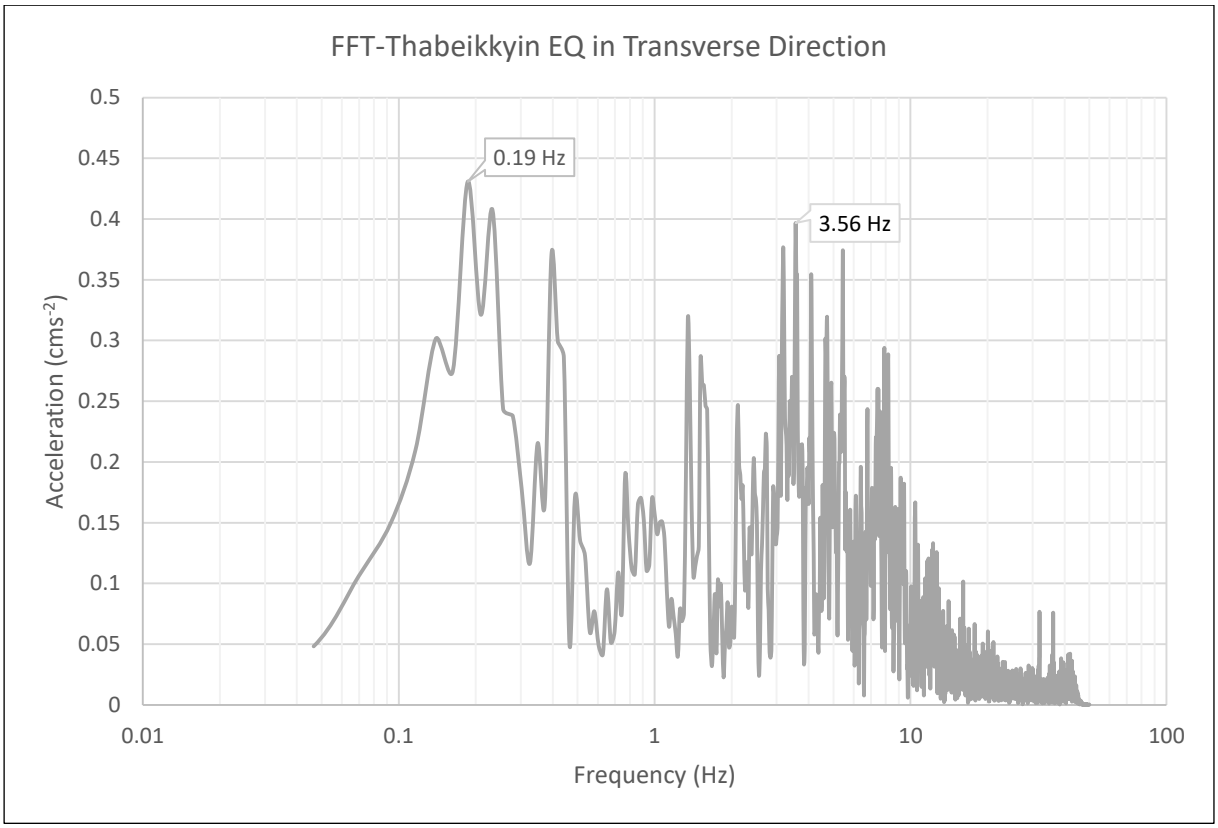

Figure 3.31: Fourier spectrum of Thabeikkyin Earthquake in transverse direction.

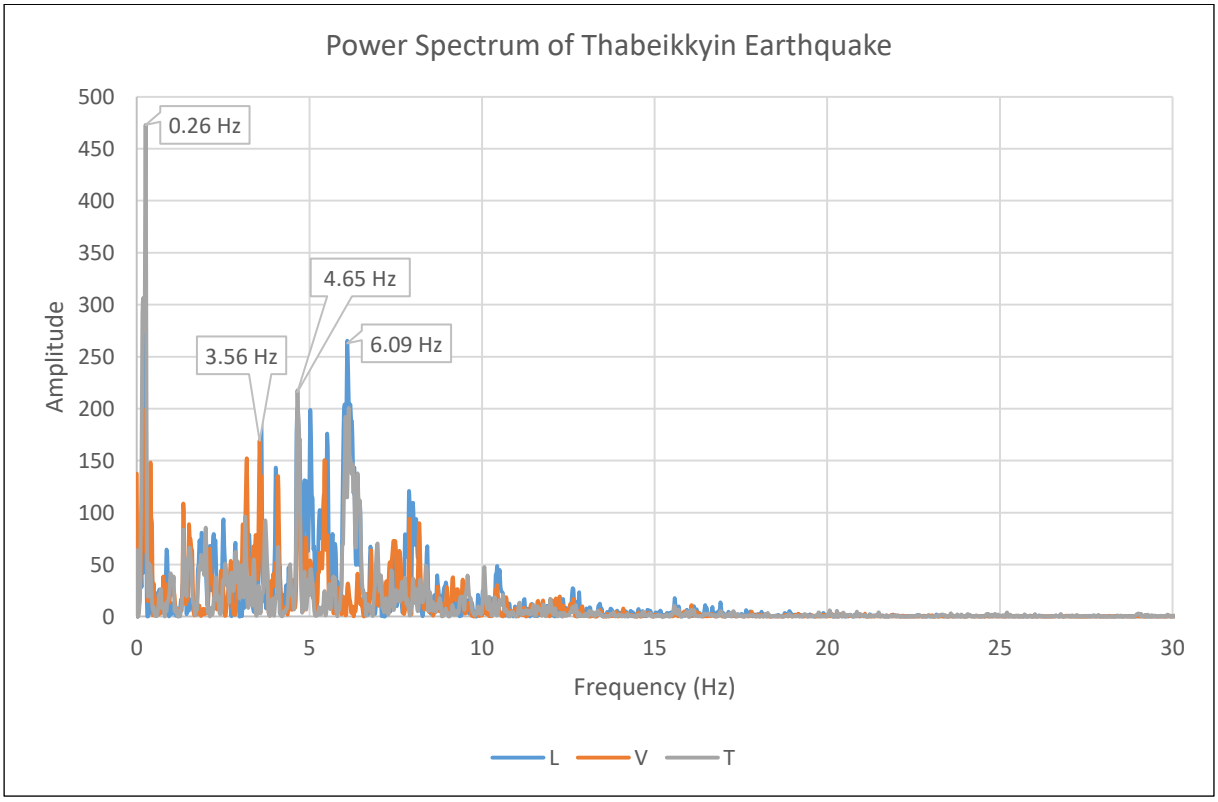

Figure 3.32: Power spectrum of Thabeikkyin Earthquake (2016).

3.5.2 Proposed Design Spectrum by Using Thabeikkyin Earthquake Data

Thabeikkyin Earthquake acceleration data used in this study was measured from the Mandalay station, which is one of the few seismic stations in Myanmar as well as the closest station to the epicenter about 100 km away [13]. As shown in Figure 3.4, the maximum acceleration values of the earthquake were measured as 26.39 gal in longitudinal direction and it is not large enough to use in the dynamic analysis of the FE bridge model in ABAQUS according to the Seismic Zone Map of Myanmar 2012 [14]. Therefore, for the purpose of using these data for the analysis of the case study bridge, the peak ground acceleration values of the original data are increased to 0.2 g and 0.4 g by multiplying with some factors.

Then, the response spectrum for modified earthquake is drawn for 5% damping ratio, and the design spectrum for the Ayeyarwady delta region (or similar regions with peak ground accelerations of 0.2g and 0.4g for Level I and II earthquakes) was proposed for level I and level II earthquakes as shown in Figure 3.33 based on Thabeikkyin Earthquake response spectrum and Seismic Zone Map of Myanmar (2012). It is just a preliminary proposal as an initiative for the emergence of the design standard for the construction of long span bridges in Myanmar and more research data is still necessary to prepare that kind of design spectrums.

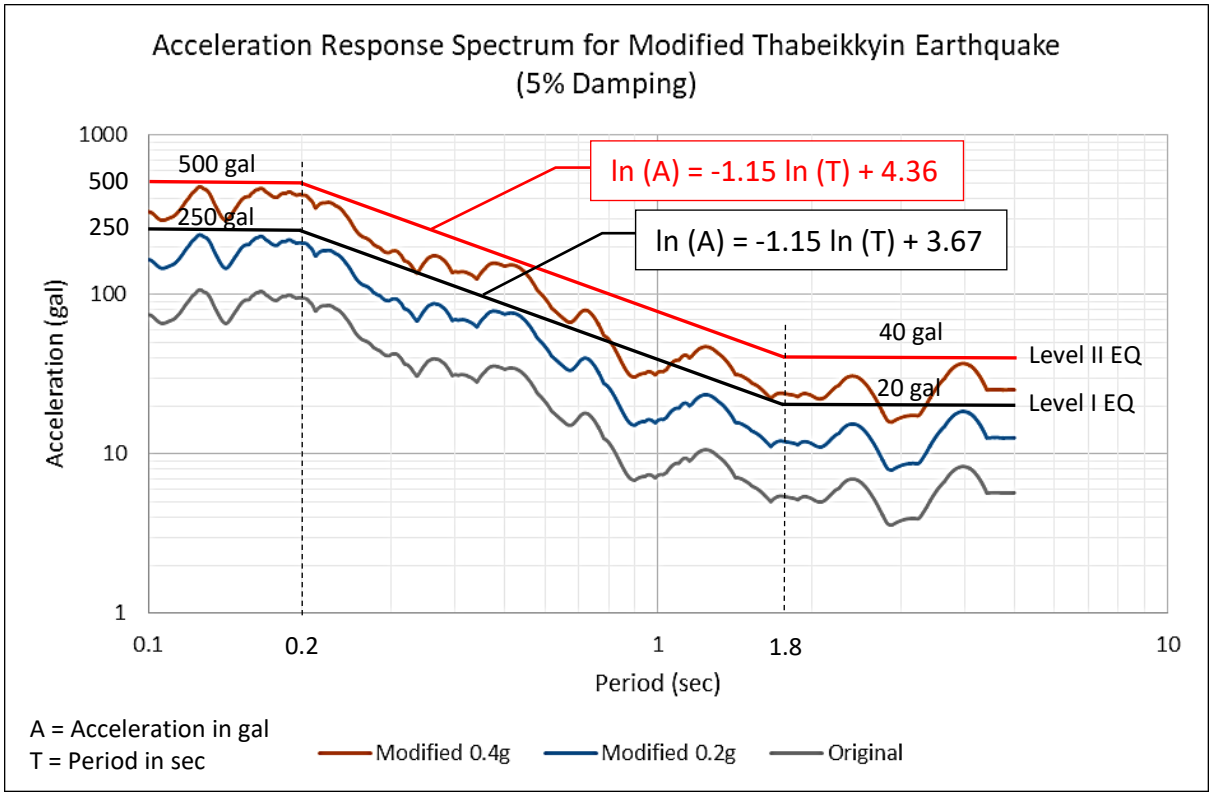

Figure 3.33: Response spectrum for modified Thabeikkyin Earthquake showing proposed design spectrums for Delta regions due to earthquakes along the Sagaing Fault.

3.6 Summary

Along with many local faults, there are two major seismic activities in Myanmar, Sagaing Fault and Sunda-Andaman Trench (also called Java Trench or Sumatra Trench). Many strong earthquakes had occurred in Myanmar during the past century on the Sagaing Fault and some local faults but Sunda-Andaman Trench caused many strong earthquakes mainly around the Sumatra and Java regions along Sumatra and Java segments frequently with great intensities.

As an academic study, linear and nonlinear response spectrums of single degree of freedom (S.D.O.F) systems were produced by writing FORTRAN programs based on Newmark's time-stepping method. Nonlinear spectrums were drawn for both elastoplastic and bilinear systems. Ductility and nonlinear response of S.D.O.F systems were also compared with linear systems by using the equal energy theorem and Thabeikkyin Earthquake data for three different normalized yield strengths. According to the results, it was found out that the ductility ratio (or ductility demand) of S.D.O.F systems increases but the resisting force decreases while decreasing the normalized yield strength.

In order to know the characteristics of earthquakes in Myanmar, Thabeikkyin Earthquake (2012) was chosen to study because it was the latest large earthquake on the Sagaing Fault and the ground motion data was recorded from Mandalay station, one of very few seismic stations in Myanmar. According to the Fourier and Power Spectrums of the earthquake, frequencies between 1 Hz to 10 Hz were dominant with the peak at 0.26 Hz and 0.19 Hz and, the maximum response acceleration occurred between 0.1 sec and 0.2 sec periods for different damping ratios according to the linear acceleration response spectrums. Moreover, the ground acceleration data of Thabeikkyin Earthquake from Mandalay station was modified in order to utilize it in the dynamic analysis of the FE bridge model in ABAQUS according to the increased possible ground acceleration values stated in Seismic Zone Map of Myanmar 2012.

The design spectrums for the Ayeyarwady delta region (or regions with peak ground accelerations of 0.2g and 0.4g) was also proposed for level I and level II earthquakes based on Thabeikkyin Earthquake response spectrum and Seismic Zone Map of Myanmar (2012). It is just a preliminary proposal as an initiative for the emergence of the design standard for the construction of long span bridges in Myanmar and more research data is still necessary to prepare that kind of design spectrums.

References

[1] Beck, M. W. et al., World Risk Report 2012, United Nations University, Institute for Environment and Human Security, 2012.

[2] Department of Population, The 2014 Myanmar Population and Housing Census – The Union Report (Volume 2), Ministry of Immigration and Population, Union of Myanmar, May 2015.

[3] Tint Lwin Swe, Earthquake Risk of Major Cities in Relation to Seismicity along Sagaing Fault, *3rd International Workshop on Seismo-tectonics in Myanmar and Earthquake Risk Management*, May 2011.

[4] Soe Thura Tun, The Sagaing Fault: A desk study report on seismo-tectonic implications in Myanmar, Myanmar Earthquake Committee, November 2005.

[5] Hla Hla Aung, Myanmar Earthquakes History, Wathan Press, Yangon, Myanmar, January 2015.

[6] https://en.wikipedia.org/wiki/Sunda_Trench

[7] Gupta, A.K., Response Spectrum Method in Seismic Analysis and Design of Structures, 1st edition, Blackwell Scientific Publications, 1990.

[8] Chopra, A.K., Dynamics of Structures, 4th edition, Prentice Hall, 2012.

[9] Clough, R.W., and Penzien, J., Dynamics of Structures, 3rd Edition, Computers & Structures, Inc., 2003.

[10] Igarashi, A., Nonlinear response and capacity design of Structures, Lecture Notes on Earthquake Engineering, Kyoto University, June 2016.

[11] SEEDS Asia, The 2012 Thabeikkyin Earthquake, Situation Report 1, November 2012.

[12] http://www.sagaingfault.info/

[13] Thiam, H. N., A Report on Upgraded Seismic Monitoring Stations in Myanmar: Station Performance and Site Response, *Seismological Research Letters*, Vol. 88(3), 2017.

[14] Myanmar Earthquake Committee, The Seismic Zone Map of Myanmar (2012), Union of Myanmar, 2012.

CHAPTER 4

Preliminary Finite Element Analysis of Maubin Bridge

4.1 Introduction

Maubin Bridge in Myanmar was constructed across the Myitmaka River, a branch of Ayeyarwady River, by the Ministry of Construction from 1994 to 1998, and it was inspected later in May 2012 because of the failure of movable bearings due to the tilting of approach span piers and abutment as a result of lateral earth pressure. Now, the bearings were already repaired, the abutment was demolished and new approach spans with steel plate girders were constructed on Maubin side in 2016. The bridge was originally designed with the assumed earthquake load of 0.1g according to AASHO 1977 [1] but the new Seismic Zone Map of Myanmar (2012) [2] stated the possible peak ground acceleration as 0.11 g ~ 0.2 g for the return period of 475 years and 0.21 g ~ 0.4 g for the return period of 2475 years [3]. Since similar types of long span steel truss bridges, mostly fabricated in China, were constructed in Myanmar after 1990, the performance of these bridges under the increased seismic loads should be evaluated again for the potential seismic retrofit.

4.2 Specifications of Maubin Bridge

Maubin Bridge, as shown in Figure 4.1 and 4.2 (a), is situated on the Myitmaka River, a branch of Ayeyarwady River in Maubin Township of the Ayeyarwady Region, which is the delta region of Myanmar forming with numerous rivers branched from the great Ayeyarwady. It was constructed by the Public Works under the Ministry of Construction in March 1994 and completed in February 1998. It is a 4 span continuous steel truss bridge with the main span length of 480 m (4 x 120 m) combined with 8 side spans, 4 on each side of the bridge having 240 m (8 x 30 m) length. The superstructure steel truss (12 m high warren trusses, each 10 m apart) of the bridge was designed and fabricated by China National Constructional and Agricultural Machinery Import and Export Corporation, Reconnaissance and Design Institute, Major Bridge Engineering Bureau, Ministry of Railways, People's Republic of China [4]. Some other superstructures such as prestressed concrete girders of side spans and all substructures including reinforced concrete piers, piles, pile caps and abutments were designed and constructed by the Public Works [5]. Steel bearing on pier P5 is a hinge or fixed bearing, and bearings on other piers are roller or movable bearings.

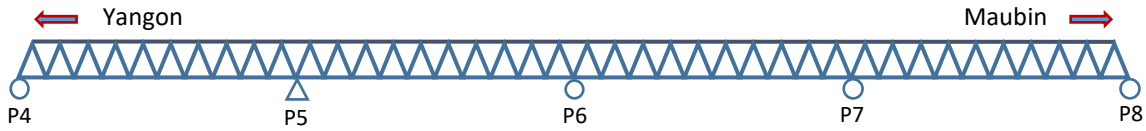

Figure 4.1: Sketch of Maubin Bridge showing roller and hinge supports over piers (P4 ~ P8).

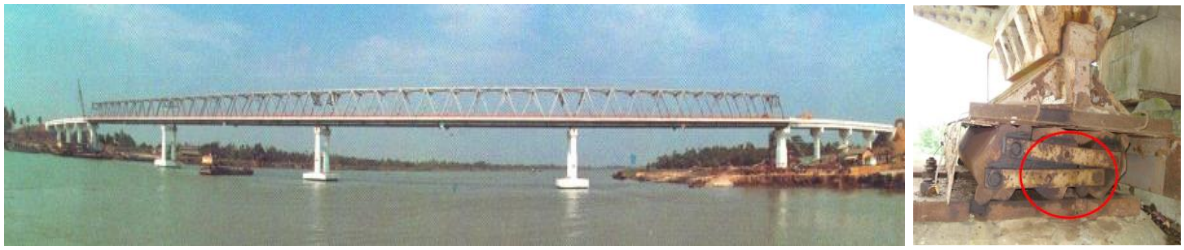

(a) (b)

Figure 4.2: (a) Side view of Maubin Bridge [5]; (b) Deformed shoes of Maubin Bridge [7].

The bridge was designed in accordance with the 12th edition of AASHO standard specifications of highway bridges [1] with the equivalent static load for the earthquake on the superstructure in vertical and horizontal directions as 10% of the dead load, meaning 0.1 g ground acceleration intensity applying on the bridge. Vehicular loads were to be applied as HS – 20 trucks (60 tons) at 10 m apart on the carriage way, and design wind velocity was assumed as 90 mph (40 m/sec). Main structural steel members were fabricated in China equivalent to the specification of GB 1591-88, 16 Mn with the yield strength (F_y) range of 325 MPa ~ 345 MPa and ultimate strength (F_u) range of 490 MPa ~ 640 MPa, depending upon the thickness of members. High strength tensile bolts conforming to GB/T 122B- 1231-91 were used with the recommended material as 20 Mn TiB. Steel bearings were also to be compliant with GB 11352-89 for the cast parts and with GB 699-88 for pins and rollers [4].

4.3 Background Problems

4.3.1 Requirements in the Construction and Maintenance of Long Span Bridges

There are three main background problems for choosing Maubin Bridge as a case study bridge for the research. The first one is concerned with the requirements in the construction and maintenance of long span bridges in Myanmar, especially for the bridges constructed after 1990. Bridges during these periods were constructed in limited construction time, materials and workmanship without almost any technical and financial assistance from foreign countries except from China. Although Myanmar engineers were trained by JICA experts for the design and construction of RC and PC girder bridges [6], they were not

familiar with the design and construction of long span steel bridges due to the lack of technology, in addition to the absence of steel production plants in Myanmar at that time.

Moreover, nearly half of these newly constructed bridges were built in the delta and coastal regions in order to develop road networks due to the location of numerous rivers within these areas. Therefore, corrosion of bridges due to the sea salt and the movement of bridge substructures on soft soil become some of the major maintenance problems. Maubin Bridge was also constructed in the Ayeyarwady delta region, where the soft soil is the major soil type and, hence, the abutments and foundations of the bridge are resting over the soft soil. In 2000, the abutment of the bridge on the Maubin side moved forward due to lateral earth pressure on its rear face and the bridge was pushed to the other side. As a result, the bridge piers become tilted (20 mm ~ 279 mm) and the bridge shoes, as shown in Figure 4.2 (b), are greatly deformed due to the horizontal shear force [5, 7].

4.3.2 Seismic Activities and Seismic Zone Map of Myanmar

Another problem is concerned with the seismic activities in Myanmar. Myanmar is one of the disaster prone countries in Southeast Asia with 51.5 million population and the population density of about 76 people/km^2, and most of the people are living along the central belts, delta regions and coastal areas [8]. Although there are some other local faults causing earthquakes in Myanmar, Sagaing Fault and Sunda-Andaman Trench, shown in Figure 4.3, are two main generators of great earthquakes according to the historical records as shown in Table 4.1. Sagaing Fault is an active fault running from the north to the south passing through the central region of Myanmar, and Sunda-Andaman Trench (also called Java Trench) is parallel to the Myanmar coastal line [9]. For example, one span of Yadana Theinga Bridge in Shwebo District of Sagain Region, a bridge being in construction, fell into the Ayeyarwady River during 2012 Thabeikkyin Earthquake (also called Shewbo Earthquake) [10].

Table 4.1: List of major earthquakes occurred in Myanmar

No.	Major Earthquakes occurred in Myanmar	Intensity (M_w)
1.	Arakan Earthquake (1762)	8.8
2.	Pyu Earthquake (1930)	7.3
3.	Myitkyina Earthquake (1931)	7.6
4.	Sagaing Earthquake (1956)	7.1
5.	Myanmar Earthquake (2011)	6.9
6.	Thabeikkyin Earthquake (2012)	6.8
7.	Myanmar Earthquake (2016)	6.8

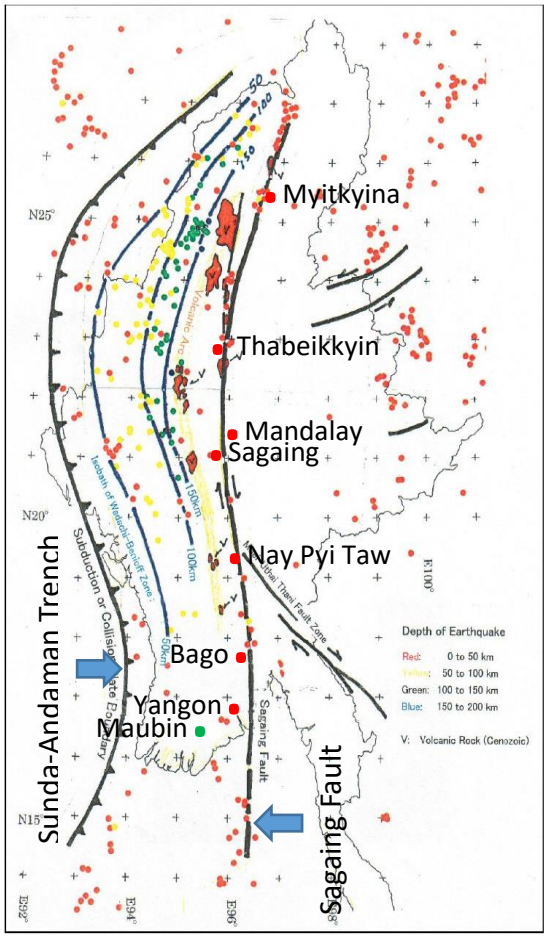

Figure 4.3: Seismic activity map of Myanmar.

(Source: Department of Meteorology and Hydrology, Myanmar)

In 2005, Myanmar Earthquake Committee issued the Seismic Zone Map of Myanmar [11] based on the deterministic and the probabilistic data, and classified five different zones according to the probable range of peak ground acceleration (PGA). According to this map, the Ayeyarwady delta region is within the moderate zone II with the expected ground acceleration of 0.1 g to 0.15 g while the regions along the Sagaing fault and the northern regions fall within zone III to V with 0.2 g to 0.5 g depending on locations. Based on more research data, Myanmar Earthquake Committee issued 2nd edition of the Seismic Zone Map of Myanmar in 2012 [12], as shown in Figure 4.4 and 4.5, with the updated values of possible PGA for 475 return period and 2475 return period (as Level I and Level II Earthquakes, JRA [3]). According to this maps, the expected PGA for Ayeyarwady delta region and Eastern region range from 0.11g to 0.2g for earthquakes with 475 year return period and from 0.21g to 0.4g for earthquakes with 2475 year return period. The expected PGA values for the regions along the Sagaing fault, and the northern regions vary from 0.2 g to greater than 0.6 g for 475 year return period, and from 0.41 g to greater than 1.0 g for 2475 year return period.

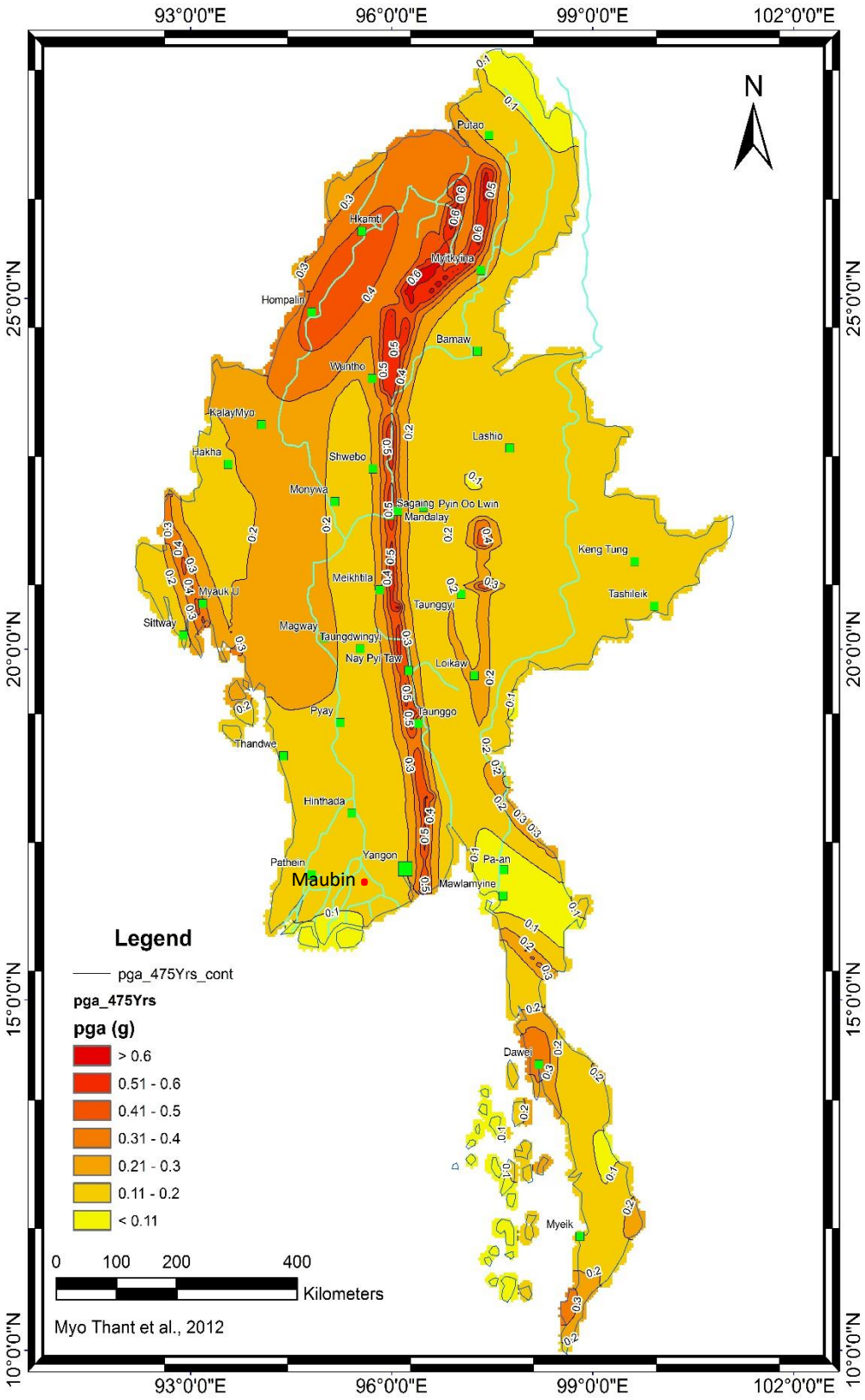

Figure 4.4: Seismic zone map of Myanmar (2012): 475 year return period [12].

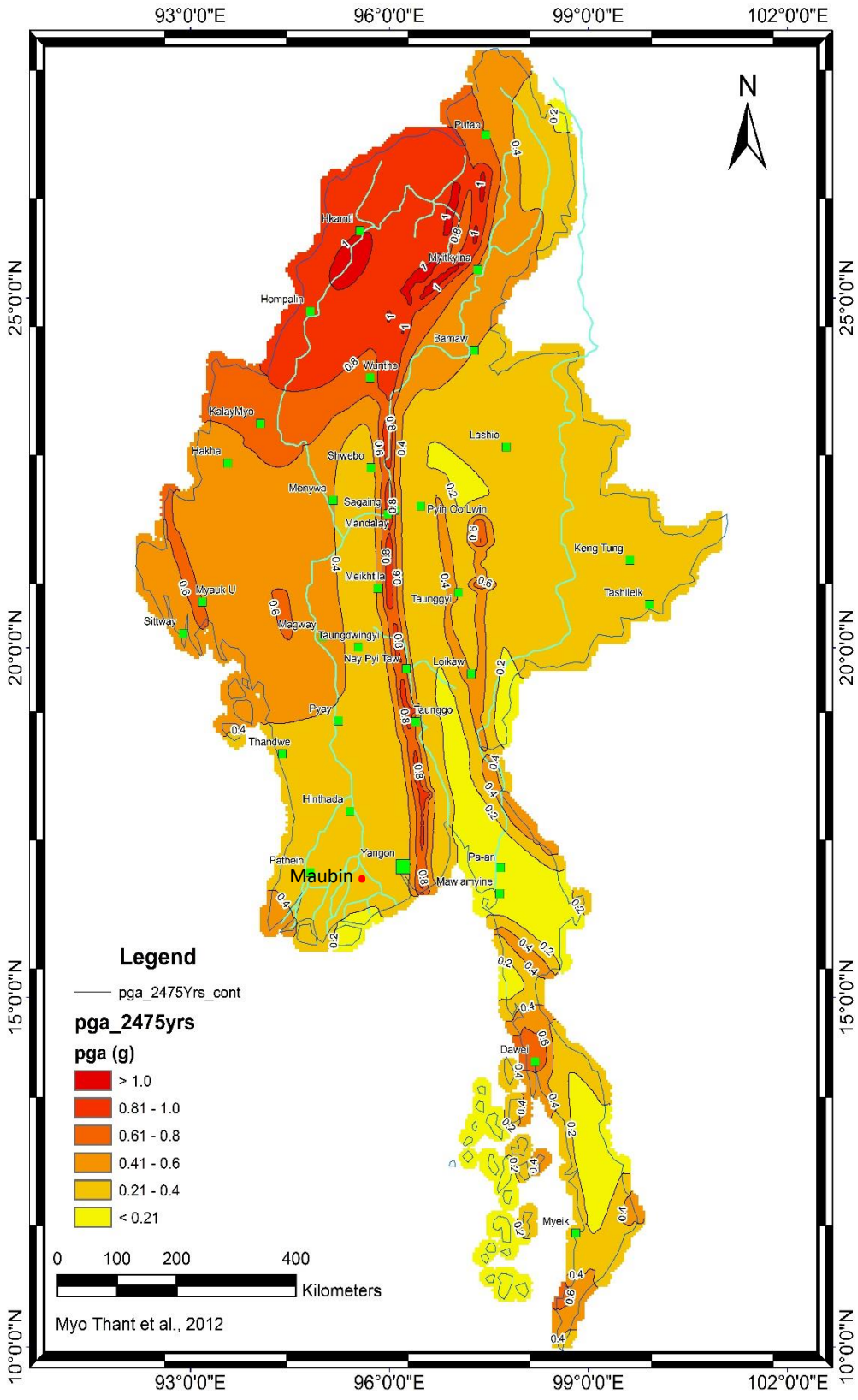

Figure 4.5: Seismic zone map of Myanmar (2012): 2475 year return period [12].

4.3.3 Assumption of Design Earthquake Load and Design Codes for Long Span Bridges

Maubin Bridge is located about 94 km away from the Sagaing Fault, which passes through near major cities like Yangon, Mandalay, Nay Pyi Taw, Bago and Sagaing. According to the 2012 Seismic Zone Maps of Myanmar [12], Maubin is located in the seismic zone where the possible ground acceleration is from 0.11 g to 0.2 g for the return period of 475 years and from 0.21 g to 0.4 g for the return period of 2475 years. However, the bridge was originally designed with the assumption of 0.1 g equivalent static load because there was no seismic zone map for Myanmar available at that time, and the 1st edition of Seismic Zone Map of Myanmar was issued only in 2005 by Myanmar Earthquake Committee.

For the design of long span bridges in Myanmar, bridge designers usually assumed the design earthquake load as 0.1 g due to the lack of sufficient data for Myanmar. Moreover, there are still no design codes and standards specifically issued for the design and construction of long span bridges in Myanmar except for Myanmar National Building Code (MNBC) which is just issued recently only for the residential buildings. MNBC was based on Uniform Building Code, ACI and ASCE Standards. Hence, the bridge designers in Myanmar often refer AASHTO and JRA standards for their design calculations which may not be suitable for Myanmar.

4.4 ABAQUS Modeling of Maubin Bridge

Maubin Bridge was designed and constructed before the Seismic Zone Map of Myanmar was first issued in 2005 with the design earthquake load of 0.1 g but the expected peak ground acceleration is 0.11 g ~ 0.2 g for the return period of 475 years and 0.21 g ~ 0.4 g for the return period of 2475 years according to 2012 Seismic Zone Map of Myanmar. Hence, the bridge was reanalyzed by using the commercial finite element software (ABAQUS) in order to check the response of the bridge according to the current data of increased seismic loads.

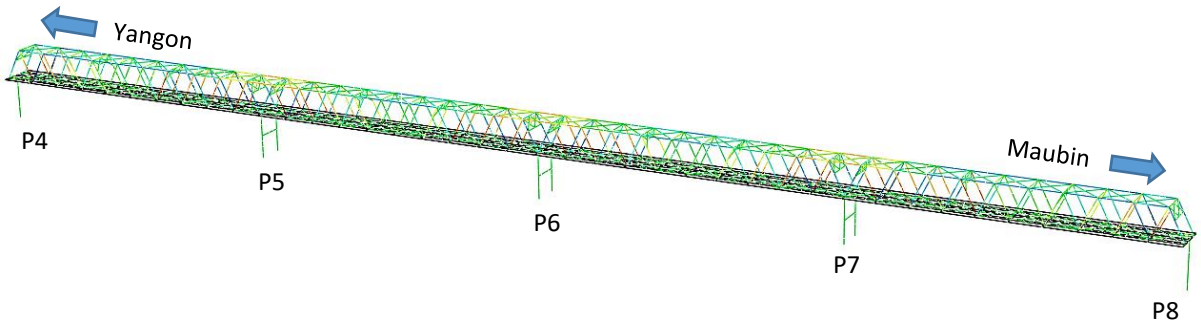

Figure 4.6: ABAQUS model of Maubin Bridge

Based on the original drawings of the bridge [4], the bridge model shown in Figure 4.6 was divided into (6) different parts without the piers: main truss of 318 members; floor system of 523 members; top bracing of 188 members; bottom bracing of 160 members; portal frames of 7 members and 10 members; and bridge decks, consisting of main deck for the traffic and side deck for the pedestrian. Connections between each part was done by tied connection or rigid connection. 3D planar shell elements (S4R) were used for the decks, and 3D beam elements (B31) are used for other parts [13].

According to the drawings, there were a total of 76 cross sections of members grouped into 3 main categories – 12 box sections for the top chord, 61 H sections for the bottom chord, diagonals, top and bottom bracings, and floor system, and 3 T-sections for the portal frames. Interior stringers of the floor system were truss members composed of angles, and only top and bottom members of inner stringers were considered in the model neglecting the diagonal members. Modulus of elasticity, density and Poisson's ratio for the materials were taken as 200 GPa, 7850 kg/m^3 and 0.3 for steel, and 30 GPa, 2400 kg/m^3 and 0.2 for concrete. Mesh size was taken as 0.6 m for the truss members and 0.5 m ~ 0.75 m for other parts.

4.5 Influence Lines for the Truss

Influence lines of the bridge truss shown in Figure 4.7 were drawn for each of the truss members by using ABAQUS software in order to point out the critical members and control loading positions in 2D truss configuration. Truss members were numbered starting from Pier P4 towards P8 (from Yangon side to Maubin side) in the figures. To draw the influence line diagrams, a 2D truss model was constructed and a unit point load is applied at each panel point for half of the four span continuous truss due to its symmetry, and evaluate the bar force for each of top chords, bottom chords and diagonal members.

According to the influence line diagrams, top chords in the middle spans were critical compression members, and lower chords in the middle spans were critical tension members while diagonal members possess smaller axial forces than both top and bottom chord members. However, in actual 3-D analysis, diagonal members, such as D13 where a transverse portal frame was attached as a bracing for lateral forces, suffer much higher tensile stresses than bottom chords due to the presence of portal frames, and member end moments. On the other hand, diagonals over the end supports (such as D1) and near inner supports (such as D18) showed much higher compressive stresses than top chords. In accordance with the influence line diagrams, top chords over the support and diagonals near the support showed higher tensile stresses than lower chords, under the design loads.

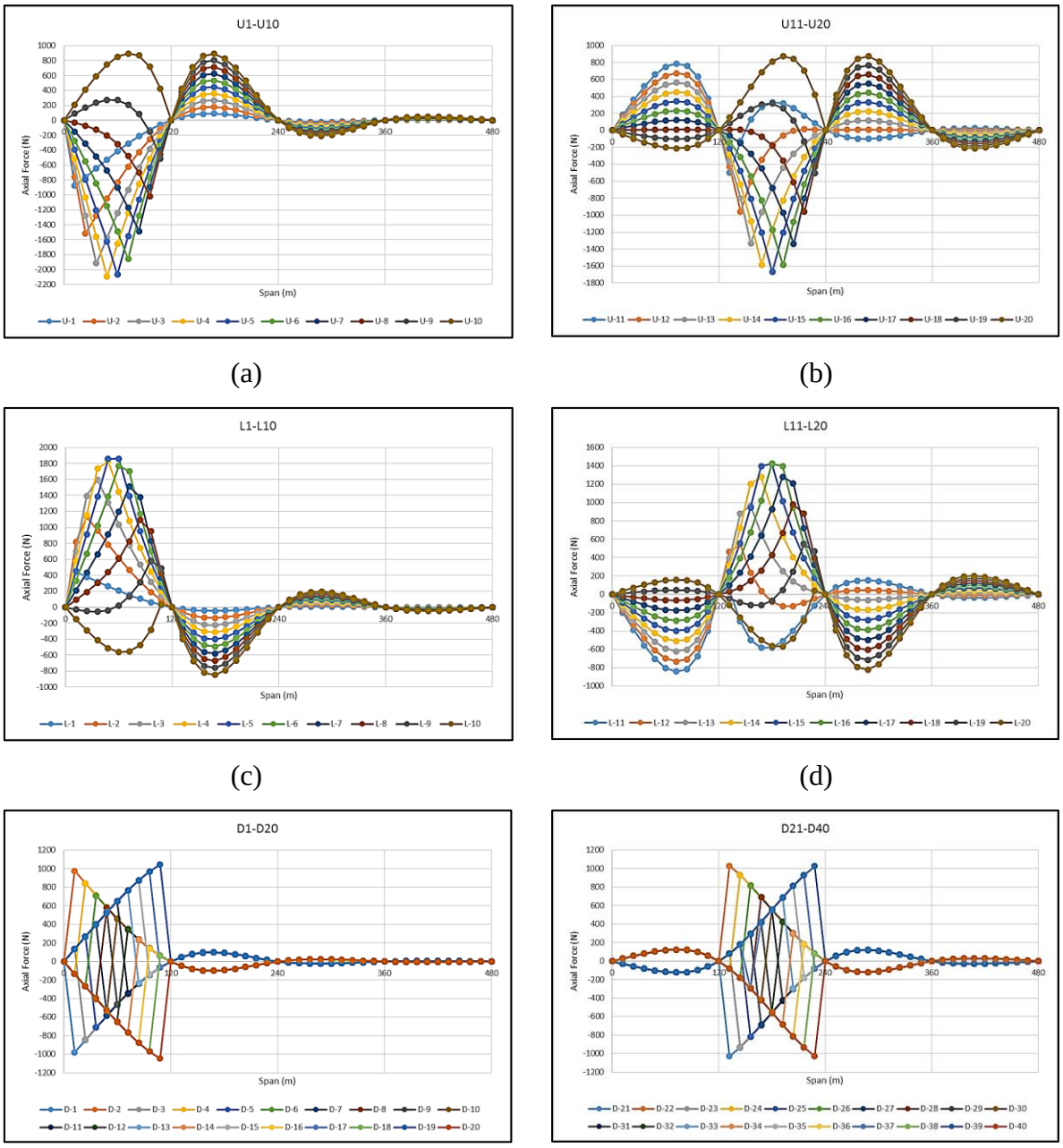

Figure 4.7: Influence lines for: (a) Top chords U1 ~ U10; (b) Top chords U11 ~ U20; (c) Bottom chords L1 ~ L10; (d) Bottom chords L11 ~ L20; (e) Diagonals D1 ~ D20; (f) Diagonals D21 ~ D40.

4.6 Application of Design Loads

Since Maubin Bridge was designed and fabricated by Reconnaissance and Design Institute of China, and design calculation sheets for the steel truss members were not available from the Public Work, the tender document for the bridge was referred to confirm the design loads for the bridge. According to the tender documents, the bridge was designed referring to the 12th edition of Standard Specifications for Highway Bridges by AASHO [1]. However, as

the 12th edition was not available as a reference for the study, 11th edition of Standard Specifications for Highway Bridges [14] was taken as the reference where 9 different load combinations were described for the design loads as shown in Table 4.2. Among them, load combinations (I, II and VII) were chosen to apply dead loads (D), vehicular live loads (L), pedestrian live loads (L), impact loads (I), wind loads (W) and earthquake loads (EQ) for the analysis of superstructure steel truss. Load factors of 1, 1.25 and 1.333 were used for dead load plus live load and impact loads, dead load plus wind loads, and dead load plus earthquake loads, respectively.

Table 4.2: Design load combinations according to AASHO 1973 [14]

Group	Load Combination	% of Unit Stress
I	D + L + I + E + B + SF	100%
II	D + E + B + SF + W	125%
III	Group I + LF + F+ 30% W + WL + CF	125%
IV	Group I + R + S + T	125%
V	Group II + R + S +T	140%
VI	Group III + R + S + T	140%
VII	D + E + B + SF + EQ	133⅓%
VIII	Group I + ICE	140%
IX	Group II + ICE	150%

Vehicular live loads were applied as HS 20-44 trucks spaced at 10 m apart placed on the bridge deck model from which the loads were transferred to the trusses through the floor system. Then, the loads were moved 12 m at a time to get various load configurations because the spacing of truss panel points was 12 m. According to AASHO 1973, impact load was calculated as 10% of live load, and wind loads in transverse direction were taken as 75 psf (3591 Pa) for the truss members and 50 psf (2394 Pa) for the floor beams with the design wind speed of 90 mph (40 ms^{-1}). Original design earthquake load was given as 0.1g (10% of dead load) but additional increased earthquake loads of 0.2 g and 0.4 g (20% and 40% of dead load) were also considered for X (longitudinal), Z (transverse) and Y (vertical) directions in order to take account of increased seismic demands from 2012 Myanmar Seismic Zone Map.

4.7 Results from Static Load Combinations and Pushover Analysis

In order to check the performance of the bridge in the preliminary stage, both the static analysis and pushover analysis with explicit method were performed on the bridge model. Static analysis was done by using design load combinations and increased earthquake loads of 0.2 g and 0.4 g. Pushover analysis was done by applying the own weight of the bridge plus unfactored earthquake loads of 0.1 g, 0.2 g and 0.4 g (as 10%, 20% and 40% of own weight) for 3 second duration in X (longitudinal), Y (vertical) and Z (transverse) directions of the bridge using explicit method.

4.7.1 Allowable Strength of Members and Deflection Limit

According to AASHO 1973 [14], the allowable stresses for tension and compression members were defined as 0.55 F_y or 0.46 F_u and the allowable deflection for the truss due to live load plus impact load was limited to span/800, which was 150 mm for the Maubin Bridge. According to the analysis results obtained from FE bridge model, the maximum deflection due to live load plus impact load was obtained as 57.5 mm, which was less than the allowable deflection (150 mm) specified in AASHO 1973. Since the yield strengths (F_y) of members according to the Chinese specifications were described in the drawings [4] as 345 MPa (for thickness $\leq$ 16 mm), 325 MPa (for 16 mm < thickness $\leq$ 25 mm) and 315 MPa (for thickness > 25 mm) based on member thickness [2], the allowable stresses for the bridge truss members became 189.75 MPa, 178.75 MPa and 173.25 MPa respectively.

4.7.2 Results from Static Load Combinations

According the static analysis of FE bridge model, diagonals suffered much higher tensile and compressive stresses than both top and bottom chords, in contrast to influence line diagrams of 2D truss. The maximum stresses under the static loading combinations were shown in Table 4.3, and the stresses highlighted in red were overstress values. Among the design load combinations being considered, stresses due to the wind load was the greatest, especially in compression diagonal members, such as D80, where the overstress value is -251.4 MPa. The stresses due to live load and impact load combinations were higher in the tension diagonal members, such as D13 and D68, where 212.2 MPa overstress occurred.

Under the design earthquake load combination (0.1 g in X, Y and Z directions), all the member stresses were within allowable stresses except for some tension diagonal members, such as D13 and D68, where the stresses are marginally higher than the allowable stresses.

For the increased earthquake load combination of 0.2 g, maximum over stresses occurred in tension diagonal members, such as D13, due to the earthquake in Y direction, as well as in some top chords over the support. Under the earthquake load 0.2 g in Z direction, over stresses occurred in end compression diagonal members, such as D80. No over stresses occurred in members due to the 0.2g earthquake in X direction.

Among the increased earthquake load combination of 0.4 g, maximum over stresses occurred in end compression diagonal members, such as D1 and D80, due to the earthquake in Z direction. Under the earthquake load 0.4 g in Y direction, over stresses occurred in both tension and compression diagonal members, such as D13 and D80, as well as in some top chords, such as U10. For the earthquake load 0.4 g in X direction, over stresses occurred in tension diagonal members, such as D13. Figures showing maximum stresses for different static loading cases from the ABAQUS analysis results were shown in Figures 4.8 to 4.15.

Table 4.3: Maximum stresses in members due to static loading combinations.

Sr.	Load Combination (AASHTO 1973)	Top Chord		Bottom Chord	Diagonal	
		Over Support	Mid Span		Tension	Compression
1.	D + L + I (10% of L)	163.0	-138.4	52.1	212.2	-162.6
2.	1.25D + 1.25W	113.2	-103.5	57.8	153.9	-251.4
3.	1.33D + 1.33EQX (0.1g)	147.3	-125.4	48.5	180.4	-141.1
4.	1.33D + 1.33EQY (0.1g)	159.2	-134.8	49.6	194.0	-152.7
5.	1.33D + 1.33EQZ (0.1g)	143.9	-128.3	57.7	178.2	-169.1
6.	1.33D + 1.33EQX (0.2g)	149.8	-124.5	47.8	184.4	-141.3
7.	1.33D + 1.33EQY (0.2g)	173.6	-147.0	54.1	211.6	-166.5
8.	1.33D + 1.33EQZ (0.2g)	143.6	-129.4	66.3	177.6	-198.6
9.	1.33D + 1.33EQX (0.4g)	154.9	-128.5	70.7	192.3	-145.5
10.	1.33D + 1.33EQY (0.4g)	202.7	-174.2	66.0	246.9	-195.4
11.	1.33D + 1.33EQZ (0.4g)	150.5	-138.7	90.2	183.5	-257.5
Allowable Stresses		173.3	-178.8	173.3	189.8	-178.8

Note: Yield stress varies from 315 MPa to 345 MPa.

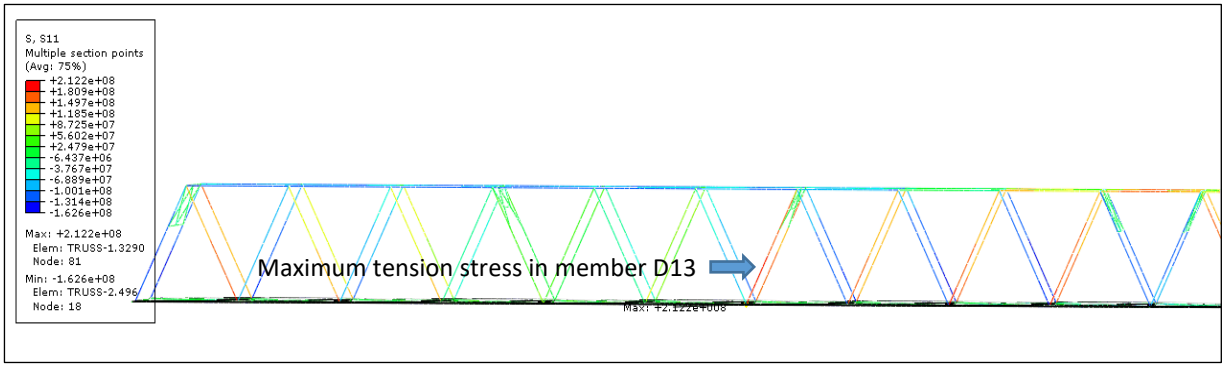

Figure 4.8: Maximum stresses under D + L + I static load combination.

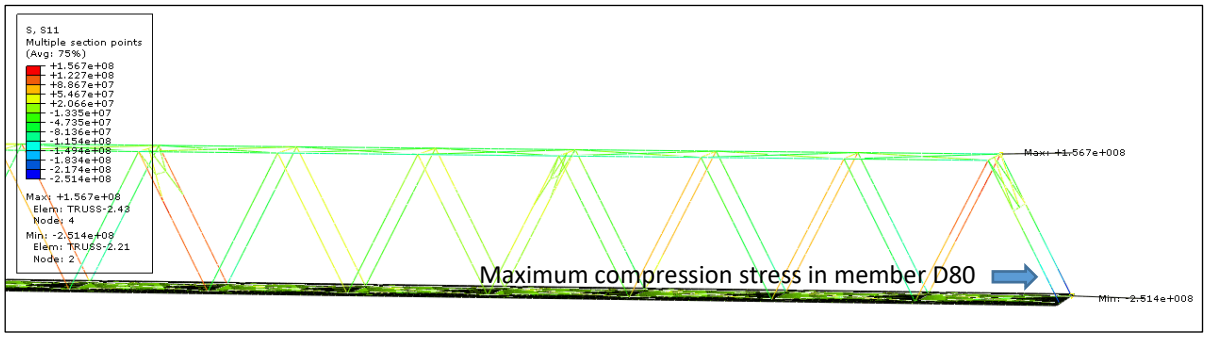

Figure 4.9: Maximum stresses under 1.25D + 1.25W static load combination.

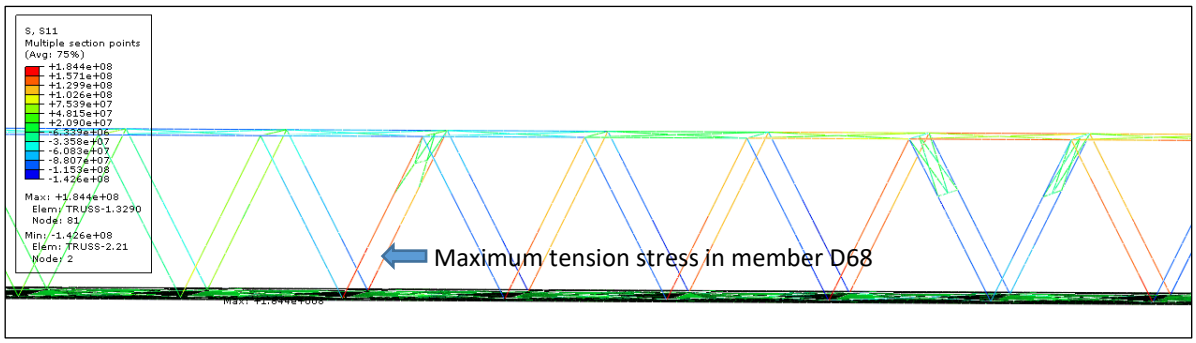

Figure 4.10: Maximum stresses under 1.33D + 1.33EQX (0.2g) static load combination.

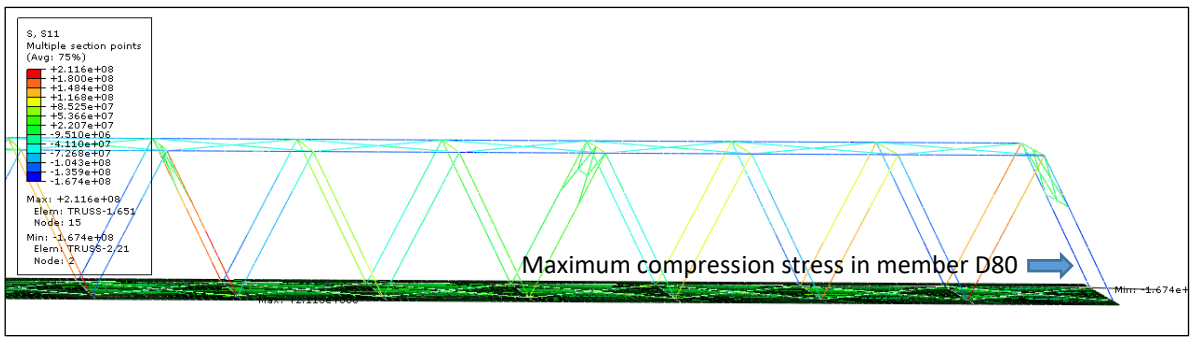

Figure 4.11: Maximum stresses under 1.33D + 1.33EQY (0.2g) static load combination.

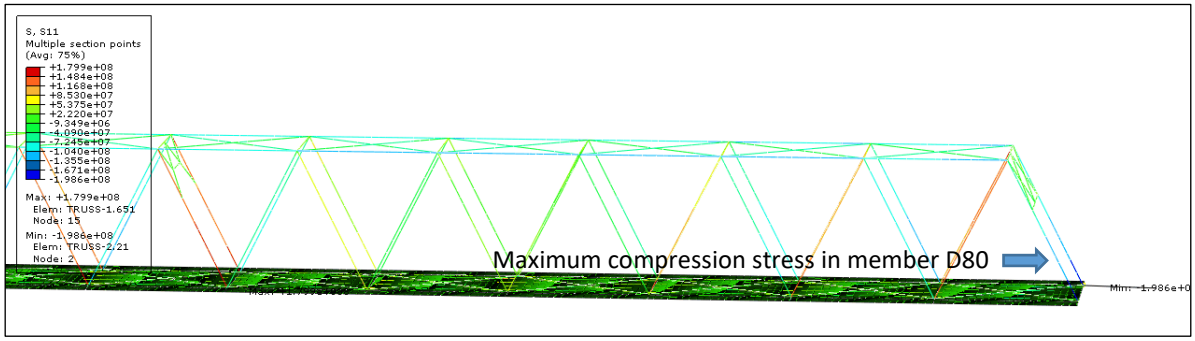

Figure 4.12: Maximum stresses under 1.33D + 1.33EQZ (0.2g) static load combination.

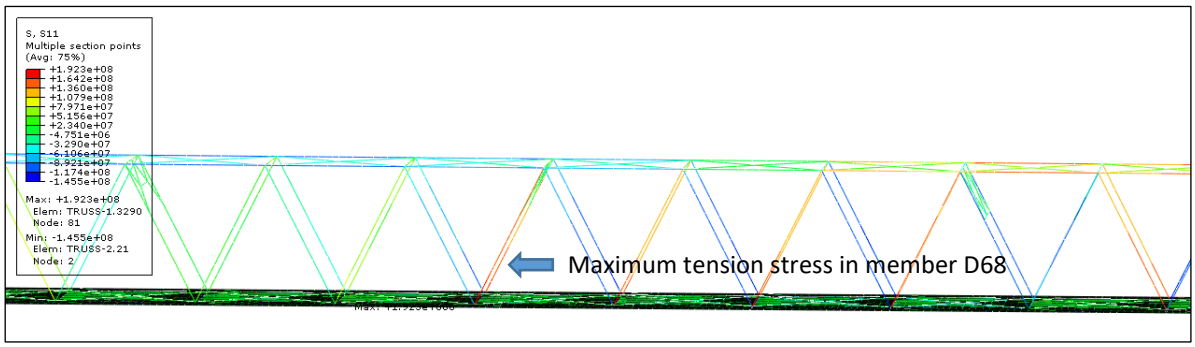

Figure 4.13: Maximum stresses under 1.33D + 1.33EQX (0.4g) static load combination.

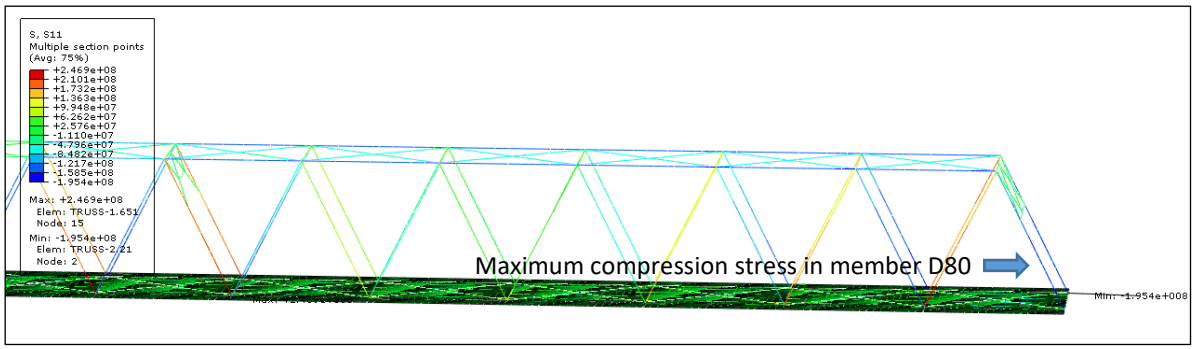

Figure 4.14: Maximum stresses under 1.33D + 1.33EQY (0.4g) static load combination.

Figure 4.15: Maximum stresses under 1.33D + 1.33EQZ (0.4g) static load combination.

4.7.3 Results from Pushover Analysis

The FE bridge model was also run by pushover analysis with explicit method under the own weight of the bridge plus unfactored earthquake load of 0.1 g, 0.2 g and 0.4 g for 3 second duration in each direction, and the results were shown in Table 4.4. The results showed that over stresses, highlighted in red, occurred in most of top chords and diagonal members except for the bottom chords for all load cases. Some stresses were even higher than yield stresses in compression diagonals under 0.4 g earthquake in transverse direction and maximum stresses for different dynamic loading cases from the ABAQUS analysis results were shown in Figures 4.16 to 4.21.

Table 4.4: Maximum stresses in members due to pushover analysis.

Sr.	Load Combination (unfactored)	Top Chord		Bottom Chord	Diagonal	
		Over Support	Mid Span		Tension	Compression
1.	DL + EQX (0.1g)	203	-176	74	262	-186
2.	DL + EQY (0.1g)	219	-193	78	283	-204
3.	DL + EQZ (0.1g)	198	-180	78	255	-216
4.	DL + EQX (0.2g)	208	-179	77	268	-189
5.	DL + EQY (0.2g)	239	-211	84	310	-223
6.	DL + EQZ (0.2g)	198	-186	94	254	-266
7.	DL + EQX (0.4g)	215	-182	113	281	-203
8.	DL + EQY (0.4g)	277	-243	104	351	-270
9.	DL + EQZ (0.4g)	203	-195	138	263	-385
Allowable Stresses		173	-179	173	190	-179

Note: Yield stress varies from 315 MPa to 345 MPa.

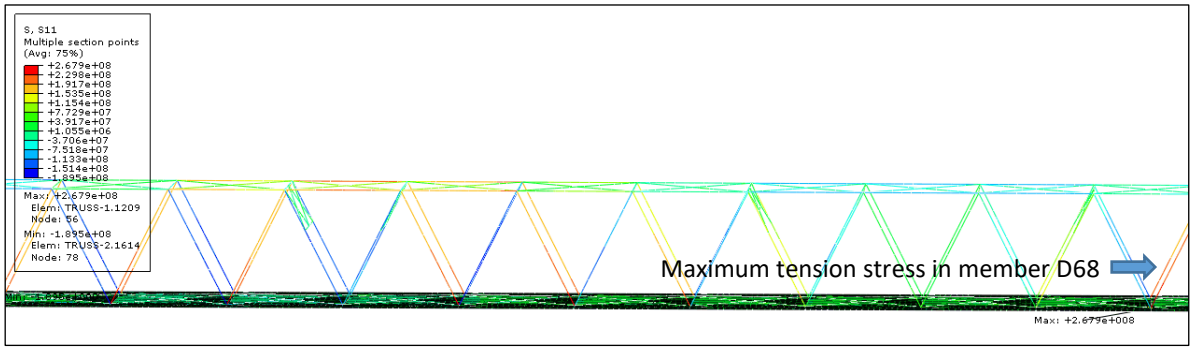

Figure 4.16: Maximum stresses under DL + EQX (0.2g) pushover analysis.

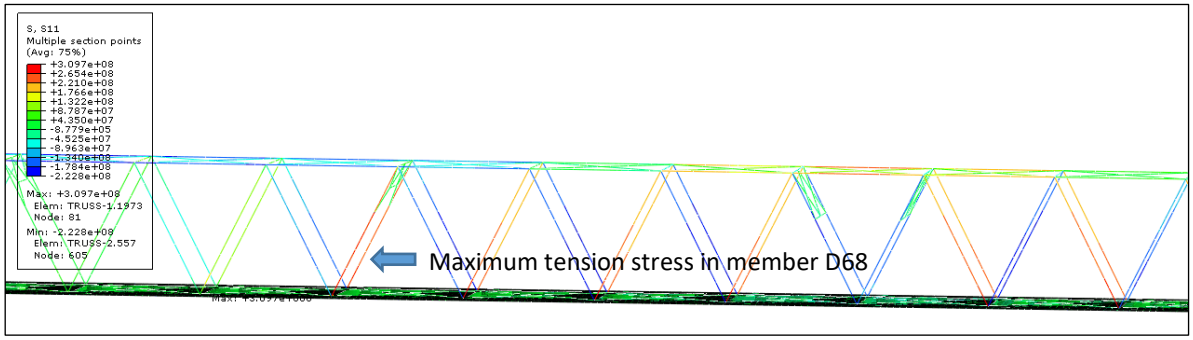

Figure 4.17: Maximum stresses under DL + EQY (0.2g) pushover analysis.

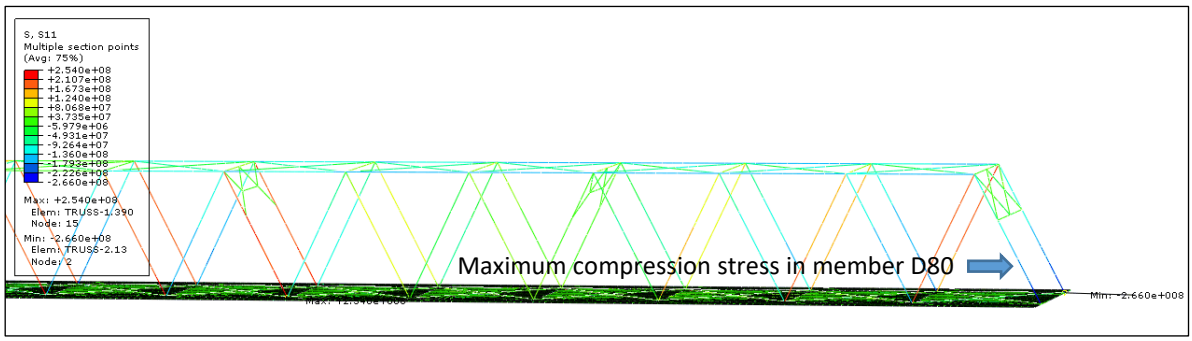

Figure 4.18: Maximum stresses under DL + EQZ (0.2g) pushover analysis.

Figure 4.19: Maximum stresses under DL + EQX (0.4g) pushover analysis.

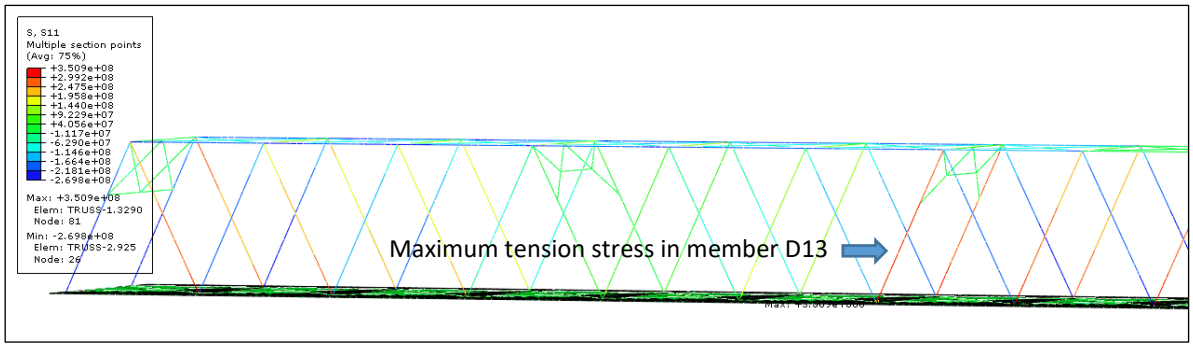

Figure 4.20: Maximum stresses under DL + EQY (0.4g) pushover analysis.

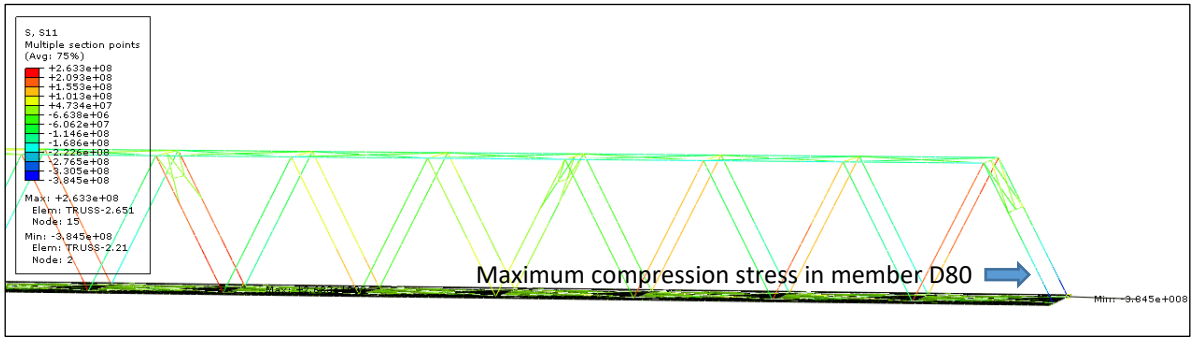

Figure 4.21: Maximum stresses under DL + EQZ (0.4g) pushover analysis.

4.8 Substructure of the Bridge and Earthquake Resistance of Pile Foundation

The substructure of the main bridge was composed of reinforced concrete piers, RC cast-in-situ piles (bored piles) and pile caps. End piers (P4 and P8) for the main truss were single column piers built on 2.8 m thick pile caps, each of which were supported by 8 Nos. x 1.8 m Φ piles each 34 m long as shown in Figure 4.22. However, middle piers (P5, P6, P7) are 15.5 m high double column piers, which were supported by 2.8 m thick pile caps with 12 Nos. x 1.8 m Φ piles each 45 m long as shown in Figure 4.23. Single column piers had hexagonal shape cross section with 2.5 m x 5.5 m largest dimensions in the breadth and in the width. Double column piers had 3 m Φ cross section until the mid-height where the cross section changes to 2.5 m Φ. Piers were then braced by (1 m x 1.5 m) cross beam at mid-height and (3 m x 2 m) cross beam at the top.

In order to check the performance of pile foundation of the bridge during the earthquake, the capacity of piles under the fixed pier (P5) was compared with the pile loads coming from the pier due to different earthquake loads. From the analysis results of the FE bridge model, the maximum load for each pile under the fixed pier (P5) due to the design earthquake load (0.1 g) in the longitudinal direction of the bridge was evaluated as 7140 kN but increased to 10836 kN for 0.2 g earthquake and 18180 kN for 0.4 g earthquake. On the other hand, the resistance of each pile and pile group capacity is checked by using α, β, λ, and SPT Methods according to AASHTO 2004 guide lines [15] and the calculations were annexed in Appendix C. These methods were semi-empirical methods to estimate the resistance of piles from undrained shear strength, effective vertical stress and number SPT blow count.

Since the detail soil test data is not available except for some borehole profile with N values, the resistance of piles are evaluated from assumed soil properties. Assuming the undrained shear strength of soil as 100 kN/m^2, unit weight of soil as 20 kN/m^3, $\alpha = 0.7$, $\beta = 0.3$, $\lambda = 0.13$, and N = 50 blows/ft, the resistance of each pile is calculated as 11302 kN, 11744 kN, 9142 kN and 7660 kN respectively for α, β, λ, and SPT Methods, and these values

are just over the applied load (7140 kN) coming from the pier. When the earthquake load is increased from 0.1g to 0.2g or 0.4g, the maximum load coming from P5 for each pile will increase from 7140 kN to 10836 kN or 18180 kN and the resistance of piles against the earthquake cannot be assured anymore. However, for block failure check of the piles, the resistance of piles as a group is 154,879 kN and is much larger than the total applied load [57,606 kN for 0.1 g (or) 73720 kN for 0.2 g (or) 105808 kN for 0.4 g] coming from the pier.

In Maubin Bridge, the piles under the middle double column piers were arranged within the pile cap in such a way that there are (4) rows of piles in the transverse direction of the bridge along which all piers will share the earthquake load as shown in Figure 4.23 (b). However, there were only (3) rows of piles in the longitudinal direction of the bridge along which only the fixed pier (P5) will resist the earthquake force. Therefore, earthquake resistance of the bridge in the longitudinal direction was relatively weaker than that in the transverse direction. Moreover, unlike plate girder bridges which usually have multiple rows of supports for each of the girders, truss bridges like Maubin Bridge consist of only two rows of supports for each of the trusses. Hence, the bridge may be prone to fall off from the bridge piers if an earthquake comes laterally from the transverse direction of the bridge.

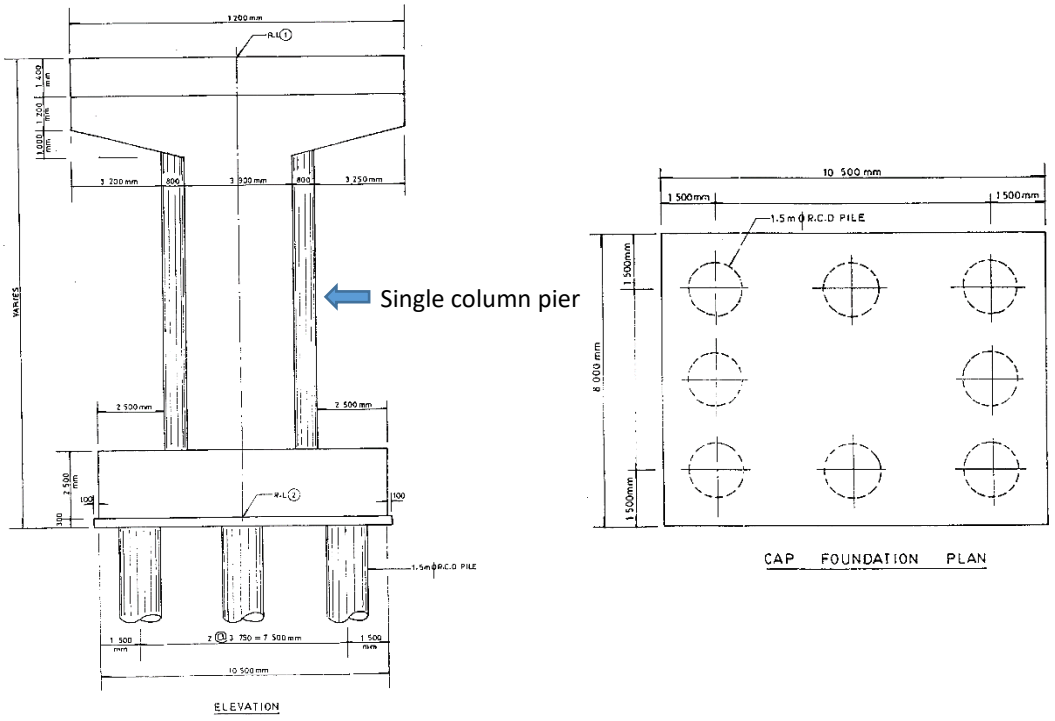

(a) (b)

Figure 4.22: (a) Single column pier P4 and P8; (b) Pile cap under pier P4 and P8.

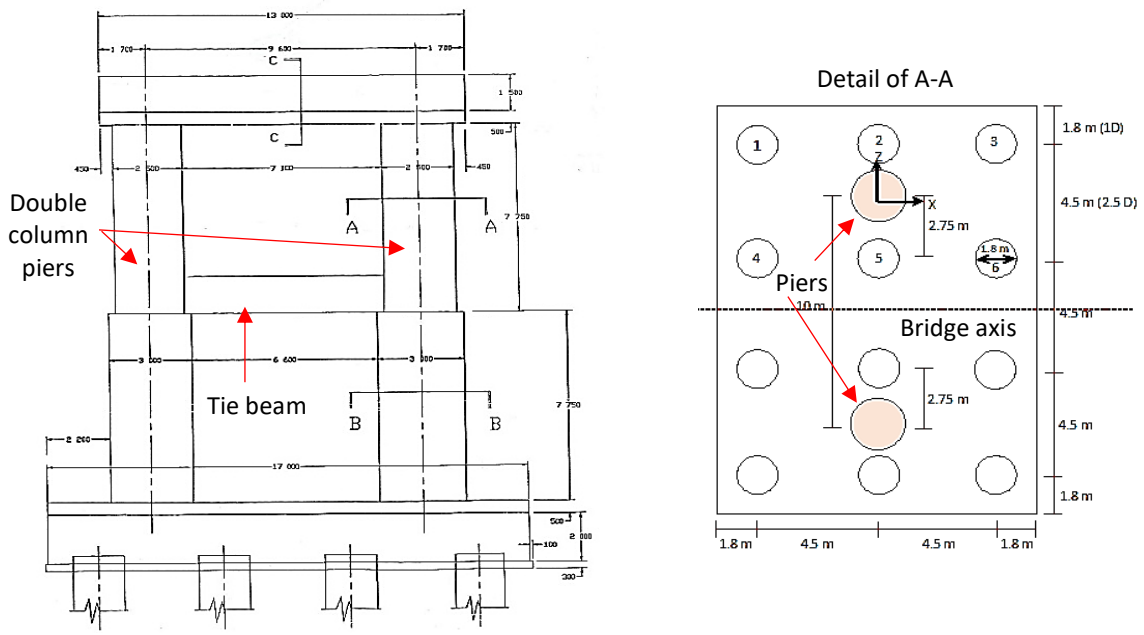

(a) (b)

Figure 4.23: (a) Double column pier P5 ~ P7; (b) Pile cap under pier P5 ~ P7.

4.9 Summary

The case study bridge, Maubin Bridge, was initially designed with the assumed earthquake load of 0.1g as an equivalent static load and opened to public in 1998. However, the new seismic zone map of Myanmar (2012) stated the possible peak ground acceleration as 0.11 g ~ 0.2 g for the return period of 475 years and 0.21 g ~ 0.4 g for the return period of 2475 years. Hence, the performance of the bridge under the increased seismic loads was urgently evaluated for the potential seismic retrofit because long span steel truss bridges of similar type were constructed in Myanmar after 1990, and the results were reported in the German-Japan Bridge Symposium at Osaka Institute of Technology in August 2016 [16].

Static analysis results showed that the design wind load and increased seismic loads of 0.2 g and 0.4 g caused the overstresses mostly in diagonal members except for some overstresses in top chords over the support due to the earthquake in vertical (Y) direction but no overstresses occurred in bottom chords. Results from pushover analysis with explicit method showed that over stresses occurred in top chords and diagonal members except in bottom chords due to unfactored seismic loads of 0.1g, 0.2g, 0.4g. Moreover, it is also verified that when the earthquake load is greater than 0.1g, the resistance of piles against the earthquake cannot be assured anymore, and the earthquake resistance of the bridge in the longitudinal direction is relatively weaker than that in the transverse direction. The bridge may also be prone to fall off from the bridge piers if an earthquake comes laterally from the transverse direction of the bridge.

References

[1] AASHO, Standard Specifications for Highway Bridges, 12th edition, American Association of State Highway and Officials, 1977.

[2] Myanmar Earthquake Committee, The Seismic Zone Map of Myanmar (2012), Union of Myanmar, 2012.

[3] JRA, Specification for Highway Bridges – Part V Seismic Design, Japan Road Association, March 2002.

[4] Reconnaissance and Design Institute, Working Drawings for Steel Truss Bridge (Maubin, Myanmar), Major Bridge Engineering Bureau, Ministry of Railways, Wuhan, China, June 1996.

[5] Public Works, Inspection of Maubin Bridge for Repair, Inspection Report, Ministry of Construction, Union of Myanmar, September 2014.

[6] JICA, Research Study on Review and Application of the Bridge Engineering Training Center Project in Myanmar, Final Report, Japan International Cooperation Agency, September 2012.

[7] JIP, "Current Situation and Issues of Myanmar's Bridge Work", Situation Report, Japan Infrastructure Partners, Japan, 2012.

[8] Department of Population, The 2014 Myanmar Population and Housing Census – The Union Report (Volume 2), Ministry of Immigration and Population, Union of Myanmar, May 2015.

[9] Kyaw Kyaw Lin, Seismic and Tsunami Activities in Myanmar, JICA Training Course, Nagoya University, Japan, July 2007 – March 2008.

[10] SEEDS Asia, The 2012 Thabeikkyin Earthquake, Situation Report 1, November 2012.

[11] Myanmar Earthquake Committee, The Seismic Zone Map of Myanmar (2005), Union of Myanmar, 2005.

[12] Myanmar Earthquake Committee, The Seismic Zone Map of Myanmar (2012), Union of Myanmar, 2012.

[13] Dassault Systems, Getting Started with ABAQUS, Version 6.14, 2014.

[14] AASHO, Standard Specifications for Highway Bridges, 11th edition, American Association of State Highway and Officials, 1973.

[15] AASHTO, LRFD Bridge Design Specifications, SI Units, 3rd edition, American Association of State Highway and Transportation Officials, 2004.

[16] Khin Maung Zaw, Suzuki, Y., Matsumura, M. and Sugiura, K., Analysis of Maubin Bridge in Myanmar for Seismic Retrofit, *Proceedings of the 11th German-Japan Bridge Symposium*, Osaka Institute of Technology, Japan, 29 - 31 August 2016.

CHAPTER 5
Field Load Testing on Maubin Bridge

5.1 Introduction

Before the actual load testing started on Maubin Bridge, preliminary tests were done on the bridge, with the permission of Ministry of Construction (MOC), on 31st May 2016 by a team of Japanese Professors from Kyoto University (KU) and a Japanese Engineer from Public Works Research Institute (PWRI), and findings were summarized in the preliminary report [1]. Based on these findings and the analysis results from ABAQUS bridge FE model [2], field load testing on the bridge was done on 21st and 22nd September 2016 in order to find out the dynamic characteristics of the bridge, and to verify the accuracy of FE bridge model.

During the field testing, static and dynamic strains on an upper chord, a lower chord and two diagonal members, static deflections at the mid span panel point between piers P4 and P5, and vibrations at four panel points were measured under various static and dynamic loading by using two (60 ton) trucks. Moreover, measurements for member thickness, surface coating thickness and surface salinity on some of bridge members were also done and, the report for static and dynamic load testing as well as the report for coating thickness and surface salinity were prepared separately [3, 4]. Load testing procedures, measured field experiment data, and analysis results are discussed in details in the following sections.

5.2 Results from Preliminary Tests on Maubin Bridge

In order to know the necessary conditions for the loading test to be done in September 2016, preliminary tests were done on Maubin Bridge on 31st May 2016 by two Professors from Kyoto University (KU) and a Japanese Engineer from Public Works Research Institute (PWRI) with the approval of Ministry of Construction of Myanmar, and the list of participants is shown in Table 5.1. The test was supported by JICA-EEHE Project for the post graduate students and staff from the Department of Civil Engineering of Yangon Technological University to be familiar with measuring equipment in the field. During the preliminary tests, ambient vibration of the bridge, strain, member thickness, and paint thickness of diagonal members (D21, D41, D50, D61, D80) as shown in Figure 5.1, and weather conditions such as wind speed, temperature, relative humidity and atmospheric pressure were measured. Bridge members were numbered starting from P4 to P8.

Table. 5.1: List of participants during the preliminary test on Maubin Bridge.

Sr.	Name	Position	Organization
1.	Dr. Kunitomo Sugiura	Professor	Kyoto University
2.	Dr. Yasuo Suzuki	Assistant Professor	Kyoto University
3.	Dr. Itaru Nishizaki	Senior Researcher	Public Works Research Institute

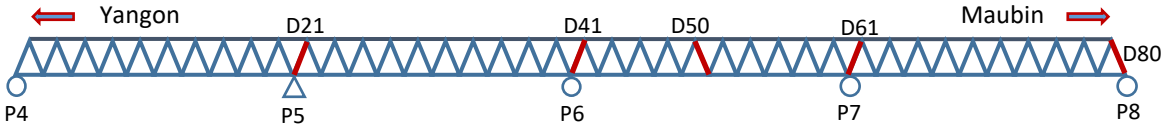

Figure 5.1: Location of measured members on Maubin Bridge in preliminary tests.

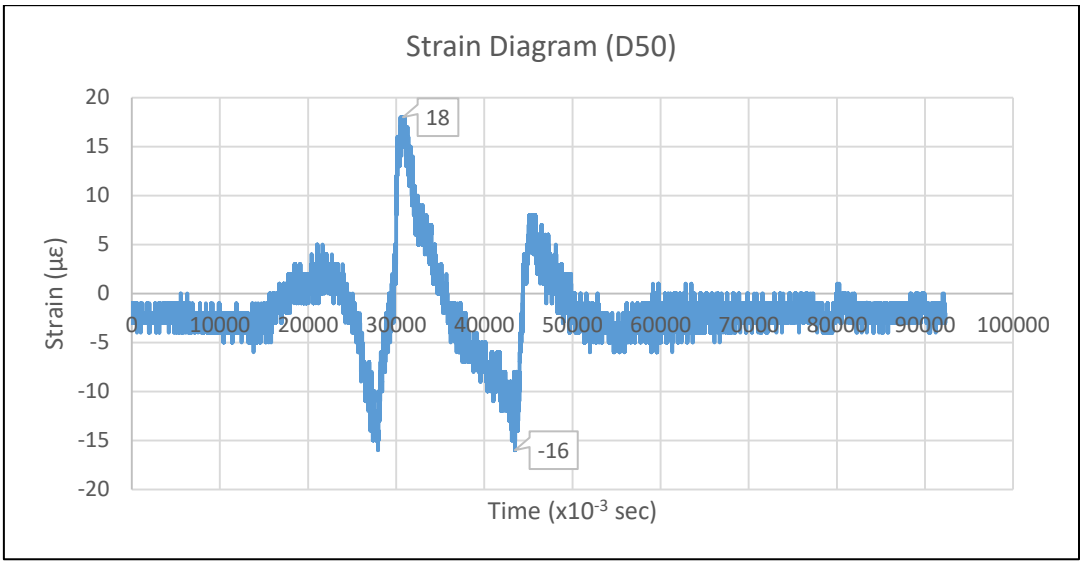

Figure 5.2: Strain variation in diagonal member (D50).

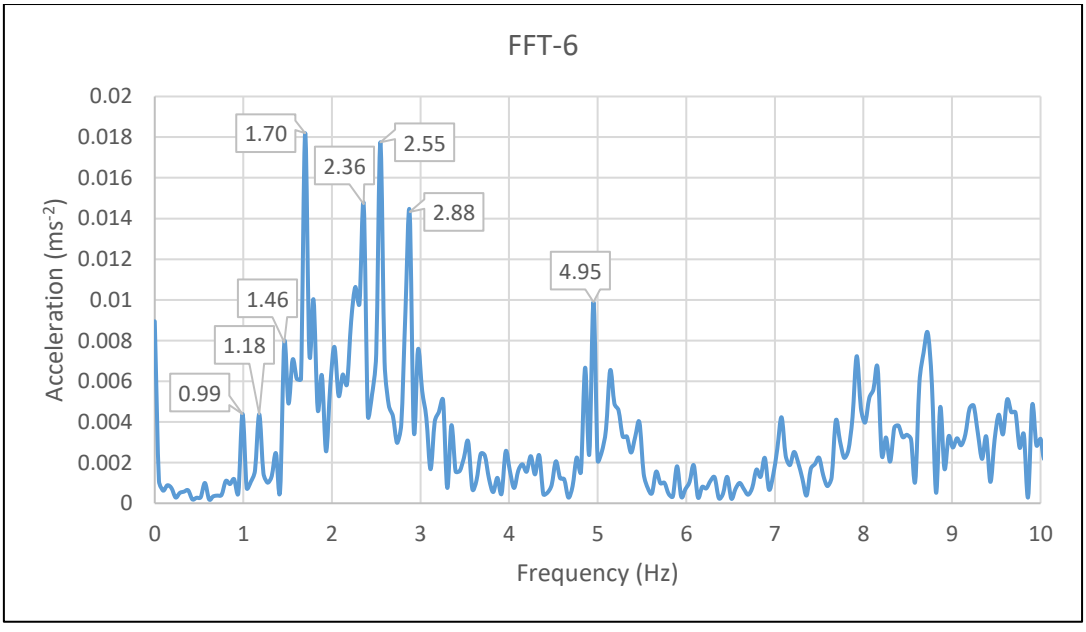

Figure 5.3: FFT graph for Maubin Bridge under ambient vibration up to 10 Hz.

As shown in Figure 5.2, the strain on diagonal member (D50) between piers P6 and P7 under normal traffic condition varied from +18 με to -16 με corresponding to the axial stress range between 3.6 MPa and -3.2 MPa, assuming the modulus of elasticity of steel as 200 GPa. Dominant frequencies of the bridge evaluated from measured vibration data after converting to FFT graphs were found to be around 0.99 Hz, 1.18 Hz, 1.46 Hz, 1.7 Hz, 2.36 Hz, 2.55 Hz, 2.88 Hz and 4.95 Hz as shown in Figure 5.3. However, due to the low traffic volume on Maubin Bridge, only some of the vibration modes were excited and heavier truck loads were still required to get the vibration modes of other frequencies.

Table 5.2: Paint thickness of diagonal members on Maubin Bridge.

Members	D80				D61	D41	D21
Position	Flange (outside)	Flange (inside)	Web (lower)	Web (upper)	Flange (outside)	Flange (outside)	Flange (outside)
Unit	μm	μm	μm	μm	μm	μm	μm
Average	227	252	259	291	246	213	283
1st	189	251	252	284	216	298	266
2nd	277	213	222	322	242	245	290
3rd	193	270	260	108	246	225	246
4th	219	227	293	265	179	173	263
5th	151	237	221	344	225	199	281
6th	246	198	262	300	221	163	252
7th	277	262	288	296	222	217	276
8th	264	361	270	300	297	186	313
9th	9.8	-	-	361	365	16.7	356
10th	81.7	-	-	329	194	379	13.7
11th	7.3	-	-	-	256	19.7	1.7
12th	7	-	-	-	232	94	11.4
13th	11.9	-	-	-	269	354	308
14th	-	-	-	-	228	20	358
15th	-	-	-	-	203	468	639
16th	-	-	-	-	-	616	-

Note: Data in gray cells are measured at peel-off paint area.

Thickness of diagonal member (D50) was measured to confirm the correctness of design cross sections, and the average thickness was measured as 11.54 mm for the web and 19.37 mm for the flange. Design thickness was mentioned in the drawings [3] as 12 mm for the web and 20 mm for the flange, and hence, values were within allowable limits. Paint thickness was also measured on both web and flange of members (D21, D41, D61, D80), and the results were shown in Table 5.2. Based on the cross-cut test results according to ISO 2409-2007, average paint thickness of members was calculated as 253 μm, but minimum

thickness as thin as 1.7 μm was measured on member (D21), and average thickness at peel-off area was calculated as 195 μm. Layer I and II of the paint system of Maubin Bridge, as shown in Figure 5.4, didn't show enough adhesive properties. Hence, in the preliminary report [1], peel-off paint areas on Maubin Bridge was suggested to be repainted as soon as possible in order to prevent the corrosion and to obtain better life cycle cost. Deteriorated layer (I and II) should be removed when repainting. Average values for the wind speed, temperature, relative humidity and atmospheric pressure were measured as 2.1 m/s, 27.2 °C, 81.2 %, 1004 hPa respectively. Even though there existed little corrosion, the protection performance of coat paint was not enough so that repainting was suggested as soon as possible.

Figure 5.4: Peeling off paint layers in Maubin Bridge

5.3 Preparations of Equipment for the Load Test

Nearly four months after the preliminary test, actual load tests on Maubin Bridge started on 21st and 22nd September 2017. The bridge was inspected in the afternoon of 20th September to determine gage points and station points, and installation of gages were done in the morning of 21st September. Then, ambient vibration was measured in the afternoon of 21st September with normal traffic. Using two (60 ton) trucks from Ministry of Construction, dynamic loading tests were done in the morning of 22nd September and static loading tests were done in the afternoon of 22nd September while closing the traffic during the tests.

Strains were measured by using a magnetic strain checker installed on the top chord, and nine normal resistance type strain gages installed on bottom chord and diagonals of the bridge on the upstream side. Vibrations on the bridge were measured by using 4 accelerometers installed on the top flange of floor beams at panel points: 3 on upstream side and 1 on downstream side. These strain gages and accelerators were then connected to different types of data loggers for static and dynamic measurements. Although the bridge is a 480 m long four span continuous bridge, only four accelerometers were able to install on two

consecutive spans due to the limited time frame, the constraint on the length of cables and available channels for hand-held data loggers, which were brought from Kyoto University. The deflection of the upstream side truss at the mid span panel point of the bridge between P4 and P5 was also measured by using a digital camera and a laser distance meter stationed on the ground, and later processed by the OpticG 2D software [5]. The list of equipment used in field loading tests were shown in Table 5.3.

Table 5.3: List of equipment for the field tests.

Sr.	Name of Equipment	Qty.	Purpose
1	Data Logger (DC-204R)	1	To measure dynamic strain and vibrations
2	Data Logger (TC-32K)	1	To measure static strain
3	Switching Box (CSW-5A)	2	To use with data logger (TC-32K)
4	Strain Gages (FLA)	9	To measure the axial strain
5	Magnetic Strain Checker (FGMH-1B)	1	To measure the axial strain
6	Accelerometers (ARF)	4	To measure the vibration/ acceleration
7	Surface Salinity Meter	1	To measure surface salt content
8	Weather Meter (Kestrel 5500)	1	To measure wind speed and direction, humidity, air pressure and temperature
9	Ultrasonic Thickness Meter	1	To measure the thickness of members
10	Electromagnetic Coating Thickness Meter	1	To measure the thickness of paint
11	Laser Distance Meter (Leica Disto D8) + Digital Camera	1+1	To measure deflection by post-processing data with OpticG-2D software
12	Temperature Gages	1	To measure temperature

Table 5.4: List of participants during the field test.

Participants from Myanmar side			Participants from Japanese side		
No.	Name	Occupation	No.	Name	Occupation
1	U Myo Win	Director, MOC	1	Dr. Kunitomo Sugiura	Professor, KU
2	U Tin Maung Htwe	Asst. Director, MOC	2	Dr. Yasuo Suzuki	Asst. Professor, KU
3	U Htun Myint	Staff Officer, MOC	3	Dr. Hisato Kato	CTI Engineering
4	U Soe Htun	Jr. Engineer II, MOC	4	Mr. Taku Hirai	Yokogawa Bridge
5	U Myo Nyunt Oo	Jr. Engineer II, MOC	5	Mr. Gen Hayashi	Ph.D. student, KU
6	U Kyaw Ye Htut	Jr. Engineer II, MOC	6	Mr. Tomohiro Tsujita	Bachelor student, KU
7	Daw Htike Htike	Jr. Engineer III, MOC	7	Mr. Khin Maung Zaw	Ph.D. student, KU and Lecturer, YTU
8	Daw Su Latt Mon	Jr. Engineer III, MOC			
9	U Kyaw Myo Hein	Work Charge, MOC			
10	Dr. Thinzar Khine	Ass. Professor, YTU			
11	Dr. Khin Su Su Htwe	Ass. Professor, YTU			
12	Ma Khin Khin Thaw	Ph.D. student, YTU			
13	Ma Khine Wutt Yee	Ph.D. student, YTU			

Note: MOC - Ministry of Construction, YTU - Yangon Technological University, KU - Kyoto University

During the field tests, engineers, researchers and government officials from both Myanmar and Japanese Institutions were working together as a team. Professors and Ph.D. students from Yangon Technological University (YTU), and engineers from Ministry of Construction participated from Myanmar side while professors and Ph.D. students from Kyoto University, and engineers from Japanese companies joined from Japanese side and the list of participants during the field test is shown in Table 5.4.

5.4 Data Measurement during the Load Test

Static and dynamic loading tests on Maubin Bridge, together with measurements for member thickness, paint coating thickness and surface salinity, were done on 21st and 22nd September 2016 while the traffic was closed sometimes during the tests. Cables and measuring instruments were installed on the bridge in the morning of 21st September, and they were removed in the morning of 23rd September followed by repainting the gage points to prevent corrosion. Ambient vibration tests were done in the afternoon of 21st September, as shown in Figure 5.5 (a), dynamic loading tests with 20 km/h and 40 km/h truck speeds in the morning of 22nd September, as shown in Figure 5.5 (b), and static loading tests in the afternoon of 22nd September, as shown in Figure 5.6 (a), with the help of two (60 ton) trucks, as shown in Figure 5.6 (b). The plan dimensions of the 60 ton truck were shown in Figure 5.7.

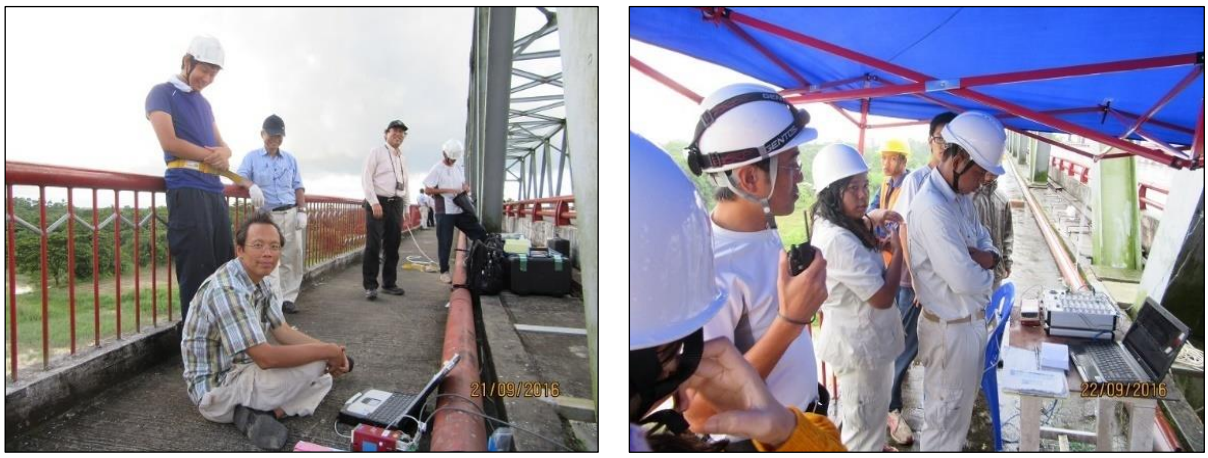

(a) (b)

Figure 5.5: (a) Measurement of ambient vibration; (b) Measurement of dynamic strain and vibration.

(a) (b)

Figure 5.6: (a) Measurement of static strain; (b) 60 ton truck resting on the bridge.

5.4.1 Measurement for Static Loading Tests

For the static tests, the trucks crawled on the bridge along the right lane (close to upstream side truss) from Yangon side to Maubin side and stopped at 8 different locations while the traffic was closed as shown in Figure 5.8. These points were selected in order to simulate truck positions for maximum shear and maximum moment effects based on ABAQUS analysis results. Then, the strains were measured on four different members, two diagonal members (D12, D13), a lower chord (L7), and a top chord (U10) as shown in Figure 5.8, with one magnetic strain checker on the upper surface of U10 as shown in Figure 5.9 (a), and three strain gages on flanges and web of each of other members, as shown in Figure 5.9 (b). Measurement team from MOC also joined the tests and their strain gages were installed close to our strain gages. Before installation, gage points were cleaned by grinders until the paints were removed completely as shown in Figure 5.10 (a), and the gages were covered by seal tapes to prevent from rain as shown in Figure 5.10 (b). Strain gages were installed at 3 m height from the node points of the truss.

Deflections of the upstream side truss at the mid-span panel point between P4 and P5, location (2) in Figure 5.8, for each static loading case were also measured by a digital camera and a laser distance meter from the ground, as shown in Figure 5.11 (a), about 17 m below the bridge near pier P4. Measured deflection values were post-processed by OpticG 2D software [5] later. During the static loading test, the slip between the magnetic strain checker and the surface of top chord (U10) occurred while two trucks parked simultaneously at location 2 and 5. Hence, static strains were measured again when the trucks returned from Maubin side to Yangon side along the center line of the bridge and stationed at locations 2 and 5.

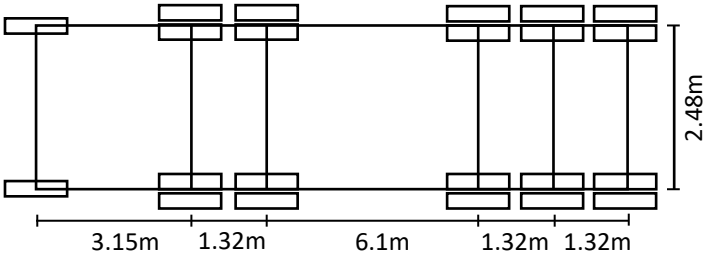

Figure 5.7: Plan dimensions of 60 ton truck.

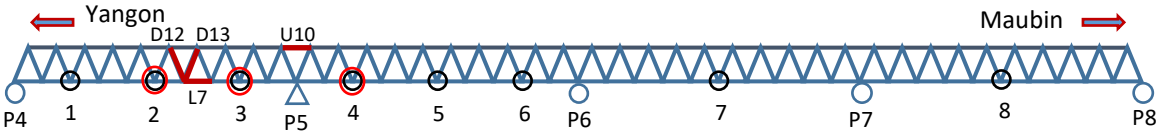

Figure 5.8: Location of 60 ton trucks load points - O, accelerometers - O, strain gages ─.

(a) (b)

Figure 5.9: (a) Magnetic strain checker on the upper surface of top chord U10; (b) Normal resistance strain gages on the web and flange of Diagonal D12.

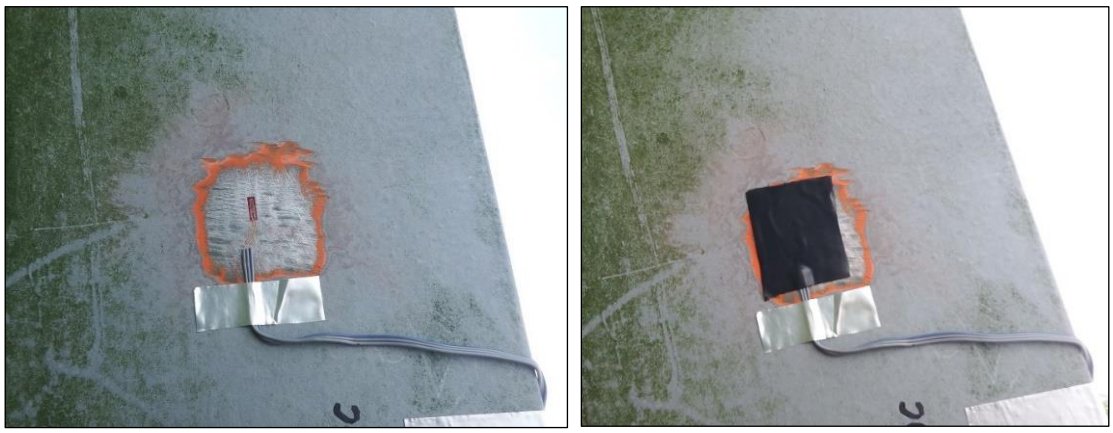

(a) (b)

Figure 5.10: (a) Strain gage installed on clean surface of diagonal D13; (b) Strain gage on diagonal D13 covered by seal tape.

(a) (b)

Figure 5.11: (a) Deflection measurement of location 2 from the ground; (b) Accelerator installed on the cross beam at location 3.

5.4.2 Measurement for Dynamic Loading Tests

For dynamic loading tests, vibrations were measured under three different loading conditions, under ambient vibration condition allowing normal traffic flow, under 20 km/h truck speed and under 40 km/h truck speed while the traffic was closed. Vibrations were measured from four accelerometers installed on the top of floor beams at locations 2, 3, 4 on upstream side truss and another at location 3 on the downstream side truss at each panel point as shown in Figure 5.8 and 5.11 (b). Ambient vibrations were measured for 20 minutes interval time while normal traffic was opened on the bridge, but two (60) ton trucks were used to run on the bridge one after another with 20 km/h speed as well as 40 km/h speed in closed traffic condition. Dynamic strains were also measured for the diagonals (D12, D13) and the lower chord (L7) while the trucks were running on the bridge.

5.4.3 Measurement for Member Thickness, Paint Thickness and Surface Salinity

While the loading tests were performing on the bridge, thickness of diagonal members on the upstream side truss between piers P4 and P6 were measured by an ultrasonic thickness meter as shown in Figure 5.12 (a). Thickness of top chords and bottom chords cannot be measured due the difficulty to access them and only half of the diagonal members were measured due to the symmetry of the bridge. Moreover, paint thickness and surface salinity on some of diagonals, bottom bracings and lower chords of the bridge over the pier P4 on Yangon side and on the new plate girders on Maubin side were also measured by using electromagnetic coating thickness meter and surface salinity meter, during the tests as shown in Figure 5.12 (b).

(a) (b)

Figure 5.12: (a) Measuring member thickness by ultrasonic thickness meter; (b) Coating thickness and surface salinity measurements on pier (P4)

According to the measurements, thickness of diagonal members were within the allowable limit (varies from -1.68% to + 12.00%) except for the thickness of the web of end diagonal D1. Average web thickness of D1 was measured as 13.01 mm, which was 18.67% lower than 16 mm thickness mentioned in the original drawings [6]. Paint thickness was measured from 199 μm to 480 μm on diagonal members, from 160 μm to 320 μm for lower chords and bracings, and from 192 μm to 388 μm for new extension girders built in 2016. In general, the coating thickness of outer webs was greater than that of inner webs, but the flange (outside) coating thickness was less than flange (inside) thickness for diagonal members. For lower chords and bracings, the flange (outside) coating thickness was larger than flange (inside) thickness at the lower chords. Average paint thickness values of each measured members were described in Table 5.5. Thinner paint thickness on lower chords and bracings may be due to the difficulties to access them during the repainting period.

Table 5.5: Average paint thickness for each measured member

Average paint thickness of members (μm)														
Diagonals						Lower Chords & Bracings				New Approach Girders				
$D1^U$	$D1^D$	D21	D41	D60	D80	L1	L2	LB1	LB2	G1	G2	G3	G4	G5
411	335	313	299	320	302	216	225	187	231	286	283	291	274	245

Surface salinity values varied from 6.7 mg/m^2 to 19.6 mg/m^2 for diagonal members, from 16 mg/m^2 to 474 mg/m^2 for lower chords and bracings, and from 21.2 mg/m^2 to 213 mg/m^2 for new extension girders. Hence, it was found out that the measured values were lowest for diagonal members and greatest for lower chords and new girders because the salt from the surface of diagonal members were washed away by the rain but not for the case of

lower chords and girders which were covered by concrete decks. Some of the measured values on lower bracings were higher than the acceptable limits. Average surface salinity values of each measured members are described in Table 5.6.

Table 5.6: Average surface salinity (NaCl) for each measured member

Average surface salinity of members (mg/m^2)														
Diagonals						Lower Chords & Bracings				New Approach Girders				
$D1^U$	$D1^D$	D21	D41	D60	D80	L1	L2	LB1	LB2	G1	G2	G3	G4	G5
9.4	16.9	12.3	8.1	9.2	8.3	54.8	86.5	103.9	261.4	102.1	151.7	97.2	115.8	109.7

5.5 Static and Dynamic Load Testing Results Comparing with FE Bridge Model

During the field tests on the bridge, static strain and deflection of members between piers P4 and P5 were measured during the static loading tests as well as dynamic strain and vibration of the bridge were measured during the dynamic loading tests by using two (60 ton) trucks from MOC. Then, the results measured from the field tests were discussed and compared with the results from FE bridge model in the following sections.

5.5.1 Results from Static Load Tests and Comparison with FE Bridge Model

During the static loading tests, static strains were measured for diagonals (D12, D13), lower chord (L7), and top chord (U10), as well as the deflection of mid-point of upstream side truss at location 2 between piers P4 and P5 as shown in Figure 5.8. Measured strain and deflection values were then compared with the results from FE bridge model as shown in Table 5.7 for the strain and Table 5.8 for the deflection. Measured strain is the average value taken from 3 strain gages from the flanges and the web. According to Table 5.7, almost all the data showed comparable results between the measured and model data, except for some data at load point 2 for the diagonal D13 where a transverse portal bracing frame was attached. The FE model strain values were generally higher than the actual strain values for the top chord U10 and the diagonal D13, but were lower for the diagonal D12 and the lower chord L7.

Differences in strain values were unusually higher for the diagonal D13 when the truck was resting at location 2, the mid-point of truss between P4 and P5. It may be due to the necessity in modeling connections between diagonal members and the transverse portal frames in the bridge model, or due to the difference between assumed support conditions and actual support conditions, or due to the inaccuracy in the load sharing from the truck. In FE

bridge model, connections were assumed as tied connections or rigid connections but the rigidity of actual connections may be different. For the load sharing from the (60 ton) truck, there was no chance to measure the axle load for each axle except for the total weight and dimensions. Smaller differences for the top chord U10 at load points 5+2, 6, 7, 8 may be due to the occurrence of slip between the magnetic strain checker and the surface of steel member.

According to Table 5.8, most of the deflection values were acceptable except for the load points 2 and 5 + 2 when the truck rested on location 2 where the model deflection was abnormally higher than the measured deflection. Differences in deflection values may be due to inaccuracies in field measurement and software errors as well as the same reasons discussed for the differences in strain values.

Table 5.7: Comparison between the measured and FE model strain by (60) ton trucks.

Load Points	Measure strain in members [a] ($x10^{-6}$)				Model strain in members [b] ($x10^{-6}$)				Difference in member strain [b-a] ($x10^{-6}$)			
	U10	D12	D13	L7	U10	D12	D13	L7	U10	D12	D13	L7
1	11	-25	39	13	17	-46	65	6	6	-21	26	-7
2	22	-29	87	38	33	-36	171	24	11	-7	84	-14
3	13	16	-16	24	27	13	-17	8	14	-3	-1	-16
4	17	-6	2	-9	36	-8	10	-5	19	-2	8	4
5	16	-5	2	-10	32	-8	10	-5	16	-3	8	5
5 + 2	41	-34	85	24	65	-44	181	19	24	-10	96	-5
6	-16	2	-2	-1	10	-3	4	-2	26	-5	6	-1
7	-31	6	-11	6	-6	2	-3	1	25	-4	8	-5
8	-26	4	-9	4	1	0	0	0	27	-4	9	-4
5	27	-7	8	-13	30	-9	13	-6	3	-2	5	7
2	27	-36	53	29	26	-57	90	14	-1	-21	37	-15
2 + 5	51	-43	60	14	56	-66	103	8	5	-23	43	-6

Table 5.8: Comparison between the measured and FE model deflection by (60) ton trucks.

Load Points	Measure deflection [c] (mm)	Model deflection [d] (mm)	Difference in deflection [d-c] (mm)
1	-7.3	-12.0	-4.7
2	-6.0	-21.1	-15.1
3	-2.9	-7.2	-4.3
4	-1.9	3.7	5.6
5	-1.5	3.7	5.2
5 + 2	-1.6	-17.4	-15.8
6	0.6	1.3	0.7
7	0.8	-0.8	-1.6
8	1.2	0.2	-1.0

5.5.2 Results from Dynamic Load Tests and Comparison with FE Bridge Model

To measure the vibration response of the bridge, four accelerometers (Ch1 ~ Ch4) were installed on the top of floor beams at locations 2, 3 and 4 on upstream side truss and at location 3 on downstream truss as shown in Figure 5.8. Vertical vibrations were measured under ambient condition (in normal traffic condition) as well as while the trucks were running with 20 km/h and 40 km/h speeds (in closed traffic condition). Dynamic strains for members (D12, D13 and L7) were also recorded while the trucks were running on the bridge. For the dynamic load tests, there had been constraints on the length (and weight) of cables and available channels for hand-held data loggers, which were brought from Kyoto University, as well as the limited time frame. Hence, only four accelerometers were able to install on the bridge although Maubin Bridge is a 480 m long four span continuous bridge.

To find out the frequencies of the bridge from the measured vibration data, a MATLAB program was written for the Fast Fourier Transform (FFT) analysis and then FFT graphs (up to 10 Hz) were drawn for each of channel (Ch1 ~ Ch4) and for each loading case as shown in Figures 5.13 to 5.15. From the FFT graphs, it was clear that the first four peak frequencies were more dominant in all channels of 40km/h truck speed test than the ambient vibration condition and 20 km/h truck speed tests except for Ch1.

Table 5.9: Percent difference between measured and model frequencies before model update

Bending Mode	Measured Frequency [a]	Model Frequency Before Updating [b]	% Difference (b-a)/a x 100%
1st	1.08 Hz	1.18 Hz	9.26 %
2nd	1.24 Hz	1.34 Hz	8.06%
3rd	1.47 Hz	1.57 Hz	6.80%
4th	1.67 Hz	1.77 Hz	5.99%

However, the frequencies may contain a mixture of bending and torsional modes of the truss and, in order to produce pure bending modes of the bridge, FFT graphs were drawn, as shown in Figure 5.16, from the half sum of vertical acceleration data from Ch2 and Ch3, which were on opposite side of the trusses at location 3. All the FFT graphs showed the first four dominant frequencies in bending mode around 1.08 Hz, 1.24 Hz, 1.47 Hz, 1.67 Hz but they were more obvious in 40 km/h truck speed test. The first four fundamental frequencies of the FE bridge model in bending were also obtained as 1.18 Hz, 1.34 Hz, 1.57 Hz and 1.77 Hz respectively with the mode shapes as shown in Figure 5.17, and the difference between the measured and model frequencies were described in Table 5.9 with differences not greater than 10%. FFT graphs show that 40 km/h speed and ambient vibration excited more frequencies than 20 km/h speed, and measured frequencies can be comparable with the frequencies obtained from FE analysis.

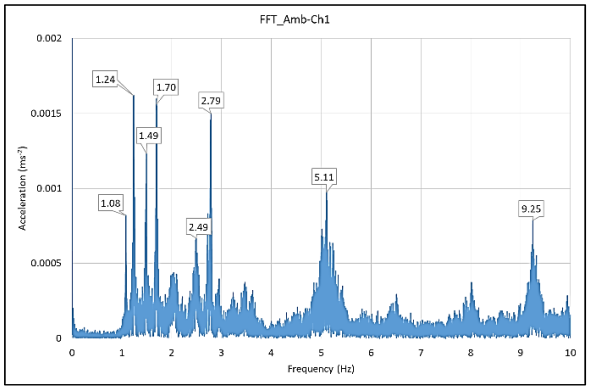

(a)

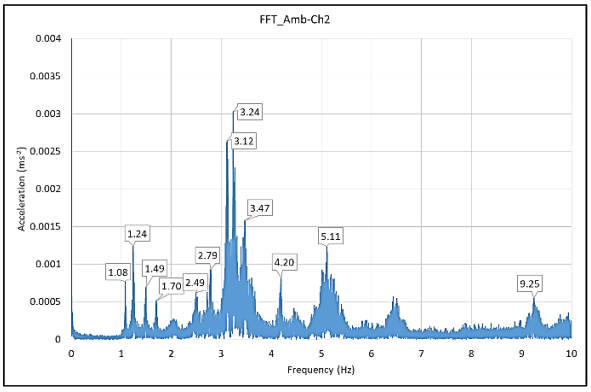

(b)

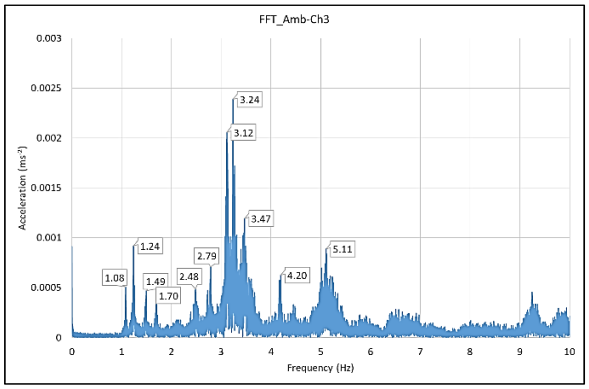

(c)

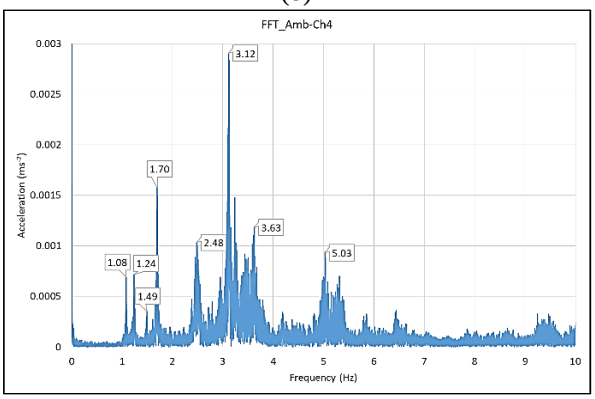

(d)

Fig. 5.13: FFT graphs for ambient vibration tests: (a) Ch1; (b) Ch2; (c) Ch3; (d) Ch4.

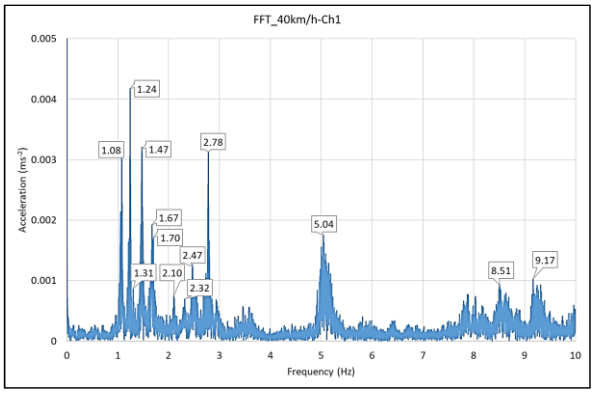

(a)

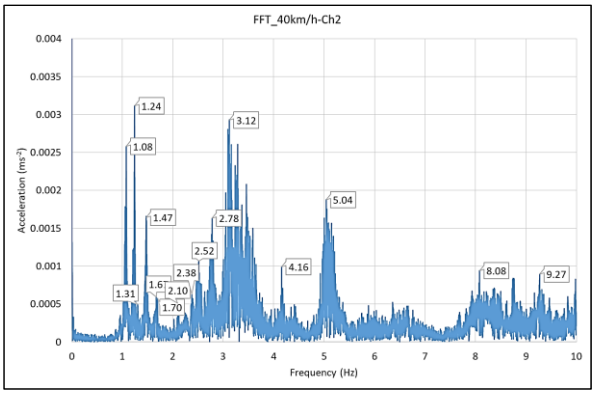

(b)

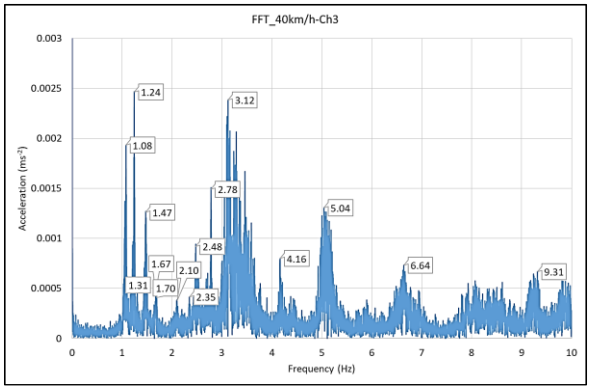

(c)

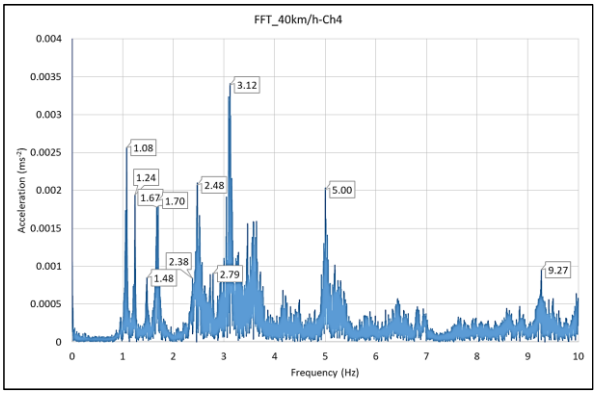

(d)

Fig. 5.14: FFT graphs for 40 km/h truck speed: (a) Ch1; (b) Ch2; (c) Ch3; (d) Ch4.

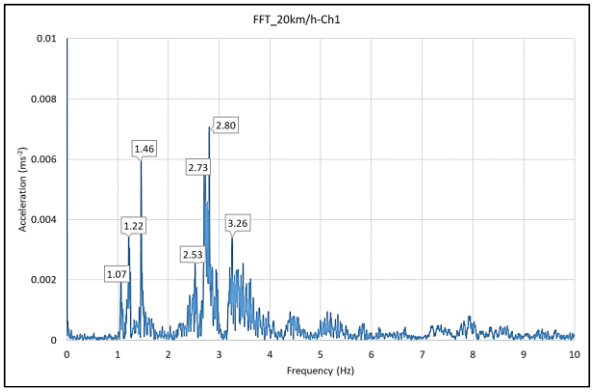

(a)

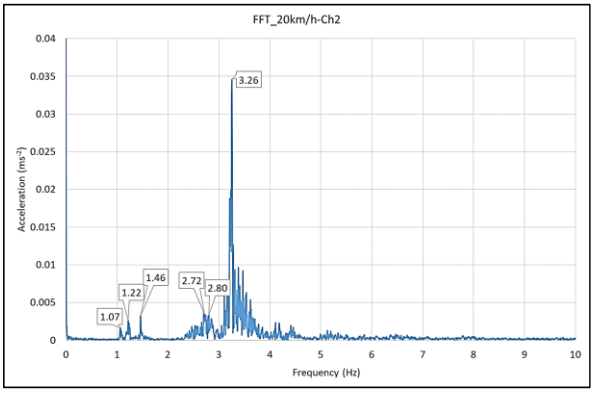

(b)

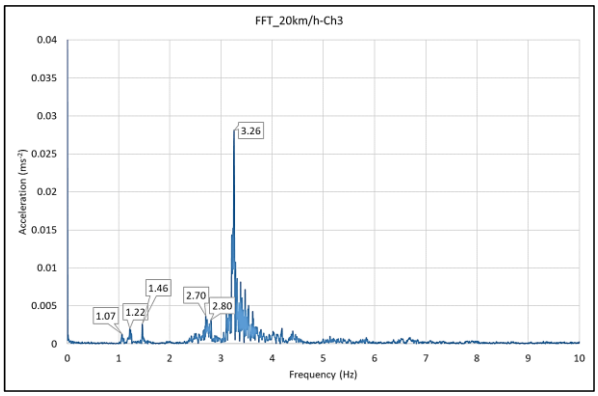

(c)

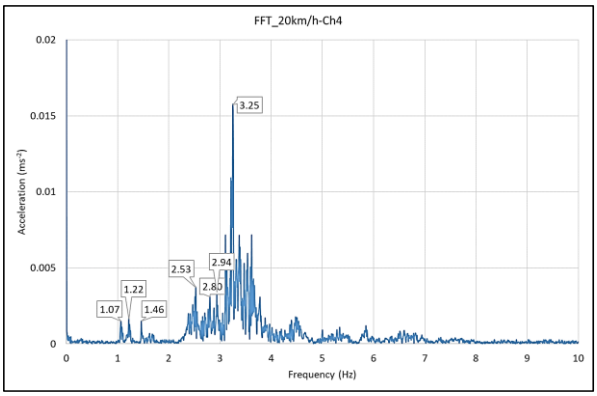

(d)

Fig. 5.15: FFT graphs for 20 km/h truck speed: (a) Ch1; (b) Ch2; (c) Ch3; (d) Ch4.

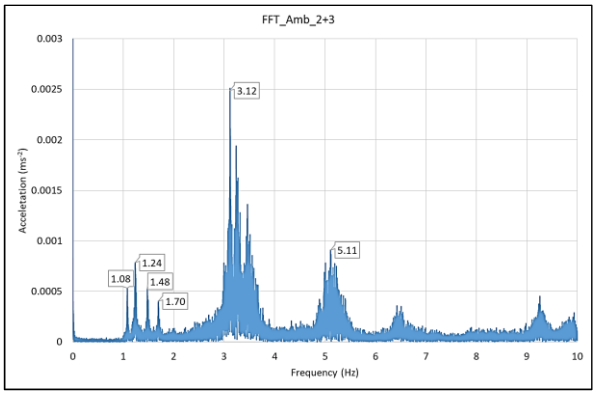

(a)

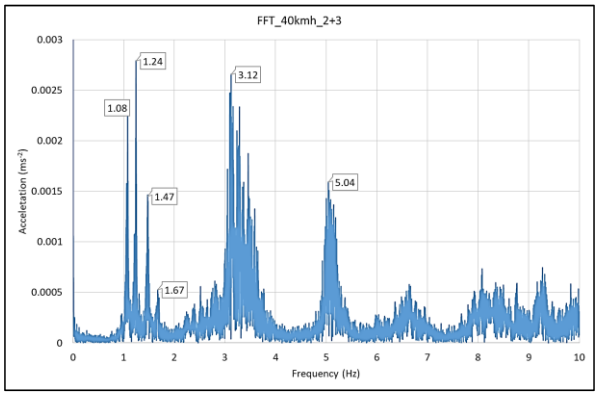

(b)

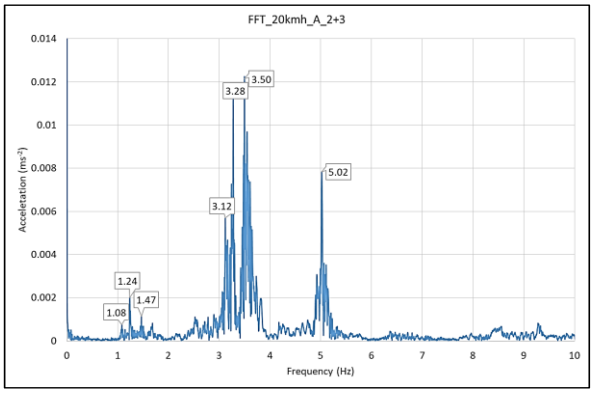

(c)

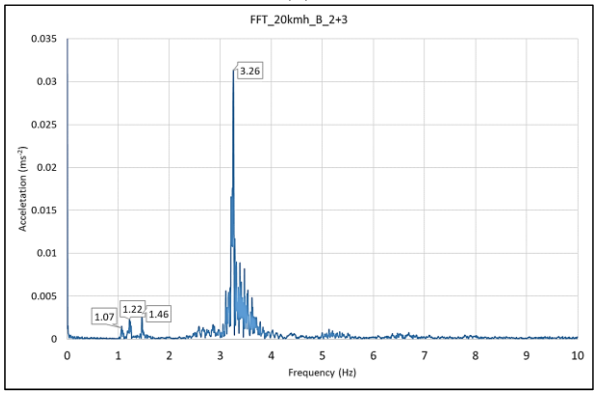

(d)

Fig. 5.16: FFT graphs showing fundamental bridge frequencies in bending mode: (a) ambient vibration test; (b) 40 km/h truck test; (c) 20 km/h truck A test; (d) 20 km/h truck B test.

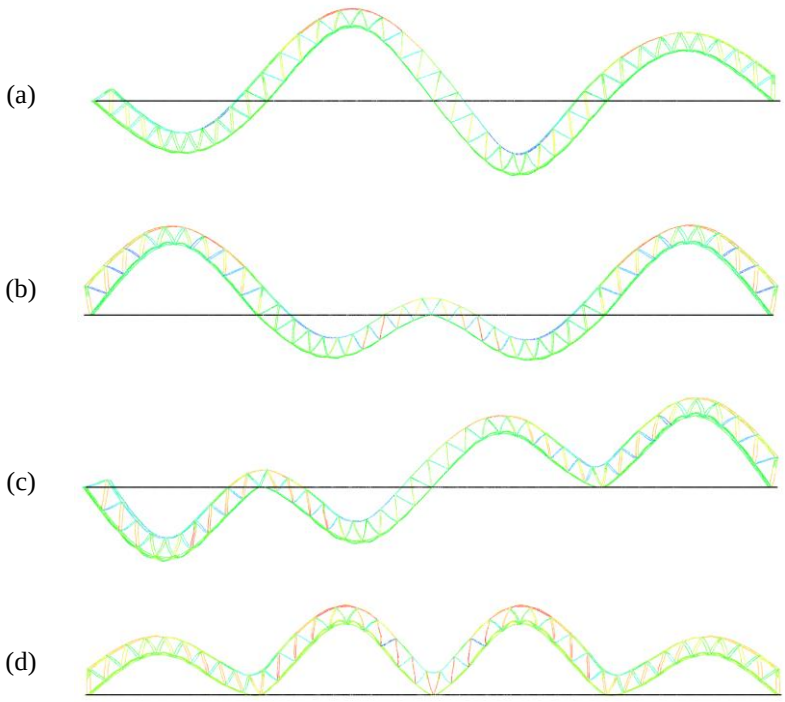

Figure 5.17: First four bending modes of FE bridge model: (a) 1st mode; (b) 2nd mode; (c) 3rd mode; (d) 4th mode.

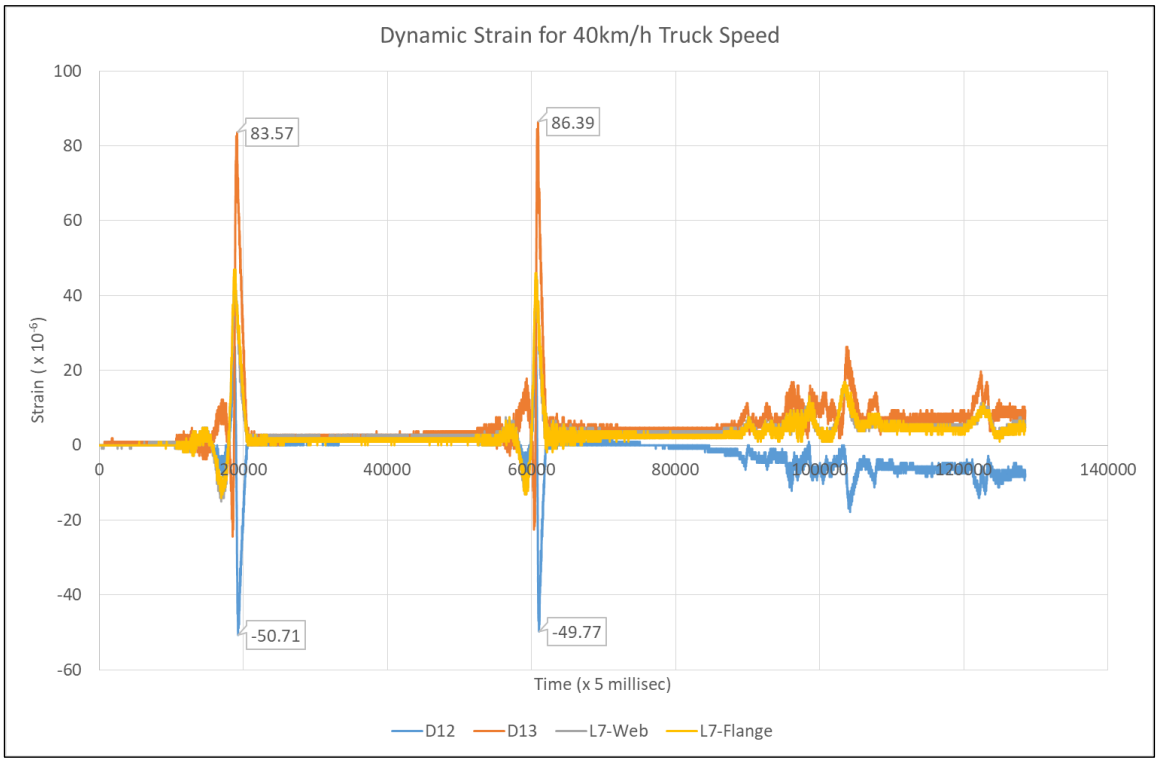

Figure 5.18: Measured dynamic strain under 40km/h truck speed

In addition to the vibration measurements, dynamic strains of the truss members (D12, D13 and L7) were also measured during the dynamic loading tests and measured dynamic strain values were shown in Figure 5.18. From the figure, it can be seen that there were two

strain peaks representing the passage of two loading trucks on the bridge one after another, with the maximum positive strain (86.39 μ) occurred in tension diagonal member (D13) and maximum negative strain (-50.71 μ) occurred in compression diagonal member (D12). These maximum strain values gave corresponding stresses of 17.28 MPa and -10.14 MPa, assuming the modulus of elasticity of steel as 200 GPa.

5.6 Adjustment of FE Bridge Model Frequency to Load Test Results

Comparing the bridge frequencies obtained from measured results and FE model results, there were some differences for the first four bending modes up to 9.26 % and, hence, the FE bridge model was necessary to be updated. According to the references [7, 8], there are two principal approaches to adjust the difference between measure and model frequency, adjusting the mass of the model or adjusting its stiffness. Adjusting the mass means adjusting the dimension of elements as well as the density of materials which are used in the model. Adjusting the stiffness of elements means adjusting the values of spring stiffness (k) for springs, elastic modulus (E) for truss elements, flexural rigidity (EI) or torsional rigidity (GJ) for beam elements, and adjusting the rigidity of connection between different parts of the model.

Table 5.10: Percent difference between measured and updated model frequencies

Bending Mode	Measured Frequency [a]	Updated Model Frequency [c]	% Difference (c-a)/a x 100%
1st	1.08 Hz	1.09Hz	0.93%
2nd	1.24 Hz	1.24 Hz	0%
3rd	1.47 Hz	1.46 Hz	-0.68%
4th	1.67 Hz	1.65 Hz	-1.20%

In the case of Maubin Bridge FE model, there are two types of elements used in the model, beam elements and plate elements, and two types of materials, steel and concrete. In order to adjust the bridge model with the measured results from the load tests, the mass of bridge decks were increased as the first step because the mass of parapet walls and handrails on both main and side decks were neglected in the previous model. In order to increase the mass, thickness of main decks were increased from 25.3 cm to 32 cm and thickness of side decks from 16.6 cm to 20 cm. After updating, fundamental frequencies of the bridge became close to measured values and the updated model frequencies are compared with measured frequencies as shown in Table 5.10 for the first four bending modes of the bridge. However,

there was no significant change in the values of strain and deflection between measured and model results because mass is not related with the stiffness of members, and the weight of the bridge is not included in the analysis for load test.

5.7 Summary

After the preliminary measurements on 31st May 2016 by a team of Japanese professors from Kyoto University (KU) and a Japanese engineer from Public Works Research Institute (PWRI), static and dynamic loading tests were done on Maubin Bridge by a team of professors and engineers from Myanmar side and Japanese side on 21st and 22nd September 2016, in order to find out the dynamic characteristics of the bridge, and to verify the accuracy of FE bridge model. Then, the results of field measurement were compared with the results from FE bridge model and the results were presented in different symposiums after the model was updated [9, 10, 11].

Static load testing results showed that the measured strain and deflection results were close to the model strain and deflection values except for load point location (2) for member D13 due to the possible errors in field measurement, or due to the necessity in modeling connection between truss members and transverse portal frames, or due to the difference between assumed support conditions and actual support conditions. Since the deflection values from the FE bridge model were generally larger than the measured deflections, it can be said that the model was a soft model in comparing with the actual bridge.

Dynamic load testing results also showed that measured bridge frequencies were close to the model frequencies for the first four bending modes with the maximum difference of 9.26% but errors became decreased to 1.2% after updating the model by increasing thickness of concrete decks. It was clear from the FFT graphs that the first four peak frequencies were more dominant in all channels of 40 km/h truck speed test than the ambient vibration condition and 20 km/h truck speed tests except for Ch1. Hence, it can be said that 40 km/h truck speed excite frequencies of stronger intensity than ambient condition and 20 km/h truck speed.

Measurement of thickness of diagonal members between piers P4 and P6 were within the allowable limit except for the end diagonal D1, whose average web thickness was about 3 mm (18.67%) lower than 16 mm thickness mentioned in the original drawings.

Paint coating thickness of lower chords and bracings was generally lowered than that of diagonal members and extension girders, which may be due to the difficulties to access them during the repainting period. In general, the coating thickness of outer webs was greater than

that of inner webs, but the coating thickness of outside flange was less than that of inside flange for diagonal members but the opposite was true for lower chords and bracings.

Surface salinity values were measured as the lowest for diagonal members and highest for lower chords and new girders because the salt from the surface of diagonal members were washed away by the rain but not for the case of lower chords and girders which were covered by concrete decks. Some of the measured values on lower bracings were higher than the acceptable limits.

References

[1] Khin Maung Zaw, Suzuki, Y., Nishizaki, I. and Sugiura, K., Report for the Preliminary Test at Yadanarpon Bridge and Maubin Bridge, Inspection Report to Ministry of Construction, August 2016.

[2] Khin Maung Zaw, Suzuki, Y., Matsumura, M. and Sugiura, K., Analysis of Maubin Bridge in Myanmar for Seismic Retrofit, *Proceedings of the 11th German-Japan Bridge Symposium*, Osaka Institute of Technology, Japan, 29 - 31 August 2016.

[3] Khin Maung Zaw, Suzuki, Y., and Sugiura, K., Report for Field Load Testing on Maubin Bridge, Inspection Report to Ministry of Construction, December 2016.

[4] Khin Maung Zaw, Suzuki, Y., Nishizaki, I., and Sugiura, K., Coating Thickness and Surface Salinity Study on Thanlwin Bridge (Mawlamyine) and Maubin Bridge, Inspection Report to Ministry of Construction, December 2016.

[5] http://www.zoomscape.net/product/

[6] Major Bridge Engineering Bureau, Working Drawings for Steel Truss Bridge (Maubin, Myanmar), Reconnaissance and Design Institute, Ministry of Railways, Wuhan, China, June, 1996.

[7] Sinha, J.K., Vibration Analysis, Instruments, and Signal Processing, 1st edition, CRC Press, Taylor and Francis Group, 2015.

[8] Adams, D.E., Health Monitoring of Structural Materials and Components, 1st edition, John Wiley & Sons, Inc., 2007.

[9] Khin Maung Zaw, Suzuki, Y., Matsumura, M. and Sugiura, K., Analysis and load testing results of Maubin Bridge in Myanmar, *Proceedings of the 29th KKHTCNN Symposium on Civil Engineering*, Hong Kong University of Science and Technology, China, 3 - 5 December 2016.

[10] Khin Maung Zaw, Suzuki, Y. Sugiura, K., and Myo Win, Comparison of Load Testing and FE Analysis Results of Maubin Bridge, *Proceedings of the 7th International*

Conference on Science and Engineering, Yangon Technological University, Myanmar, 10 - 11 December 2016.

[11] Khin Maung Zaw, Suzuki, Y. and Sugiura, K., Study of Maubin Bridge in Myanmar for Seismic Retrofit, *Proceedings of the 10th Taiwan - Japan Workshop on Structural and Bridge Engineering*, Kyoto University, Japan, 31 March – 2 April 2017.

CHAPTER 6

Experiments on Elastomeric Rubber Bearings

6.1 Introduction

In order to acquire fundamental information of the bridge bearings, which were intended to use in the retrofitting of long span steel bridges in Myanmar, tests on elastomeric rubber bearings were scheduled to be done with the sample bearings provided by Sumitomo Riko Company Limited. These sample bearings were scaled down to replace the actual bearings to be installed in the bridges in Myanmar but they were large enough to perform cyclic shear tests in the six degree of freedom (DOF) testing machine in the Structural Engineering Laboratory at Katsura Campus of Kyoto University. The dimensions of sample bearings for the experiments were shown in Figure 6.1 and their specifications were described in Table 6.1 and 6.2.

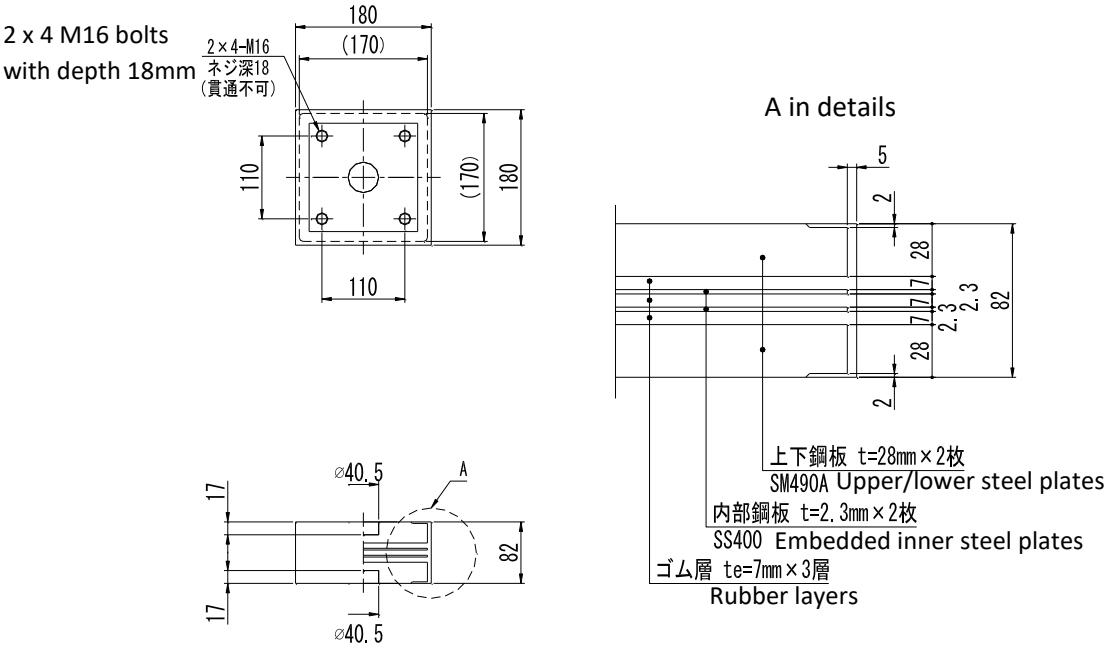

Figure 6.1: Dimensions of sample bearings (all dimensions in mm).

Table 6.1: Specifications of sample elastomeric rubber bearings.

Type	Shear Modulus	Rubber Thickness & No. of Layers		Shape Factor		Horizontal Stiffness K_H (kN/mm)	Damping Ratio h_B (%)	Vertical Stiffness K_v (kN/mm)
		t_e (mm)	n	S1	S2			
HDR-S	G12	7	3	6.07	8.10	1.66	16.9	451

Table 6.2: Lateral loads for various lateral displacements (drift) of sample bearings.

Type	Shear Modulus	Lateral Force（kN）		
		175% drift	250% drift	300% drift
HDR-S	G12	89	196	324

The plan dimension of the bearings was 180 mm x 180 mm and the height was 82 mm. Three layers of 7 mm thick high damping elastomeric rubber were used in the bearing with 2.3 mm thick steel plates (SS400) sandwiched between them for reinforcement. Top and bottom parts of the bearing were covered by 28 mm thick (SM490A) steel plates with 16 mm diameter bolt holes for the connection. Shear modulus (G) of the bearing was 1.2 MPa with horizontal stiffness of 1.66 kN/mm, vertical stiffness of 451 kN/mm and equivalent damping ratio of 16.9%. According to the documents from the manufacturer, 89 kN (9.076 ton), 196 kN (19.986 ton) and 324 kN (33.039 ton) lateral forces were required to make the lateral displacement (drift) of the bearing to 175% (36.75 mm), 250% (52.5 mm) and 300% (63 mm).

6.2 Experimental Setup

For the experiments, the six DOF universal testing machine in Structural Engineering Laboratory was used to test the properties of elastomeric rubber bearings. This testing machine, shown in Figure 6.2, was jointly developed by Kyoto University and Shimadzu Corporation of Japan. It was controlled by nine hydraulic actuators, which were fitted with built-in load cells and LVDTs so that it can apply loads in three axial directions and three rotations along X, Y and Z axes. The capacity of each actuator is 10 tons except for the actuator in vertical Z direction, which can apply 50 tons in compression and 30 tons in tension. The stroke of each actuator is ± 100 mm in displacement and ± 10.3 degree in rotation [1].

Two bearing specimens were planned to test in five different loading configurations as shown in Table 6.3. The first bearing (No. 1213) is to be tested by applying constant vertical compression force (6 MPa or 19.823 ton) and two levels of cyclic lateral force: five loading cycles to get 175% drift or 36.75 mm; and another three loading cycles to get 250% drift or 52.5 mm, as shown in Figure 6.3. The second bearing (No. 1214) is also to be tested in the same way for the lateral displacement of 175% drift or 36.75 mm but under three different vertical compressive forces: 6 MPa (19.823 ton); 3 MPa (9.912 ton); and 9 MPa (29.735 ton). Two displacement transducers (T1 and T2) were attached to the top and bottom steel plates of the bearing to measure the lateral displacement (drift) and another two transducers (T3 and T4) to measure the displacement of the bearing along the vertical loading direction (Z axis) as shown in Figure 6.4.

Figure 6.2: Six DOF universal testing machine in Structural Engineering Laboratory.

Table 6.3: Five different loading configurations for testing of bearing specimens.

Sr.	Test Number	Specimen Number	Vertical Load (P) (ton)	Lateral Displacement (mm)	No. of Loading Cycles
1.	Test 1-A	1213	19.823	± 36.75 mm	5
2.	Test 1-B	1213	19.823	± 52.50 mm	3
3.	Test 2-A	1214	19.823	± 36.75 mm	5
4.	Test 2-B	1214	9.912	± 36.75 mm	3
5.	Test 2-C	1214	29.735	± 36.75 mm	3

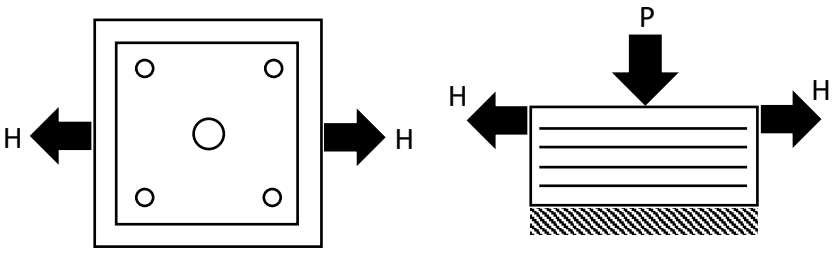

(a) Plan view of bearing (b) Side view of bearing

Figure 6.3: Loadings applied for bearing specimens.

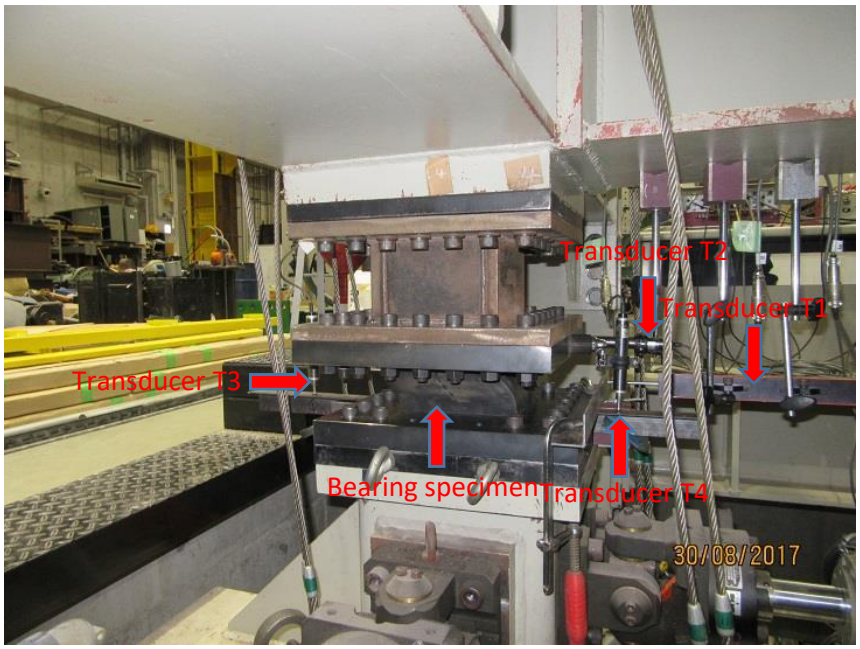

Figure 6.4: Displacement transducers attached to the specimen.

6.3 Results of Cyclic Loading Tests for Bearing Specimens

The bearing samples provided by Sumitomo Riko Company Limited were already tested to 175% lateral drift while compressed under 6 MPa pressure in their laboratory before sending the samples to the Structural Mechanics Lab at Kyoto University, and the complete test data was attached together with the bearings for further references. Hence, it was a good chance to compare the current test data with the original data provided by the manufacturer. Figure 6.5 showed the deformation of sample bearing (No. 1214) under the lateral load being pushed to 36.75 mm displacement.

Figure 6.5: Bearing Specimen (No. 1214) being pushed to 36.75 mm displacement.

6.3.1 Rate of Loading for Bearing Specimens

Preliminary tests for bearings were done by the manufacturer in their laboratory with the loading rate of 0.043 Hz (23.256 sec per loading cycle) to 10 cycles under pure sine wave loading. However, the loading rate for the experiments in Kyoto University was set up at 0.1 mm/sec (1470 sec per loading cycle for 36.75 mm lateral displacement or 2100 second per loading cycle for 52.5 mm lateral displacement) under triangular cyclic loading in order to get more stable loading condition for the testing machine.

6.3.2 Determination of Shear Modulus and Vertical Stiffness of Bearings

Shear modulus or horizontal stiffness is the most important property of the bearing because of its effects to the forces transmitted between the superstructure and substructure, and the shear modulus of sample bearings was evaluated from the slope of load-displacement graphs drawn from the experiment data according to AASHTO specifications [2].

There were five different loading configurations, as shown in Table 6.3, to test two bearing specimens under different values of lateral displacements and compressive stresses, and each of the bearings was initially loaded for five cycles to 36.75 mm lateral displacement under 6 MPa or 19.823 ton compressive force, which was the reference condition provided by the manufacturer. In order to evaluate the shear modulus (horizontal stiffness), vertical stiffness and equivalent damping ratio of the bearings, load-displacement graphs for each of the load cases were drawn, as shown in Figure 6.6 to 6.10, from the test results. The shear modulus or horizontal stiffness (K_H) of bearings was then determined from the slope of the red line, connecting maximum and minimum load points of the third loading cycle, as shown in Table 6.4, with the values of vertical stiffness (K_V) of bearings which were calculated from vertical load (P) and vertical displacement values.

Table 6.4 Shear modulus (horizontal stiffness) and vertical stiffness of bearings.

Sr.	Test Number	Specimen Number	Maximum Lateral Load (H) (ton)	Maximum Vertical Load (P) (ton)	Maximum Displacement (mm)	Shear Modulus (kN/mm)	Vertical Stiffness (kN/mm)
1.	Test 1-A	1213	5.33	19.82	± 36.72	1.415	141
2.	Test 1-B	1213	8.14	19.82	± 52.46	1.510	121
3.	Test 2-A	1214	5.13	19.82	± 36.72	1.331	131
4.	Test 2-B	1214	4.86	9.91	± 36.72	1.282	99
5.	Test 2-C	1214	5.35	29.74	± 36.72	1.327	142

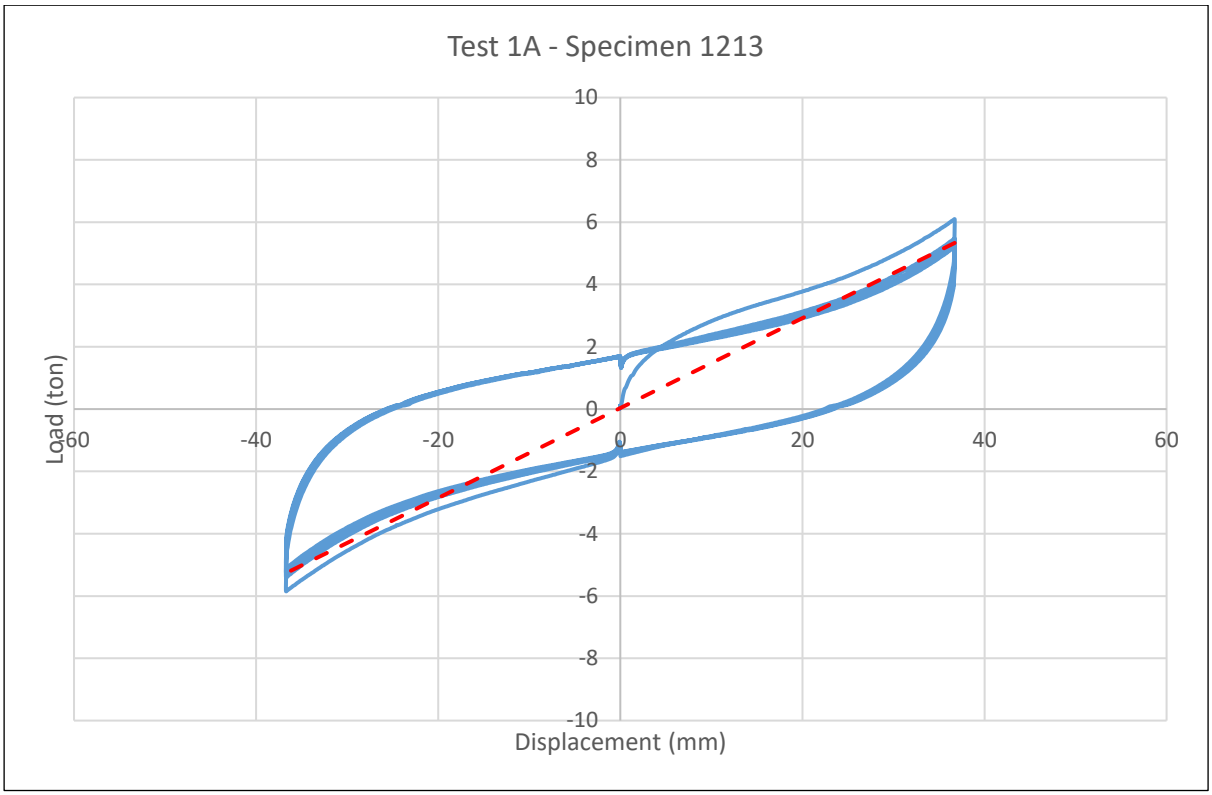

Figure 6.6: Load-displacement curve of Test 1-A.

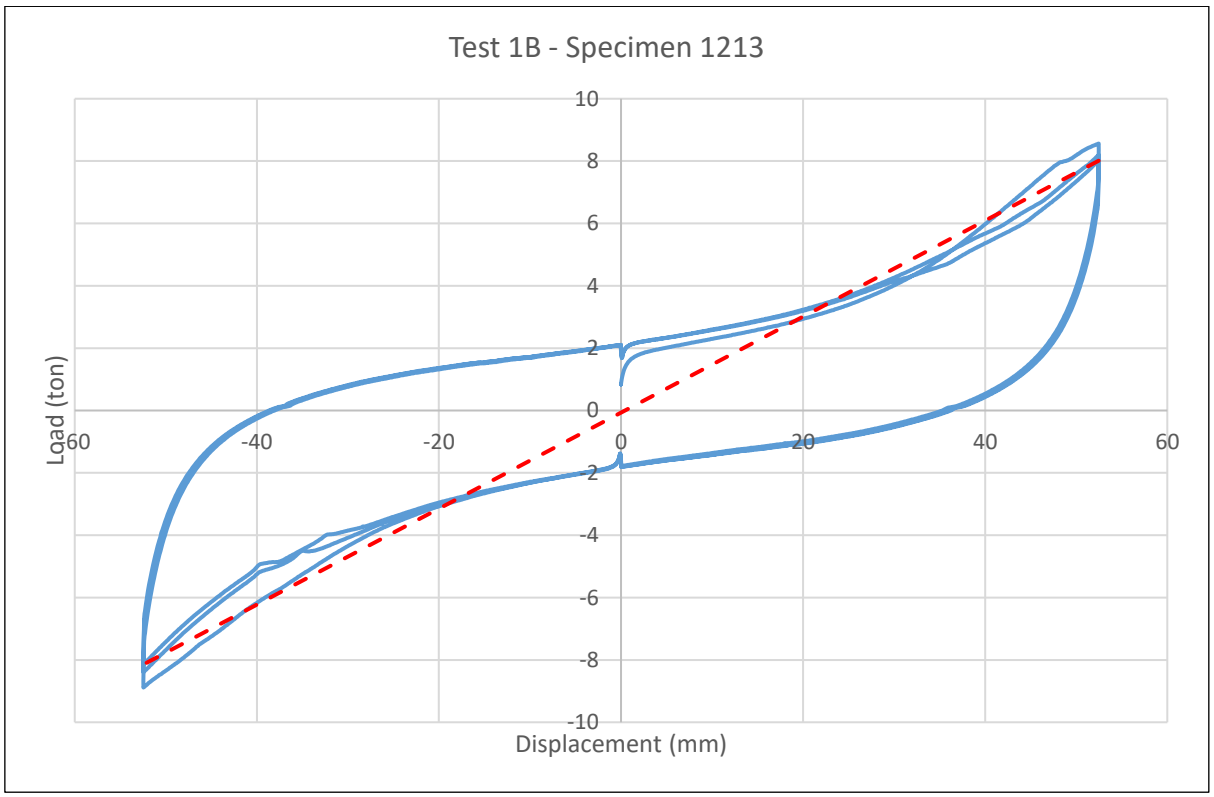

Figure 6.7: Load-displacement curve of Test 1-B.

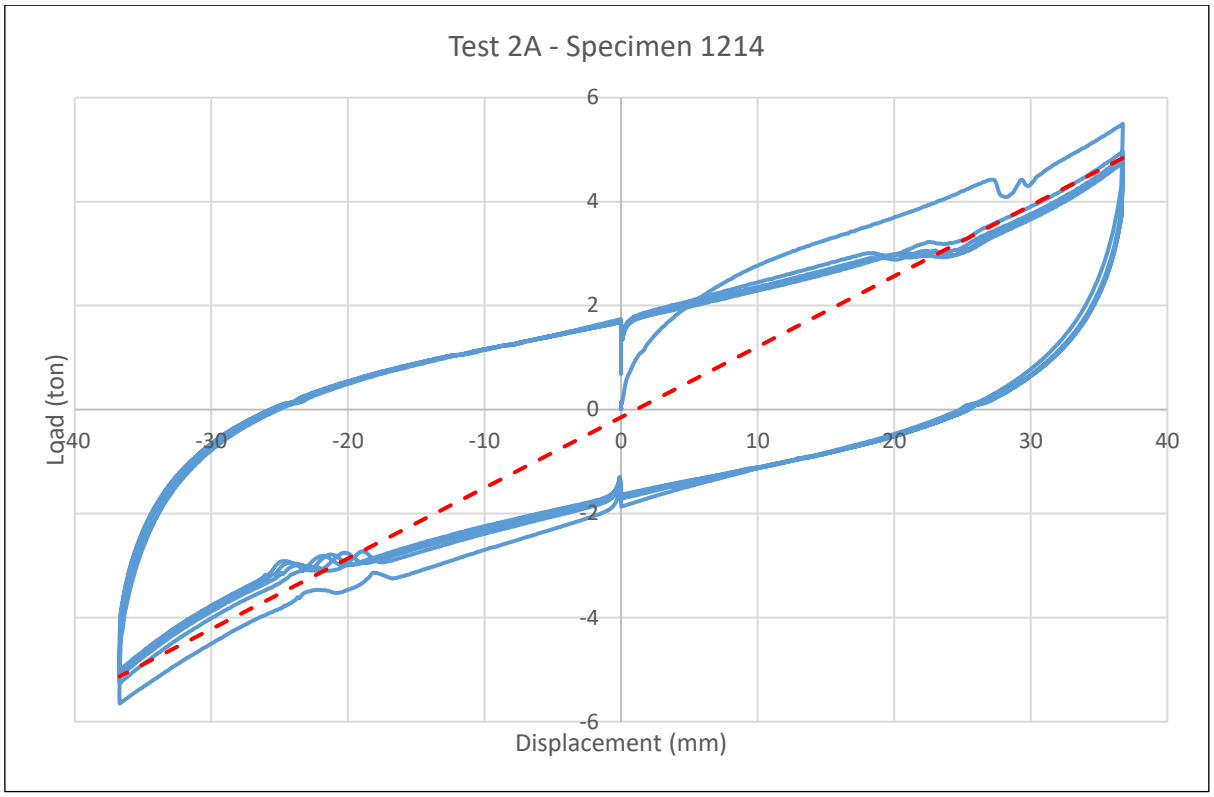

Figure 6.8: Load-displacement curve of Test 2-A.

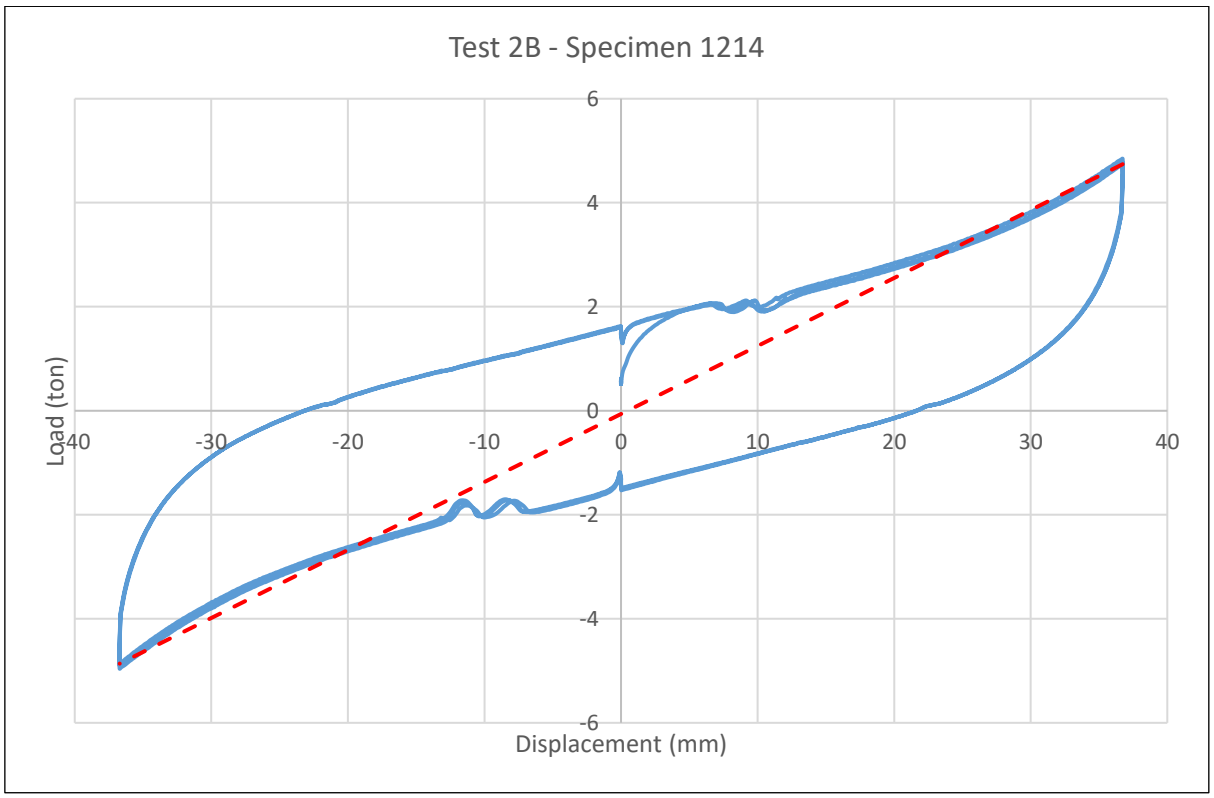

Figure 6.9: Load-displacement curve of Test 2-B.

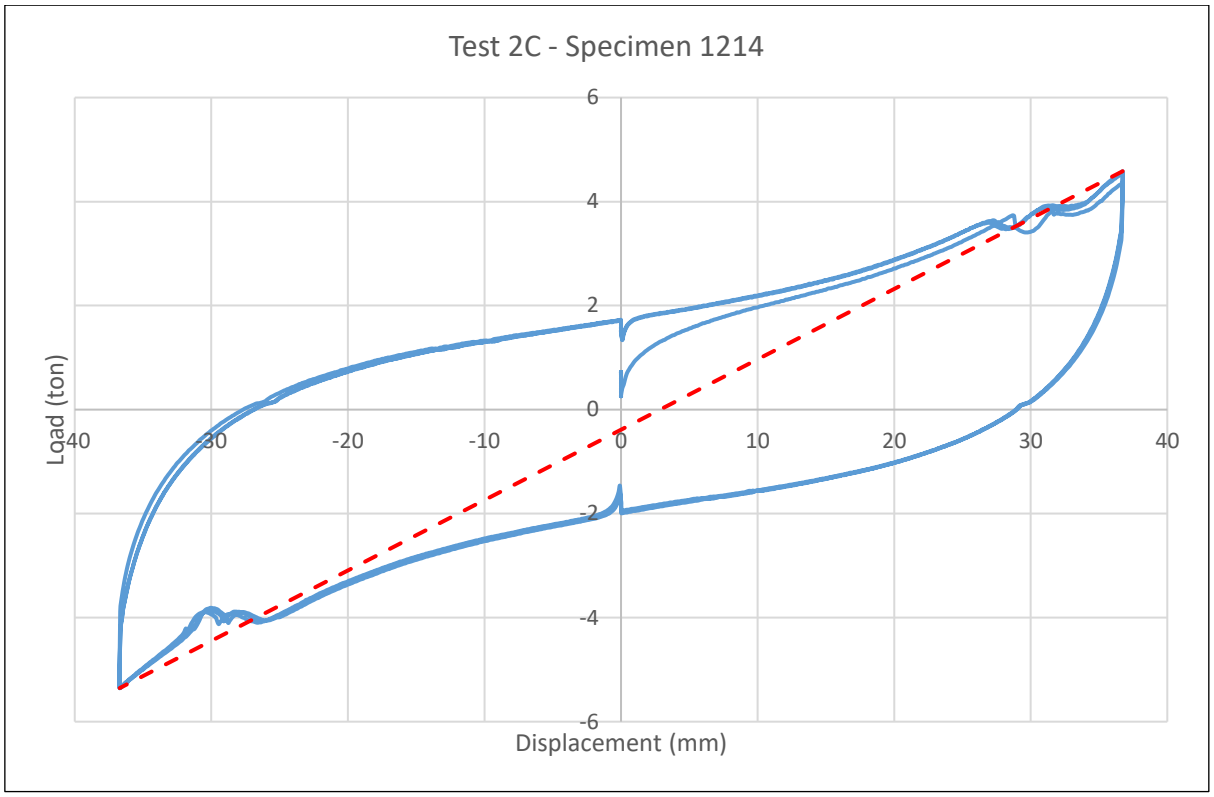

Figure 6.10: Load-displacement curve of Test 2-C.

6.3.3 Determination of Equivalent Damping Ratio of Bearings

The equivalent damping ratio (ζ_{eqv}) of a system can be calculated by equating the energy dissipated by the system in a vibration cycle and that of an equivalent system [3]. Hence, the equivalent damping ratio (ζ_{eqv}) of the bearings were evaluated from the enclosed area of load-displacement curve, which represents the dissipated energy (E_D) of the bearing, and the area under the straight line connecting the origin and maximum deformation point, which represents the strain energy (E_{S0}) as shown in Figure 6.11 by using the following equation (6.1). Then, Table 6.5 showed the dissipated energy (E_D), the strain energy (E_{S0}) and the equivalent damping ratios (ζ_{eqv}) of sample bearings evaluated from the third cycle of load-displacement curves (shown in Figure 6.6 to 6.10) for different load cases by using the equation (6.1).

$$\zeta_{eqv} = \frac{1}{4\pi}\frac{E_D}{E_{S0}} \qquad (6.1)$$

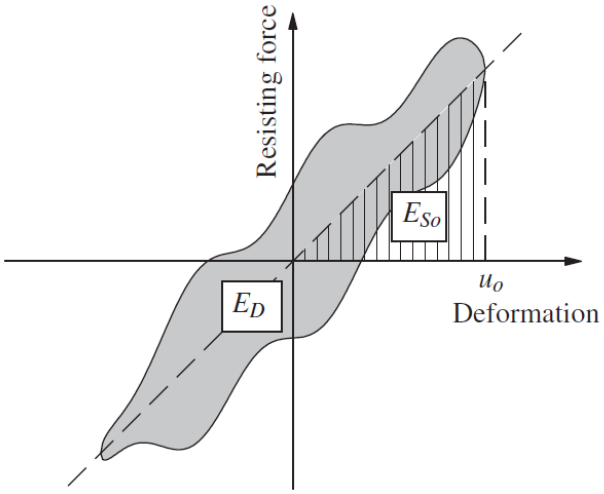

Figure 6.11: Strain energy (E_{S0}) and energy dissipated (E_D) during the experiment [3].

Table 6.5: Equivalent damping ratio of bearings determined from load-displacement curves

Sr.	Test Number	Specimen Number	Lateral Displacement (mm)	Vertical Load (P) (ton)	Dissipated Energy (E_D) (kN.m)	Strain Energy (E_S) (kN.m)	Equivalent Damping Ratio (ζ_{eqv}) (%)
1.	Test 1-A	1213	36.75	19.82	2.84	0.96	23.55
2.	Test 1-B	1213	52.50	19.82	5.53	2.06	21.37
3.	Test 2-A	1214	36.75	19.82	2.87	0.87	26.18
4.	Test 2-B	1214	36.75	9.91	2.64	0.85	24.63
5.	Test 2-C	1214	36.75	29.74	3.03	0.83	29.25

6.4 Comparison of Test Results

From Table 6.4, the shear modulus or stiffness of bearing sample No. 1213 was found to be generally higher than that of sample No. 1214 especially for Test 1-B with maximum displacement (drift), showing the effect of increasing drift on higher value of shear modulus due to increased lateral loads.

According to Table 6.5, it can be seen that the bearing from Test 1-B dissipated more energy with minimum damping ratio than other load cases because it was pushed to higher displacement (52.5 mm) comparing with other specimens. The dissipated energy of the bearing from Test 2-C was found to be the second largest with the maximum damping ratio, and it may be due to the high vertical compressive load it suffered.

For the bearing specimen No. 1214 under varying vertical compressive loads with the same lateral displacement, dissipated energy as well as damping ratio gradually increases from Test 2-B under the lowest vertical load to Test 2-C under the highest vertical load. These results confirmed the effect of increasing vertical loads which caused the bearing to dissipate more energy with higher damping ratio. The occurrence of wavy ups and downs in the load-deflection curves of specimen No. 1214 may be due to the occurrence of slip between the specimen and connecting steel plates.

Moreover, the values of shear modulus (horizontal stiffness) obtained from experiments, shown in Table 6.4, were found to be lower than the design value of 1.66 kN/mm provided by the manufacturer. Vertical stiffness values of the bearings were also found to be much lower than the design value of 451 kN/mm. However, the values of equivalent damping ratio from experiments, shown in Table 6.5, were found to be larger than the design value of 16.9% and the measured value 21.8% to 22.7% described by the manufacturer.

6.5 Summary

In order to acquire necessary information in conducting cyclic loading tests for bridge bearings, which were intended to use in the retrofitting of long span steel bridges in Myanmar, two elastomeric rubber bearings were tested in five different loading configuration with the courtesy of Sumitomo Riko Company Limited.

Load-displacement curves were drawn for each load cases and, accordingly, shear modulus or horizontal stiffness, vertical stiffness, dissipated energy, strain energy and equivalent damping ratio of sample bearings were evaluated from the experiment data of the third loading cycle. Test results showed the effect of increasing lateral displacement (drift) on higher value of shear modulus and dissipated energy due to increased lateral load, and the effect of increasing vertical loads causing the bearing to dissipate more energy with higher damping ratio.

References

[1] Oyawa, W. O., Structural Response of Filled Steel Composite Members, D.Eng. Thesis, Kyoto University, January 2000.

[2] NCHRP, Elastomeric Bridge Bearings: Recommended Test Methods, National Cooperative Highway Research Program, National Academic Press, 2001.

[3] Chopra, A.K., Dynamics of Structures, 4th edition, Prentice Hall, 2012.

CHAPTER 7
Dynamic Assessment of Retrofitted Maubin Bridge

7.1 Introduction

There is a rapid increase in the number of long span steel bridges in Myanmar within the last two decades and most of them were steel-through-truss bridges as well as few suspension bridges and few steel arch bridges. Most of the bridges were designed and fabricated in China and some of them were constructed close to the fault line. Until recently, there was no reliable data concerning with the intensity of earthquakes for various regions of the country except for the Seismic Zone Map of Myanmar issued by Myanmar Earthquake Committee in 2005 [1] as the first edition and later in 2012 for the second edition [2]. Since the design earthquake load for the long span bridges in Myanmar were usually assumed as 0.1g before these maps were issued, it is essential to assess the seismic performance of these bridges for the future earthquakes. As a preliminary review for such kind of study, Maubin Bridge was selected as a case study bridge, and numerical analyses as well as field load testing were performed with the results described in Chapter 4 and 5, and also reported in previous symposiums [3, 4, 5, 6]. Then, after running the dynamic implicit analysis of FE bridge model using the acceleration-time series of a typical earthquake in Myanmar, the bridge will be proposed to retrofit with steel reinforced elastomeric rubber bearings.

7.2 Preliminary Design of Elastomeric Bearings for Seismic Retrofit

7.2.1 Preliminary Static and Pushover Analyses

Maubin Bridge was initially designed with the assumed earthquake load of 0.1 g according to AASHO 1977 [7], but the new Seismic Zone Map of Myanmar (2012) stated the possible ground acceleration as 0.11 g ~ 0.2 g for the return period of 475 years (Level I earthquake) and 0.21 g ~ 0.4 g for the return period of 2475 years (Level II earthquake) for the bridge site. Hence, the seismic performance of the bridge under the increased seismic loads was evaluated in the preliminary study by the static analysis under the design load combinations as well as pushover analysis under the own weight plus 20% and 40% of own weight in horizontal and vertical directions (representing 0.2 g and 0.4 g earthquake) for the potential seismic retrofit, and the results were discussed in Chapter 4.

Static analysis results of the FE bridge model showed that stresses in some tension and compression diagonal truss members were greater than the allowable stresses in original wind

load and increased earthquake load combinations, but stresses were lower for bottom chords, top and bottom bracings, floor beams and portal bracings. However, according to the pushover analysis, some top chords and most tension and compression diagonal members suffered stresses greater than the allowable stresses and sometimes even larger than yield stresses for the increased earthquake loads. Hence, the bridge will be proposed to conduct seismic retrofit by using elastomeric rubber bearings. Piers were not included in the bridge model for the above preliminary static and pushover analyses.

7.2.2 Calculations of Bearing Dimensions according to AASHTO Specifications

Maubin Bridge is a four span continuous warren steel truss bridge, supported by five reinforced concrete piers (P4 ~ P8) with 120 m span length for each span. End piers (P4 and P8) are single column piers and middle piers (P5 ~ P7) are double column piers with the height of 15.5 m [8]. The width of the piers in the top are 2.5 m for P4 and P8, and 3.0 m for P5 ~ P7, which were wide enough for the installation of new elastomeric rubber bearings. The existing bearings used for the bridge on the top of piers are steel bearings of two different types, fixed (hinge) bearings on pier P5 and movable (roller) bearings on other piers (P4, P6, P7, P8).

For seismic retrofitting of the bridge, existing steel bearings will be proposed to replace with steel reinforced elastomeric rubber bearings for the better load sharing in the longitudinal direction of the bridge as well as for the isolation between superstructure and substructure. In order to estimate the dimensions of the elastomer and steel, the bearings were designed preliminarily in accordance with the method B of AASHTO-LRFD specifications [9]. A typical elastomer with hardness 60 Shore A Durometer, and a shear modulus of 150 psi (1MPa) is assumed for the proposed bearing with 1.75 ksi (12 MPa) delamination stress limit. Then the dimensions of the bearing are calculated as shown in Table 7.1 and detail calculations are described in Appendix D.

Table 7.1: Dimensions of proposed steel reinforced elastomeric bearings.

Sr.	Bearing Location	Plan Dimension	Interior Elastomer		Exterior Elastomer		Steel Plate Thickness
			Thickness	Layers	Thickness	Layers	
1.	P5 and P7	1.3 m x 0.75 m	40 mm	7	30 mm	2	5 mm
2.	P6	1.1 m x 0.75 m	35 mm	5	25 mm	2	4 mm
3.	P4 and P8	0.5 m x 0.75 m	25 mm	3	15 mm	2	3 mm

7.3 Application of Thabeikkyin Earthquake Record for Dynamic Analysis

The case study bridge, Maubin Bridge, was constructed over the Myitmaka River, a branch of Ayeyarwady River in Maubin Township of the Ayeyarwady Region and it is situated about 90 km west of the famous Sagaing Fault. Hence, Thabeikkyin Earthquake acceleration time history was used for the dynamic analysis of the bridge model because it was the last greatest earthquake recorded in Sagaing Fault. The data used in this study was measured from the Mandalay station, which is one of the few seismic stations in Myanmar as well as the closest station to the epicenter about 100 km away. But the maximum acceleration values of the earthquake were measured only as 26.39 gal in longitudinal direction and it is not large enough to use in the dynamic implicit analysis of the FE bridge model in ABAQUS according to the Seismic Zone Map of Myanmar 2012. Therefore, for the purpose of using these data for the analysis of case study bridge, the peak ground acceleration of the original data was increased to 0.2 g and 0.4 g by multiplying with some factors as discussed in Chapter 3 of the thesis. The modified acceleration time series of the Thabeikkyin Earthquake to 0.2 g and 0.4 g were shown in Figure 7.1 and 7.2.

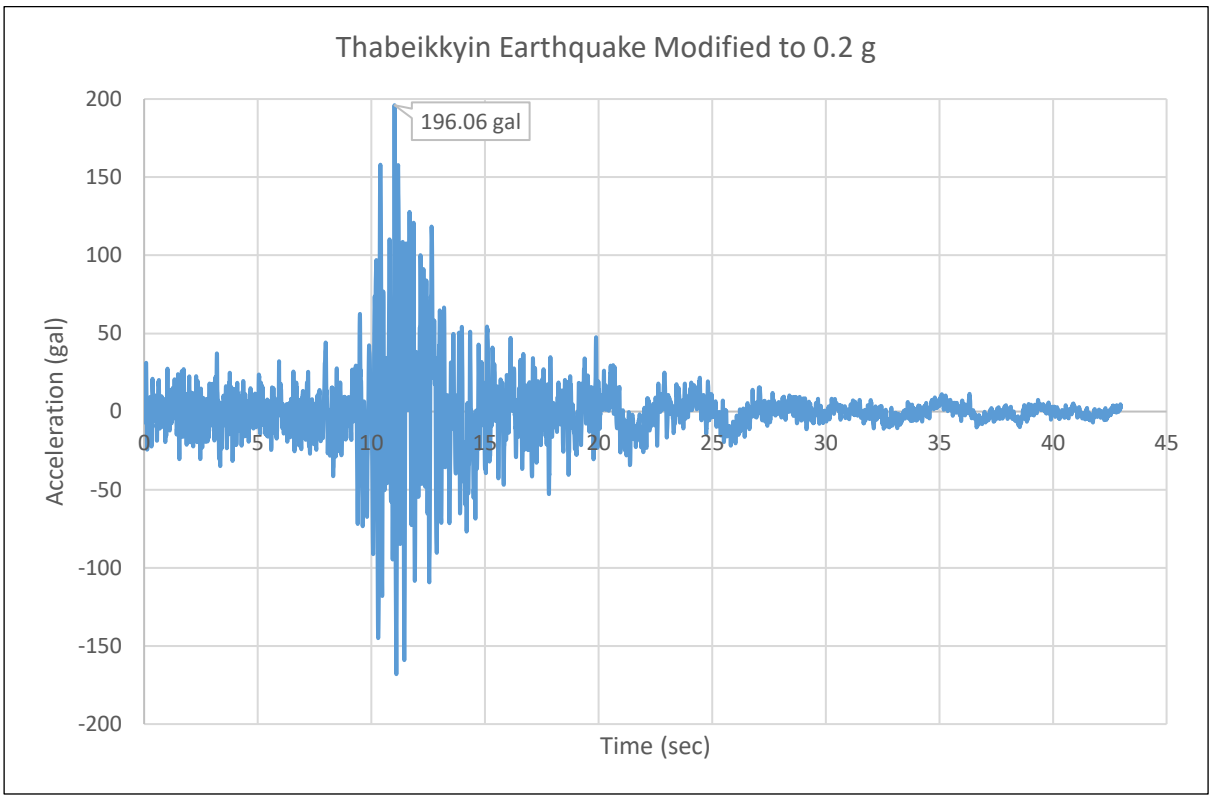

Figure 7.1: Acceleration time history of Thabeikkyin Earthquake modified to 0.2 g.

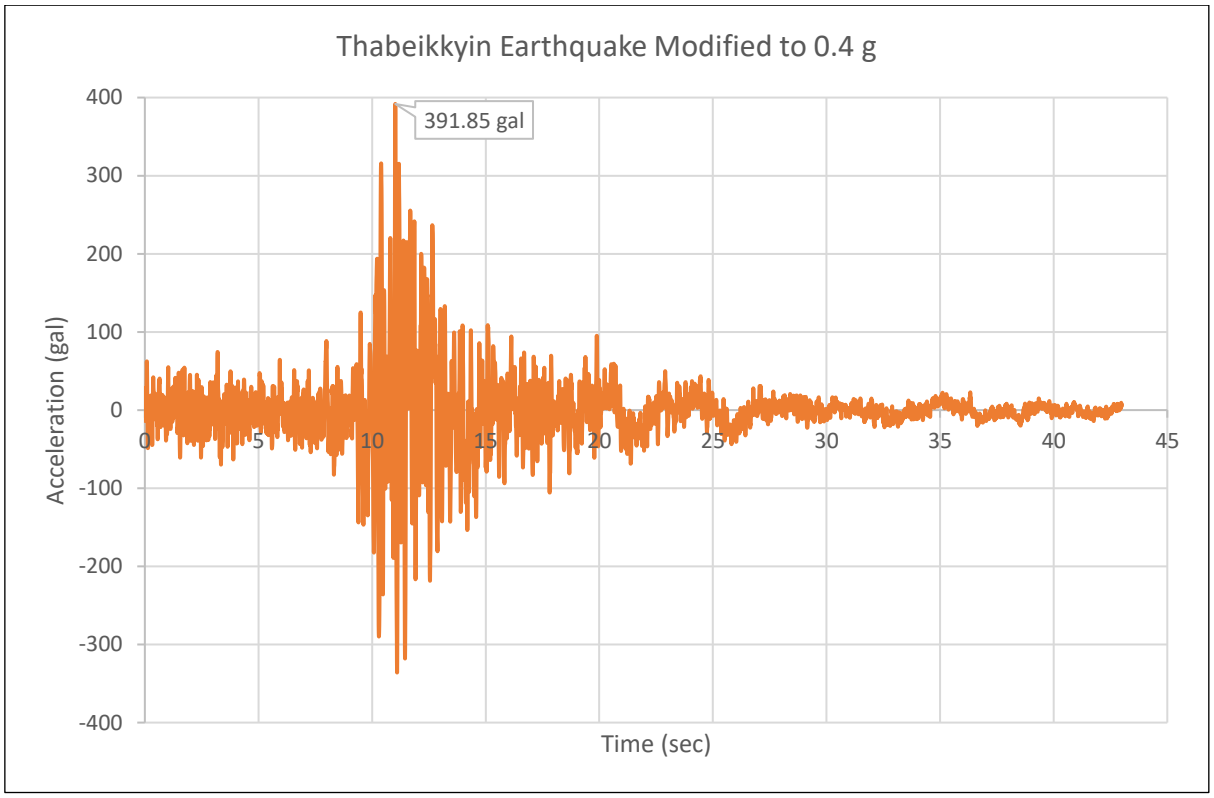

Figure 7.2: Acceleration time history of Thabeikkyin Earthquake modified to 0.4 g.

7.4 Dynamic Assessment of Retrofitted Maubin Bridge

After the FE bridge model was analyzed by static and pushover analyses as described in the previous Chapter 4 of the thesis, the analysis results confirmed overstressed members due to the increased seismic loads. Then, the accuracy of the FE bridge model was confirmed and adjusted by using the results of static and dynamic field load testing on the actual bridge as discussed in the Chapter 5 of the thesis. As a final step, the retrofitted bridge model will be analyzed again by dynamic implicit analysis, comparing between the stresses with the existing bearings and the stresses with retrofitted elastomeric bearings under the modified Thabeikkyin Earthquake data. Only the superstructure steel truss was considered in the bridge model for the preliminary analysis, but bridge piers were included in the retrofitted bridge model because acceleration time history record of Thabeikkyin Earthquake in Myanmar was applied at the base of bridge piers in the dynamic implicit analysis.

7.4.1 Spring Stiffness Values for Existing Bearings and Elastomeric Rubber Bearings

In addition to the bridge model adjusted by the results of field load tests, spring elements were used in the analysis to represent the existing hinge and roller bearings as well as to represent the elastomeric rubber bearings with proper spring stiffness values. The spring

stiffness values in six degree of freedom (DOF) directions for existing bearings and propose rubber bearings used in the bridge model were shown in Table 7.2, and spring stiffness values between the piers and the ground were assumed as 10^{17} kN/mm (infinity) for K_1, K_2, K_3, and 10^{17} kN/rad for K_4, K_5, K_6, where K_1, K_2, K_3 referred displacement spring stiffness values and K_4, K_5, K_6 referred rotational spring stiffness values in longitudinal (X), vertical (Y) and transverse (Z) directions of the bridge. The values of stiffness K_1 and K_2 for elastomeric bearings were found out by trial and error to get minimum stresses in truss members.

Table 7.2: Values of spring stiffness in six DOF directions for bearings.

Sr.	Bearing Type	K_1 (kN/mm)	K_2 (kN/mm)	K_3 (kN/mm)	K_4 (kN/rad)	K_5 (kN/rad)	K_6 (kN/rad)
1.	Hinge (existing)	10^{17}	10^{17}	10^{17}	10^{17}	10^{17}	10^{-5}
2.	Roller (existing)	10^{-5}	10^{17}	10^{17}	10^{17}	10^{17}	10^{-5}
3.	Elastomeric	1	300	10^{17}	10^{17}	10^{17}	10^{17}

7.4.2 Analysis Results with Existing Bearings under Modified Thabeikkyin Earthquake

With the spring stiffness values described in Table 7.2, the FE bridge model with the existing bearings was run by the dynamic implicit analysis under the own weight of the bridge. The acceleration time series of modified Thabeikkyin Earthquake data (0.2 g and 0.4 g) were applied at the base of piers in each of three different directions, longitudinal (X), vertical (Y) and transverse (Z) directions of the bridge, and the analysis results were shown in Table 7.3.

According to Table 7.3, there were four tension diagonal members (D35 and D46, each on upstream truss and downstream truss) suffered maximum tensile stresses of 386 MPa, which were higher than their yield strength of 345 MPa. Besides these over-yield-stress members, 18 top chords over the supports at three middle piers, 36 top chords in the middle and side spans, 54 tension diagonal members, and 48 compression diagonal members suffered higher stresses greater than the allowable stress values under two different modified Thabeikkyin Earthquake intensity of 0.2 g and 0.4 g. Bottom chords, top bracings, bottom bracings, floor system and piers did not show overstresses due to the earthquake.

Maximum stresses in the truss members were found to be 250 MPa for top chords over the support (U9 ~ U11, U19 ~ U21, U29 ~ U31 on two trusses), -238 MPa for top chords in the middle and side spans (U1 ~ U6, U14 ~ U16, U24 ~ U26, U34 ~ U39 on two trusses), 386 MPa for tension diagonal members (D2, D4, D6, D13, D15, D 17, D19, D22, D24, D26, D28, D33, D35, D37, D39 in the first two spans and symmetric members on next two spans of two

trusses), and -295 MPa for compression diagonal members (D1, D3, D14, D16, D18, D 20, D23, D25, D27, D34, D36, D38, D40 in the first two spans and symmetric members on next two spans of two trusses). Figures showing maximum stresses for different loading cases with original bearings from the ABAQUS analysis results were shown in Figures 7.3 to 7.8.

Table 7.3: Number of overstress members and maximum stresses with existing bearings.

Sr.	Earthquake Intensity and Direction	Overstress Case	Total No. of Overstressed Top Chord Members		Total No. of Overstressed Diagonal Members	
			Over Support	Mid span	Tension	Compression
1.	0.2g in X-dir	Over Allowable Stress	18 Nos. (248 MPa)	36 Nos. (-238 MPa)	58 Nos. (386 MPa)	48 Nos. (-293 MPa)
		Over Yield Stress	-	-	4 Nos. (386 MPa)	-
2.	0.2g in Y-dir	Over Allowable Stress	18 Nos. (248 MPa)	36 Nos. (-238 MPa)	58 Nos. (386 MPa)	48 Nos. (-292 MPa)
		Over Yield Stress	-	-	4 Nos. (386 MPa)	-
3.	0.2g in Z-dir	Over Allowable Stress	18 Nos. (249 MPa)	36 Nos. (-238 MPa)	58 Nos. (385 MPa)	48 Nos. (-292 MPa)
		Over Yield Stress	-	-	4 Nos. (385 MPa)	-
4.	0.4g in X-dir	Over Allowable Stress	18 Nos. (248 MPa)	36 Nos. (-238 MPa)	58 Nos. (386 MPa)	48 Nos. (-293 MPa)
		Over Yield Stress	-	-	4 Nos. (386 MPa)	-
5.	0.4g in Y-dir	Over Allowable Stress	18 Nos. (248 MPa)	36 Nos. (-238 MPa)	58 Nos. (387 MPa)	48 Nos. (-291 MPa)
		Over Yield Stress	-	-	4 Nos. (387 MPa)	-
6.	0.4g in Z-dir	Over Allowable Stress	18 Nos. (250 MPa)	34 Nos. (-238 MPa)	58 Nos. (384 MPa)	48 Nos. (-295 MPa)
		Over Yield Stress	-	-	4 Nos. (384 MPa)	-

Note: Allowable stress of members – 173 MPa ~ 190 MPa; yield stress – 315 MPa ~ 345 MPa.

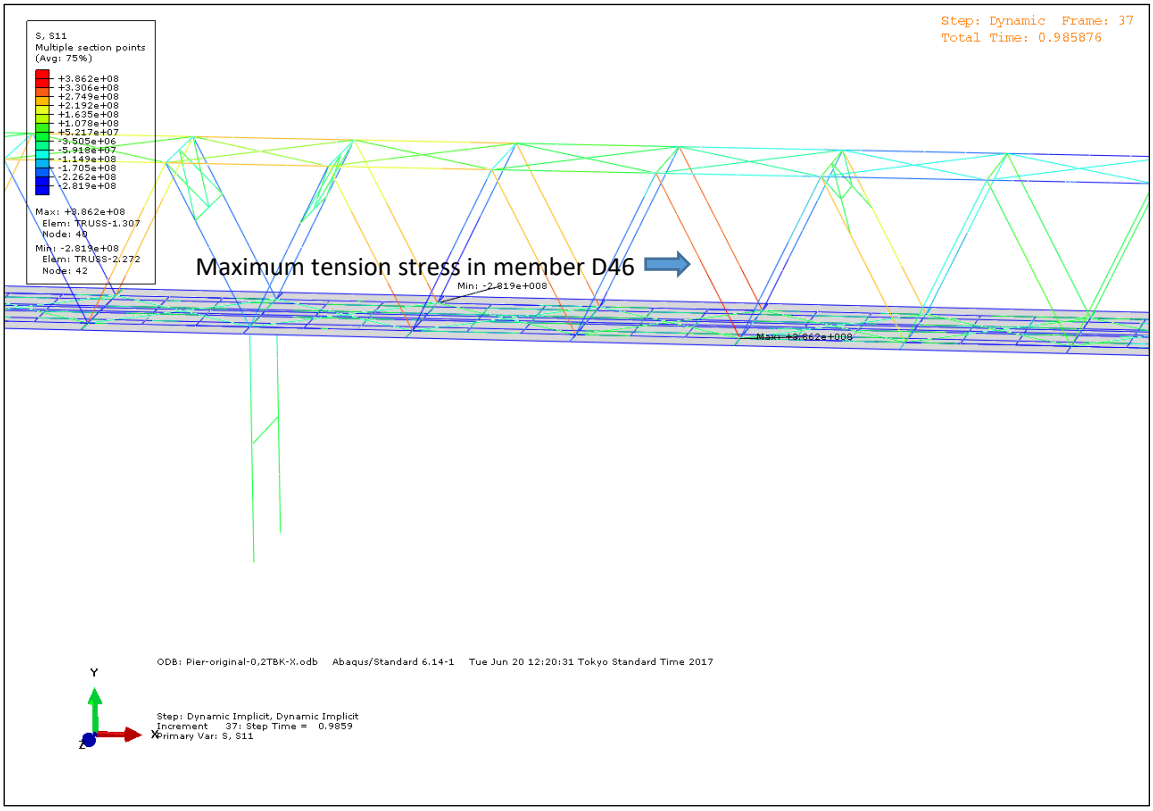

Figure 7.3: Maximum stresses with existing bearings due to 0.2g Thabeikkyin Earthquake in X-direction.

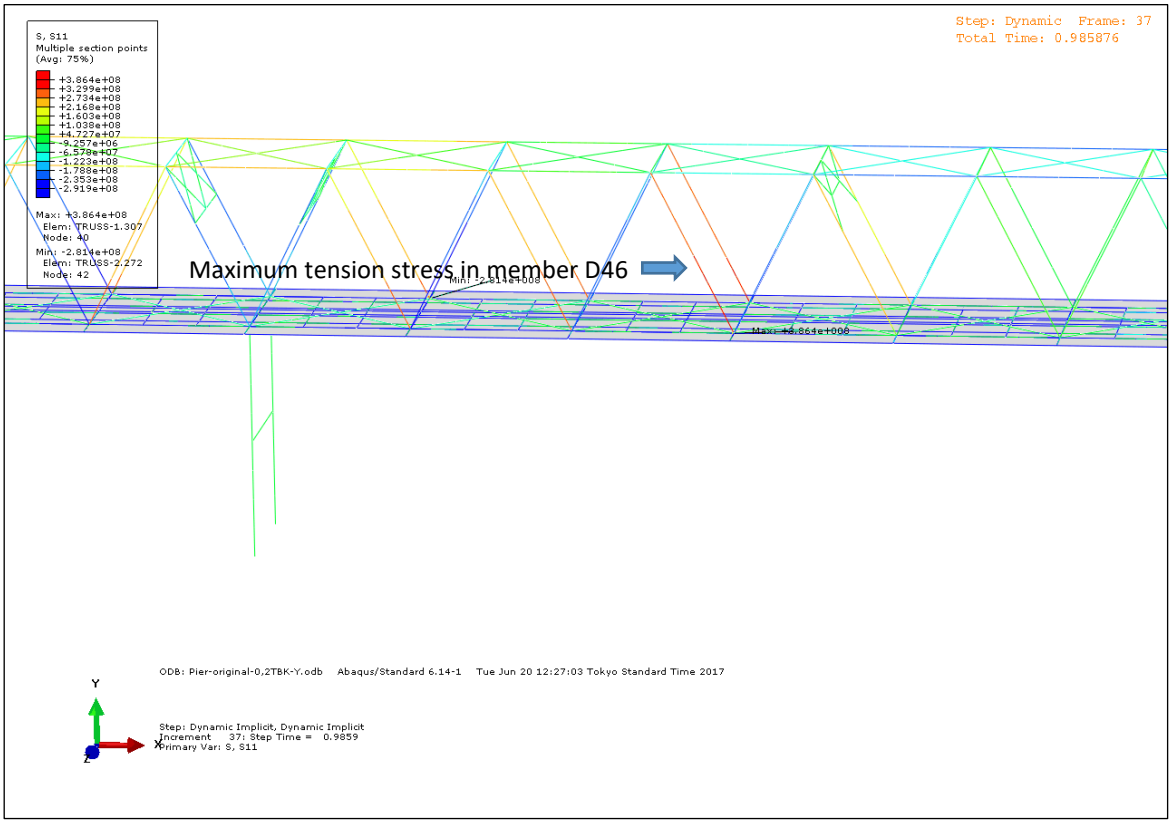

Figure 7.4: Maximum stresses with existing bearings due to 0.2g Thabeikkyin Earthquake in Y-direction.

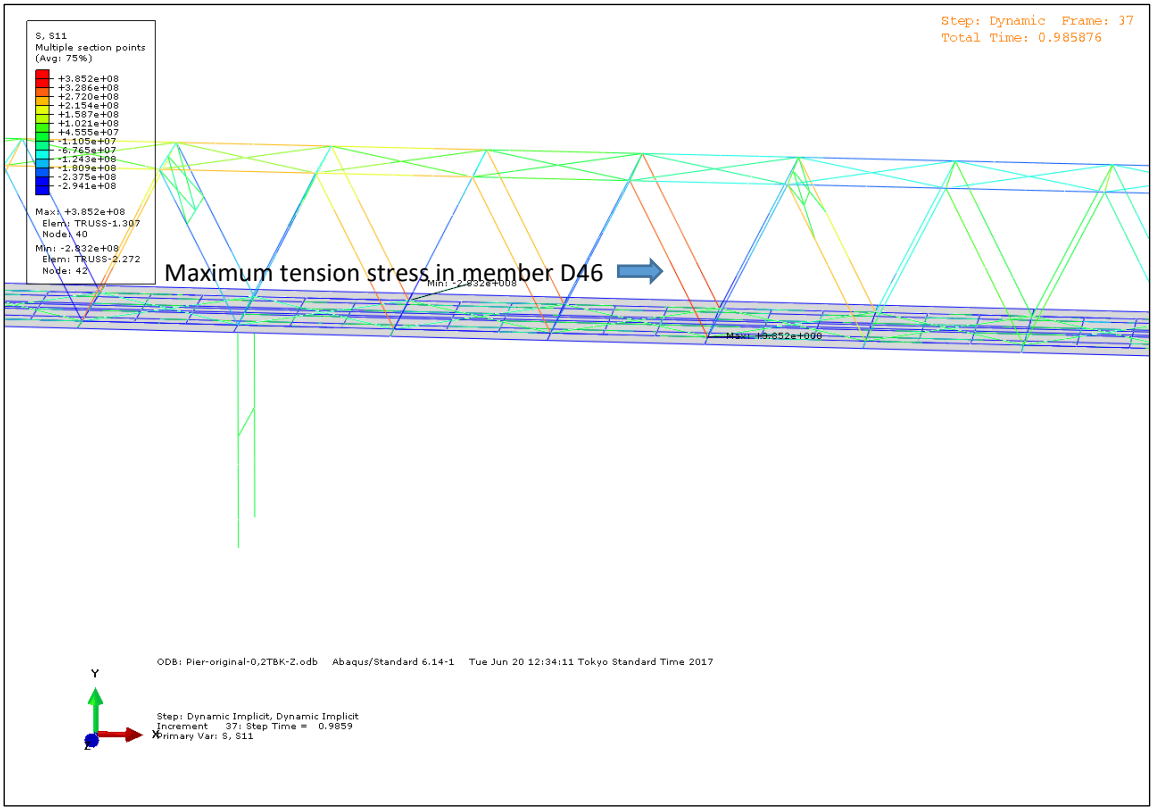

Figure 7.5: Maximum stresses with existing bearings due to 0.2g Thabeikkyin Earthquake in Z-direction.

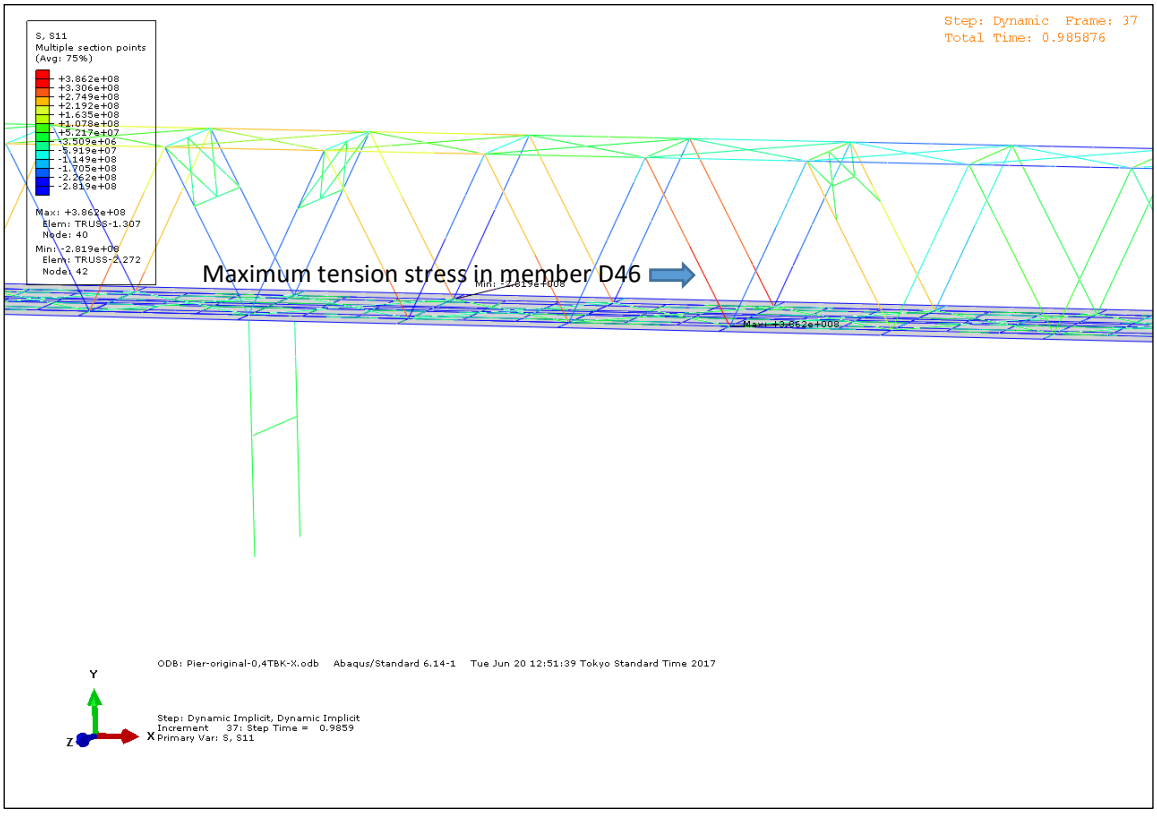

Figure 7.6: Maximum stresses with existing bearings due to 0.4g Thabeikkyin Earthquake in X-direction.

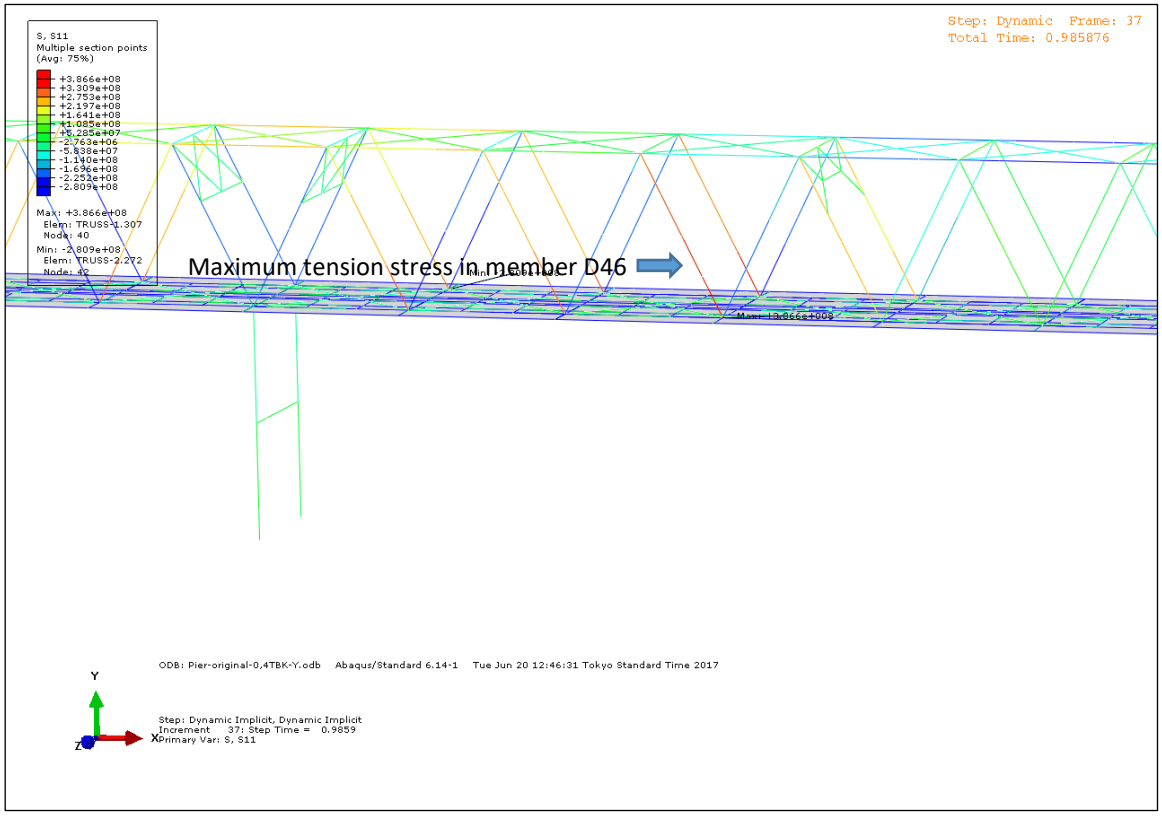

Figure 7.7: Maximum stresses with existing bearings due to 0.4g Thabeikkyin Earthquake in Y-direction.

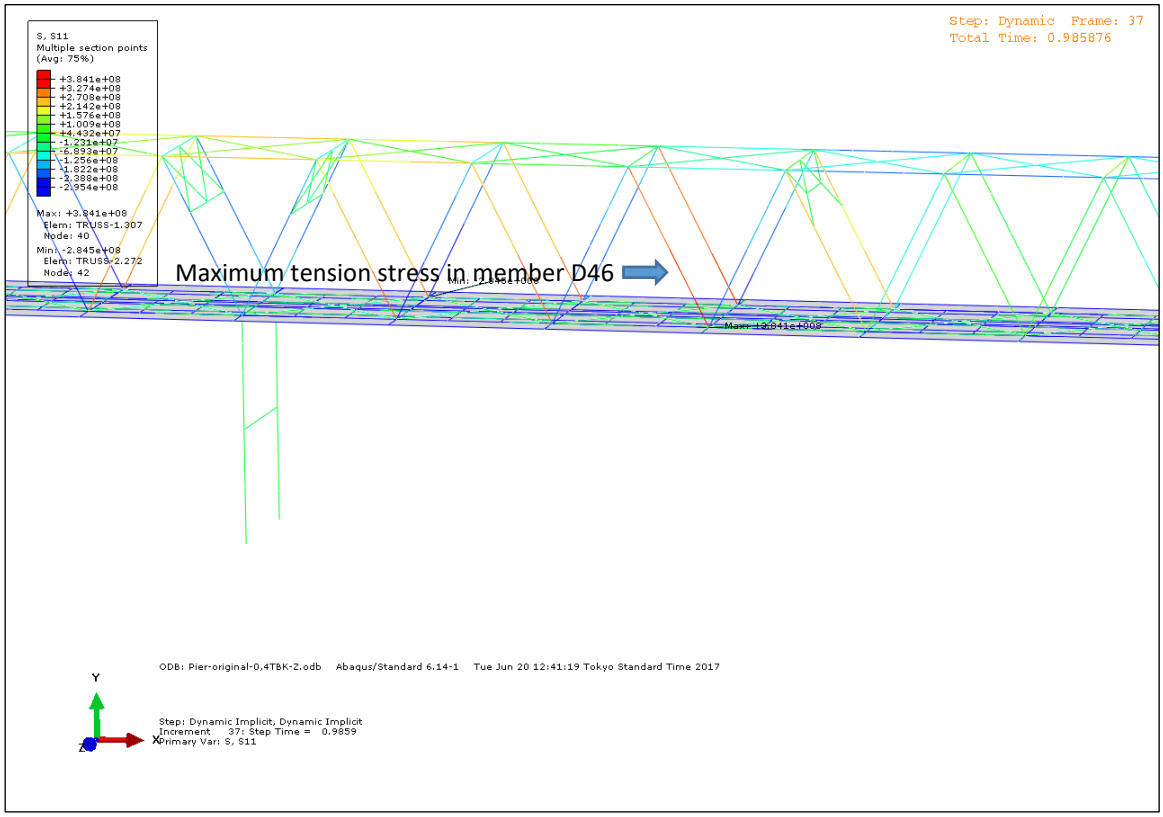

Figure 7.8: Maximum stresses with existing bearings due to 0.4g Thabeikkyin Earthquake in Z-direction.

7.4.3 Analysis Results with Elastomeric Bearings under Modified Thabeikkyin Earthquake

After analyzing the bridge model with the existing bearings, the bearings were replaced with elastomeric rubber bearings in the bridge model, assuming the retrofitted condition, using the spring stiffness values shown in Table 7.2. Then, as in the previous case, the bridge model was run again by dynamic implicit analysis under the own weight of the bridge, and the acceleration time series of modified Thabeikkyin Earthquake data (0.2 g and 0.4 g) were applied at the base of piers in each of three different directions, longitudinal (X), vertical (Y) and transverse (Z) directions of the bridge, and the analysis results were shown in Table 7.4.

Table 7.4: Number of overstress members and maximum stresses with elastomeric bearings.

Sr.	Earthquake Intensity and Direction	Overstress Case	Total No. of Overstressed Top Chord Members		Total No. of Overstressed Diagonal Members	
			Over Support	Mid span	Tension	Compression
1.	0.2g in X-dir	Over Allowable Stress	18 Nos. (252 MPa)	28 Nos. (-216 MPa)	56 Nos. (340 MPa)	38 Nos. (-320 MPa)
		Over Yield Stress	-	-	-	-
2.	0.2g in Y-dir	Over Allowable Stress	18 Nos. (252 MPa)	28 Nos. (-217 MPa)	56 Nos. (341 MPa)	38 Nos. (-320 MPa)
		Over Yield Stress	-	-	-	-
3.	0.2g in Z-dir	Over Allowable Stress	18 Nos. (253 MPa)	28 Nos. (-216 MPa)	56 Nos. (340 MPa)	38 Nos. (-320 MPa)
		Over Yield Stress	-	-	-	-
4.	0.4g in X-dir	Over Allowable Stress	18 Nos. (252 MPa)	28 Nos. (-216 MPa)	56 Nos. (341 MPa)	38 Nos. (-321 MPa)
		Over Yield Stress	-	-	-	-
5.	0.4g in Y-dir	Over Allowable Stress	18 Nos. (253 MPa)	28 Nos. (-217 MPa)	56 Nos. (342 MPa)	38 Nos. (-321 MPa)
		Over Yield Stress	-	-	-	-
6.	0.4g in Z-dir	Over Allowable Stress	18 Nos. (253 MPa)	28 Nos. (-216 MPa)	56 Nos. (340 MPa)	38 Nos. (-320 MPa)
		Over Yield Stress	-	-	-	-

Note: Allowable stress of members – 173 MPa ~ 190 MPa; yield stress – 315 MPa ~ 345 MPa.

According to Table 7.4, there were no over-yield-stress members, as in the case with existing bearings, but there were still 18 top chords over the supports in three middle piers, 28 top chords in the middle and side spans, 56 tension diagonal members, and 38 compression diagonal members suffering stresses greater than the allowable stress values under two different modified Thabeikkyin Earthquake intensity of 0.2 g and 0.4 g. As in the previous case, there were no overstresses occurred in bottom chords, top bracings, bottom bracings, floor system and piers due to the earthquake.

Maximum stresses in the truss members were found to be 253 MPa for top chords over the support (U9 ~ U11, U19 ~ U21, U29 ~ U31 on two trusses), -217 MPa for top chords in the middle and side spans (U2 ~ U6, U14 ~ U15, U25 ~ U26, U34 ~ U38 on two trusses), 342MPa for tension diagonal members (D2, D4, D6, D13, D15, D 17, D19, D22, D24, D26, D28, D33, D35, D37, D39 in the first two spans and symmetric members on next two spans of two trusses), and -321 MPa for compression diagonal members (D3, D14, D16, D18, D 20, D23, D25, D27, D34, D36, D38, D40 in the first two spans and symmetric members on next two spans of two trusses). Figures showing maximum stresses for different loading cases with elastomeric rubber bearings from ABAQUS analysis results were shown in Figures 7.9 to 7.14.

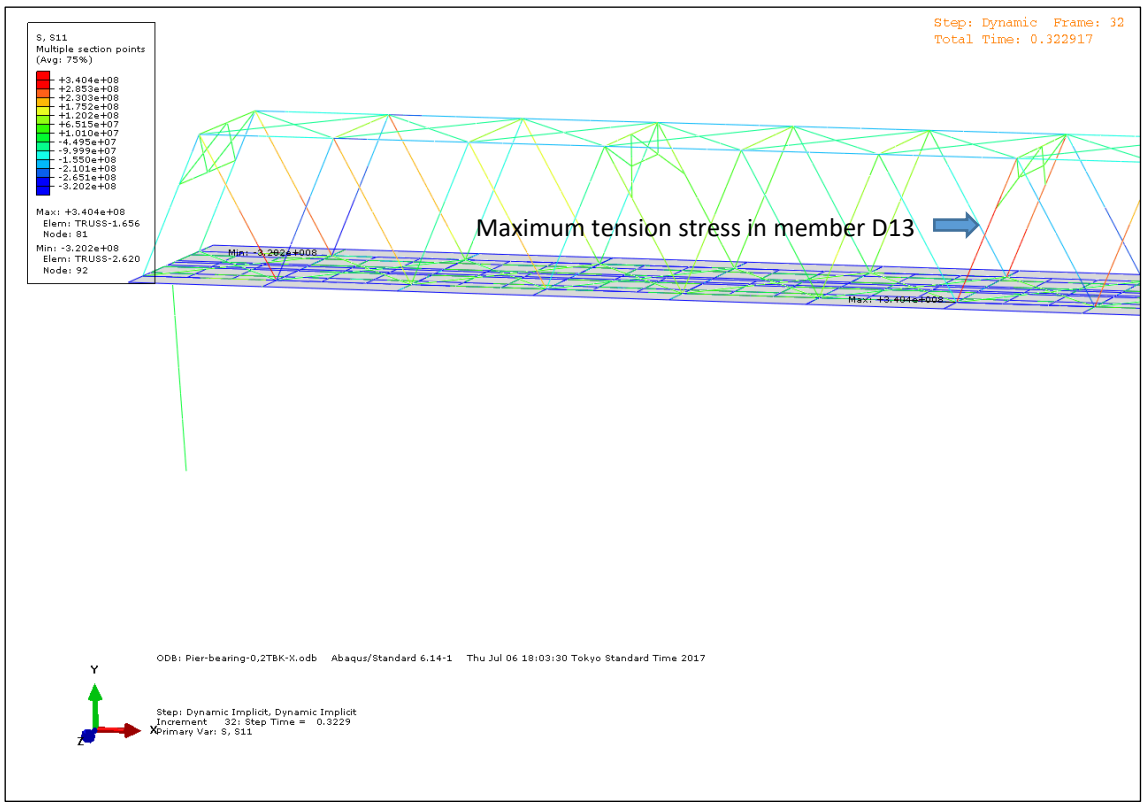

Figure 7.9: Maximum stresses with elastomeric bearings due to 0.2g Thabeikkyin Earthquake in X-direction.

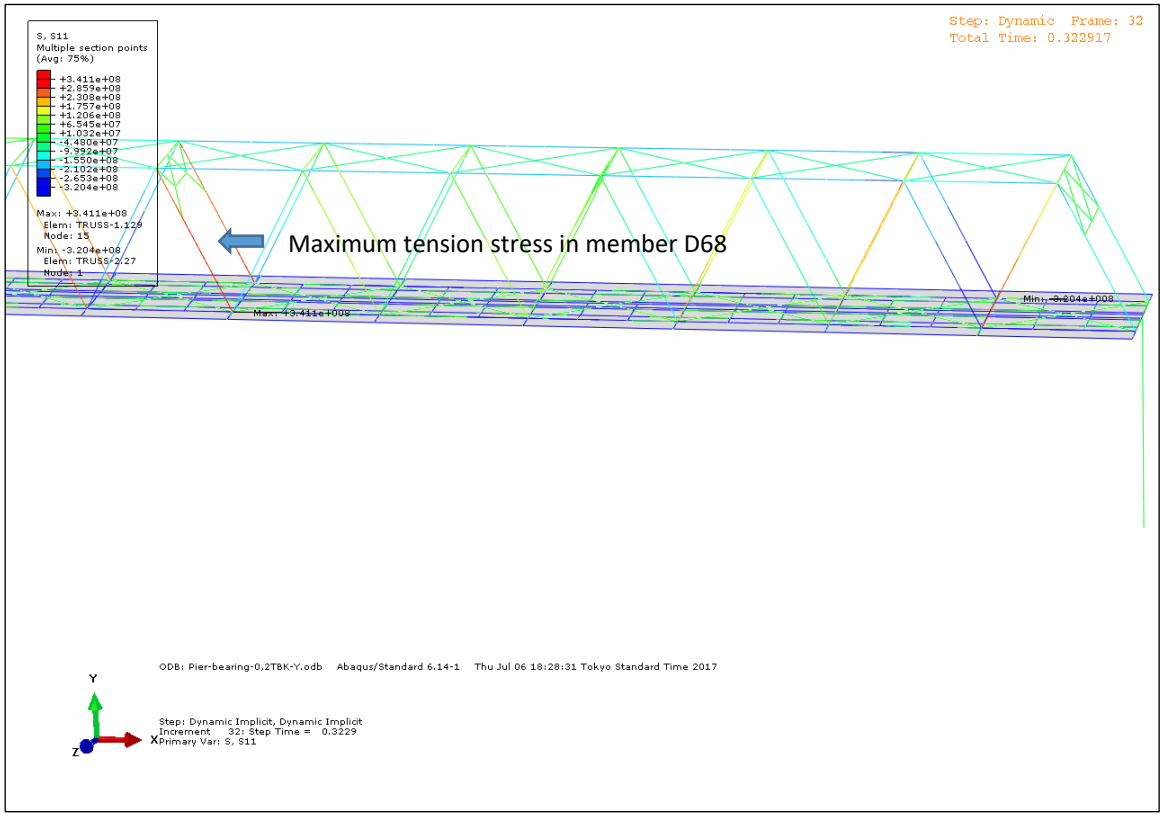

Figure 7.10: Maximum stresses with elastomeric bearings due to 0.2g Thabeikkyin Earthquake in Y-direction.

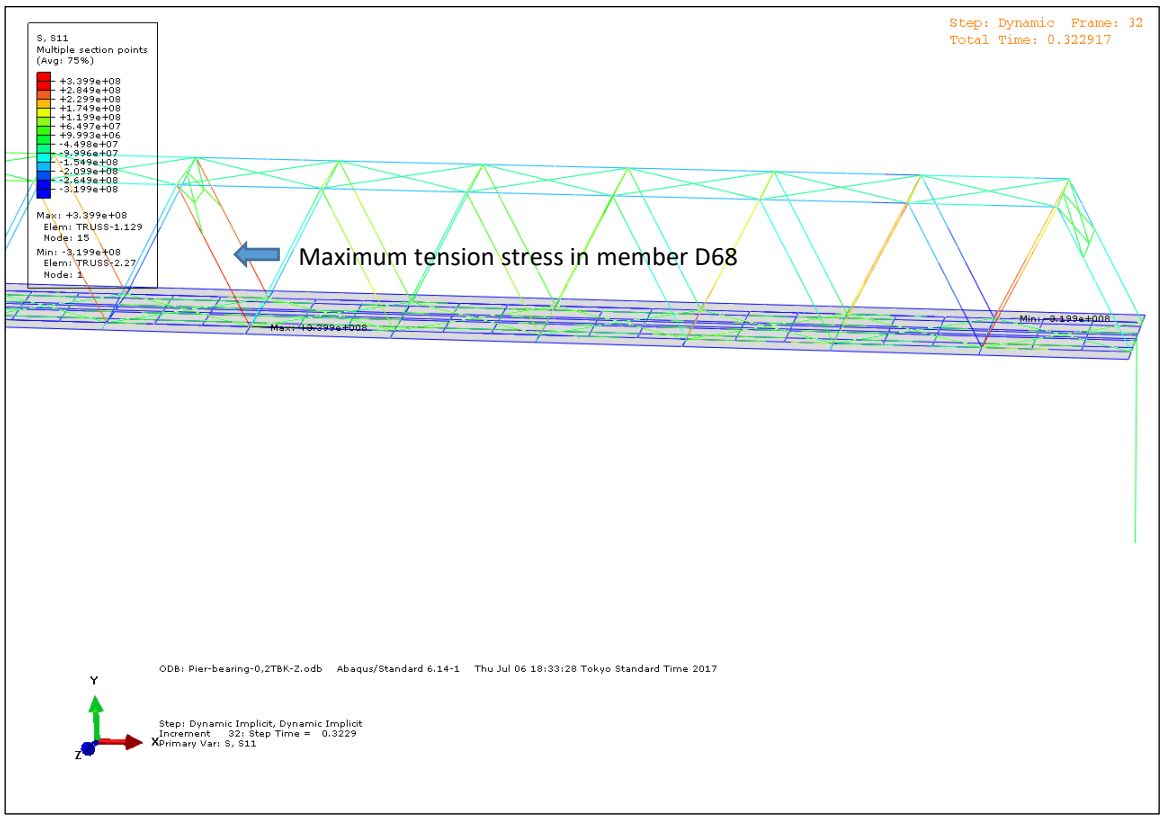

Figure 7.11: Maximum stresses with elastomeric bearings due to 0.2g Thabeikkyin Earthquake in Z-direction.

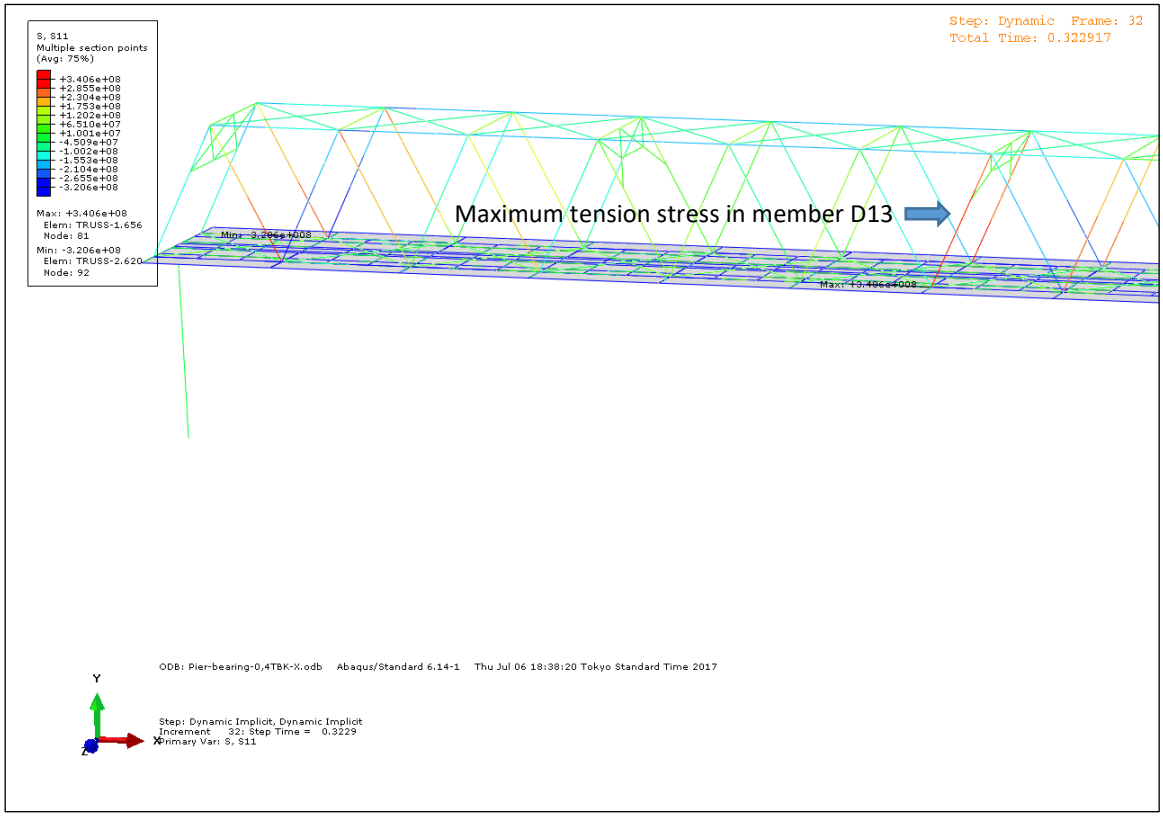

Figure 7.12: Maximum stresses with elastomeric bearings due to 0.4g Thabeikkyin Earthquake in X-direction.

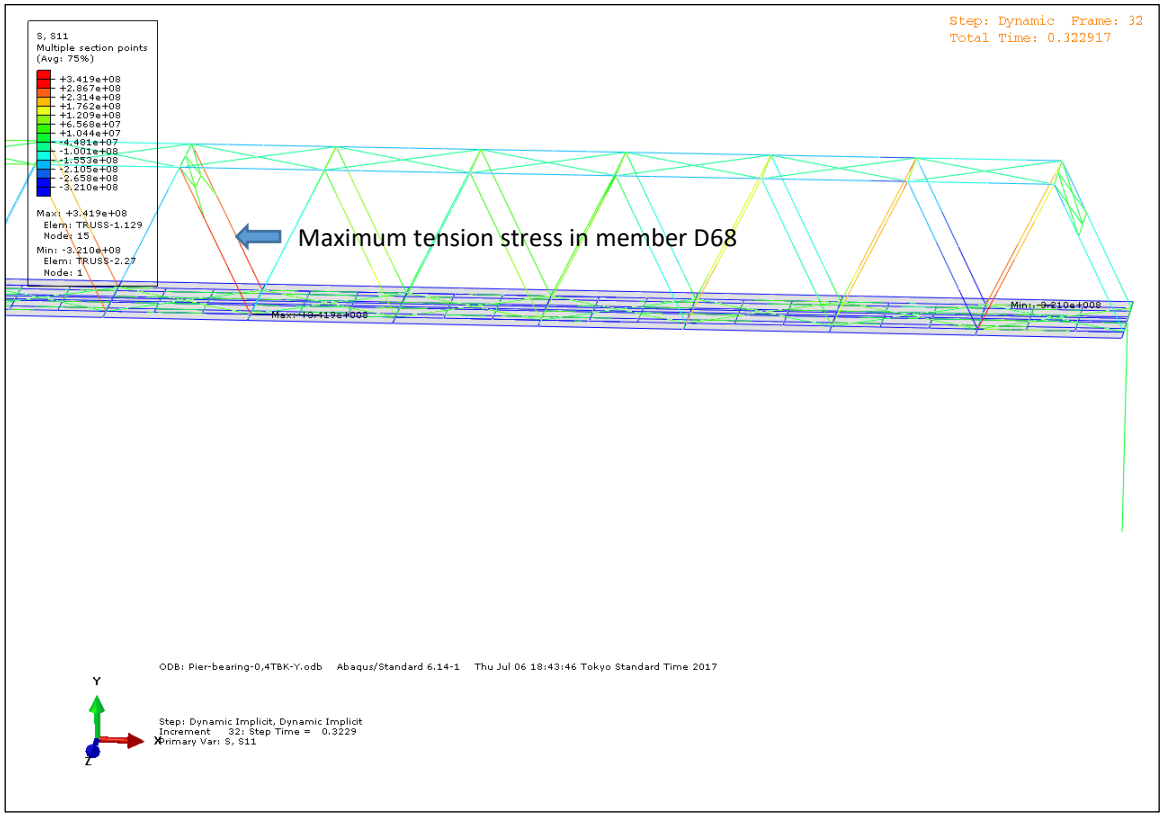

Figure 7.13: Maximum stresses with elastomeric bearings due to 0.4g Thabeikkyin Earthquake in Y-direction.

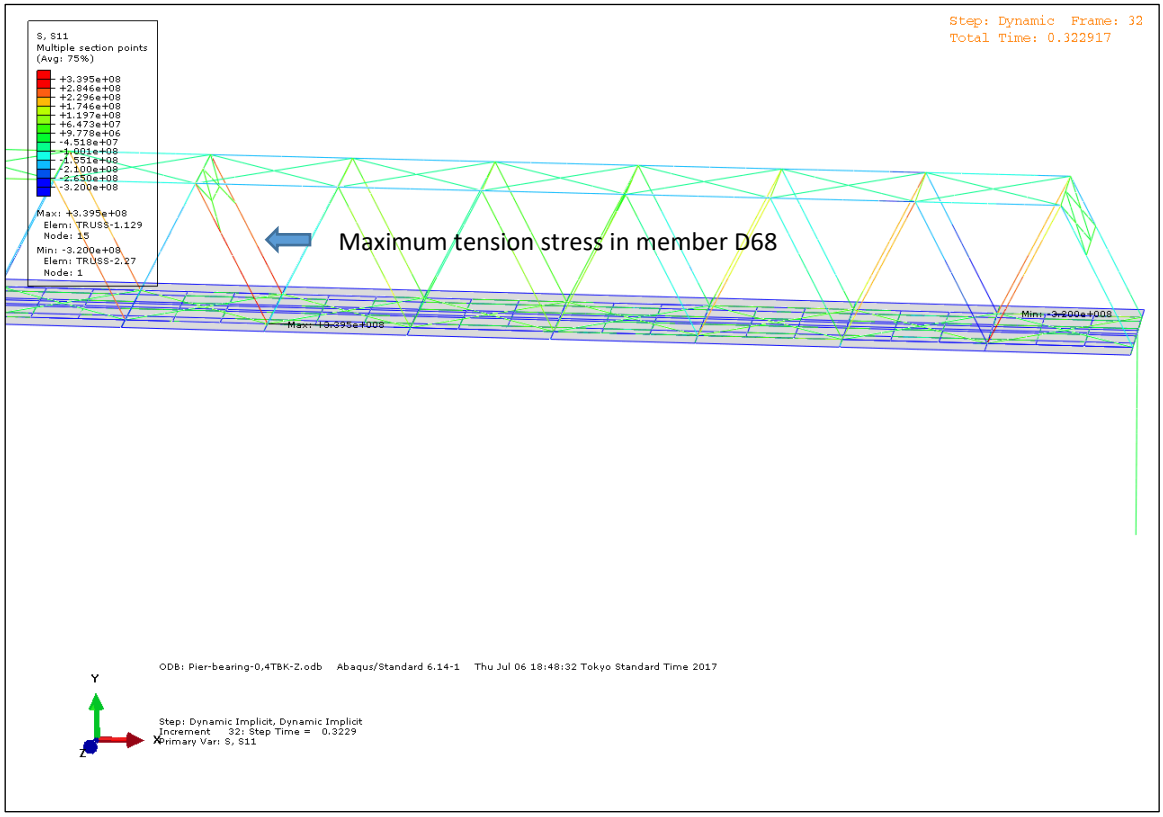

Figure 7.14: Maximum stresses with elastomeric bearings due to 0.4g Thabeikkyin Earthquake in Z-direction.

7.5 Comparison of Results Before and After Retrofitting

When comparing the results of dynamic analysis for before and after the retrofitting conditions by replacing the existing bearings with elastomeric rubber bearings, it was found out that the members which were previously stressed beyond the yield strength in the original model showed lower stresses below the yield limit in the retrofitted model. The number of overstressed members were also reduced from 36 to 28 for top chords in the middle and side spans, from 58 to 56 for tension diagonal members, and from 48 to 38 for compression diagonal members. Therefore, comparing with existing bearing condition, the retrofitted bridge model with elastomeric rubber bearings eliminates the over-yield-stress members, and also reduce the number of over-allowable-stress members from 160 to 140 in total. Although the overstress values were reduced in tension diagonal members and top chords in middle and side spans, some overstress values were found to be increased for compression diagonal members.

Most importantly, the ratio of horizontal reactions (R_x) in the longitudinal direction of the bridge on top of pier P5 (pier with original fixed bearings) between after-retrofitting condition and before-retrofitting condition were evaluated as 0.16 for 0.2g modified

earthquake, and 0.15 for 0.4g modified earthquake. Hence, it can be seen that the magnitudes of horizontal reactions (R_x) were reduced significantly after retrofitting the bridge with elastomeric rubber bearings due to the load sharing effect. As a result, the weakness in earthquake resistance of the bridge foundation (piles under pier P5) in longitudinal direction (previously discussed in section 4.8 of Chapter 4) was greatly improved accordingly. In conclusion, it can be said that the retrofitted bridge model showed better results than the original bridge model with lower overstress values and less number of overstress members.

7.6 Summary

The case study bridge, Maubin Bridge, was initially designed with the assumed earthquake load of 0.1 g according to AASHO 1977, but the new Seismic Zone Map of Myanmar (2012) stated the possible ground acceleration for the bridge site as 0.11 g ~ 0.2 g for the return period of 475 years (Level I earthquake) and 0.21 g ~ 0.4 g for the return period of 2475 years (Level II earthquake). Hence, static and pushover analyses were done as a preliminary study and the presence of overstressed members were confirmed. Then, the bridge was proposed to retrofit by changing the existing steel hinge and roller bearings into elastomeric rubber bearings, and the FE bridge model was run by dynamic implicit analysis by using the modified acceleration record of Thabeikkyin Earthquake for before and after retrofitted conditions.

From the results, four tension diagonal members (D35 and D46, each on upstream truss and downstream truss) suffered maximum tensile stresses of 386 MPa, which was higher than their yield strength of 345 MPa for the bridge model with existing bearings. Moreover, 18 top chords over the supports in three middle piers, 36 top chords in the middle and side spans, 54 tension diagonal members, and 48 compression diagonal members suffered higher stresses greater than the allowable stress values.

For the retrofitted bridge model, there were no more over-yield-stress members, and the number of overstressed members were also reduced to 28 from 36 for top chords in the middle and side spans, to 56 from 58 for tension diagonal members, and to 38 from 48 for compression diagonal members. Although the overstress values were reduced in tension diagonal members and top chords in middle and side spans, some overstress values were found to be increased for compression diagonal members.

Moreover, comparing with before-retrofitting condition, the magnitudes of horizontal reactions (R_x) for after-retrofitting condition were reduced significantly about 6 times due to the load sharing effect. As a result, the weakness in earthquake resistance of the bridge piers

in longitudinal direction (previously discussed in section 4.8 of Chapter 4) was greatly improved accordingly. Therefore, it can be concluded that the retrofitted bridge model showed better results than the original bridge model with lower overstress values and less number of overstress members.

References

[1] Myanmar Earthquake Committee, The Seismic Zone Map of Myanmar (2005), Union of Myanmar, 2005.

[2] Myanmar Earthquake Committee, The Seismic Zone Map of Myanmar (2012), Union of Myanmar, 2012.

[3] Khin Maung Zaw, Suzuki, Y., Matsumura, M. and Sugiura, K., Analysis of Maubin Bridge in Myanmar for Seismic Retrofit, *Proceedings of the 11th German-Japan Bridge Symposium*, Osaka Institute of Technology, Japan, 29 - 31 August 2016.

[4] Khin Maung Zaw, Suzuki, Y., Matsumura, M. and Sugiura, K., Analysis and load testing results of Maubin Bridge in Myanmar, *Proceedings of the 29th KKHTCNN Symposium on Civil Engineering*, Hong Kong University of Science and Technology, China, 3 - 5 December 2016.

[5] Khin Maung Zaw, Suzuki, Y. Sugiura, K., and Myo Win, Comparison of Load Testing and FE Analysis Results of Maubin Bridge, *Proceedings of the 7th International Conference on Science and Engineering*, Yangon Technological University, Myanmar, 10 - 11 December 2016.

[6] Khin Maung Zaw, Suzuki, Y. and Sugiura, K., Study of Maubin Bridge in Myanmar for Seismic Retrofit, *Proceedings of the 10th Taiwan-Japan Workshop on Structural and Bridge Engineering*, Kyoto University, Japan, 31 March - 2 April 2017.

[7] AASHO, Standard Specifications for Highway Bridges, 12th edition, American Association of State Highway and Officials, 1977.

[8] Public Works, Inspection of Maubin Bridge for Repair, Inspection Report, Ministry of Construction, Union of Myanmar, September 2014.

[9] AASHTO, LRFD Bridge Design Specifications, SI Units, 3rd Edition, American Association of State Highway and Transportation Officials, 2004.

CHAPTER 8
Summary and Recommendations

8.1 Summary of Thesis

There have been some background problems for the design, construction and maintenance of long span bridges in Myanmar, especially for those bridges constructed after the change of government in 1988. In order to increase the surface transportation network of the county, former Myanmar government constructed several long span bridges starting around 1990's with limited resources in limited construction time and, as a result, the number of long span steel bridges all over the country rapidly increased from 198 to 528 within 20 years [1]. Almost all of the newly constructed long span steel bridges were designed and fabricated by Chinese companies except for very few bridges with Japanese companies at that time, and many of them were constructed in the coastal and delta regions and some were constructed near the active faults without considering local seismic activities.

According to various investigation reports from local and foreign experts, the deterioration of most long span bridges in Myanmar was generally caused by the chloride attack, the movement of substructures on soft ground, unqualified bridge painting works, fracture of high tension bolts, cracks in floor beams and pavements, settlement and scouring at the base of piers, soil erosion and corroded substructures due to high flood and poor maintenance [2, 3]. Professors and postgraduate students from Kyoto University and Osaka City University also formed a joint research group to study the dynamic characteristics of Yadanarpon Bridge, and to find out the cause of cracks in the end of floor beams in order to give suggestions to the Ministry of Construction for proper retrofitting of the bridge. The current situation of construction and maintenance of bridges in Myanmar had been reported by the author in JSSC symposium in November 2015 [4].

Moreover, according to the higher probable ground acceleration values indicated in the second edition of Seismic Zone Map of Myanmar (2012) [5], the earthquake performance of former long span bridges should be evaluated again, especially for the bridges located in higher seismic zones near the Sagaing Fault and other local faults. There are two major seismic activities in Myanmar, Sagaing Fault and Sunda-Andaman Trench (also called Java Trench or Sumatra Trench) along with many local faults. Many strong earthquakes had occurred in Myanmar during the past century related to the Sagaing Fault and some local

faults, and Sunda-Andaman Trench caused tsunamis along the coastline in addition to many strong earthquakes around the Sumatra and Java regions [6, 7, 8].

In order to know the characteristics of earthquakes in Myanmar, Thabeikkyin Earthquake (2012) has been studied because it was the latest large earthquake recorded on the Sagaing Fault, using the ground motion data recorded from Mandalay station. Response spectrums, Fourier spectrums and Power spectrums were drawn to study the characteristics of Thabeikkyin Earthquake. According to the Fourier and Power spectrums of the earthquake, frequencies between 1 Hz to 10 Hz were dominant with the peak at 0.26 Hz and 0.19 Hz and, the maximum response acceleration occurred between 0.1 sec and 0.2 sec periods for different damping ratios according to the linear acceleration response spectrums. Design spectrums for the Ayeyerwady delta region (or regions with peak ground accelerations of 0.2g and 0.4g) due to the earthquakes along the Sagaing Fault were also proposed based on Thabeikkyin Earthquake response spectrum and Seismic Zone Map of Myanmar (2012).

Linear and nonlinear response spectrums of (SDOF) systems for Thabeikkyin Earthquake were produced by writing FORTRAN programs based on Newmark's time-stepping method [9]. Ductility and response of nonlinear SDOF systems were also compared with the response of linear systems by using the equal energy theorem [10] for three different normalized yield strengths. According to the results, it was found out that the ductility ratio increases but the resisting force decreases while decreasing the normalized yield strength.

Moreover, the ground acceleration data of Thabeikkyin Earthquake was modified to 0.2g and 0.4g in order to propose a design spectrum according the Seismic Zone Map of Myanmar 2012. The design spectrum for the Ayeyarwady delta region (or similar regions with peak ground accelerations of 0.2g and 0.4g for Level I and II earthquakes) was proposed for level I and level II earthquakes but it is just a preliminary proposal as an initiative for the emergence of the design standard for the construction of long span bridges in Myanmar and more research data is still necessary to prepare that kind of design spectrums.

In order to find out the earthquake resistance performance of long span bridges in Myanmar, Maubin Bridge was selected as the case study bridge, which was initially designed according to AASHO 1977 with the assumed earthquake load of 0.1g, because similar long span steel truss bridges were constructed in Myanmar after 1990. However, the new Seismic Zone Map of Myanmar (2012), issued by Myanmar Earthquake Committee, stated the possible ground acceleration of the bridge site as 0.11 g ~ 0.2 g for the return period of 475 years and 0.21 g ~ 0.4 g for the return period of 2475 years. Hence, the performance of the

bridge under the increased seismic loads were evaluated for the potential seismic retrofit and the results were presented in the German-Japan Bridge Symposium in August 2016 [11].

Preliminary static analysis and pushover analysis with explicit method were performed by creating three dimensional finite element bridge model in ABAQUS according to the original drawings of the bridge as well as the resistance of piles under the pier due to static earthquake load was checked by using the results from FE analysis and soil report data. The bridge model is composed of 318 truss members, 188 top lateral bracing members, 160 bottom lateral bracing members, 523 floor system members, 16 transverse portal frames and 120 floor decks.

According to static analysis results, the design wind load and increased seismic loads of 0.2g and 0.4g caused the overstresses mostly in diagonal members except for some over stresses in top chords over the support due to the earthquake in vertical (Y) direction. Results from pushover analysis with explicit method showed that over stresses occurred in almost all truss members except bottom chords due to unfactored seismic loads of 0.1g, 0.2g, 0.4g. Moreover, it is also verified that when the earthquake load is increased from 0.1g to 0.2g or 0.4g, the resistance of piles against the earthquake cannot be assured anymore and the earthquake resistance of the bridge in the longitudinal direction is relatively weaker than that in the transverse direction. The bridge may also be prone to fall off from the bridge piers if an earthquake comes laterally from the transverse direction of the bridge.

After the FE bridge model was analyzed by the ABAQUS, static and dynamic loading tests were performed on the bridge in September 2016 in order to find out the dynamic characteristics of the real bridge structure and to verify the accuracy of the bridge model. Before the actual loading tests, preliminary measurements were done on the bridge in 31st May 2016 by a team of Japanese professors from Kyoto University (KU) and a Japanese engineer from Public Works Research Institute (PWRI). Based on the results from numerical analysis and preliminary measurements, actual static and dynamic loading tests were done on the Maubin Bridge from 21st to 22nd September 2016, and the results of field measurement were compared with the results from FE bridge model and the results were presented in symposiums after the model was updated [12, 13, 14].

Static load testing results showed that the measured strain and deflection results were close to the model strain and deflection values except for load point location (2) for member D13 due to the possible errors in field measurement, or due to the necessity in modeling connection between truss members and transverse portal frames, or due to the difference between assumed support conditions and actual support conditions. Since the deflection

values from the FE bridge model were generally larger than the measured deflections, it can be said that the model was a soft model in comparing with the actual bridge. Dynamic load testing results also showed that measured bridge frequencies were close to the model frequencies for the first four bending modes with the maximum difference of 9.26% but these errors became decreased to 1.2% after updating the model by increasing the thickness of concrete decks.

Since long span steel bridges in Myanmar were intended to retrofit with elastomeric rubber bearings, two elastomeric rubber bearings were tested in five different loading configuration in order to acquire the fundamental information in conducting tests for bridge bearings. Load-displacement curves were drawn for each load cases, and shear modulus or lateral stiffness, vertical stiffness, dissipated energy, strain energy and equivalent damping ratio of sample bearings were evaluated from the experimental data of the third loading cycle. Test results showed the effect of increasing lateral displacement on higher value of shear modulus and dissipated energy due to the increased lateral load, and the effect of increasing vertical loads causing the bearing to dissipate more energy with higher damping ratio.

After the FE bridge model was updated, the bridge was proposed to retrofit by replacing existing steel hinge and roller bearings with elastomeric rubber bearings, and the FE bridge model was run by dynamic implicit analysis by using the modified acceleration record of Thabeikkyin Earthquake for before and after retrofitted conditions. According to the analysis results, four tension diagonal members suffered maximum tensile stresses of 386 MPa, which was higher than their yield strength of 345 MPa for the bridge model with original bearings. Apart from these four members, 18 top chords over the supports in three middle piers, 36 top chords in the middle and side spans, 58 tension diagonal members, and 48 compression diagonal members suffered higher stresses greater than the allowable stress values.

For the retrofitted bridge model, there were no more over-yield-stress members, and the number of overstressed members were also reduced to 28 from 36 for top chords in the middle and side spans, to 56 from 58 for tension diagonal members, and to 38 from 48 for compression diagonal members. Therefore, comparing with existing bearing condition, the number of over-allowable-stress members reduced from 160 to 140 in total. Although the overstress values were reduced in tension diagonal members and top chords in middle and side spans, some overstress values were found to be increased for compression diagonal members.

Moreover, the magnitudes of horizontal reactions (R_x) for after-retrofitting condition were reduced significantly about 6 times comparing with before-retrofitting condition, due to

the load sharing effect. As a result, the weakness in earthquake resistance of the foundation of the bridge in longitudinal direction was greatly improved accordingly. Therefore, it can be concluded that the retrofitted bridge model showed better results than the original bridge model with lower overstress values and less number of overstress members.

8.2 Recommendations for Future Research

The results of the study pointed out the requirements for the seismic retrofitting of the former long span steel truss bridges in Myanmar to meet the local seismic demands according to the Seismic Zone Map of Myanmar 2012. Retrofitting can be accomplished by replacing existing steel bearings with elastomeric rubber bearings and, if necessary, buckling restrained braces (BRB) members can be installed in place of top and bottom lateral bracings as well as transverse portal bracings. However, the earthquake resistance of bridge piers were not included in this study and it is still necessary to check their performance in future researches.

Hence, the seismic performance of former long span bridges, especially near the faults, should be reviewed one-by-one by using the preliminary static analysis as well as the proper time history dynamic analysis, referring to the latest Seismic Zone Map of Myanmar issued by the Myanmar Earthquake Committee. Then, the dynamic characteristics of the bridges should also be checked by performing vibration tests on the bridge to find out its dynamic characteristics, and then to confirm the appropriate retrofitting method.

Moreover, when designing a long span bridge especially located near the faults, static analysis should be used as a preliminary step to determine the cross section dimensions of bridge members, but dynamic analysis using proper time history records should also be used to check the performance of the bridge during the future expected earthquakes.

Although the design spectrum for the Ayeyarwady delta region (or similar regions) was proposed for level I and level II earthquakes based on Thabeikkyin Earthquake response spectrum and Seismic Zone Map of Myanmar (2012), it is just a preliminary proposal and more research is still required to prepare that kind of design spectrums. Since the standard specifications for the design and construction of long span bridges for Myanmar is not established yet, the findings of the present study should be used as one of the references for further researches.

References

[1] Public Works, Current Situation of Road Networks and Bridges, Ministry of Construction, Union of Myanmar, February 2013.

[2] JIP, Current Situation and Issues of Myanmar's Bridge Work, Situation Report, Japan Infrastructure Partners, Japan, 2012.

[3] Oriental Consultants, JICA, Investigation Record Books for Substructures of Bridges (Reference Data), The National Transport Development Plan, Rehabilitation and Modernization of Yangon-Mandalay Railway Project, September 2013.

[4] Khin Maung Zaw, Suzuki, Y. and Sugiura, K., Current Situation of Construction and Maintenance of Bridges in Myanmar, *Proceedings of Construction Steel*, Vol. (23), pp. 364-371, JSSC Symposium, Tokyo, Japan, 19 - 20 November 2015.

[5] Myanmar Earthquake Committee, The Seismic Zone Map of Myanmar (2012), Union of Myanmar, 2012.

[6] Tint Lwin Swe, Earthquake Risk of Major Cities in Relation to Seismicity along Sagaing Fault, *3rd International Workshop on Seismo-tectonics in Myanmar and Earthquake Risk Management*, May 2011.

[7] Soe Thura Tun, The Sagaing Fault: A desk study report on seismo-tectonic implications in Myanmar, Myanmar Earthquake Committee, November 2005.

[8] Hla Hla Aung, Myanmar Earthquakes History, Wathan Press, Yangon, Myanmar, January 2015.

[9] Chopra, A.K., Dynamics of Structures, 4th edition, Prentice Hall, 2012.

[10] Igarashi, A., Nonlinear response and capacity design of Structures, Lecture Notes on Earthquake Engineering, Kyoto University, June 2016.

[11] Khin Maung Zaw, Suzuki, Y., Matsumura, M. and Sugiura, K., Analysis of Maubin Bridge in Myanmar for Seismic Retrofit, *Proceedings of the 11th German-Japan Bridge Symposium*, Osaka Institute of Technology, Japan, 29 - 31 August 2016.

[12] Khin Maung Zaw, Suzuki, Y., Matsumura, M. and Sugiura, K., Analysis and load testing results of Maubin Bridge in Myanmar, *Proceedings of the 29th KKHTCNN Symposium on Civil Engineering*, Hong Kong University of Science and Technology, China, 3 - 5 December 2016.

[13] Khin Maung Zaw, Suzuki, Y. Sugiura, K., and Myo Win, Comparison of Load Testing and FE Analysis Results of Maubin Bridge, *Proceedings of the 7th International Conference on Science and Engineering*, Yangon Technological University, Myanmar, 10 - 11 December 2016.

[14] Khin Maung Zaw, Suzuki, Y. and Sugiura, K., Study of Maubin Bridge in Myanmar for Seismic Retrofit, *Proceedings of the 10th Taiwan-Japan Workshop on Structural and Bridge Engineering*, Kyoto University, Japan, 31 March - 2 April 2017.

APPENDIX A

FORTRAN Program for Linear Response Spectrum

```
      Program Newmark_Linear
      Implicit None
      Real GA(5000),RA,RV,RU,D(5),T(5000),P,dp,pd,w,dt,gamma,beta,k,a,b
      Real TAmax,Amax,Vmax,Umax,dU,dV,dA
      Integer I,J,M,nd,np,N
      dt=0.02
      nd=1
      np=4901
      N=1560
      gamma=0.5
      beta=0.25
      Open(Unit=1,FILE="C:\\MSDEV\\DAMP.dat")
      Read(1,*)(D(I),I=1,nd)
      Open(Unit=2,FILE="C:\\MSDEV\\PERIOD.dat")
      Read(2,*)(T(J),J=1,np)
      Open(UNIT=3,FILE="C:\\MSDEV\\ACC-TBK.dat")
      Read(3,*)(GA(M),M=1,N)
      Open(UNIT=4,FILE="C:\\MSDEV\\TBK-spectrum.txt")
      Do 3 I=1,nd
            dp=D(I)
            Write(4,30)dp
30          Format(5X,8HDamping=,F4.2/5X,6HPeriod,5X,4HDmax,8X,4HVmax,10X,
            4HAmax/6X,4Hsec.,6X,4Hcms.,7X,8Hcms./sec,4X,12Hcms./sec/sec)
            Do 4 J=1,np
                  pd=T(J)
                  w=2*3.141592654/pd
                  k=w**2+gamma/(beta*dt)*2*dp*w+1./(beta*((dt)**2))
                  a=1./(beta*dt)+(gamma/beta)*2*dp*w
                  b=1./(2*beta)+dt*(gamma/(2*beta)-1)*2*dp*w
                  TAmax=0.0
                  Amax=0.0
                  Vmax=0.0
                  Umax=0.0
                  RU=0.0
                  RV=0.0
                  RA=0.0
                  Do 5 M=1,N
```

```
                        P=-(GA(M+1)-GA(M))+a*RV+b*RA
                        dU=P/k
                        dV=(gamma/(beta*dt))*dU-(gamma/beta)*RV+dt*
                        (1-(gamma/(2*beta)))*RA
                        dA=dU/(beta*(dt)**2)-RV/(beta*dt)-RA/(2*beta)
                        RU=RU+dU
                        RV=RV+dV
                        RA=RA+dA
                        TA=RA+GA(M+1)
                        If(Abs(TA).GT.TAmax)then
                              TAmax=Abs(TA)
                        else
                              TAmax=TAmax
                        End If
                        If(Abs(RA).GT.Amax)then
                              Amax=Abs(RA)
                        else
                              Amax=Amax
                        End If
                        If(Abs(RV).GT.Vmax)then
                              Vmax=Abs(RV)
                        else
                              Vmax=Vmax
                        End If
                        If(Abs(RU).GT.Umax)then
                              Umax=Abs(RU)
                        else
                              Umax=Umax
                        End If
5                 Continue
                  Write(4,100)pd,Umax,Vmax,TAmax
100               Format(6X,F5.3,4X,F8.3,5X,F8.3,7X,F8.3)
4           Continue
3     Continue
      Stop
      End
```

APPENDIX B

FORTRAN Program for Nonlinear Response Spectrum

```
      Program Newmark_NonLinear_AM
      Implicit None
      Real GA(25000),RA,RV,RU,D(1),T(4901),P,dp,pd,w,dt,gamma,beta,K,a,b
      Real TAmax,Amax,Vmax,Umax,dU,dV,dF,F,Fy0,Fy,nFy,Ke,Kp,Kf,V0
      Integer I,J,M,nd,np,N,Count
      dt=0.01
      nd=1
      np=1
      N=4997
      gamma=0.5
      beta=0.25
      Fy0=200
      Open(Unit=1,FILE="C:\\MSDEV\\DAMP.dat")
      Read(1,*)(D(I),I=1,nd)
      Open(Unit=2,FILE="C:\\MSDEV\\PERIOD.dat")
      Read(2,*)(T(J),J=1,np)
      Open(UNIT=3,FILE="C:\\MSDEV\\ACC-TBK.dat")
      Read(3,*)(GA(M),M=1,N)
      Open(UNIT=4,FILE="C:\\MSDEV\\Spectrum-TBK.txt")
      Do 3 I=1,nd
            dp=D(I)
            Write(4,30)dp
30          Format(5X,8HDamping=,F4.2/5X,6HPeriod,5X,4HDmax,8X,4HVmax,10X,
            4HAmax/6X,4Hsec.,6X,4Hcms.,7X,8Hcms./sec,4X,12Hcms./sec/sec)
            Do 4 J=1,np
                  pd=T(J)
                  w=2*3.141592654/pd
                  Kf=gamma/(beta*dt)*2*dp*w+1./(beta*((dt)**2))
                  Ke=w**2
                  Kp=0.0
                  a=1./(beta*dt)+(gamma/beta)*2*dp*w
                  b=1./(2*beta)+dt*(gamma/(2*beta)-1)*2*dp*w
                  TAmax=0.0
                  Amax=0.0
                  Vmax=0.0
                  Umax=0.0
```

```
RU=0.0
RV=0.0
RA=0.0
V0=0.0
F=0
K=Ke
Count=1
Do 5 M=1,N
      P=-(GA(M+1)-GA(M))+a*RV+b*RA
      dU=P/(K+Kf)
      dV=(gamma/(beta*dt))*dU-(gamma/beta)*RV+dt*
      (1-(gamma/(2*beta)))*RA
      dF=K*dU
      RU=RU+dU
      RV=RV+dV
      F=F+dF
      If((Count.EQ.1).AND.(F.GT.Fy0))then
            Fy=Fy0
            nFy=-Fy0
            F=Fy0
            RU=Fy0/Ke
            RV=RV-dV
            K=Kp
            Count=Count+1
      Else if((Count.EQ.1).AND.(F.LT.-Fy0))then
            Fy=Fy0
            nFy=-Fy0
            F=-Fy0
            RU=-Fy0/Ke
            RV=RV-dV
            K=Kp
            Count=Count+1
      Else if((Count.GT.1).AND.(MOD(Count,2).EQ.0).AND.
      (V0.GT.0).AND.(RV.GT.0))then
            Fy=F
            nFy=(Fy-2*Fy0)
            K=Kp
      Else if((Count.GT.1).AND.(MOD(Count,2).NE.0).AND.
      (V0.LT.0).AND.(RV.LT.0).AND.(F.LT.nFy))then
            RU=RU+(nFy-F)/Ke
            F=nFy
```

```
      RV=RV-dV
      K=Kp
      Count=Count+1
Else if((Count.GT.1).AND.(MOD(Count,2).EQ.0).AND.
(V0.LT.0).AND.(RV.LT.0))then
      nFy=F
      Fy=(nFy+2*Fy0)
      K=Kp
Else if((Count.GT.1).AND.(MOD(Count,2).NE.0).AND.
(V0.GT.0).AND.(RV.GT.0).AND.(F.GT.Fy))then
      RU=RU-(F-Fy)/Ke
      F=Fy
      RV=RV-dV
      K=Kp
      Count=Count+1
Else if((Count.GT.1).AND.(MOD(Count,2).EQ.0).AND.
((V0*RV).LT.0))then
      Fy=F-dF
      nFy=(Fy-2*Fy0)
      RV=RV-dV
      K=Ke
      Count=Count+1
Else if((Count.GT.1).AND.(MOD(Count,2).EQ.0).AND.
(V0.LT.0).AND.(RV.GT.0))then
      nFy=F-dF
      Fy=(nFy+2*Fy0)
      RV=RV-dV
      K=Ke
      Count=Count+1
Else
      K=Ke
End If
V0=RV
RA=-GA(M+1)-2*dp*w*RV-F
TA=RA+GA(M+1)
If(Abs(TA).GT.TAmax)then
      TAmax=Abs(TA)
else
      TAmax=TAmax
End If
If(Abs(RA).GT.Amax)then
```

```
                        Amax=Abs(RA)
                    else
                        Amax=Amax
                    End If
                    If(Abs(RV).GT.Vmax)then
                        Vmax=Abs(RV)
                    else
                        Vmax=Vmax
                    End If
                    If(Abs(RU).GT.Umax)then
                        Umax=Abs(RU)
                    else
                        Umax=Umax
                    End If
5               Continue
                Write(4,100)pd,Umax,Vmax,TAmax
100             Format(6X,F5.3,4X,F8.3,5X,F8.3,7X,F8.3)
4           Continue
3     Continue
      Stop
      End
```

APPENDIX C

Calculation of Earthquake Resistance of Piles under the Pier P5 of Maubin Bridge

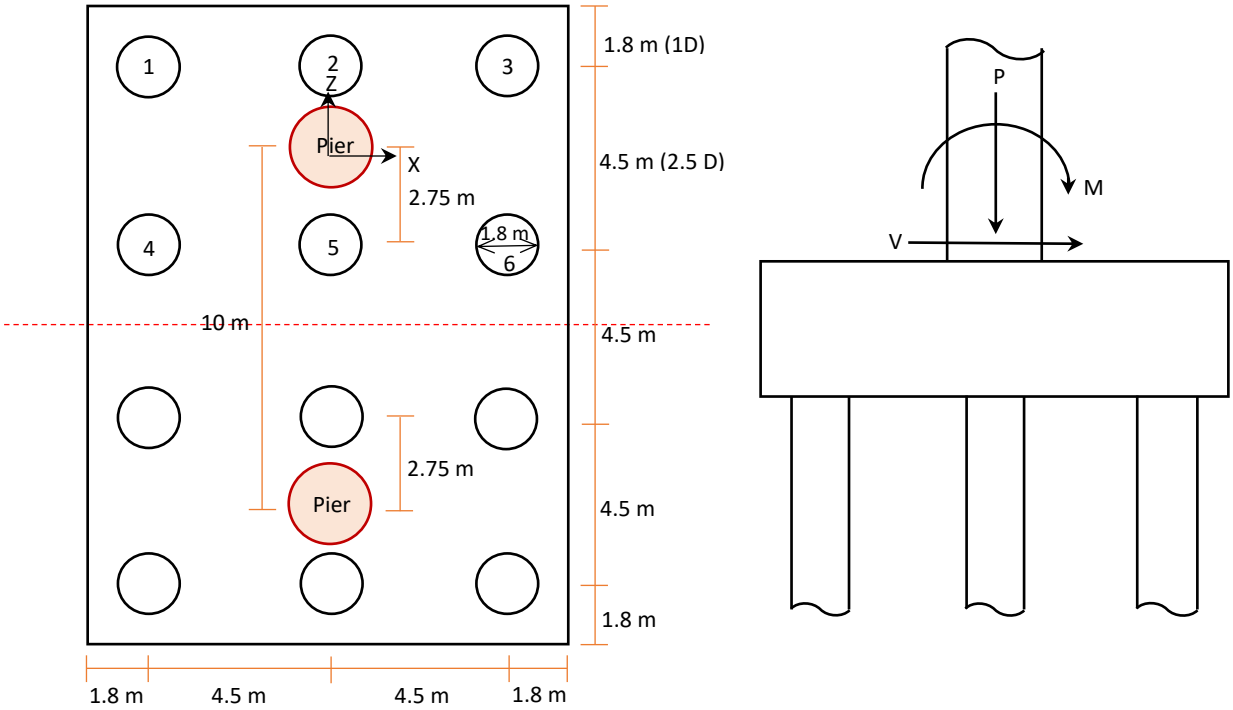

Figure C.1: Arrangement of piles and pier columns in the pile cap of pier P5.

Earthquake resistance of piles under the pier P5 of Maubin Bridge was calculated by referring AASHTO Bridge Design Specifications 2004, using the SPT values from soil reports as follows:

1. <u>Load on Each Pile under Factored DL + EQ (0.1g)</u>

   Consider only the half of pile cap (6 piles) due to symmetry.

   R = 11190 kN (reaction from ABAQUS); n = 6 (no. of piles); h_p = 17.5 m (height of pier)

   V = 3610 kN (horizontal reaction from ABAQUS)

   $W_{pilecap}$ = (12.6 m x 17.1 m x 2.8 m) x 2400 kg/m^3 x 9.81 = 14204 kN

   $W_{pier} = \pi\ (2.75/2)^2$ x 17.5 x 2400 x 9.81 = 2447 kN (assuming average pier dia. as 2.75 m)

   W_{beam} = (1 x 1.5 x 7.1 + 3 x 2 x 13) x 9.81 x 2400 = 2087 kN

   $P = (R + W_{pier} + W_{beam}/2 + W_{pilecap}/2)/6 = (11190 + 2447 + 2087/2 + 14204/2)/6$

   P = (21783/6) = 3630 kN

   $M_z = V \times h_p$ = 63175 kN.m

$x_1 = x_4 = -4.5$ m; $x_2 = x_5 = 0$ m; $x_3 = x_6 = 4.5$ m.

$I_z = \Sigma x^2 = 81\ m^2$

$P_1 = P_4 = (P/n) + (M_z.x_1/I_z) = 3630\ kN - 3510\ kN = 120\ kN$

$P_2 = P_5 = (P/n) + (M_z.x_2/I_z) = 3630\ kN + 0 = 3630\ kN$

$P_3 = P_6 = (P/n) + (M_z.x_3/I_z) = 3630\ kN + 3510\ kN =$ 7140 kN #

2. Load on Each Pile under Factored DL + EQ (0.2g)

R = 12190 kN; P = 3797 kN; V = 7240 kN; $M_z = V \times h_p = 126700$ kN.m

$P_1 = P_4 = (P/n) + (M_z.x_1/I_z) = 3797\ kN - 7039\ kN = -3242\ kN$

$P_2 = P_5 = (P/n) + (M_z.x_2/I_z) = 3797\ kN + 0 = 3797\ kN$

$P_3 = P_6 = (P/n) + (M_z.x_3/I_z) = 3797\ kN + 7039\ kN =$ 10836 kN #

3. Load on Each Pile under Factored DL + EQ (0.4g)

R = 14225 kN; P = 4136 kN; V = 14445 kN; $M_z = V \times h_p = 252788$ kN.m

$P_1 = P_4 = (P/n) + (M_z.x_1/I_z) = 4136\ kN - 14044\ kN = -9908\ kN$

$P_2 = P_5 = (P/n) + (M_z.x_2/I_z) = 4136\ kN + 0 = 4136\ kN$

$P_3 = P_6 = (P/n) + (M_z.x_3/I_z) = 4136\ kN + 14044\ kN =$ 18180 kN #

Resistance of Piles according to AASHTO 2004

Assuming length of pile in soil = 35 m, length of pile in water = 10 m

A. SPT Method (based on SPT values from soil report)

Assuming $\sigma'_v = 0.357$ MPa, N = 50 blows/ft, $N_{avg} = 25$ blows/ft, $D_b = 5$ m

$R = q_p.A_x + q_s.A_s$ (10.7.3.4.2)

$q_p = 0.038\ N_{corr}\ D_b/D$; $N_{corr} = [0.77 \log_{10}(1.92/\sigma'_v)].N$; $q_s = 0.0019 N_{avg}$;

$N_{corr} = 25$ blows/ft; $q_p = 2.956$ MPa; $q_s = 0.048$ MPa

$R = 2956\ \pi\ (1.8/2)^2 + 48\ \pi\ (1.8) \times 35 = 17022$ kN

$\varphi R = 0.45\ R =$ 7660 kN (Control) > 7140 kN #

B. α Method

Assuming $\alpha = 0.7$, undrained shear strength of soil, $S_u = 100\ kN/m^2$

$R = 9S_u.A_x + \alpha S_u.A_s$ (10.7.3.3)

$R = 9 \times 100 \times \pi\ (1.8/2)^2 + 0.7 \times 100 \times \pi\ (1.8) \times 35 = 16145$ kN

$\varphi R = 0.7\ R = 11302$ kN #

C. β Method

Assuming $\beta = 0.3$, unit weight of soil (γ) = 20 kN/m^3

Effective vertical stress (σ'_v) = 35 x (20 – 9.81) = 357 kN/m^2

$R = 9S_u.A_x + \beta\sigma'_v.A_s$ (10.7.3.3)

$R = 9 \times 100 \times \pi (1.8/2)^2 + 0.3 \times 357 \times \pi (1.8) \times 35 = 23487$ kN

$\varphi R = 0.5\ R = 11744$ kN #

D. λ Method

Assuming $\lambda = 0.13$, $S_u = 100$ kN/m^2, $\sigma'_v = 357$ kN/m^2

$R = 9S_u.A_x + \lambda (\sigma'_v + 2\ S_u).A_s$ (10.7.3.3)

$R = 9 \times 100 \times \pi (1.8/2)^2 + 0.13 \times (357 + 2 \times 100) \times \pi (1.8) \times 35 = 16622$ kN

$\varphi R = 0.55\ R = 9142$ kN #

Check as a Group of Pile

I. Load on Pile Group under Factored DL + EQ

$P_{0.1g}$ = (21783 x 2) + (3510 x 4) = 57606 kN

$P_{0.2g}$ = (22782 x 2) + (7039 x 4) = 73720 kN

$P_{0.4g}$ = (24816 x 2) + (14044 x 4) = 105808 kN #

II. Pile Group Capacity (block failure check according to AASHTO 2004)

$R = (2X + 2Y).Z.S_u + X.Y.N_c.S_u$ (10.7.3.10)

X, Y, Z = length, width and depth of pile group

$N_c = 7.5\ (1 + 0.2X/Y) = 7.5\ (1 + 0.2 \times 9/13.5) = 8.5$, $S_u = 100$ kN/m^2

$R = 2(9 + 13.5) \times 30 \times 100 + (9 \times 13.5 \times 8.5 \times 100) = 238275$ kN

$\varphi R = 0.65 \times 238275 = 154879$ kN > 105808 kN #

APPENDIX D

Preliminary Design of Elastomeric Bearings for Maubin Bridge

Elastomeric rubber bearings for Maubin Bridge were designed preliminarily in accordance with the method B of AASHTO-LRFD specifications. A typical elastomer with hardness 60 Shore A Durometer and a shear modulus (G) of 150 psi (1 MPa) is assumed for the proposed bearing with 1.75 ksi (12 MPa) delamination stress limit (σ_d).

Step 1: To determine the minimum area of bearing

In order to satisfy the maximum compressive stress limit for bearings fixed against shear deformation, the minimum bearing area is determined from the reaction due to total load at each pier divided by the delamination stress (σ_d) as follows:

For pier P5 and P7: $A_{min} = \frac{F_R}{\sigma_d} = \frac{11.4\ MN}{12\ MPa} = 0.95\ m^2$

For pier P6: $A_{min} = \frac{F_R}{\sigma_d} = \frac{9.7\ MN}{12\ MPa} = 0.81\ m^2$

For pier P4 and P8: $A_{min} = \frac{F_R}{\sigma_d} = \frac{4.0\ MN}{12\ MPa} = 0.33\ m^2$

Since the width of the bearing plate under the lower chord is 780 mm, the width of the bearing is assumed as 750 mm for all the bearings, and the length as 1300 mm for P5, P7, 1100 mm for P6 and, 500 mm for P4, P8, giving the area of 0.975 m^2, 0.825 m^2 and 0.375 m^2 respectively, which are greater than the required area of 0.95 m^2, 0.81 m^2 and 0.33 m^2. Since the width of the piers in the top are from 2.5 m to 3.0 m, the length of bearings were within limits for the installation in the top of piers.

Step 2: To determine the shape factor and elastomer thickness

The shape factor (S) of a layer of an elastomeric bearing is defined as the plan area of the layer divided by the area of perimeter free to bulge. Since the relationship between the shear stress and the applied compressive load depends directly on the shape factor, the shape factor

is estimated first from the compressive stress (σ_s) divided by twice the shear modulus (G) as follows:

For pier P5 and P7: $S = \frac{\sigma_s}{2G} = \frac{11.4/(0.75)(1.3)}{2\ (1)} = 5.85$

For pier P6: $S = \frac{\sigma_s}{2G} = \frac{9.7/(0.75)(1.1)}{2(1)} = 5.88$

For pier P4 and P8: $S = \frac{\sigma_s}{2G} = \frac{4.0/(0.75)(0.5)}{2(1)} = 5.33$

Then the thickness of elastomer is determined from the estimated shape factor and, the length and width of the bearing as follow:

For pier P5 and P7: $h_i = \frac{LW}{[2S_i(L+W)]} = \frac{(0.75)(1.3)}{2(5.85)(0.75+1.3)} = 41\ mm$

For pier P6: $h_i = \frac{LW}{[2S_i(L+W)]} = \frac{(0.75)(1.1)}{2(5.88)(0.75+1.1)} = 38\ mm$

For pier P4 and P8: $h_i = \frac{LW}{[2S_i(L+W)]} = \frac{(0.75)(0.5)}{2(5.33)(0.75+0.5)} = 28\ mm$

Hence 40 mm, 35 mm, 25 mm thicknesses are used for an interior elastomeric layer of the bearings. Then the actual shape factor is calculated again using the actual thickness of elastomeric layers as follows:

For pier P5 and P7: $S = \frac{LW}{2(h_i)(L+W)} = \frac{(0.75)(1.3)}{2(0.04)(0.75+1.3)} = 5.95$

For pier P6: $S = \frac{LW}{2(h_i)(L+W)} = \frac{(0.75)(1.1)}{2(0.035)(0.75+1.1)} = 6.37$

For pier P4 and P8: $S = \frac{LW}{2(h_i)(L+W)} = \frac{(0.75)(0.5)}{2(0.025)(0.75+0.5)} = 6.0$

Step 3: To determine the number of interior elastomeric layers

Then, the number of interior elastomeric layers is determined from the uplift requirement under the combination of compression and rotation as follows:

For pier P5 and P7: $$n_u = \frac{1.0GS(\theta_s)\left(\frac{W}{h_i}\right)^2}{\sigma_s} = \frac{1.0(1)(6.79)(0.005)\left(\frac{1.3}{0.04}\right)^2}{11.69} = 4$$

$$n_c = -\frac{0.167(\theta_s)\left(\frac{W}{h_i}\right)^2}{\frac{\sigma_s}{2.25GS}-1} = -\frac{0.167(0.005)\left(\frac{1.3}{0.04}\right)^2}{\frac{11.69}{2.25(1)(5.95)}-1} = 7 \text{ (Control)}$$

For pier P6: $$n_u = \frac{1.0GS(\theta_s)\left(\frac{W}{h_i}\right)^2}{\sigma_s} = \frac{1.0(1)(6.37)(0.005)\left(\frac{1.1}{0.035}\right)^2}{11.76} = 3$$

$$n_c = -\frac{0.167(\theta_s)\left(\frac{W}{h_i}\right)^2}{\frac{\sigma_s}{2.25GS}-1} = -\frac{0.167(0.005)\left(\frac{1.1}{0.035}\right)^2}{\frac{11.76}{2.25(1)(6.37)}-1} = 5 \text{ (Control)}$$

For pier P4 and P8: $$n_u = \frac{1.0GS(\theta_s)\left(\frac{W}{h_i}\right)^2}{\sigma_s} = \frac{1.0(1)(6)(0.005)\left(\frac{0.5}{0.025}\right)^2}{10.67} = 2$$

$$n_c = -\frac{0.167(\theta_s)\left(\frac{W}{h_i}\right)^2}{\frac{\sigma_s}{2.25GS}-1} = -\frac{0.167(0.005)\left(\frac{0.5}{0.025}\right)^2}{\frac{10.67}{2.25(1)(6)}-1} = 2 \text{ (Control)}$$

Hence, 7 layers of 40 mm thick interior elastomeric sheets are used for P5 and P7 with 30 mm thick exterior layers, 5 layers of 35 mm thick interior elastomeric sheets for P6 with 25 mm thick exterior layers, 3 layers of 25 mm thick interior elastomeric sheets for P4 and P8 with 15 mm thick exterior layers.

Step 4: To check the stability of bearings

Then the stability of bearings is checked by two conditions whether $2A \leq B$ is satisfied or $\sigma_s \leq GS/(A - B)$.

For pier P5 and P7: $$A = \frac{1.92\frac{h_t}{L}}{\sqrt{1+\frac{2L}{W}}} = \frac{1.92\left(\frac{0.34}{1.3}\right)}{\sqrt{1+\frac{2(1.3)}{0.75}}} = 0.24$$

$$B = \frac{2.67}{(S+2)\left(1+\frac{L}{4W}\right)} = \frac{2.67}{(5.95+2)\left(1+\frac{1.3}{4(0.75)}\right)} = 0.23$$

So $2A \nleq B$

Then check $\sigma_s \leq GS/(A-B)$

But $\frac{GS}{A-B} = \frac{1(5.95)}{0.01} = 595 > \sigma_s$ (It's OK)

Therefore, the bearing on P5 and P7 is stable.

For pier P6: $A = \frac{1.92\frac{h_t}{L}}{\sqrt{1+\frac{2L}{W}}} = \frac{1.92\left(\frac{0.225}{1.1}\right)}{\sqrt{1+\frac{2(1.1)}{0.75}}} = 0.20$

$B = \frac{2.67}{(S+2)\left(1+\frac{L}{4W}\right)} = \frac{2.67}{(6.37+2)\left(1+\frac{1.1}{4(0.75)}\right)} = 0.23$

So $2A \nleq B$

Then check $\sigma_s \leq GS/(A-B)$

But $(A-B) = -0.03$ (It's OK)

Therefore, the bearing on P6 is stable.

For pier P4 and P8: $A = \frac{1.92\frac{h_t}{L}}{\sqrt{1+\frac{2L}{W}}} = \frac{1.92\left(\frac{0.105}{0.5}\right)}{\sqrt{1+\frac{2(0.5)}{0.75}}} = 0.26$

$B = \frac{2.67}{(S+2)\left(1+\frac{L}{4W}\right)} = \frac{2.67}{(6+2)\left(1+\frac{0.5}{4(0.75)}\right)} = 0.27$

So $2A \nleq B$

Then check $\sigma_s \leq GS/(A-B)$

But $(A-B) = -0.01$ (It's OK)

Therefore, the bearing on P4 and P8 is stable.

Step 5: To determine the thickness of reinforcing steel plates (SM490A)

For pier P5 and P7: $h_s = \frac{3h_i\sigma_s}{F_y} = \frac{3(0.04)(11.69)}{355} = 4.0$ mm

For pier P6: $h_s = \frac{3h_i\sigma_s}{F_y} = \frac{3(0.035)(11.76)}{355} = 3.5$ mm

For pier P4 and P8: $h_s = \frac{3h_i\sigma_s}{F_y} = \frac{3(0.025)(10.67)}{355} = 2.3$ mm

Use 5 mm thick (SM490A) reinforcing steel plates for P5 and P7, 4 mm thick steel plates for P6, and 3 mm thick steel plates for P4, P8.

Step 6: To evaluate the stiffness values in horizontal and vertical directions

For pier P5 and P7: $K_L = K_T = \frac{GA}{\Sigma h_i} = \frac{1(0.975)}{0.34} = 2.9$ kN/mm

$E = \alpha.\beta.S_1.G_e = (45)(1)(5.95)(1) = 267.75$ MPa

$K_v = \frac{AE}{\Sigma h_i} = \frac{(0.975)(267.75)}{0.34} = 768$ kN/mm

For pier P6: $K_L = K_T = \frac{GA}{\Sigma h_i} = \frac{1(0.825)}{0.225} = 3.67$ kN/mm

$E = \alpha.\beta.S_1.G_e = (45)(1)(6.37)(1) = 286.65$ MPa

$K_v = \frac{AE}{\Sigma h_i} = \frac{(0.825)(286.65)}{0.225} = 1051$ kN/mm

For pier P4 and P8: $K_L = K_T = \frac{GA}{\Sigma h_i} = \frac{1(0.375)}{0.105} = 3.57$ kN/mm

$$E = \alpha.\beta.S_1.G_e = (45)(1)(6.0)(1) = 270 \text{ MPa}$$

$$K_v = \frac{AE}{\Sigma h_i} = \frac{(0.375)(270)}{0.08} = 1266 \text{ kN/mm}$$